LOW TEMPERATURE ELECTRICAL RESISTIVITY AND GALVANOMAGNETIC EFFECTS IN Mn-RICH CuMn AND Ni-RICH NiFeCr ALLOYS

by
SWAPAN CHAKRABORTY

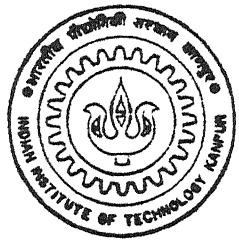

DEPARTMENT OF PHYSICS

Indian Institute of Technology Kanpur

FEBRUARY, 1998

LOW TEMPERATURE ELECTRICAL RESISTIVITY AND GALVANOMAGNETIC EFFECTS IN Mn - RICH CuMn AND Ni-RICH NiFeCr ALLOYS

A Thesis Submitted

in Partial Fulfilment of the Requirements

for the Degree of

Doctor of Philosophy

by

SWAPAN CHAKRABORTY

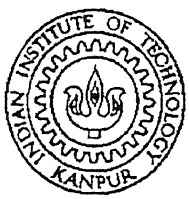

to the

DEPARTMENT OF PHYSICS

INDIAN INSTITUTE OF TECHNOLOGY, KANPUR

February, 1998

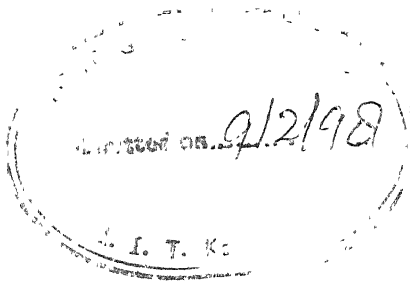

CERTIFICATE

It is certified that the work contained in the thesis entitled *LOW TEMPERATURE ELECTRICAL RESISTIVITY AND GALVANOMAGNETIC EFFECTS IN Mn - RICH CuMn AND Ni-RICH NiFeCr ALLOYS* by *Swapan Chakraborty* has been carried out under my supervision and that this work has not been submitted elsewhere for a degree.

Ashok Kumar Majumdar

Professor A. K. Majumdar
Department of Physics
Indian Institute of Technology, Kanpur
India 9/2/98

February, 1998

Synopsis

In recent times, disordered systems have generated great interest due to some fascinating problems emerging from the study of their electrical, galvanomagnetic, and thermal properties. A disordered system, in general, means liquid and amorphous materials, where the atoms are randomly arranged without any crystalline structure. The last few decades have witnessed an explosion of experimental activities on amorphous alloys because of their large technological applications. Some of the important behaviours so far observed are : the Mooij correlation, resistivity minima, resistivity saturation at high temperatures, negative temperature dependence of ordinary Hall coefficient in non-magnetic alloys, etc. It has now been realised that many of these properties cannot be explained in the mould of ordered systems. As a matter of fact, in moderately disordered alloys the conduction electrons are no longer nearly free since the mean free path becomes almost comparable to the interatomic spacing. The value of electrical resistivity is a measure of the disorder in any alloy. Disorder in any material can exist in varying degrees, ranging from a few impurities in an otherwise perfectly crystalline host to the strongly disordered alloys or glassy structures.

Till now, most of the studies in disordered materials involved amorphous alloys where the electrical resistivity is of the order of (100-200) $\mu\Omega$cm. On the other hand, crystalline alloys are usually considered to be more ordered than amorphous alloys. In this work, random substitutional concentrated crystalline alloys are made from transition metals where the high-temperature crystalline phase is preserved by proper quenching. It is to noted that these alloys are as resistive ($\rho \simeq$ (50 - 200) $\mu\Omega$cm) as many amorphous alloys. Hence these crystalline alloys can be considered as another form of disordered systems where some of the behaviours mentioned above are expected to be observed. But ironically, not much attention has been paid till now to these crystalline alloys. The main hurdle lies in the alloy preparation where retaining the isophasic high - temperature crystalline

phase down to low temperatures is found to be rather difficult. The present thesis deals with two such alloy series, γ - $Cu_{100-x}Mn_x$ ($36 \leq x \leq 83$) and γ - $Ni_{100-x-y}Fe_xCr_y$ ($6 \leq x \leq 23$; $2 \leq y \leq 21$).

The present γ-$Cu_{100-x}Mn_x$ (x = 36, 60, 73, 76, and 83) alloys have exotic magnetic structures at low temperatures. According to the magnetic phase diagram, they are cluster glasses for x = 36, 60, and 73 with T_{sg} between 135 and 149 K and are in the mixed cluster-glass and long-range antiferromagnetic phase for x = 76 and 83 with $T_{sg} \approx$ 145 and 45 K, respectively. These substitutionally disordered alloys have resistivities between 93 and 197 $\mu\Omega$cm. Electrical resistivity (1.2 - 40 K) and magnetoresistance till 7.5 T in both longitudinal and transverse orientations are measured in these γ-CuMn alloys. On the other hand, the γ - $Ni_{100-x-y}Fe_xCr_y$ ($6 \leq x \leq 23$; $2 \leq y \leq 21$) alloys are all ferromagnetic. The initial permeability (μ) for these alloy compositions are very high making them useful as transformer core materials, heat resistant steel, etc. However, according to the earlier neutron diffraction and dc-magnetisation studies, the Cr-rich alloys ($\geq$ 18 at.%) are expected to have a spin - glass phase at low temperatures besides the ferromagnetic one at higher temperatures. The electrical resistivity in these alloys are found to be widely varying between 31 and 90 $\mu\Omega$cm. Electrical resistivity, magnetoresistance, ferromagnetic anisotropy of resistivity (FAR) and the Hall effect are studied in these γ-NiFeCr alloys.

The **motivation** behind the present studies is to try to answer some of the following questions :
Does resistivity minimum occur in concentrated γ - CuMn and NiFeCr alloys? If it does, then what are the possible mechanisms responsible for its occurrence?
Is it possible to identify as well as isolate the spin-glass (in CuMn) and ferromagnetic (in NiFeCr) contributions to the electrical resistivity from other contributions? It is rather important to find how different competing physical mechanisms give rise to the resistance minimum. Since magnetoresistance data provide useful information regarding different scattering phenomena, a consistent interpretation of electrical resistivity remains incomplete without it.
Is it possible to find a correlation between the values of the FAR and the earlier observed $R_s = \lambda_s = 0$ line in the ternary composition diagram? This will give useful information regarding their electronic band structure. Moreover, this will tell us whether the split-band model can provide a

satisfactory explanation for such low - FAR alloys and also its applicability in general. Also, why are the values of FAR so small in Cr-rich alloys. Is it possible to interpret the FAR data using the two-current model?

Does the extra-ordinary Hall coefficient ($R_s \propto \rho^n$) exhibit a negative temperature dependence reflecting the resistivity minimum?

Chapter 1 introduces the subject illustrating various properties of ordered and disordered materials and highlighting some of the important anomalous behaviours observed in disordered systems. The theoretical models proposed so far to interpret these anomalies and the motivation behind the present study are also discussed in details.

Chapter 2 begins with a description of the experimental procedures involved in the sample preparation and their characterisation. The design and fabrication of dc - resistivity and Hall effect / magnetoresistance cryostats along with their electrical circuit lay-out are discussed next. The measurement techniques used in the present study are also spelt out in details. Special stress is given to illustrate the techniques adapted for minimising noise in the present measurements.

Chapter 3 contains the electrical resistivity (ρ(T)) study of both γ - CuMn and γ - NiFeCr alloys. The measurements on γ-$Cu_{100-x}Mn_x$ ($36 \leq x \leq 83$) alloys are done in the temperature range $1.2 \leq T \leq 30$ K. The data show resistivity minima at T_{min} lying between 2.5 and 24.5 K. The resistivity well below the minima follows a $\sqrt{T}$ type of behaviour and these has been interpreted in terms of the electron-electron (e-e) interaction effects in the presence of weak localisation. The e-e interaction effects have dominant contributions to the resistivity in the temperature range of 1.2 $K \leq T \leq T_{min}/3$ whereas those from magnetic and phonon scattering are found to be negligible. In the higher temperature range of $T_{min}/3 \leq T \leq 30$ K, besides the e-e interaction effects, magnetic contribution of the type $T^{3/2}$ and phonon contribution given by the standard Bloch - Grüneissen relation have been observed.

On the other hand, in Ni-rich γ - $Ni_{100-x-y}Fe_xCr_y$ ($8 \leq x \leq 17.5$, $8 \leq y \leq 21$) ternary alloys,

the electrical resistivity is measured in the temperature range of $1.2 \leq T \leq 290$ K. The data in all the alloys exhibit distinct minima lying between 7 and 35.5 K. Below the minima, the resistivity is well described by the e-e interaction effects ($\rho \propto \sqrt{T}$), independent of the magnetic state of the alloys. In the temperature range of $T_{min}/3 \leq T \leq 2T_{min}$, besides the e-e interaction effects, magnetic ($\propto T^2$) and phonon ($\propto T^3$) contributions have been distinctly isolated. At higher temperatures (> 100 K), a linear electron - phonon term along with the magnetic term are observed till about 200 K for the low-Cr alloys. But above 200 K, only a linear term is obtained in the low-Cr alloys whereas in the high-Cr ones, it is found right from 100 K onwards. Interestingly, the values of the coefficient of the magnetic term ($\propto T^2$) come out to be of the same order as the theoretical one (10^{-5} $\mu\Omega$cm K^{-2}). Moreover, the residual resistivity of all the alloys, calculated using the two-current model and the Matthiessen's rule, are in reasonable agreement with the experimental values.

Chapter 4 consists of detailed studies of magnetoresistance in both the alloy series and ferromagnetic anisotropy of resistivity for only NiFeCr alloys. Here high - resolution transverse magnetoresistance (TMR) data in γ - $Cu_{100-x}Mn_x$ alloys (x = 36 - 83) are presented till 7.5 T at 4.2, 20.5, and 63 K and longitudinal (LMR) magnetoresistance at 4.2 K. They show positive magnetoresistance till 7.5 T in the Mn-rich ($x \geq 60$) alloys while an overall negative one in the alloy with x=36 at all temperatures. However, the data at 4.2 K in x=36 clearly demonstrate a positive magnetoresistance till 3 T which becomes negative at higher fields. The data for the Mn-rich alloys ($x \geq 60$) at 4.2 and 20.5 K are well described by the electron - electron interaction (EEI) effects along with localisation and normal magnetoresistance. In the two regions of high (4 to 7.5 T) and low (0 to 1 T) fields, distinctly dominant contribution of EEI effects compared to that of localisation has been observed. For x=36, an additional term due to the cluster-glass (CG) phase (= - $\beta_{CG}H^2$) has to be considered in explaining its overall negative magnetoresistance. The contribution of the combined EEI and localisation effects has been separated convincingly from the normal magnetoresistance (C_N) and the cluster-glass (β_{CG}) terms. The temperature dependence of the normal magnetoresistance follows the Kohler's rule while the cluster-glass term shows a behaviour similar to those of the dilute spin glasses. Moreover, the present interpretation of magnetoresistance is found to be very much consistent with that of the electrical resistivity (ρ(T)).

On the contrary, high-resolution magnetoresistance data ($\Delta\rho/\rho$) in both longitudinal (LMR) and transverse (TMR) orientations in some fifteen different compositions of Ni-rich γ - $Ni_{100-x-y}Fe_xCr_y$ ($6 \leq x \leq 23$; $2 \leq y \leq 21$) alloys are presented at 4.2 K in magnetic inductions till 1.4 T. In the low Cr-content alloys ($y \leq 18$), the LMR is found to be positive while the TMR is negative. However, beyond technical saturation, the slope of both LMR and TMR data are found to be positive. This low-field anisotropy in the magnetoresistance arises from the inherent spin - orbit interaction present in a ferromagnet. Both the LMR and TMR data till 1.4 T (beyond technical saturation) have shown an H^2 dependence which is attributed to the dominant presence of the EEI effects in the low - field limit. The contribution of the normal magnetoresistance to the present data is estimated to be negligibly small. In the high Cr-content alloys ($y \geq 18$) both the LMR and the TMR are found to be negative and nearly isotropic which is ascribed to the dominant SG/CG term.

The ferromagnetic anisotropy of resistivity (FAR) for the present $Ni_{100-x-y}Fe_xCr_y$ ($6 \leq x \leq 23$; $2 \leq y \leq 21$) alloys are evaluated from the LMR and the TMR data. The FAR values in the present alloys are found to be very small. A maximum value of 0.76 % is found in the alloy $Ni_{77}Fe_{21}Cr_2$ with 2 at.% of Cr. But as the Cr content increases, the FAR decreases drastically and becomes almost zero for the alloys with more than 18 at.% Cr. These results are discussed in terms of the split-band (SB) as well as the two-current conduction (TCC) model. In addition, Hall resistivity (ρ_H) for alloys of composition $Ni_{75}Fe_{13}Cr_{12}$, $Ni_{70}Fe_{12}Cr_{18}$, $Ni_{73.5}Fe_8Cr_{18.5}$, $Ni_{72}Fe_8Cr_{20}$, and $Ni_{71}Fe_8Cr_{21}$ is measured till 1.4 T at 4.2 K only. The experimental extra-ordinary Hall conductivity, γ_{HS}=0 line in the ternary phase diagram (using the present data and the earlier reported values) exhibits a pronounced curvature in the Cr-rich ($\simeq$ 20 at.%) region, contrary to the straight line, predicted by the SB model. But the most important observation is that the ridges of the constant FAR lines are found to follow exactly the experimental γ_{HS}=0 line. All these are in good agreement with the idea behind the SB model. However, the above consistent behaviour of the experimental γ_{HS}=0 line and the line joining the ridges of the constant FAR lines in the ternary phase diagram is found to lie far away from where they are theoretically expected. This is quite puzzling. One of the reasons for such a discrepancy is attributed to the composition dependence of Z_{eff} which was taken as a

constant in the SB model. Another possible reason is the uncertainty of the complete band splitting of Cr from Ni and Fe bands. Intensive theoretical as well as experimental investigations are needed to resolve it. In addition, such small values of FAR in the present alloys are ascribed to the large energy difference between the spin-up bands for Cr and Ni as shown by the CPA calculations. The decrease in the FAR with Cr can also be interpreted using the two-current conduction model as the alloys move towards weak-itinerant ferromagnetism with increasing Cr, in excellent agreement with the earlier dc-magnetisation data. This is probably the only work where detailed description of such small FAR's in high Cr-content alloys are presented.

In **Chapter 5**, high - resolution data for the temperature dependence of the Hall resistivity (ρ_H) are presented in magnetic inductions till 1.4 T and temperatures down to 1.4 K. The samples are ferromagnetic Ni-rich γ-$Ni_{75}Fe_{13}Cr_{12}$ (S29), $Ni_{70}Fe_{12}Cr_{18}$ (S48), and $Ni_{73.5}Fe_8Cr_{18.5}$ (S41) alloys where ρ_H beyond saturation exhibits a decrease with increasing temperature. The values of the ordinary (R_0) and the extra-ordinary (R_s) Hall coefficients are found to be positive in alloys S48 and S41 whereas they are negative in S29. Electrical resistivity (ρ(T)) study in these alloys has shown resistivity minima (at T_{min}) which are described by the electron - electron interaction effects. The extra-ordinary Hall coefficient (EHC) comes out to be two orders of magnitude greater than the ordinary Hall coefficient (OHC). This large extra-ordinary contribution can be attributed to the side-jump effect ($R_s \propto \rho^2$). R_0 is found to be almost temperature independent in all the alloys. On the other hand, R_s(T), irrespective of its sign, has shown a decrease with increasing temperature with a minimum around T_{min}. The temperature dependence of the positive EHC in alloys S41 and S48 is consistent with the minima observed in ρ(T). On the other hand, the negative EHC in alloy S29 behaves exactly opposite to that theoretically expected. Instead of getting more negative, it becomes more positive below as well as above T_{min}. This is found to be rather puzzling and, in no way, can be interpreted by current theories. Nevertheless, this is the only study where such a strong negative temperature dependence of EHC has been observed in any concentrated crystalline ferromagnetic system.

Finally, **Chapter 6** concludes the thesis by summarising some of the important observations and spelling out the scope of future work.

Acknowledgments

It is a great pleasure for me to express my deep sense of gratitude to Prof. A.K. Majumdar for his sincere and constant guidance throughout the present work. I specially remember those days when I was struggling with my experiments; the inspiration and the confidence he had given me was indispensable at that crucial juncture. Perhaps it would not have been possible for me to bring the present work to a logical conclusion without his active support and encouragement. His attitude towards experimental research and foresight are really amazing. Besides an acknowledged good teacher and expert, I find him very approachable, communicative, and always willing to help in all aspects of life.

I am indebted to Prof. K. Shahi and Prof. V.N. Kulkarni for the valuable suggestions and advice they gave me from time to time. I also acknowledge Drs. K.P. Rajeev and C.V. Tomy for their help and co-operation at various stages of my work. My sincere thanks go to Profs. D. Chowdhury, R.C. Budhani, and V. Ravi Shankar, who gave me the necessary morale booster for carrying out experimental research.

This is, in fact, a very good opportunity to recollect my sweet memories of my seniors and colleagues with whom I have shared the work and the laboratory. I am grateful to my seniors Drs. Alok Banerjee, Amitabh Das, Rita Singhal, and S.V. Sharma for their training, advice, and help at the initial stages of my work. Especially, I am indebted to Drs. A.K. Gangyopadhyay and Alok Banerjee for providing samples for the present work. I am grateful to my labmates Gautam Sinha, Dr. T. K. Nath, N. Sudhakar, Dr. G.D. Mukherjee, and A. Tewari for their help and cooperation. I always find them beside me whenever there is any need.

My heartful thanks to M/S D.C. Banerjee, Ram Ashray, and Ram Prakash Pal for their immense support and help during the course of my experiments. The timely cooperation that I received from the staff members of the Physics Workshop, the Liquid Nitrogen Plant, the Glass Blowing Workshop, and the Physics Office, is beyond comparison. I gratefully acknowledge all of them.

During my stay in IIT / Kanpur, I had come across several friends whose company will be remembered forever. Among them, I should mention Mr. and Mrs. Shankar, Shudhansu, Wasan, Giri, Rajan, Anil, Tapo, Ani, Deba, Kishore, Saurabh, Prabal, Patnaik, Sunu, Atanu, Joydeep, Prem, Biswarup, Khan, Dada, Bogada, Pandeyji, Johri, Himanshu and many others for their close to heart relation with me.

I would also like to acknowledge our core group comprising of Sujay, Shanti, Alok, GK, Behera, Dipak, Abir, and Rahul. I have always found them in unison whenever there is a decision of going to a trip or a picnic or even to a movie. Their lively association with me will remain in my heart forever.

During initial stage of my stay, I have always enjoyed to be associated with the "BODHI GRANTHAGAR" and its various cultural programmes. But its fateful closing was one of the most tearful events of my stay in the campus.

I would like to thank Mrs. S. Majumdar for extending warm hospitality during my stay in the campus. In this regard, I would also like to acknowledge the members of the family of Mr. D.C. Banerjee and Prof. D. Chowdhury. All of them made my stay in IIT, Kanpur very pleasant and memorable.

At last, it is very difficult for me to express in a few words my deep feelings towards my family and their sacrifice fulfilling my needs. I must express my deep sense of gratitude to my parents and brother for their whole hearted love, support, and encouragement which always inspired me to achieve my goals in life. Also the affection and the inspiration that I receive from the other

members, relatives, and friends, always gives me a morale boost to overcome all odds in all fro
of life. Finally, I would like to express my deep appreciation for Suni, with whom I decided
share my life, for her whole hearted cooperation and tremendous moral support which has help
me to become a member of this elite society.

Swapan Chakrabor

Dedicated
to
my parents

Contents

List of Tables

List of Figures

Chapter 1

Introduction

1.1 Preamble

Condensed matter physics in recent times has been tackling fascinating problems connected with magnetic, galvanomagnetic, electrical, and thermal properties of different materials, especially in the disordered state. Earlier, a disordered system, in general, meant liquid and amorphous materials[1], where atoms are randomly arranged without any crystalline structure. In the last few decades, lot of attention has been paid on amorphous alloys because of their large technological applications which, as a result, has led to an explosion of experimental activities. Interestingly, it has been observed that addition of transition metals can enhance both structural and chemical disorder in amorphous alloys. This, in turn, reveals some interesting anomalous behaviours[2]. The understanding of these properties has been found rather difficult and controversial with the existing free-electron model[3, 4]. It is important to note here that the value of electrical resistivity ($\rho(T) \simeq 0$) is generally considered as a measure of disorder in any alloy[4]. Most of these anomalies reported so far are in electrical transport, galvanomagnetic, and thermal properties. Some of them are listed below.

1. The temperature coefficient of resistivity (TCR) is found to be positive in alloys with $\rho_0 < 150$ $\mu\Omega$cm while it is negative for alloys with $\rho_0 > 150$ $\mu\Omega$cm. This is better known as the Mooij correlation[5]. In addition, values of the TCR are found to be very small compared to that of crystalline metals[2, 3].

2. At low temperatures, the alloys with positive TCR often exhibit an increase in resistivity with decreasing temperature, giving rise to resistivity minima[2, 3].

3. At high temperatures, the alloys with positive TCR show resistivity saturation[6–8].

4. Breakdown of the Matthiessen's rule[9, 10].

5. The ordinary Hall coefficients (R_0) in metals and alloys (where majority charge carriers are electrons) are usually temperature independent and negative[11]. But in amorphous alloys, R_0 is often found to be positive[12–16]. Interestingly, very recently R_0 has also exhibited a negative temperature dependence in non-magnetic amorphous alloys[2].

It has been realised now that many of these anomalies[3, 4] cannot be explained by forcing these systems into the mould of the ordered systems. Here conduction electrons are not so free as it is expected in the free electron model. The mean free path of the conduction electrons may be as large as the interatomic spacing in these disordered alloys. As a result, the Boltzmann transport equations do not hold. In fact, disorder in any material can exist in varying degrees, ranging from a few impurities in an otherwise perfect crystalline host to the strongly disordered limit of alloys or glassy structures.

Crystalline alloys are in general considered to be comparatively more ordered than amorphous alloys. Recently, random substitutional concentrated crystalline alloys are made from transition metals where the high-temperature crystalline phase is preserved at low temperatures by rapid quenching. It is important to note that these alloys are quite resistive with $\rho \simeq (70 - 200)\ \mu\Omega$cm, which is of the same order as that of some amorphous alloys. Hence these crystalline alloys can also be considered as another form of disordered system, but now with chemical disorder, where all the above anomalies are expected to be observed. But ironically, not much attention has been paid till now to these crystalline alloys. In this thesis, the prime intention is to study electrical resistivity, magnetoresistance, ferromagnetic anisotropy of resistivity, and Hall effect in such systems of crystalline alloys.

1.2 Brief Review

1.2.1 Magnetism in ordered and disordered materials

Instead of going directly to electron transport and galvanomagntic properties, here we have presented a brief review of magnetic properties of ordered and disordered materials.

Magnetism is always considered as a fundamental property of any solid. New sophisticated and precise experimental techniques (e.g. SQUID, neutron diffraction, ac - susceptibility, nuclear magnetic resonance, etc.) have led to the recognition of a wide variety of magnetic ordering in different materials. The most commonly known among them are ferromagnetism, paramagnetism, diamagnetism, ferrimagnetism, and antiferromagnetism[17–19]. Except the closed shell diamagnetism, all other magnetic properties can be understood classically by the molecular field theories. To describe the origin of the molecular field theory, several magnetic - exchange interactions are proposed for different kinds of magnetic materials. Important among them are: *(1) direct exchange* ($H_{ij} = -\sum_{ij} J_{ij} S_i \cdot S_j$, where i and j represent the spins at different lattice sites; J_{ij} is positive for ferromagnets and negative for ferri and antiferromagnets), *(2) superexchange* (for magnetic oxides and semiconducting materials), *(3) indirect exchange interaction* (for spin and cluster glasses), *(4) hyperfine interaction* (to describe the Mössbauer effect, nuclear magnetic resonance and nuclear specific heat, etc.), etc.. The most fascinating one is the indirect exchange (RKKY) interaction which can be written as

$$J(r) = -\frac{J_0 cos(2k_F r)}{(2k_F r)^3}, \tag{1.1}$$

where k_F is the Fermi wave vector. This interaction, J(r), is oscillatory in nature, i.e., it becomes positive and negative depending on the separation between the spins / moments. However, the strength of J(r) reduces with inverse cube of the distance between spins.

Kondo regime

The disorder in any material could be varied widely by changing impurity concentration. It was discovered long back that, by adding a few parts per million (ppm) of magnetic impurities ($\leq$ 100

ppm) in noble metal hosts, one can get the so - called **Kondo regime**. Here magnetic impurities are completely isolated from each other and, as a result, there are no direct interactions among them. Even the RKKY interaction is negligibly small due to their large separation ($J(r) \propto 1/r^3$). Above some characteristic temperature, known as the Kondo temperature (T_K), these alloys behave like paramagnets. The important features of the Kondo alloys below T_K are: **(1)** The susceptibility falls below its paramagnetic value at Curie temperature, i.e., there is a loss of moment as the conduction electrons begin to form a surrounding cloud of oppositely (antiferromagnetically) polarized spin and **(2)** the electrical resistivity shows a logarithmic[20] upturn (i.e., minimum) at low temperatures. The value of resistivity in these dilute alloys is of the order of a few $\mu\Omega$cm. However, the Kondo effect disappears when the impurity concentration is increased.

Spin glass

Addition of a few atomic percent of magnetic impurity ($\simeq$ (1 - 10) at.%) in non - magnetic / noble metal hosts can give rise to a new magnetic state where isolated impurity spins / moments are randomly distributed without any long-range magnetic ordering. Below some characteristic temperature, known as the spin-freezing temperature (T_f), these spins are found to be frozen or locked in random orientations and hence it is called a **spin - glass** (SG) state. The interaction between the spins is of RKKY type (Eq.(1.1)) and thus the coupling (J(r)) between them can be either ferromagnetic or antiferromagnetic depending on their separation. The direct interaction, however, is negligibly small. Thus, randomness invokes a competition between the impurity spins/moments as to how they should order themselves. In fact, several arrangements of connecting them are possible in forming different sets of spin - disordered states with equivalent energy. This is called "frustration"[21]. Randomness and frustration are two most basic prerequisites for the formation of a spin - glass phase. Some of the most exciting experimental features of spin glasses are sharp peaks in ac-susceptibility[22–24] at T_f, hysteresis and remanence in dc-magnetisation below T_f[25–27], time-decay of remanent magnetisation[28], rounded - peak in Hall resistivity near T_f[29, 30], knee in molar heat capacity at T_f[31], etc. Good reviews on various experimental observations can be found elsewhere[22, 32–34].

There was an explosion of theoretical activities to explain the behaviour of the spin - glass state. The scaling theory[35], based on RKKY interaction, was proposed first where magnetisation, saturation remanence and molar specific heat are described by universal functions of reduced variables H/C and T/C (where C is the impurity concentration). However, at higher concentration (> 1 at. %), the scaling theory breaks down due to the enhanced short-range direct interaction. Later, Edwards and Anderson[36] suggested an elegant approach where the cusp in ac-susceptibility is shown as a manifestation of a magnetic phase transition due to sudden random freezing of spins at T_f. To describe the phase transition, an order parameter q was defined as

$$q = \langle S_i(0) \cdot S_i(t) \rangle. \tag{1.2}$$

Here a spin is initially (at t=0) observed with a value of $S_i(0)$. After a long time t ($t \rightarrow \infty$), there is a non-vanishing probability that the same spin $S_i(t)$ will lie in the same direction resulting in $q \neq 0$. As the temperature approaches zero, $q \rightarrow 1$. But above T_f, the order parameter becomes zero. The magnetic state of a spin glass is quite different from those of conventional para and ferromagnets. A comparison between the order parameter q and the magnetisation m ($\langle S_z \rangle$) in them are given below.

	Net moment	**Order parameter**
Spin glass	m=0	$q \neq 0$
Paramagnet	m=0	q=0
Ferromagnet	$m \neq 0$	$q \neq 0$

Sherrington and Kirkpatrick (SK)[37] have extended the Edward - Anderson model to real systems using a mean - field theory. Later, de Almeida and Thouless[38] have pointed out some instability in the SK solution at low temperatures and in both spin - glass and ferromagnetic phases. They have proposed a phase diagram illustrating the stability limits of the SK solution (known as AT line). Till today, several theories on different approaches have been proposed, such as the Thouless - Anderson - Palmer (TAP) solvable model[39], replica-symmetry-breaking (RSB) scheme, droplet model[40], fractal-cluster model[41], etc.. But all these theories suffer from one drawback or the

other.

Cluster glass

As the impurity concentration increases (> 10 at.%), the probability for impurities to come close to each other is greatly enhanced (described in Fig.1.1). As a result, each impurity will have another as a first or second - nearest neighbour. Hence, there will be a direct magnetic exchange and, as a result, short - range magnetic clusters form. Intra-cluster interaction might be ferro- as well as antiferromagnetic depending on the nature of the impurity and the neighbouring position. As for example, intra-cluster interaction in $Au_{100-x}Fe_x$ ($16 \leq x \leq 24$) is ferromagnetic[42] while it is antiferromagnetic[43] in $Cu_{100-x}Mn_x$ ($72 \leq x \leq 84$). However, the inter - cluster interaction will be of RKKY type. Hence, cluster moments are randomised in the long range. In cluster glass, values of magnetisation and saturation remanence are enhanced compared to those in dilute spin - glass alloys. The value of electrical resistivity also increases. Soukoulis and Levin[44, 45] have proposed a model for cluster glass using mean field theory. This theory is found to be fairly successful in interpreting the experimental observations of sharp peak in ac-susceptibility and rounded maximum in specific heat.

Percolation limit

Further increase in concentration will lead to a situation where each magnetic impurity will have at least one nearest neighbour. Above some particular concentration, impurities will appear as an uninterrupted long chain spread over the whole sample and then the alloy is said to have reached the percolation limit. In this concentration regime, interactions between impurities are still mixed in character, i.e., a combination of RKKY as well as direct exchange interactions. Here magnetic clusters are coupled without any long-range order. The main controversy in the percolation limit is that frustration is completely neglected here.

Re-entrant spin glass / Mixed phase

At the percolation boundary, a strange magnetic behaviour emerges where both long-range and spin - glass orderings coexist. This is known as a re-entrant spin glass (RSG) or mixed phase (M)

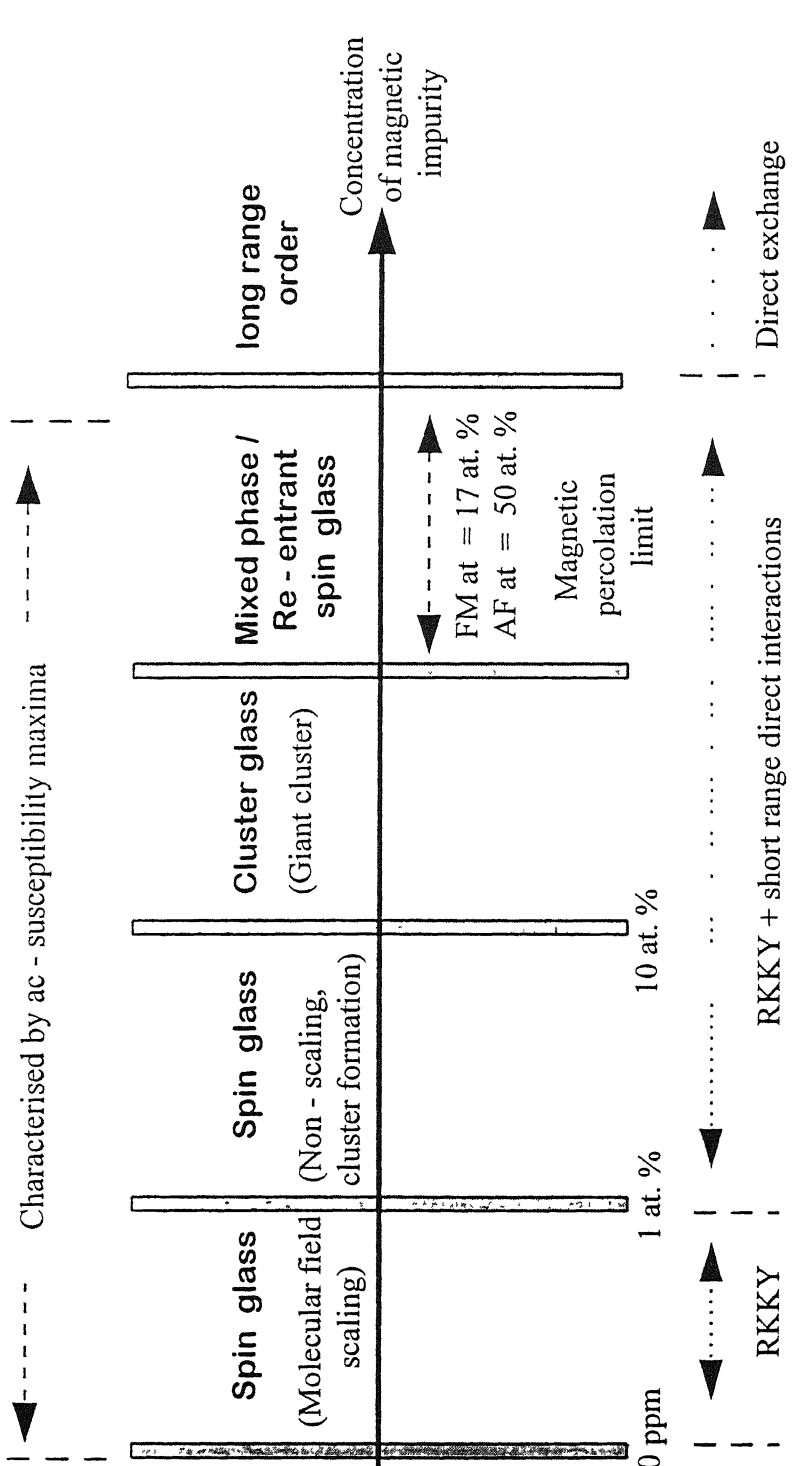

Figure 1.1 : Magnetic behaviours of various impurity concentration regimes.
Here FM = ferromagnetic and AF = antiferromagnetic.

(see Fig.1.1). This is puzzling in the sense that, as temperature is reduced, a disordered state arises from a comparatively more ordered state. In other words, a long-range magnetic order breaks up into a large number of randomly frozen clusters at low temperatures. Experimentally, it has been found that a paramagnet (P), on lowering of temperature, becomes a ferromagnet (FM) or an antiferromagnet (AF) below T_c (Curie temperature) or T_N (Neel temperature), respectively, and on further cooling, it re-enters a frozen state below T_f, e.g., in $Au_{100-x}Fe_x$ ($16 \leq x \leq 24$)[42] as P $\rightarrow$ FM $\rightarrow$ RSG (SG + FM) whereas in $Cu_{100-x}Mn_x$ ($70 \leq x \leq 85$)[43, 46] as P $\rightarrow$ AF $\rightarrow$ M (CG + AFM). In this regime, long-range magnetic ordering is inhomogeneous compared to that in pure ferro- or antiferromagnets.

Sherrington and Kirkpatric[37] had first shown theoretically, using mean - field theory and Ising model, that ferromagnetic and spin - glass phases can coexist. Later Gabay and Toulouse[47] suggested a dynamical "non-Ising spin glass" approach which is found to be more effective in describing this mixed phase. According to this model, in the presence of an applied magnetic field, the randomly oriented spins will split into two components. One is longitudinal (along the field direction) and the other is transverse (perpendicular to the field direction). At T_c, the longitudinal component becomes ordered while the transverse component freezes at much lower temperatures (below T_f) because of inhomogeneous local moments giving rise to the mixed phase. The proposed phase diagram by Gabay and Toulouse has shown convincingly the existence of a paramagnetic, a ferromagnetic, and a spin - glass along with the mixed phase. Mixed phase or re-entrant spin glass is usually found in concentrated crystalline as well as in amorphous alloys. Some of the examples are $Au_{100-x}Fe_x$[42], $Cu_{100-x}Mn_x$[43], $Fe_{80-x}Ni_xCr_{20}$[48], $Ni_{80-x}Fe_xCr_{20}$[49], $Ni_{100-x}Mn_x$[50], $(Fe_xNi_{100-x})_{80}$ $P_{14}B_6$[51], $(Fe_xNi_{100-x})_{79}$ Si_9B_6[52], etc.. Recently, in magnetic semiconductors (Hg_{100-x} Mn_xTe, Cd_{100-x} Mn_xTe, etc.), mixed phase and / or cluster - glass kind of behaviour (AF $\rightarrow$ CG) has been observed below the percolation limit.

Magnetism in concentrated alloys

Most of the concentrated transition metal alloys (crystalline as well as amorphous) studied so far are Fe, Ni, or Co - based. Hence, almost all of them have long - range ferromagnetic order.

However, the magnetic behaviours of both crystalline and amorphous alloys are found to be broadly of similar kind. The magnetisation below T_c of these alloys is generally described by two well - known mechanisms which are: (1) Generation of spin waves in the localised model and (2) Stoner excitation in itinerant electron model. According to the spin-wave theory[53], specific magnetisation σ(H,T) (emu/gm) well below T_c can be written as

$$\frac{\Delta\sigma(H,T)}{\sigma(0,0)} = \frac{\sigma(H,T) - \sigma(0,0)}{\sigma(0,0)} = AT^{3/2} + BT^{5/2}. \tag{1.3}$$

Here the first term ($T^{3/2}$) arises from the harmonic term of the spin-wave dispersion relation and the second term ($T^{5/2}$) represents the anharmonic contribution. On the other hand, Stoner[54] had put forward the idea of itinerant electron ferromagnetism in 3d metals and alloys where the 3d bands are split into spin-up and spin-down subbands due to large exchange energy. The electrons, thus, becomes itinerant in the sense that as temperature increases, they move from one subband to the other. This idea was later modified by Thompson et al.[55] by classifying the itinerant ferromagnetism into two categories : (1) strong and (2) weak. In a strong ferromagnet, one subband (i.e., spin-up) is completely full while in a weak ferromagnet both the spin-up and the spin-down subbands are partially filled. The relative change of specific magnetisation due to Stoner excitations is given by

$$\frac{\Delta\sigma(T)}{\sigma(0)} = AT^{3/2}e^{-E/k_BT} \qquad \text{(strong ferromagnets)} \tag{1.4}$$

$$= BT^2. \qquad \text{(weak ferromagnets)} \tag{1.5}$$

Typical examples of a strong ferromagnet is Ni and NiFe, while Fe and FeCr are weak ferromagnets. Later Wohlfarth and co-workers[56–59] have enriched the itinerant model by proposing some useful criteria, such as Rhodes-Wohlfarth ratio, etc..

1.2.2 Electrical resistivity

From the very beginning of condensed matter studies, electrical resistivity ($\rho(T)$) is found to be one of the most important and extensively studied phenomena which provides many useful information regarding the electronic band structure as well as the interaction of conduction electrons with different scattering centres. In recent times, $\rho(T)$ in disordered alloys have attracted a lot of attention

due to some of their anomalous behaviours. It is well known that electrical resistivity comes from random incoherent scattering of conduction electrons and, as a result, it is a measure of disorder in a given material. In a perfect periodic crystalline metal (i.e., without defects), electron waves can propagate without any attenuation and the resistivity arises from scattering by boundaries only. But in reality there are always some defects and impurities, however small they might be. This gives rise to the residual resistivity (ρ_0) measured at T=0. Addition of impurities, thermal disorder at finite temperatures, and application of a magnetic field can enhance the electrical resistivity. The band structure in transition 3d metals is more complex than in simple non-transition metals. In 3d transition metals and alloys, the 3d bands are much narrower in energy than the s and the p bands, and as a result, the density of state of 3d electrons is much higher than those of the s and p electrons. Hence the conduction electrons will have much higher velocity than the d electrons. In other words, the comparatively static d electrons act as additional source of scattering for the conduction electrons and hence resistivity anomalies appear. Thus, the interpretation of electrical resistivity in 3d metals and alloys is found to be rather difficult and controversial.

Phonon contribution

In simple metals and alloys, one of the major contributions to resistivity comes from the scattering of conduction electrons by lattice vibrations (i.e., phonons). Long back, a single-band phonon scattering using the Bloch theory[60] was proposed where ρ_{phonon} is given by

$$\rho_{phonon}(T) = A\left(\frac{T}{\theta_D}\right)^5 \int_0^{\theta_D/T} \frac{z^5 dz}{(e^z-1)(1-e^{-z})}, \tag{1.6}$$

where A is a constant and θ_D is the Debye temperature. This is known as the Bloch - Grüneissen relation which, on simplification, gives

$$\rho_{phonon}(T) = BT^5 \qquad T << \theta_D \tag{1.7}$$

$$= CT \qquad T >> \theta_D. \tag{1.8}$$

In transition metals and alloys, Mott[61] had first proposed that s-d transition has to be incorporated in the electron - phonon scattering. Later Wilson[62] had included s-d transition in calculating the phonon contribution for 3d metals and their alloys. This is known as the Bloch-Wilson relation

which is written as

$$\rho_{phonon}(T) = A\left(\frac{T}{\theta_D}\right)^3 \int_0^{\theta_D/T} \frac{z^3 dz}{(e^z-1)(1-e^{-z})}. \quad (1.9)$$

On simplifying the above relation (Eq.(1.9)), one gets

$$\rho_{phonon}(T) = BT^3 \quad T << \theta_D \quad (1.10)$$

$$= CT \quad T >> \theta_D. \quad (1.11)$$

Ferromagnetic contribution

In ferromagnetic 3d metals and alloys, a magnetic contribution to resistivity arises mainly from scattering of conduction electrons by 3d moments. According to the spin-wave theory, the resistivity much below T_c goes as ω^2 (where $\hbar\omega = k_B T$) and hence $\rho \propto T^2$. Baber[63] had shown that the resistivity at very low temperatures, using the itinerant electron theory, also behaves in a similar manner ($\propto T^2$). Later, Kasuya[64] and Mannari[65] modified the ferromagnetic contribution by considering the s-d transition which is given by

$$\rho_{mag}(T) = \frac{\pi^2 V m G^2 (g-1)^2 J}{8 N e^2 \hbar E_F}\left(\frac{k_B T}{k_F^2 \Re}\right)^2, \quad (1.12)$$

where G represents the strength of the s-d interaction, J is the total angular momentum quantum number, g the Lande - g - factor, $\Re$ is a constant coming from spin - wave dispersion relation, and $E_F = \hbar^2 k_F^2/2m$, the Fermi energy of the conduction electrons. Here V and N are the volume and the number of atoms, respectively in the crystal. Later, in an extensive study, Goodings[66] had shown that the coefficient of T^2 in Eq.(1.12) bears the most important information regarding s-s and s-d scattering and theoretically it's value should be of the order of 1×10^{-11} $\Omega cm T^{-2}$ for Fe and Ni-based alloys. On the other hand, in amorphous ferromagnetic materials, a $T^{3/2}$ term comes from incoherent momentum nonconserving s-d scattering[67]. It is important to note that the $T^{3/2}$ term vanishes for crystalline ferromagnets.

Spin / Cluster - glass contribution

In a very dilute spin glass, Laborde and Radhakrishna[68] had first shown that the resistivity goes

as T^2 at very low temperatures (T < 1 K). Later, Rivier and Adkins[69, 70] proposed a model to describe resistivity of spin glasses above 1 K, but much below their T_f. The idea behind this model is that the conduction electrons are scattered by long - wavelength spin excitations. For pure spin diffusive modes, which is also one of the prime criteria for a spin glass, the spin/cluster glass contribution to the resistivity is found to be

$$\rho(T) = A[1 - D/(1 + CDT^{3/2})], \tag{1.13}$$

where A and C depend on impurity concentration while D represents the temperature independent non-magnetic scattering. At low temperatures ($T << T_f$), Eq.(1.13) reduces to $\rho(T) \propto T^{3/2}$, which is confirmed experimentally[71]. This model is also very successful in describing the high - temperature ($T \simeq T_f$) inflexion points beyond which the resistivity flattens out as in dilute AuCr, AuMn, AgMn, and CuMn alloys[71, 72].

Later, Fisher[73] suggested that the resistivity in spin/cluster glass can arise from two main scattering centres: (1) static disorder of the impurity spins and (2) spin excitations. According to his theory, the resistivity goes as

$$\rho(T) = \rho_{el} + \rho_{inel}, \tag{1.14}$$

where ρ_{el}, the elastic contribution, is proportional to some spin-glass order parameter q, which has a very small temperature dependence. On the other hand, the inelastic part, ρ_{inel}, is responsible for the spin-diffusive contribution to resistivity which is written as

$$\rho_{inel}(T) = BT^2 - CT^{5/2}. \tag{1.15}$$

Here both B, C > 0 and hence the total resistivity ρ(T) in Eq.(1.14) will have the temperature dependence as that of Eq.(1.15). It is also suggested that a $T^{3/2}$ term, similar to that in Eq.(1.13), can arise only when the intra-cluster interaction is ferromagnetic. In addition, this theory is claimed to be reliable for concentrated alloys and valid at comparatively much higher temperatures than those in the work of Rivier and Adkins[70], and Laborde and Radhakrishna[68]. Experimentally,

this has been found to be valid in concentrated CuMn alloys[43].

Amorphous alloys

The non-transition metal amorphous alloys are the simplest of amorphous materials. The Ziman model[74] based on free electron theory has been widely accepted as a proper description of the electrical resistivity of simple liquid and amorphous alloys. The expression for ρ is given[1, 2] by

$$\rho = \frac{3\pi e^2 \Omega}{\hbar m v_F N} \int_0^1 |V(q)|^2 S(q) 4(q/2k_F)^3 d(q/2k_F), \tag{1.16}$$

where S(q) is the structure factor, V(q) the pseudo potential, N/Ω the number of atoms per unit volume, and v_F is the Fermi velocity. Good reviews on this work can be found elsewhere[1, 2]. Later, the above model is extended to amorphous 3d transition metal alloys[2, 75] to describe the anomalous behaviour of their ρ(T) which is given by

$$\rho = \frac{30\pi^2\hbar^3}{me^2 E_F k_F \Omega} \Gamma N_d(E_F) S(2k_F), \tag{1.17}$$

where Γ is a parameter related to the virtual bound state and N_d (E_F) is the d-density of states. The temperature dependence of the structural factor S(k_F) goes as

$$S(k_F) = \int_{-\infty}^{+\infty} S(q,\omega) z (e^z - 1)^{-1} d\omega, \tag{1.18}$$

where $z=\hbar\omega/k_B T$. At very low temperatures ($T<<\theta_D$), the structure factor goes as T^2 and at high temperatures ($T>>\theta_D$) as T[76]. Later, with the introduction of a new idea of "phonon ineffectiveness"[77, 78], the low temperature T^2 dependence is found as a manifestation of phonon scattering in the disordered state. This is not limited to amorphous alloys only, but it is a feature of disordered alloys.

Resistivity minima

Kondo effect

In recent times, the low temperature resistivity minima in disordered alloys have attracted a lot of attention. As it has been discussed earlier, the decrease in resistivity with increasing temperature

was found long back in very dilute alloys and was interpreted in terms of the Kondo effect[20, 60] which gives $\rho(T) = \rho_0$ - m ln(T). The reason for such minima is ascribed to the localised magnetic impurities which are far apart and interact indirectly with each other by polarising the conduction electrons. Later, Rivier and Zuckermann[79] showed that spin-fluctuations in dilute alloys can explain the resistivity at very low temperatures (below Kondo minima) giving

$$\rho(T) = \rho_0(1 - (T/T_K)^2), \tag{1.19}$$

where T_K is the Kondo temperature. Some of the salient features[20] of the Kondo effect are: (1) usually the minima are expected in very low-resistive alloys, (2) the depth of minima and T_{min} depend on the impurity concentration as well as the magnetic state of the alloys, and (3) the last but not the least is that the Kondo minima disappear with the application of a magnetic field. In many amorphous alloys, similar type of low-temperature resistivity minima are observed. Initially, they were described by the Kondo effect[80, 81]. But these amorphous alloys are highly resistive and, moreover, the minima are found in some non-magnetic alloys where the constituents are not at all magnetic. Above all, the minima do not vanish even in magnetic fields as high as 4 tesla. This strongly contradicts the predictions of Kondo effect. Hence it is concluded that the Kondo effect is not responsible for such minima in amorphous alloys.

Two-level tunnelling states

Later, to interpret the resistivity minima in amorphous alloy, Cochrane et al.[82] and Tsuei[83] proposed a two-level tunnelling model following the idea of Anderson et al.[84] and Phillips[85]. The amorphous alloys, in fact, form metastable (glassy) states and, hence, there must be many local atomic configurations of equivalent energy, which are inaccessible. In other words, in terms of position coordinate, the energy (E(x)) of these atomic configurations can be represented by a double potential - well separated by a barrier. As temperature increases, these atoms can tunnel from one well to another of roughly equivalent energy to retain thermal equilibrium. In disordered metallic alloys, scattering of conduction electrons by the two - level states leads to a negative temperature dependence of resistivity which is quite analogous to that of the Kondo effect[82] and is given by

$$\rho \propto -ln(T^2 + \Delta^2), \tag{1.20}$$

where Δ is the energy splitting parameter. Experimentally, this was found successful in interpreting the resistivity minima and low - temperature resistivity saturation in some amorphous alloys[86]. However, Black and Gyorfy[87] had pointed out some important anomalies in the concept of the equivalent spin label of coupled electrons. Later, in another report, Black et al.[88] showed that the contribution arising from the two-level tunnelling model is very small and hence it is very unlikely to be observed in the ρ(T) data.

Quantum interference effects

Most of the above theories suffer from one flaw or the other in explaining the resistivity minima in amorphous alloys. All these theories are more or less based on the free - electron model. Two most important criteria for Boltzmann transport to hold are: (1) $k_F l >> 1$, where $k_F = 2\pi/\lambda_F$ is the Fermi wavevector and l is the mean free path of electrons and (2) multiple scattering is neglected. In disordered alloys ($\rho \simeq 150\ \mu\Omega$cm), one can easily find using Drude's formula ($\rho = m/ne^2\tau$) that the mean free path of the conduction electrons is of the order of interatomic diatance, a ($l \simeq a$). As a result, the interacting electrons in these alloys do not follow classical Boltzmann trajectory. Now they are better considered as diffusing from site to site with multiple elastic scattering[89]. This leads to a phase-coherence in the electron partial waves which, in turn, enhances the probability for an electron to return to its origin (see Fig.1.2). The electrons thus get localised resulting in a higher resistivity. Any inelastic process like electron - magnon, electron - phonon scattering or electron - electron interaction or application of a magnetic field can destroy the phase coherence and hence reduces the resistivity of these alloys. The correction to conductivity due to the quantum interference effects for three-dimensional systems is given by[90, 91]

$$\Delta\sigma \propto \sqrt{T} \qquad T \geq \theta_D \tag{1.21}$$

$$\propto T \qquad T \leq \theta_D. \tag{1.22}$$

Electron - electron interaction effects

It is to be noted that interaction between localised electrons is not taken into account in the above

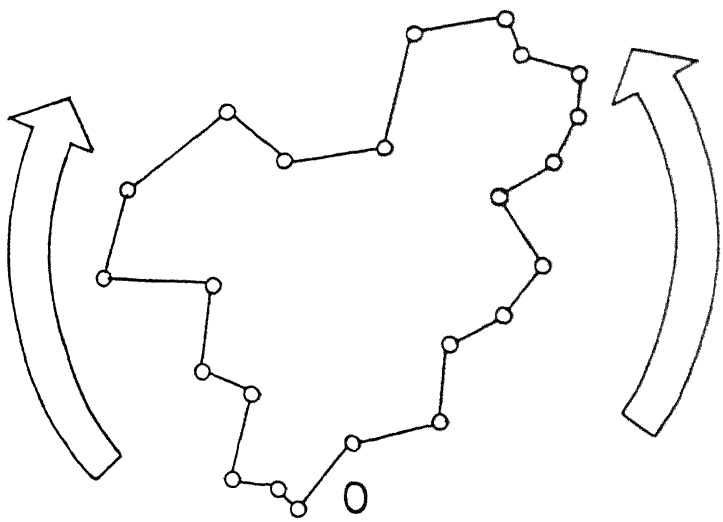

FIG. 1.2. The closed path of coherent electrons moving diffusively. The arrows indicate that the electrons can travel along both clockwise and anticlockwise paths returning to the origin **O** in phase. It shows that the probability of returning to **O** is two times greater than that calculated classically and thus the electrons get localised.

quantum interference effect. In the weak - localization limit, the interaction between two electrons is another source of dephasing of the phase coherence. Theoretically, this phenomenon is expected to occur at the lowest temperatures. According to Lee and Ramakrishnan[4], the conductivity due to the electron-electron (e-e) interaction effects for 3-dimensional systems is given by

$$\Delta\sigma = \frac{1.3e^2}{4\sqrt{2}\pi^2\hbar}\left[\frac{4}{3} - \frac{3}{2}F_\sigma\right]\left[\frac{k_BT}{\hbar D}\right]^{1/2}, \qquad (1.23)$$

where F_σ is the screening constant and D the diffusion constant. Rapp et al.[92] have reanalysed the ρ(T) data in terms of e-e interaction effects for a series of amorphous alloys which were earlier described by the tunnelling and the Kondo effects. Oliver et al.[93] later confirmed experimentally that the e-e interaction effects indeed show up at temperatures much below that of the weak localization effects. Some of the earlier studies[94–97] on metallic glasses and concentrated crystalline

alloys had shown a near-universal value of 6 $(\Omega cmK^{1/2})^{-1}$ for the coefficient of the $\sqrt{T}$ term (Eq.(1.23)). Later, resistivity studies on metallic glasses also show double minima[98]. Bergmann and co-workers[99] have extended the quantum interference effects to dilute spin - glass alloys. Very recently, they have shown that weak localisation is an effective method to study Stoner excitations on the surface of thin films[99, 100]. Moreover, the presence of quantum interference effects is also observed in AlCuFe quasicrystals[101].

Resistivity saturation

It has been found that disordered alloys with positive TCR at 300 K ($\rho_0 < 150$ $\mu\Omega$cm) exhibit resistivity minima at low temperatures and resistivity saturation at high temperatures[102]. Wiessmann et al.[9] have successfully proposed a model for resistivity saturation where the Blotzmann transport channel ($\rho_{Boltzmann}$) acts in parallel to a non-classical channel resulting in

$$\frac{1}{\rho} = \frac{1}{\rho_{sat}} + \frac{1}{\rho_{Boltzmann}}, \tag{1.24}$$

where ρ_{sat} is the saturation resistivity ($\simeq$ (150-200) $\mu\Omega$cm). This essentially demonstrates a deviation from Matthiessen's rule. However, later Chakraborty and Allen[10] have raised some questions regarding the arguments in formulating this model. Gurvitch[103] modified the above model by suggesting an expression of ρ_{sat} $(= 3\hbar a/\alpha^{2/3}e^2)$ using statistical distribution of relaxation times. Several theories have been suggested so far to explain the resistivity saturation. Most important among them are "phonon ineffectiveness"[78] theory, interaction theory[104], etc. The resistivity saturation is observed in many disordered alloys at high temperatures such as TiAl[105], NbSn[106], FeNiCr[107], etc..

1.2.3 Magnetoresistance

It is well known that the electrical resistivity in any material can be varied by applying a magnetic field. This is known as magnetoresistance which is usually measured in two orientations, one is longitudinal and the other is transverse. In the longitudinal mode, the magnetic field is applied along the direction of the electric current while the field is perpendicular in the transverse mode. The study of magnetoresistance is considered to be one of the most essential investigations to get

a complete idea about the different scattering mechanisms responsible for the electrical resistivity.

Normal magnetoresistance

In metals and alloys, a positive magnetoresistance usually appears as a result of the anisotropy in electron relaxation time[11] and is given by

$$\Delta\rho/\rho = \frac{Q^2}{n^2e^2}\frac{B^2}{\rho^2}, \tag{1.25}$$

where Q is a measure of the anisotropy and n is the number of electrons per unit volume. It can be seen from Eq.(1.25) that normal magnetoresistance becomes dominant at high fields (i.e., large B) and at low temperatures (i.e., small ρ). Later, using the two-band model, a more comprehensive relation for the normal magnetoresistance was written as

$$\Delta\rho/\rho = \left(\frac{1}{\rho 2ne}\right)^2 B^2. \tag{1.26}$$

Besides this, dependence of normal magnetoresistance on temperature, magnetic field, and impurity can be expressed universally[11] as

$$\Delta\rho/\rho = f\left(\frac{B}{\rho}\right). \tag{1.27}$$

This is known as the Kohler's rule. This is valid for both transverse and longitudinal orientations.

Magnetoresistance in ferromagnets

In ferromagnetic materials, magnetoresistance in both longitudinal (LMR) and transverse (TMR) orientations are quite different from the normal magnetoresistance due to the presence of spontaneous magnetisation. In general, the longitudinal (LMR) and the transverse magnetoresistances (TMR) are positive and negative, respectively at low fields. At higher fields, often called the technical saturation[11], they show only a small decrease with field. This negative magnetoresistance (i.e., $\frac{1}{\rho}\frac{d\rho}{dH}$) beyond technical saturation was considered earlier as characteristics of ferromagnets and could be understood from the localised model. According to this model, the magnetoresistance is proportional to $(M_s(H,T)^2 - M_s(0)^2)$ (where $M_s(0)$ is the spontaneous magnetisation). Now, as the magnetic field increases, the value of the magnetisation ($M_s(H,T)$) dominates over the spontaneous one ($M_s(0)$) and hence a negative slope in magnetoresistance[11]. However, at very low

temperatures ($T << T_c$), this slope disappears[108] since $M_s(T) \simeq M_s(0)$.

Considering a random distribution of domains in a polycrystal, the zero - field magnetoresistance is written[109] as

$$\rho = (1/3)\rho_{\|s} + (2/3)\rho_{\perp s}, \tag{1.28}$$

where

$$\frac{\rho_{\|s} - \rho}{\rho_{\perp s} - \rho} = \frac{\Delta\rho_{\|s}}{\Delta\rho_{\perp s}} = -2. \tag{1.29}$$

On the other hand, the ferromagnetic anisotropy of resistivity (FAR) is defined as

$$FAR = \frac{\Delta\rho_{\|s} - \Delta\rho_{\perp s}}{\rho}, \tag{1.30}$$

where the values of $\Delta\rho_{\|s}/\rho$ and $\Delta\rho_{\|s}/\rho$ are obtained from the high-field LMR and TMR data extrapolated to zero internal magnetic field (H_{int}). The internal field H_{int} is defined as $H_{int} = H_{ext} - \beta M_s$ where β is the demagnetisation factor which depends on the dimensions of the sample and its orientation with respect to the applied field. It is interesting to note that the FAR is an inherent property of ferromagnetic materials which does not depend on the value of the zero - field resistivity. The origin of FAR is generally attributed to the spin-orbit interaction present in a ferromagnet.

Two-current conduction model

Campbell et al. had proposed a model, called the two-current conduction[110, 111] (TCC), to describe the composition as well as the temperature dependence of electrical resistivity and FAR in binary and ternary Fe and Ni-based ferromagnetic alloys. The basic idea behind this model is that the 3d band of transition metals and alloys splits into spin-up and spin-down subbands due to the ferromagnetic exchange interaction. As a result, the electrical conduction takes place in parallel through both spin-up and spin-down channels. The resistivity in each spin-up ($\rho\uparrow$) and spin-down ($\rho_\downarrow$) channels has a series of contributions arising from s-s (ρ_{ss}) and s-d (ρ_{sd}) scattering of conduction electrons (i.e., s electrons). The residual resistivity, according to the TCC model, can be written as

$$\rho_0 = \rho_\uparrow^0 \rho_\downarrow^0 / (\rho_\uparrow^0 + \rho_\downarrow^0). \tag{1.31}$$

Now as the temperature increases, mixing of spin-up and spin-down subbands due to the electron - magnon scattering gives rise to a spin-mixing term ($\rho_{\uparrow\downarrow}$). In addition, the temperature - dependent resistivity terms $\rho_\uparrow^P$(T) and $\rho_\downarrow^P$(T) must be included in the residual spin-up and spin-down resistivities, respectively. Here it is to be noted that $\rho_{\uparrow\downarrow}$, $\rho_\uparrow^P$(T), and $\rho_\downarrow^P$(T) are characteristics of host only and do not depend on the impurity. The general expression for the total resistivity is then given[110] by

$$\rho(T) = \frac{\rho_\uparrow \rho_\downarrow + \rho_{\uparrow\downarrow}(\rho_\uparrow + \rho_\downarrow)}{\rho_\uparrow + \rho_\downarrow + 4\rho_{\uparrow\downarrow}}, \tag{1.32}$$

where

$$\rho_\sigma(T) = \rho_\sigma^0 + \rho_\sigma^P(T). \tag{1.33}$$

Here σ represents the resistivity of spin-up and spin-down subbands.

On the other hand, the FAR arises due to the spin-orbit interaction. The mixing of spin-up and spin-down states is not possible at low temperatures. This is also true even in the absence of spin-orbit interaction. In these circumstances, $\rho\uparrow$ arises mainly from s-s scattering (ρ_{ss}) of like-spin states (since there are no vacant d$\uparrow$ states at the Fermi level) while the contribution to $\rho\downarrow$ comes from both s-s and s-d scattering of like-spin states. But in the presence of spin-orbit interaction, spin-up states acquire sufficient energy so that certain amount of d$\uparrow$ electrons can move into the d$\downarrow$ states at the Fermi level resulting in d$\uparrow$-d$\downarrow$ mixing. However, the transfer of d$\downarrow$ electrons to d$\uparrow$ states is found to be highly anisotropic. The reason is that the magnetisation direction induces a preferred axis for the spin-orbit coupling which, in turn, gives rise to resistivity anisotropy. After a rigorous calculation, the FAR is expressed[110] as

$$FAR = \frac{\gamma(\rho_\downarrow - \rho_\uparrow)\rho_\downarrow}{\rho_\uparrow \rho_\downarrow + \rho_{\uparrow\downarrow}(\rho_\uparrow + \rho_\downarrow)}, \tag{1.34}$$

where γ is a constant[112], of the order of 0.01. A good review of FAR can be seen elsewhere[113]. Later on, Malozemoff[114] proposed a modified TCC model for describing the FAR in amorphous and concentrated crystalline alloys. In addition, the FAR is found to depend strongly on electron

- impurity scattering rather than on electron - phonon scattering[115]. Very recently, Berger[116] has correlated the TCC model with Nordhiem's rule. In another theory, Banhart and Ebert have proposed a model[117] for FAR in disordered magnetic alloys based on the Kubo-Greenwood formalism and the spin-polarised relativistic coherent potential approximation.

Magnetoresistance in spin glass/cluster glass

Long back, Béal-Monod and Weiner[118] had shown a negative magnetoresistance for dilute spin glasses, essentially in the Kondo regime. Later, Mookerjee[119] proposed a theory for spin glasses where the impurity and the s-d couplings are assumed to be isotropic. This is possible only when no magnetic cluster is formed. In this circumstance, magnetoresistance is found to be varying as (-H^2) near T_f at low fields and also it is proportional to the impurity concentration. Experimentally, this is found to be more or less valid for AuFe, AuMn, CuMn, and AuFe[120] alloys.

Magnetoresistance due to localisation effects

In highly disordered alloys, irrespective of their magnetic state, some interesting anomalous behaviours are observed which cannot be described by the above models. Here, as it has been mentioned earlier, the mean free path of conduction electrons is of the order of inter-atomic separation and the electrons start getting localised due to the phase coherence between the scattered partial waves. The application of a magnetic field is a source of dephasing like the inelastic scattering. However, this phenomenon is found to be quite complex and depends on many factors. According to Altshuler et al.[121–123], the magnetoresistance due to weak localisation in the presence of spin-orbit interaction for a three dimensional system can be written as

$$(\Delta\rho/\rho) = \alpha\frac{e^2\rho}{2\pi^2\hbar}\left(\frac{eH}{\hbar}\right)^{1/2}\left[\frac{1}{2}f_3\left(\frac{H}{H_i}\right) - \frac{3}{2}f_3\left(\frac{H}{H_{so}}\right)\right], \tag{1.35}$$

where

$$\begin{aligned} f_3(x) &\simeq x^{3/2}/48, \qquad (x << 1) \\ &\simeq 0.605. \qquad (x >> 1) \end{aligned}$$

Here $H_i = (\hbar/4eD)\tau_i^{-1}$, $H_{so} = H_i + H'_{so}$, and $H'_{so} = (\hbar/4eD)\tau_{so}^{-1}$ where τ_i^{-1} and τ_{so}^{-1} are the relaxation rates for inelastic and spin-orbit scattering, respectively and the prefactor $\alpha \simeq 1$. The exact

nature of the magnetoresistance depends on the relative strength of spin-orbit interaction and inelastic scattering[124]. For weak spin-orbit interaction[124] ($\tau_{so}^{-1} << \tau_i^{-1}$, i.e., $H_{so} \simeq H_i$), the magnetoresistance in Eq.(1.35) becomes negative and can be expressed as

$$(\Delta\rho/\rho)_{loc} \simeq -\alpha\frac{e^2\rho}{96\pi^2\hbar}\left(\frac{e}{\hbar}\right)^{1/2} H^2/H_i^{3/2} \qquad (H << H_i) \tag{1.36}$$

$$\simeq -\alpha\frac{0.605e^2\rho}{2\pi^2\hbar}\left(\frac{eH}{\hbar}\right)^{1/2}. \qquad (H >> H_i) \tag{1.37}$$

On the other hand, for a strong spin-orbit interaction ($\tau_{so}^{-1} >> \tau_i^{-1}$, i.e., $H_{so} >> H_i$), the magnetoresistance in Eq.(1.35) becomes positive and is given by

$$(\Delta\rho/\rho)_{so} \simeq +\alpha\frac{e^2\rho}{192\pi^2\hbar}\left(\frac{e}{\hbar}\right)^{1/2} H^2/H_i^{3/2} \qquad (H << H_i) \tag{1.38}$$

$$\simeq +\alpha\frac{0.605e^2\rho}{4\pi^2\hbar}\left(\frac{eH}{\hbar}\right)^{1/2}. \qquad (H_i << H << H_{so}) \tag{1.39}$$

However, at very high fields where $H >> H_{so}$, Eq.(1.35) reduces to Eq.(1.37) as if it is in the weak spin-orbit limit. The behaviour of magnetoresistance is illustrated in Fig.1.3 in the presence of weak, moderate, and strong spin - orbit interaction. Moreover, the above model also predicts that there is no effect of orientation of magnetoresistance, viz. TMR and LMR should be identical.

Magnetoresistance in interaction effects

In electron - electron interaction effects (EEI), the energy difference between the two interacting electrons acts as an additional source of dephasing at the lowest temperatures. EEI contributes to the magnetoresistance and adds a correction term to the Boltzmann conductivity which is found to be positive. According to Lee and Ramakrishnan[4], if only the spin-splitting of the interacting electrons is considered, the magnetoresistance can be expressed as

$$(\Delta\rho/\rho)_{int} = \frac{e^2\rho F_\sigma}{4\pi^2\hbar}\left(\frac{kT}{2D\hbar}\right)^{1/2} g_3\left(\frac{g\mu_B H}{kT}\right), \tag{1.40}$$

where F_σ is a screening constant and

$$g_3(h) \simeq \sqrt{h} - 1.3, \qquad (h >> 1) \tag{1.41}$$

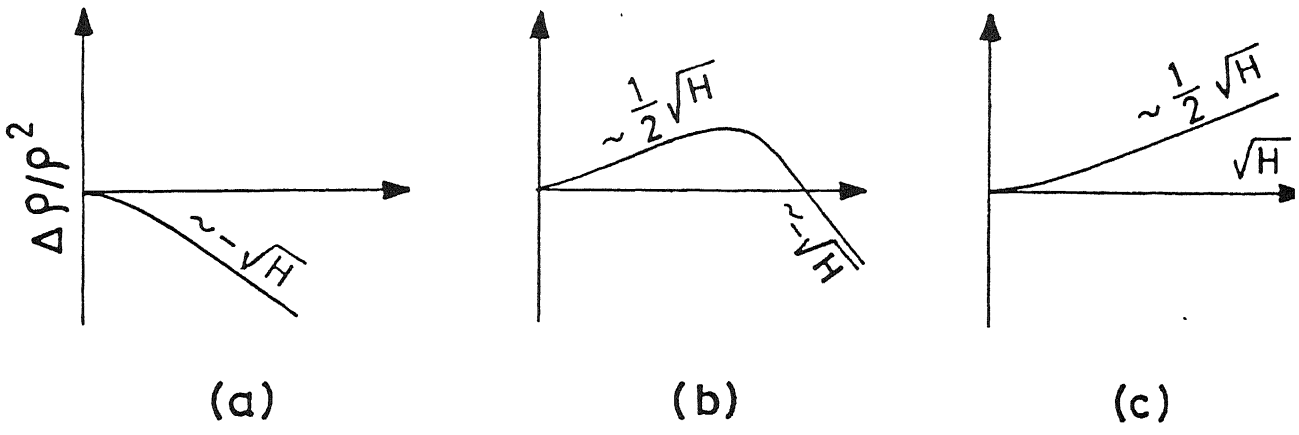

FIG. 1.3. Main features of magnetoresistance in three dimensional systems arising from spin - orbit (SO) interaction in the weak - localisation limit : (a) weak SO, (b) moderate SO, and (c) strong SO.

$$\simeq 0.053h^2. \qquad (h << 1) \qquad (1.42)$$

On the other hand, if the same arguments are used for the orbital contribution, the magnetoresistance[121] can be written as

$$(\Delta\rho/\rho)_{orb} = \frac{\mathrm{g(T)}e^2\rho}{2\pi^2\hbar}\left(\frac{eH}{\hbar}\right)^{1/2}\phi_3\left(\frac{2eDH}{\pi kT}\right), \qquad (1.43)$$

where g(T) is an interaction parameter and

$$\phi_3(h) \simeq 1.9 \qquad (h >> 1) \qquad (1.44)$$

$$\simeq 0.33h^{3/2}. \qquad (h << 1) \qquad (1.45)$$

Thus the orbital and the spin - splitting contributions of the interacting electrons to the magnetoresistance have the same field dependence.

Earlier studies by Howson and Greig[125, 126] on CuZr and CuTi amorphous alloys have clearly shown the presence of interaction effects in ρ(T) in the temperature range of 100 mK to 20 K But in the interpretation of the magnetoresistance data[126], they had concluded that the field dependence of EEI effects along with localisation term comes into play only below 1 K which is inconsistent with the interpretation of ρ(T) data. Later Bieri et al.[124, 127] had shown that strong spin - orbit scattering is responsible for the positive magnetoresistance of $Cu_{50}Lu_{50}$, $Pd_{80}Si_{20}$, and some other amorphous alloys. The study on FeZr[128] amorphous alloys have shown the presence of weak-localisation and e-e interaction effects in the temperature range (4.2 - 77)K in magnetic induction up to 5 T. Very recently, magnetoresistance data in CaAl[129] and FeCr[130] amorphous alloys have been analysed in terms of the strong spin-orbit interaction in the weak-localisation limit.

1.2.4 Hall effect

The Hall effect in metals and alloys is considered to be one of the most important experimental techniques to get useful information about their electronic structure. The Hall resistivity in any simple non-magnetic material[11] is defined as

$$\rho_H = \frac{E_{xy}}{j_{xx}} = R_0 B_z, \tag{1.46}$$

where R_0 is known as the ordinary Hall coefficient (OHC), E_{xy} the transverse electric field, j_{xx} the longitudinal current density, and B_z the magnetic induction. The origin of R_0 is the Lorentz force acting on the conduction electrons. For any simple metal, the sign and the magnitude of R_0 can be obtained using the two-band model[11].

In any ferromagnetic material, an additional term is required to explain the Hall resistivity which is then expressed as

$$\begin{aligned} \rho_H &= R_0 B_z + \rho_H^{Ext} \\ &= R_0 B_z + R_s M_s. \end{aligned} \tag{1.47}$$

Here ρ_H^{Ext} is known as the spontaneous or the extra-ordinary part of the Hall resistivity, M_s the saturation magnetisation, and R_s the extra-ordinary Hall coefficient (EHC). The origin of ρ_H^{Ext} is

attributed to the spin-orbit interaction[131–133] present in a ferromagnet.

Ordinary Hall coefficient

According to the free - electron theory, the magnitude and the sign of the ordinary Hall coefficient R_0 depends on the majority charge carriers and their concentration. In the two-band model, the general expression for R_0 is given[11] by

$$R_0 = \frac{1}{e} \frac{\left(\frac{\sigma_e^2}{n_e} - \frac{\sigma_h^2}{n_h}\right) + \frac{B^2\sigma_e^2\sigma_h^2(n_e - n_h)}{e^2 n_e^2 n_h^2}}{(\sigma_e + \sigma_h)^2 + \frac{B^2\sigma_e^2\sigma_h^2(n_e - n_h)^2}{e^2 n_e^2 n_h^2}}, \tag{1.48}$$

where n and σ are the carrier concentration and the conductivity, respectively. The suffix e and h represent electron and hole, respectively as charge carriers. For high fields ($B \rightarrow \infty$), the above relation gives

$$R_0 = \frac{1}{e(n_e - n_h)}. \tag{1.49}$$

For simple metals and alloys, the majority charge carriers are electron ($n_e >> n_h$) and hence $R_0 = 1/en_e$. It is important to note that, according to the free electron theory, R_0 in any metal is negative and is independent of temperature.

Hall effect in spin glass

In spin glasses, the behaviour of the OHC R_0 deviates strongly from what is expected in the free-electron theory. The most important one is the temperature dependence of R_0. Experimental data in dilute AuFe and AuCr alloys[134] show that

$$R_0(T) = R_0(0) + A/T. \tag{1.50}$$

This is ascribed to the skew scattering arising from the left - right asymmetry of conduction electrons after interacting with the polarised local 3d impurities. A good review of these studies can be found in references[134, 135].

Hall effect in disordered non-magnetic alloys

Recently in amorphous transition metal alloys, a positive R_0 is observed which in no way can be explained by the free - electron theory. Several explanations have been proposed so far[136–138]. The most successful and well accepted one is the s-d hybridisation[13–15]. Good reviews on these works are given in literature[2, 138, 139]. In transition - metal alloys, it is known that the s-band (i.e., conduction band) overlaps with the 3d-band and thus s-d hybridisation takes place. In amorphous alloys, disorder can induce a broadening of energy levels where s and d bands meet and, as a result, the dispersion curve (E vs. k) of conduction electrons is modified into an "S" - shape (see Fig.1.4). The group velocity (dE/dk) is negative in the vicinity of s-d hybridisation (between E_1 and E_2) and hence R_0 becomes positive.

Recently, the OHC in non - magnetic PdZr, NiZr, FeZr, CuTi, and PdZi have shown a negative temperature dependence[140–142] which is interpreted in terms of electron-electron interaction effects[121, 122] and is given by

$$\frac{\Delta R_0}{R_0} = \frac{2\Delta\sigma}{\sigma} \simeq \frac{1.3e^2}{2\sigma\pi^2\hbar}(4/3 - 2F_\sigma)\sqrt{\frac{k_B T}{2\hbar D}}. \qquad (1.51)$$

Their analysis is found to be consistent with the interpretation of the ρ(T) data. Very recently, in some amorphous paramagnetic transition metal alloys, R_0 is found to have a dominant anomalous contribution[138, 143] which is explained in terms of the side-jump effect[133].

Extra-ordinary Hall coefficient

In any ferromagnetic material, the Hall resistivity (ρ_H) usually follows Eq.(1.47) in the temperature range $T << T_c$ where T_c is the Curie temperature. The values of R_sM_s and OHC are obtained from the intercept and the slope, respectively of a linear fit of the high-field data. For any crystalline ferromagnetic material, R_s is generally found to be at least an order of magnitude[131] larger than R_0 and it is more so in amorphous 3d alloys[132]. Hence the value of ρ_H is nearly equal to that of the spontaneous term (R_sM_s).

Localised models

Any spontaneous contribution in a ferromagnet is mainly dependent on its saturation magnetisation,

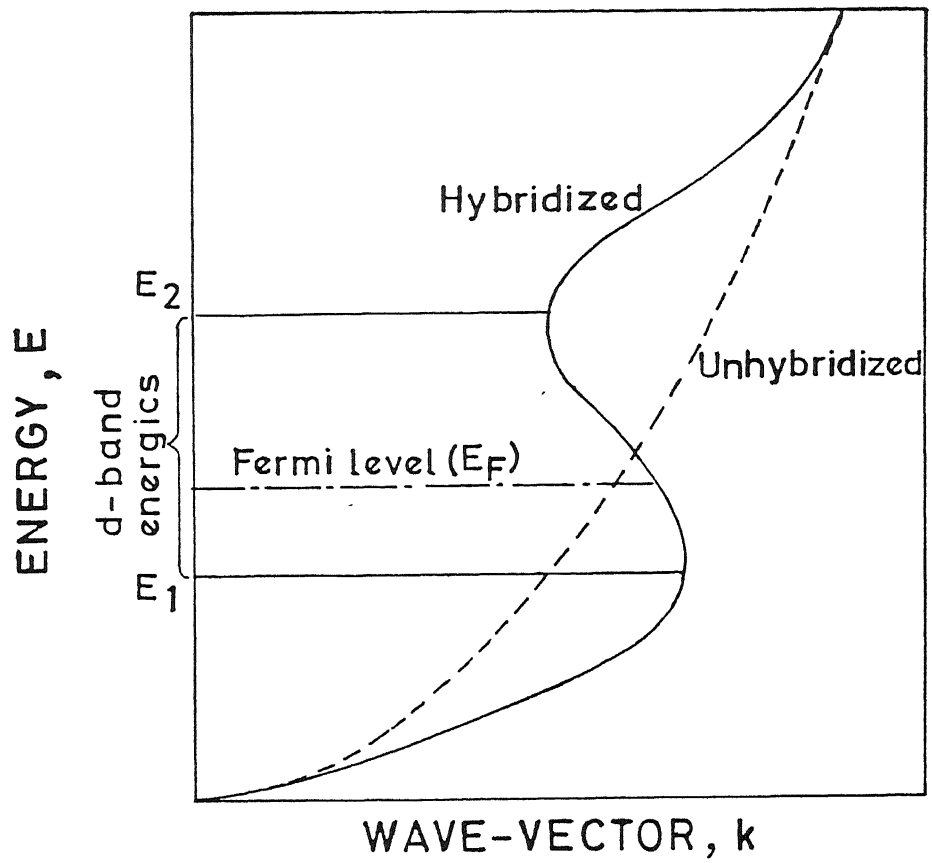

FIG. 1.4. The s-d hybridisation on the dispersion curve (energy (E) vs. wave vector (k)). The dashed line is unhybridised conduction band (i.e., s band). Between E_1 and E_2, the slope of the dispersion curve (i.e., the group velocity) is negative.

i.e., on the electron spin/moment. This indicates that the electron spin and its interaction[131, 132] (i.e., spin-orbit interaction) have a major influence on ρ^{ext}(H). According to Kondo[144], d and f electrons are localised at their lattice sites, moments of which, however, contribute to the total magnetisation of an alloy. The conduction electrons (i.e., s electrons) are the majority charge carriers. It has been shown that the extra-ordinary contribution to Hall resistivity arises only when an intrinsic spin-orbit interaction of d/f electrons is taken into consideration. According to this model, the Hall resistivity is expressed as

$$\rho_H \propto \left\langle (M - \langle M \rangle)^3 \right\rangle . \tag{1.52}$$

Later, Kagan and Maksimov[145] have modified this model by introducing a mixed type of s(orbit) - d/f(spins) interaction in addition to the intrinsic spin - orbit interaction which under the molecular - field approximation (S = 1/2) is written as

$$\rho_H \propto (M_s^2(0) - M_s^2(T)). \tag{1.53}$$

Experimentally, the behaviour of extra - ordinary Hall resistivity in any 3d alloy is found to be strongly temperature dependent and most importantly it exhibits a correlation with electrical resistivity. This had attracted a lot of theoretical attention. Karplus and Luttinger[146] first suggested that the extra - ordinary Hall resistivity is a consequence of the left-right asymmetry of magnetic electrons which arises due to their spin-orbit interaction. As a result, when an electric field is applied, a current appears perpendicular to both magnetisation and the electric field. The calculation also shows that this current is proportional to the magnetisation and finally to ρ^2. It is also predicted that the coefficient of ρ^2 is independent of temperature and impurity concentration. Later, Smit[147] pointed out that this approach can not produce any net current in perfectly periodic crystals. In his original calculation[147], the spin-orbit interaction of 3d electron was considered in the form

$$\lambda_{so}(E_F) = A_{so}\chi d^2 \sum_n \frac{|\text{matrix el.}|^2}{E_n - E_F}, \tag{1.54}$$

where d is the distance between the nearest - neighbour atoms, E_n is the energy of a band state, χ is an overlap integral, and A_{so} is the atomic spin - orbit parameter.

Scattering mechanisms

Following Smit's formalism, two types of scattering mechanisms have been developed so far to explain the spontaneous Hall contribution in 3d metals and alloys. The first one is called the skew scattering where it is thought that an electron wavepacket might get deflected at an angle θ (see Fig.1.5(a)) after getting scattered by a potential in a periodic crystal. In other words, the electron wavepacket assumes a left - right asymmetry normal to the plane containing the electron spin and

its velocity. Theoretically, the skew scattering[132] is characterised by a constant spontaneous Hall angle ($\tan\theta = \rho_H/\rho$) which, in turn, gives

$$\begin{aligned} \rho_H &\propto \rho \\ i.e.\ R_s M_s &\propto \rho. \end{aligned} \tag{1.55}$$

In the low-field limit, the concentration as well as the temperature dependence of M_s was found to be weaker than those of ρ and hence Eq.(1.55) could be written as

$$R_s \propto \rho. \tag{1.56}$$

On the other hand, it is well known that for any strongly correlated system the dimensionless parameter, $\lambda_F/\pi\Lambda$ (where λ_F is the Fermi wavelength and Λ the mean free path of the electron) becomes very large due to the smaller electron mean free path. Under these circumstances, the classical Boltzmann equation does not hold[133]. This gives rise to the second possibility where the electron wavepacket might get transversely displaced from its original path after getting scattered. This is known as the side-jump effect. This transverse displacement is generally written as Δy (Fig.1.5(b)) which is found to be of the order of an atomic distance[131] ($\simeq 10^{-10}$ m). The side-jump parameter[132] Δy is related to θ_s by

$$tan\theta_s \simeq \theta_s \simeq \Delta y/\Lambda \propto \rho\Delta y, \tag{1.57}$$

which, in turn, shows that

$$\rho_H \propto \rho^2. \tag{1.58}$$

Hence, assuming M_s as a constant, R_s can be expressed as

$$\begin{aligned} R_s &\propto \rho^2 \\ &= K\rho^2, \end{aligned} \tag{1.59}$$

where K is the proportionality constant which depends only on the composition. The side-jump parameter Δy in the one-band model[148] can be expressed as

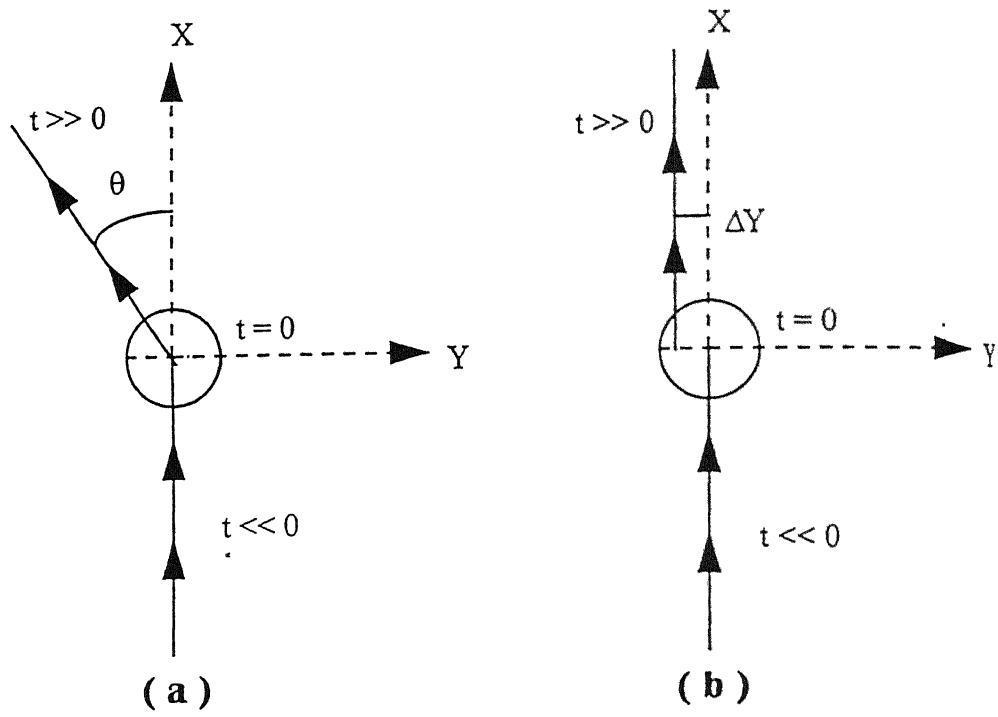

FIG. 1.5. The trajectory of a wavepacket is deflected by (a) skew scattering and (b) side - jump mechanism.

$$\Delta y = \alpha M_s \hbar k_F / n e^2, \tag{1.60}$$

where k_F is the Fermi wave number of the electron and n the number of electrons per unit volume.

The extra-ordinary Hall coefficient in pure metals and dilute alloys[131, 132] follows the behaviour as predicted by the skew - scattering theory. On the other hand, the side-jump effect is found to be dominant in concentrated alloys where the value of ρ is large. However, both the effects could be found together in one system in different temperature regimes[148]. In the present context, it is to be noted that the skew scattering can be dominant in the low temperature regime and the side-jump effect at high temperatures. In interpreting the temperature dependence of R_s in any ferromagnetic material, it is always controversial whether only the magnetic disorder contribution

to the resistivity ρ or the total contribution from all scattering[149] is responsible for the sharp change of data below T_c. In amorphous alloys, R_s is found to be varying as ρ(T) even above T_c. This is attributed to the structural disorder[132]. However, the electrical resistivity can be varied by changing temperature as well as composition. Hence, to interpret the temperature dependence of the EHC, several authors[11, 131, 150] work with a quantity called the extra-ordinary Hall conductivity, which is expressed as

$$\gamma_{HS} = \frac{\rho_H}{\rho^2} = \frac{R_s M_s}{\rho^2}. \tag{1.61}$$

Here the concentration and temperature dependence of the EHC is eliminated by dividing by ρ^2. Thus γ_{HS} should have a weaker temperature dependence than ρ_H.

Split-band model

Smit's theory[147] (Eq.(1.54)) had first pointed out that the spin-orbit interaction can change sign when the scattering potential is reversed with respect to the Fermi level. Later, Kondorskii[151] suggested that the sign of the EHC will be understood if the information regarding the shape of the Fermi surface is known. The latter is not only not available readily but also very difficult to calculate, especially in 3d alloys.

Later on, the extra-ordinary Hall coefficient in binary Ni and Fe based alloys[152] (R_s) was found to change their sign exactly at the same e/a ratio ($\simeq$ 27.7)[152, 113]. This seemed to be in good agreement with the rigid - band model. But in ternary NiFeCu alloys[150], the above correlation did not hold, since the line $R_s \simeq \lambda_s \simeq 0$ lies far away from the line of constant electron concentration. Berger had predicted[152] that some orbital degeneracy exists in the 3d spin - down band near the Fermi level and the change of sign of R_s occurs when this orbital degeneracy crosses the Fermi level. It is to be noted here that the sign change of linear magnetostriction coefficient ($\lambda_s = 0$)[153, 154] and a maximum in FAR[150, 152, 155], are also expected during this crossover. Later, Ashworth et al.[150] had extended this idea and proposed a model, called the split-band (SB) model, for describing the sign change of R_s and λ_s in ternary NiFeM alloys (where M = Cr, V, Ti, W, Mo, etc.). According to the SB model, constituents of a given alloy have their own distinct 3d

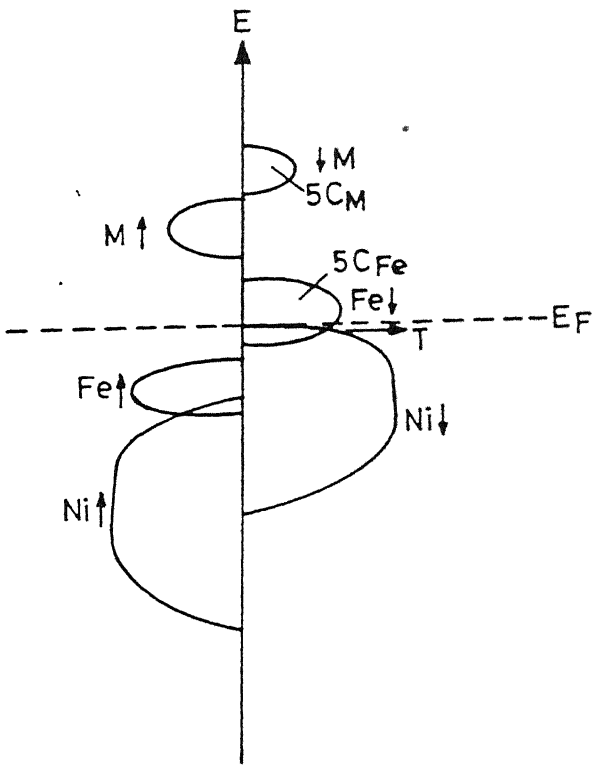

FIG. 1.6. Schematic band states for ternary NiFeM (M = Cr, V, etc.) alloys according to the split-band model.

subbands separated from each other on the energy scale (see Fig.1.6). This is possible only when the bands of all the constituents differ in energy by more than their average band width[156]. The above condition is generally satisfied for concentrated alloys where valence difference (Z) between any two constituents is greater than two, i.e., $Z \geq 2$. In fact, the split-band model is found to be an extension of Friedel's virtual bound state (VBS) model[157]. The constituent of an alloy with the largest atomic number (i.e., whose nuclei is most attractive to electrons) will have their subbands at the bottom while that with the smallest atomic number at the top. For NiFeM (where M = Cr, V, Ti, W, Mo, etc.) alloys, the bands for Ni are at the bottom whereas those of M are at the top (as shown in Fig. 1.6). Theoretical calculations show that the composition variation of $R_s \simeq \lambda_s \simeq 0$ is found to be associated with the zero expectation value of the Z-component of the 3d orbital

angular momentum[152, 158] ($\langle L_z(E_F)\rangle = 0$). This happens when the Fermi energy (E_F) lies at the boundary or the gap between Fe 3d↓ and Ni 3d↓ bands. In other words, the EHC and the linear magnetostriction coefficient change sign when the point T (where 3d spin-down bands of the Ni and Fe meet) crosses the Fermi level. According to Friedel's VBS model[157], the total number of states in a given 3d subband is found to be equal to five times the atomic concentration of the respective constituent. The Fermi level crossover will occur when the total number of holes in the 3d band of the alloy is equal to the total number of 3d↓ states of the Fe atom, i.e., for ternary NiFeM alloys, this condition can be written as

$$\begin{aligned} & 5C_{Fe} = 0.55 + 2C_{Fe} - \quad (10+Z)C_M \\ i.e., \quad & 3C_{Fe} + (10+Z)C_M = \quad 0.55, \end{aligned} \tag{1.62}$$

where 0.55 is the number of holes per atom in Ni, C the atomic concentrations, and Z the valence difference between M and Ni (e.g., -4 for Cr, -5 for V, etc). However, the above equation (i.e., Eq.(1.62)) can also be applied to binary alloys. As for example, in NiFe alloys, such a change of sign will occur when $3C_{Fe} = 0.55$, i.e., around 18 at.% of Fe which is consistent with the experimental results[108, 109]. As a matter fact, the above theory is found to be in good agreement with the experimental findings of the maximum value of the FAR and the change of sign of R_s and λ_s in Ni and Fe - based binary, and to some extent in ternary NiFeCu alloys. Later Berger has extended this model[158] to explain the minimum in electronic specific heat. In addition, there are some direct experimental evidences for such band splitting in NiCu alloys[159] from ultraviolet photoelectron spectroscopy and reflectivity measurements. The coherent potential approximation (CPA) calculations[160] for band structures in various Ni and Fe-based alloys provide another strong theoretical support to the validity of the split-band model. But, ironically, there is no detailed experimental study of FAR along with the location of $R_s = \lambda_s = 0$ lines in any other ternary system suggested in the split - band model except NiFeCu alloy series.

1.3 Motivation behind the Present Study

1.3.1 General introduction

The above discussion has clearly illustrated how the electrical resistivity and the galvanomagnetic properties of disordered alloys deviate from what is expected from the free electron theory. In recent times, this is considered to be a subject of great interest from the physics point of view. Till now, most of the studies have dealt with amorphous alloys where the resistivity is found to be of the order of (100 - 200) $\mu\Omega$cm. A good review on these can be found in the literature[2, 3, 138]. Recently, some concentrated crystalline transition metal alloys are found to be fairly resistive ($\rho \simeq$ (50 - 200) $\mu\Omega$cm). But there is as such no careful and systematic study in these alloys. The main hurdle lies in the alloy preparation where retaining the isophasic high - temperature crystalline phase at low temperatures is found to be very difficult. The present thesis deals with two such alloy series, namely γ - $Cu_{100-x}Mn_x$ ($36 \leq x \leq 83$) and γ - $Ni_{100-x-y}Fe_xCr_y$ ($6 \leq x \leq 23$; $2 \leq y \leq 21$) To keep their high - temperature γ-phase (i.e., face centered cubic phase), the alloys are heat treated and subsequently quenched properly in water. This kind of heat treatment is essential for preserving the random substitutional disorder in these alloys and avoiding any chemical clustering.

CuMn system is always a subject of great interest among physicists from the Kondo effect era. The dilute regime of these γ - $Cu_{100-x}Mn_x$ alloys had exhibited resistivity minima which were later interpreted by the Kondo effect. As it was mentioned earlier that the magnetic phase of spin glass was observed in this alloy series for $x \leq 10$ at.% below T_f. It is interesting to note here that CuMn along with AuFe and (EuSr)S are a very few examples of "ideal spin glass"[22] where the experimental behaviours follow exactly the predictions of some basic theories, like Ising - model, random bond, mean - field theory, etc. Also these alloys, in the dilute regime of spin glass, exhibit an overall negative magnetoresistance in both longitudinal and transverse directions. Earlier, Kouvel[27] simulated the magnetic behaviour of $Cu_{100-x}Mn_x$ alloys ($x < 25$ at.%) by a simple model where spin / cluster - glass phase is described by an ensemble of mutually - interacting ferro and antiferromagnetic domains. The neutron - diffraction study by Sato et al.[161] has shown short-range antiferromagnetic ordering in $Cu_{75}Mn_{25}$ alloy.

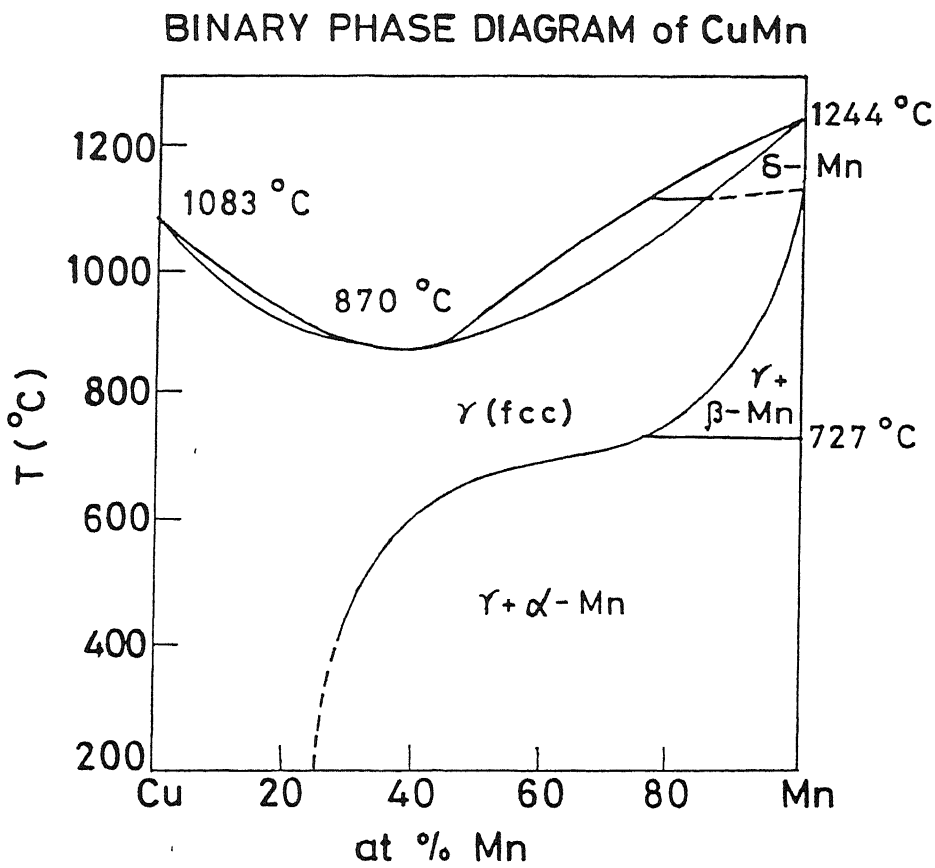

FIG. 1.7. Phase diagram of binary CuMn alloys.

Later, a detailed neutron diffraction study by Cowlam and Samah[162] over a wide range of concentration revealed some interesting features about the magnetic ordering in the concentrated regime of γ - $Cu_{100-x}Mn_x$ ($x \geq 72$) alloys. It has been found that, for $x \leq 72$, both the nearest and the next - nearest neighbour interactions of Mn are antiferromagnetic. This is known as the AF3 structure. But, in the concentration range of $72 \leq x \leq 84$, only the nearest neighbour interaction is antiferromagnetic while the next - nearest one is ferromagnetic. This is called the AF1 structure. Thus, there is a high probability of forming a cluster glass / mixed phase in the concentration range of $72 \leq x \leq 84$.

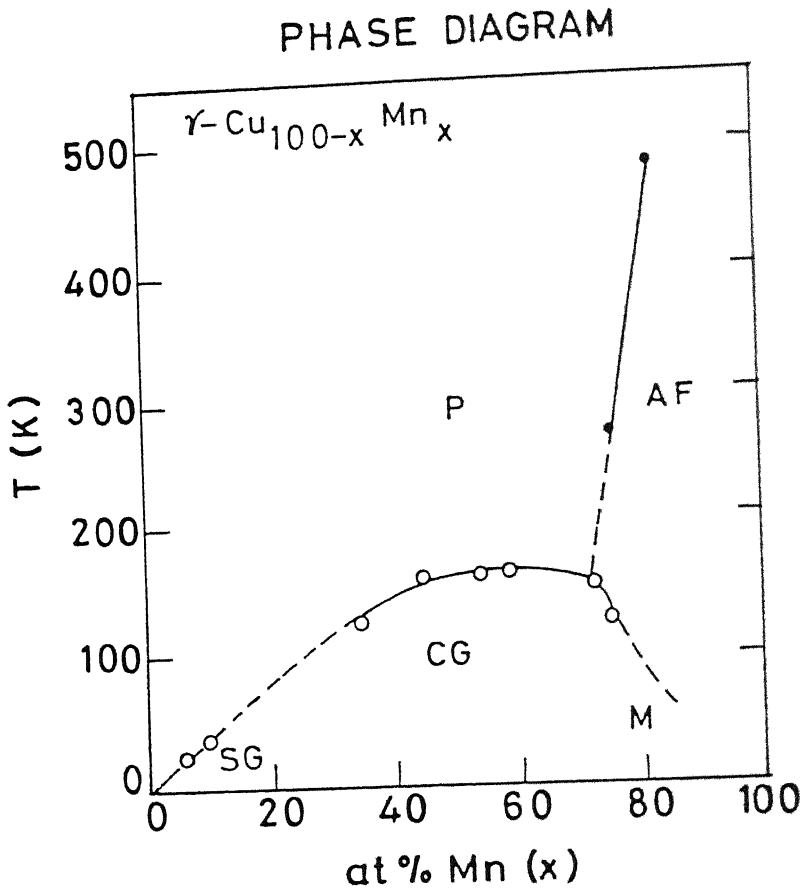

FIG. 1.8. Magnetic phase diagram of concentrated binary CuMn alloys.

However, a problem comes from the metastable state of the high - temperature isophasic γ-phase in this regime. According to the metallurgical phase diagram (see Fig.1.7), the low - temperature crystallographic phase of $Cu_{100-x}Mn_x$ for $x > 25$ at.% is found to be a mixture of γ (fcc) and α (simple cubic) phases. The high - temperature γ-phase is isophasic, but metastable (see Fig.1.7), which makes the high temperature studies unreliable. Due to all these complications, the concentrated regime of CuMn alloys has not been paid much attention. Very recently, Banerjee and Majumdar, in a detailed study[43], have established the complete magnetic phase diagram (see Fig.1.8) over

a wide composition range of 4.4 $\leq$x$\leq$ 83 using ac-susceptibility and dc-magnetisation studie Moreover, their phase diagram is found to be in good agreement with the theoretically propose one[46]. Thus the alloys studied in this work are in cluster - glass / mixed phase region. On th other hand, the electrical resistivity study[43] in $Cu_{100-x}Mn_x$ (36 $\leq$x$\leq$ 83) alloys have shown th these substantially disordered materials have large values of residual resistivity ($\rho \simeq$ (97 - 20($\mu\Omega$cm). Long back Coles had shown that even the concentrated CuMn alloys might have resistivit minima[163] at low temperatures. Later, Banerjee and Majumdar have confirmed it. Since the study is restricted only down to 10 K[43], interpretation of the resistivity minima was not possibl Nevertheless, a dominant (BT^2 - $CT^{5/2}$) - type of cluster-glass contribution was clearly obtained i the temperature range of T > 25 K. However, Ford and Mydosh[71] found a dominant $T^{3/2}$ type c spin-glass contribution at low temperatures (much below 20 K) for x$\leq$10 at.%.

NiFeCr alloys are well known for their wide range of technological applications, such as elir vars, heat - resistant steel, non-magnetic stainless steel, etc. (shown in Fig.1.9). Recently, this allo series has attracted a lot of attention due to its fascinating magnetic behaviour[164], especially th γ-phase composition region. The present γ - $Ni_{100-x-y}Fe_xCr_y$ ($6 \leq x \leq 23$; $2 \leq y \leq 21$) alloy are in the range of chrome permalloy and heat - resistant steel (see Fig.1.9). It is well known tha the high temperature γ-phase of Fe is antiferromagnetic (AFM). Hence Cr is added to stabilise th AFM phase of Fe. In fact, this is true for the Fe-rich side of γ - $Ni_{100-x-y}Fe_xCr_y$ (x > 50) alloys But, in the Ni-rich NiFeCr (the present alloy series), Cr is added to enhance the electrical resistivit (i.e., disorder) and to decrease the eddy - current losses[165].

Earlier, the present alloy series at 77 K was found to be ferromagnetic[165, 166]. Howeve neutron diffraction study[167, 168] in NiFeCr alloys has revealed that the exchange interactio among the constituents are J(Fe-Fe) = -7 meV, J(Ni-Ni) = 52 meV, J(Cr-Cr) = -227 meV, J(Fe-N = 36 meV, J(Fe-Cr) = 39 meV, and J(Ni-Cr) = 122 meV. Hence the mixed/cluster-glass phase ca be expected to be observed in certain composition range of this alloy series. Later, Majumda and Blanckenhagen[48] have hit upon a series of γ - $Fe_{80-x}Ni_xCr_{20}$ (10 $\leq$x$\leq$ 30) alloys wher ferromagnetic, mixed, spin - glass, and antiferromagnetic phases are obtained within the sam

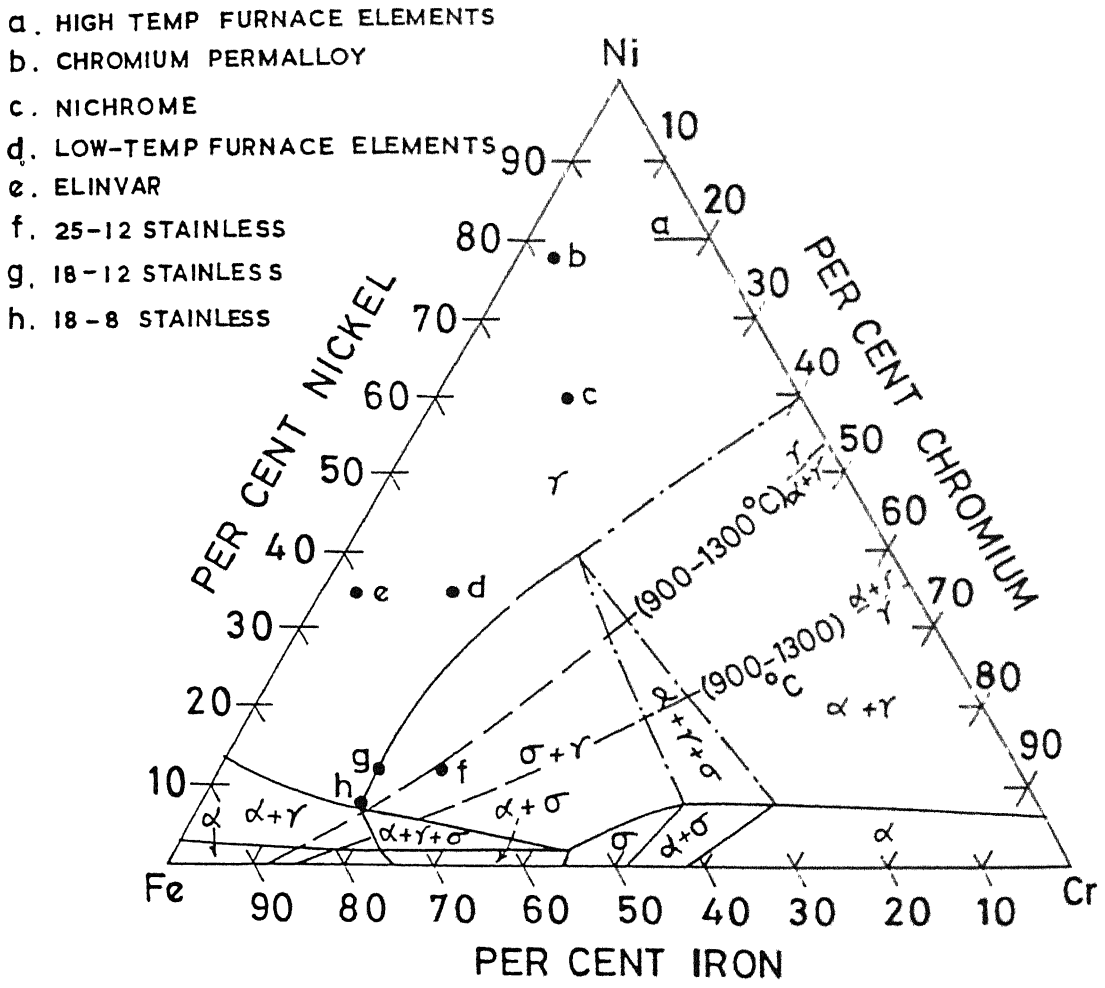

FIG. 1.9. Phase diagram of ternary NiFeCr alloys at 600^0 C (solid lines) and at 1200^0 C (dotted lines).

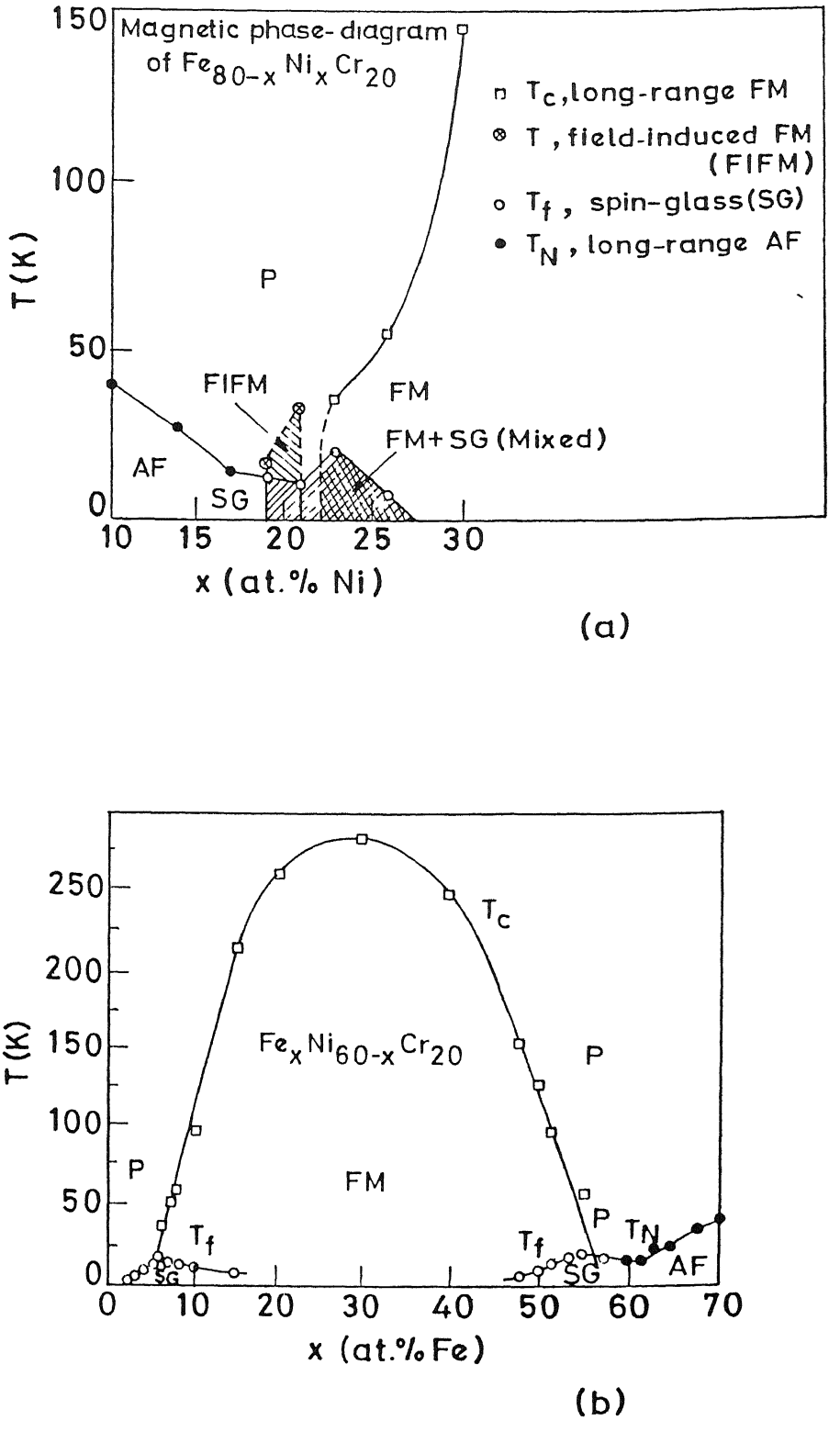

FIG. 1.10. Magnetic phase diagram of (a) Fe-rich γ - $Fe_{80-x}Ni_xCr_{20}$ and (b) Ni-rich γ - $Ni_{80-x}Fe_xCr_{20}$ alloys.

crystallographic phase (i.e., γ-phase) (see Fig.1.10(a)). Menshikov et al [19] have shown that ferromagnetic and spin - glass behaviours can be observed in Ni rich γ - $Ni_{82-x}Fe_xCr_{18}$ ($2 \leq x \leq 15$) alloys as well (see Fig.1.10(b)). This seems to be quite exciting in the sense that, for the same crystallographic phase, both ferromagnetic and spin/cluster glass phases are observed in both Fe and Ni-rich sides of NiFeCr series.

Recently, the electrical resistivity study in γ - $Ni_{82-x}Fe_xCr_{18}$ ($2 \leq x \leq 37$) alloys have shown resistivity minima[169, 170] around 20 K. But the interpretation of the data is found to be somewhat confusing. Later, in Fe-rich $Fe_{80-x}Ni_xCr_{20}$ alloys, resistivity minima[96] are observed at very low temperatures which are interpreted in terms of electron - electron interaction effects. Also a high-temperature resistivity saturation[107] is reported for the same alloy series which is well described by the parallel - resistor model[9]. However, the magnetoresistance[171] of these alloys show some anomalies which could not be explained consistently with the interpretation of the electrical resistivity.

Another aspect of these NiFeCr alloys, which is interesting, is the fact that Cr has always reduced the ferromagnetic anisotropy of resistivity (FAR) drastically. Earlier, in an extensive study[108], Van Elst had pointed out that addition of 10.1 at.% Cr in Ni host decreases the value of FAR to almost zero. Since then, there is as such no detailed systematic report on FAR in Cr-rich alloys. On the other hand, the change of sign of the extra-ordinary Hall coefficient in the present NiFeCr alloys[172], i.e., R_s=0 line, exhibited a gross disagreement with the prediction of the split-band model on the ternary composition diagram. Later, the deviation (though smaller) of λ_s=0 line on the same diagram (where λ_s is the linear - magnetostriction coefficient) confirmed the above disagreement[173].

1.3.2 Motivation

Keeping in mind all the above facts, various measurements like electrical resistivity and galvano-magnetic properties are planned accordingly. The present γ-$Cu_{100-x}Mn_x$ (x = 36, 60, 73, 76, and 83) alloys have exotic magnetic structures at low temperatures. According to the magnetic phase

diagram[43] (Fig.1.8) they are cluster glasses for x = 36, 60, and 73 with T_{sg} between 135 and 149 K and are in the mixed cluster-glass and long-range antiferromagnetic phase for x = 76 and 83 with $T_{sg} \approx$ 145 and 45 K, respectively[43]. The values of ρ(T) are found in the range of (93 - 197) $\mu\Omega$cm. Thus, these alloys are substantially disordered. Electrical resistivity (1.2 - 40 K) and magnetoresistance till 7.5 T in both longitudinal and transverse orientations are measured in these γ-$Cu_{100-x}Mn_x$ alloys.

On the other hand, the γ - $Ni_{100-x-y}Fe_xCr_y$ ($6 \leq x \leq 23$; $2 \leq y \leq 21$) alloys are all ferromagnetic below their respective T_c's. However, according to the earlier neutron diffraction and dc-magnetisation studies[49], the Cr-rich alloys ($\geq$ 18 at.%) are expected to have a spin - glass phase as well at low temperatures besides the ferromagnetic one at higher temperatures. The values of the electrical resistivity in these alloys are found to be widely varying between 31 and 90 $\mu\Omega$cm, depending on the alloy composition. Electrical resistivity, magnetoresistance, ferromagnetic anisotropy of resistivity (FAR) and the Hall effect are studied in these alloys.

The motivation behind these studies are :

1. Do resistivity minima occur in concentrated γ - CuMn and NiFeCr alloys? If yes, then what are the possible mechanisms responsible for their occurrence?

2. Is it possible to identify as well as to isolate the spin-glass (in CuMn) and ferromagnetic (in NiFeCr) contributions to the electrical resistivity from other contributions? It is rather important to find how different competing physical mechanisms give rise to the resistance minima.

3. On the other hand, magnetoresistance data always provides useful information regarding different scattering phenomena, without which the interpretation of electrical resistivity remains incomplete. Hence, it is very important to check whether the interpretation of the magnetoresistance data is consistent with that of the electrical resistivity (ρ(T)) or not.

4. The motivation behind the study of FAR in NiFeCr alloys is three-fold. The first one is to find a correlation between the values of the FAR and the earlier observed $R_s = \lambda_s = 0$

line in the ternary composition diagram. This will give some useful information regarding their electronic band structures. Moreover, this will tell us whether the split-band model can provide a satisfactory explanation for such low - FAR alloys or not. Also it is very essential to check the general applicability of the split-band model. The second aim is to explore possible reasons for such small values of FAR in Cr-rich alloys. The last one is to try to interpret the FAR data using the two-current conduction model[110, 112].

5. The temperature dependence of the Hall effect is measured in some NiFeCr alloys where resistivity minima are observed. The motivation behind this study is that the extraordinary Hall coefficient ($R_s \propto \rho^n$) should exhibit a negative temperature dependence, reflecting the resistivity minima. As a matter of fact, the ordinary Hall coefficient (R_o) should also have a negative temperature dependence, as predicted by the e-e interaction effects.

References

[1] U. Mizutani, Progress in Material Science **28**, 97 (1983).

[2] M.A. Howson and B.L. Gallagher, Physics Reports **170**, 265 (1988).

[3] J. S. Dugdale, Contemp. Phys. **28**, 547 (1987).

[4] P. A. Lee and T. V. Ramakrishnan, Rev. Mod. Phys. **57**, 287 (1985).

[5] J.H. Mooij, Phys. Stat. Sol. A **17**, 521 (1973).

[6] M. Gurvitch, Phys. Rev. B **24**, 544 (1981).

[7] P.B. Allen, Phys. Rev. Lett. **37**, 1638 (1976).

[8] Z. Fisk. and G.W. Webb, Phys. Rev. Lett. **36**, 1084 (1976).

[9] H. M. Wiessmann, M. Gurvitch, H. Lutz, B. Schwarz, M.Strongin, P.B. Allen, and J.W. Halley, Phys. Rev. Lett. **38**, 782 (1977).

[10] B. Chakraborty and P.B. Allen, Phys. Rev. Lett. **42**, 736 (1979); P.B. Allen and B. Chakraborty, Phys. Rev. B **23**, 4815 (1980).

[11] J.P. Jan, in Solid State Physics, edited by F. Seitz and D. Turnbull (Academic, New York, 1957), Vol. 5, P. 1.

[12] H.U. Kunzi and H.J. Güntherodt, The Hall Effect and its Applications (Plenum, New York, 1980).

[13] G.F. Weir, M.A. Howson, B.L. Gallagher and G.J. Morgan, Phil. Mag. **47**, 163 (1983).

[14] M.A. Howson and G.J. Morgan, Phil. Mag. **51**, 439 (1985).

[15] D. Nguyen-Manh, D. Mayou, G.J. Morgan, and A. Paturel, J. Phys. F : Metal Phys. **17**, 999 (1987).

[16] Z. Marhonovic, M. Guberovic, E. Babic, and G.J. Morgan, J. Phys. F : Metal Phys. **17**, 1123 (1987).

[17] A.H. Morrish, The Physical Principles of Magnetism (John Wiley Sons., 1965).

[18] S. Chikazumi, Physics of Magnetism (John Wiley Sons., 1964).

[19] J. Crangle, The Magnetic Properties of Solids (The Structures and Properties of Solids, Vol. 6, Edward Arnold, London, 1977).

[20] J.Kondo, Prog. of Theo. Physics **32**. 37 (1964); in Solid State Physics, edited by F. Seitz and D. Turnbull (Academic Press., New York, 1969), Vol. 23, P.183.

[21] G. Toulouse, Comm. Phys. **2**, 115 (1977).

[22] J. Mydosh, Spin Glasses : An Experimental Introduction (Taylor and Francis, London, Washington DC, 1993).

[23] Peter J. Ford, Cont. Phys. **23**, 141 (1982).

[24] V. Canella and J.A. Mydosh, Phys. Rev. B **6**, 4220 (1972).

[25] C.N. Guy, Physica **86-88**, 877 (1977); J. Phys. F : Metal Phys. **7**, 1505 (1977).

[26] J.L. Tholence and R. Tournier, J. Physique C **35**, 229 (1974); Physica B **86-88**, 873 (1977).

[27] J.S. Kouvel, J. Phys. Chem. Solids **24**, 795 (1963).

[28] C.N. Guy, J. Phys. F : Metal Phys. **8**, 1309 (1978).

[29] S.P. McAlister and C.M. Hurd, Phys. Rev. Lett. **37**, 1017 (1976).

[30] S.P. McAlister, J.Appl. Phys. **49**, 1616 (1978).

[31] D.L. Martin, Phys. Rev. B **20** 368 (1979); **21**, 1902 (1980); 1906 (1980).

[32] J.A. Mydosh, Amorphous Magnetism II, edited by R.A. Levy and R. Hasegawa (Plenum, 1977), p.73.

[33] A.P. Murani, J. Magn. Magn. Mater. **5**, 95 (1977).

[34] A.P. Murani, J. Physique C **6**, 1517 (1978).

[35] J. Souletie and R. Tournier, J. Low Temp. Phys. **1**, 95 (1969).

[36] S.F. Edwards and P.W. Anderson, J. Phys. F **5**, 965 (1975); **6**, 1927 (1976).

[37] D. Sherrington and S. Kirkpatrick, Phys. Rev. Lett. **35**, 1792 (1975).

[38] J.R.L. de Almeida and D.J. Thouless, J. Phys. A **11**, 983 (1978).

[39] D.J. Thouless, P.W. Anderson, and R.G. Palmer, Phil. Mag. B **23**, 1371 (1981).

[40] D.S. Fisher and D.A. Huse, Phys. Rev. Lett. **47**. 201 (1986); Phys. Rev. B **38**, 386 (1988).

[41] A.P. Malozemoff and B. Barbara, J. Appl. Phys. **57**, 3410 (1985).

[42] B.R. Coles, B.R. Sarkissian, and R.H. Taylor, Phil. Mag. B **37**, 489 (1978).

[43] A. Banerjee and A. K. Majumdar, Phys. Rev. B **46**, 8958 (1992).

[44] C.M. Soukoulis and K. Levin, Phys. Rev. Lett. **39**, 581 (1977); Phys. Rev. B **18**, 1439 (1978).

[45] K. Levin, C.M. Soukoulis, and G.S. Grest, Phys. Rev. B **22**, 3500 (1980).

[46] A. Mookerjee and S.B. Roy, Pramana (To be published).

[47] M. Gabay and G. Toulouse, Phys. Rev. Lett. **47**, 201 (1981).

[48] A.K. Majumdar and P.V. Blanckenhagen, Phys. Rev. B **29**, 4079 (1984).

[49] A.Z. Menshikov, G.A. Takzey, and A. Ye. Teplylykh, Phys. Met. Metall. **54**, 41 (1982).

[50] R.G. Aliken, T.D. Chemang, J.S. Kouvel, and H. Hurdequint, J. Magn. Magn. Mater. **30**, L1, (1982).

[51] L.M. Kistler and S.M. Bhagat J. Phys. C **15**, L929 (1982).

[52] V Manves, R.A. Brand, W. Kenne, and R. Marx, Solid State Comm. **48**, 871 (1983).

[53] F. Keffer in Handbuch der Physik, Vol. XVIII/2, edited by S. Flugge Springer Verlag, Berlin, 1966).

[54] E.C. Stoner, Proc. Roy. Soc. (London) **A 165**, 372 (1938).

[55] E.D. Thompson, E.P. Wohlfarth, A.C. Bryan, Proc. Phy. Soc. **83**, 59 (1964).

[56] P. Rodes and E.P. Wohlfarth, Proc. Roy. Soc. (London) **A 273**, 247 1963.

[57] J. Mathon and E.P. Wohlfarth, Proc. Roy. Soc. (London) **A 302**, 409 (1968).

[58] D.M. Edwards and E.P. Wohlfarth, Proc. Roy. Soc. (London) **A 303**, 127 (1967)

[59] E.P. Wohlfarth, J. Magn. Magn. Mater. **7**, 113 (1978).

[60] J. S. Dugdale in The Structures and Properties of Solids 5 - The Electrical Properties of Metals and Alloys (Edward Arnold, London, 1977).

[61] N.F. Mott, Proc. Phys. Soc. **47**, 571 (1935); Proc. Roy. Soc. (London) **A 153**, 699 (1936).

[62] A.H. Wilson, Proc. Roy. Soc. (London) **A 167**, 580 (1938).

[63] W.G. Baber, Proc. Roy. Soc. (London) **A 158**, 383 (1937).

[64] T. Kasuya, Prog. Theo. Phys. (Kyoto) **22**, 227 (1959).

[65] I. Mannari, Prog. Theo. Phys. (Kyoto) **22**, 335 (1959).

[66] D.A. Goodings, Phys. Rev. B. **132**, 542 (1963).

[67] R. Richter, M. Wolf, and F. Goedsche, Phys. Stat. Solidi B **95**, 473 (1979).

[68] O. Laborde, P. Radhakrishna, J. Phys. F : Metal Phys. **3**, 1731 (1973).

[69] N. Rivier, J. Phys. F : Metal Phys. **4**, L249 (1974).

[70] N. Rivier and J. Adkins, J. Phys. F: Metal Phys. **5**, 1745 (1975).

[71] P. J. Ford and J. A. Mydosh, Phys. Rev. B **14**, 2057 (1976).

[72] J.A. Mydosh, P.J. Ford, M.P. Kawarta, and T.E. Whall, Phys. Rev. B **10**, 2845 (1974).

[73] K. H. Fischer, Z. Phys. B **34**, 45 (1979).

[74] J.M. Ziman, Phil. Mag. **6**, 1013 (1961).

[75] R. Evans, D.A. Greenwood, and P. Loyd, Phys. Lett. A **35**, 71 (1971).

[76] S.R. Nagel, Phys.Rev. B **16**, 1694 (1977).

[77] D. Markowitz, Phys. Rev. B **15**, 3617 (1977).

[78] P.J. Cote and L.V. Meisel, Phys. Rev. Lett. **39**, 102 (1977).

[79] N. Rivier and M.J. Zuckermann, Phys. Rev. Lett. **21**, 904 (1968).

[80] J. Kastner, H.J. Schmit, and E.F. Wasserman, Solid State Commun. **33**, 527 (1980).

[81] T.K. Kim, S. Ishio, and M. Takahashi, Proc. 4th Int Conf. on Rapidly Quenched Metals. Sendai (edited by T. Masumoto and K. Suzuki), Vol. 2, p. 1323 (1981).

[82] R. Cochrane, R. Harris, J. Ström-Olsen and M. Zuckerman, Phys. Rev. Lett. **35**, 676 (1975).

[83] C.C. Tsuei, Solid State Commun. **27**, 1591 (1978).

[84] P.W. Anderson, B.I. Halperin, and C.M. Verma, Phil. Mag. **25**, 1 (1972).

[85] W.A. Philips, J. Low Temp. Phys. **7**, 351 (1972).

[86] Ö. Rapp, J.E. Grindborg, and K.V. Rao, J. Appl. Phys. **49**, 1733 (1978).

[87] J.L. Black and B.L. Gyorffy, Phys. Rev. Lett. **41**, 1591 (1978).

[88] J.L. Black, K. Vladar, and A. Zawadowski, Phys. Rev. B **26**, 1559 (1982).

[89] G. Bergmann, Phys. Rep. **107**, 1 (1984).

[90] B. L. Altshuler and A. G. Aranov, Solid State Commun. **30**, 115 (1979); in *Electron Interactions in Disordered Solid*, edited by A.L. Efros and M. Pollak (North-Holland,Amsterdam, 1985).

[91] M.A. Howson, J. Phys. F : Metal Phys., **14**, L25 (1986).

[92] Ö. Rapp, S.M. Bhagat, and H. Gudmundson, Solid State Commun. **42**, 741 (1982).

[93] M. Oliver, J. O. Ström-Olsen, Z. Altounian, R.W. Cochrane, and M. Trudeau, Phys. Rev. B **33**, 2799 (1986).

[94] R. W. Cochrane and J. O. Störm-Olsen, Phys. Rev. B **29**, 1088 (1984).

[95] A. Das and A. K. Majumdar, Phys. Rev. B **43**, 6042 (1991).

[96] S. Banerjee and A. K. Roychowdhury, Phys. Rev. B **50**, 8195 (1994).

[97] S. Chakraborty and A.K. Majumdar, Phys. Rev. B **53**, 6235 (1996).

[98] M. Oliver, J. O. Störm-Olsen, and Z. Altounian, Phys. Rev. B **35**, 333 (1987).

[99] Wei Wei, G. Bergmann, and Ralf-Peter Peters, Phys. Rev. B **38**, 11751 (1988).

[100] G. Bergmann and H. Beckmann, Phys. Rev. B **52**, R15 687 (1995).

[101] A. Sahnoune, J. O. Ström-Olsen, and A. Zaluska, Phys. Rev. B **46**, 10269 (1992).

[102] P.J. Cote and L.V. Meisel in Glassy Metals I, edited by H.J. Güntherodt and H. Beck (Springer, Berlin, 1981).

[103] M. Gurvitch, Phys. Rev. B **28**, 544 (1983).

[104] R.B. Laughlin, Phys. Rev. B **26**, 3479 (1982).

[105] C.Y. Wu and J.J. Lin, Z. Phys. B **93**, 269 (1994); J.J. Lin, C.Y. Wu, and Y.D. Yao, Phys. Rev. B **48**, 4864 (1993).

[106] M. Gurvitch, Phys. Rev. B **24**, 7404 (1981).

[107] T.K. Nath and A.K. Majumdar, Phys. Rev. B **53**, 12148 (1996).

[108] H.C. Van Elst, Physica **25**, 708 (1959).

[109] J. Smit, Physica **16**, 612 (1951).

[110] I.A. Campbell, A. Fert, and O. Joul, J. Phys. C **3**, S95 (1970).

[111] I.A. Campbell, A. Fert, and O. Joul, J. Phys. F : Metal Phys. **6**, 849 (1976).

[112] I.A. Campbell, A. Fert, and O. Joul, J. Magn. Magn. Mater. **5**, 23 (1977).

[113] T.R. McGuire and R.I. Potter, IEEE Trans. Magnetics **MAG-11**, 1018 (1975).

[114] A.P. Malozemoff, Phys. Rev. B **32**, 6080 (1985).

[115] L. Berger, P.P. Freitas, J.D. Warner, and J.E. Schmidt, J. Appl. Phys. **64**, 5459 (1988).

[116] L. Berger, J. Appl. Phys. **67**, 5549 (1990).

[117] J. Banhart and H. Ebert, Europhys. Lett. **32**, 517 (1995).

[118] M.T. Béal-Monod and R.A. Weiner, Phys. Rev. B **170**, 552 (1968).

[119] Abhijit Mookerjee, J. Phys. F : Metal Phys. **10**, 1559 (1980).

[120] A.K. Nigam and A.K. Majumdar, Phys. Rev. B **27**, 495 (1983).

[121] B.L. Altshuler, A.G. Aronov, A.I. Larkin, and D. Khmelnitskii, Sov. Phys. JETP **54**, 411 (1981).

[122] H. Fukuyama, in Anderson Localisation, edited by T. Nagaoka and H. Fukuyama (Springer, Berlin, 1982).

[123] D.V. Baxter, R. Richer, A.L. Trudeau, R.W. Cochrane, and J.O. Ström-Olsen, J. Phys. France **50**, 1673 (1989).

[124] J.B. Bieri, A. Fert, G. Creuzet, and A. Schuhl, J. Phys. F : Metal Phys. **16**, 2009 (1986).

[143] K. Rhie, D.G. Naugle, Beom-hoan O, and J.T. Markert, Phys. Rev. B **49**, 12688 (1994); **48**, 5973 (1993).

[144] J. Kondo, Prog. Theor. Phys. (Japan) **27**, 772 (1962).

[145] Yu. Kagan and L.A. Maksimov, Sov. Phys. Solid State **7**, 422 (1965).

[146] R. Karplus and J.M. Luttinger, Phys. Rev. **95**, 1154 (1954).

[147] J. Smit, Physica **24**, 39 (1958); **21**, 877 (1955).

[148] A.K. Majumdar and L. Berger, Phys. Rev. B **7**, 4203 (1973).

[149] D. Müller, J.W. Schünemann, and K. Bärner, J. Magn. Magn. Mater. **110**, 161 (1991).

[150] H. Ashworth, D. Sengupta, G. Schnakenberg, L. Shapiro, and L. Berger, Phys. Rev. **185**, 172 (1969).

[151] E.I. Kondorskii, Sov. Phys. JETP **28**, 291 (1969).

[152] L. Berger, Physica **30**, 1141 (1964).

[153] L. Berger, Phys. Rev. **138**, A1083 (1965).

[154] R.C. O'Handley, Phys. Rev. B **18**, 930 (1978); R.C. O'Handley and L. Berger, Int. Phys. Conf., Ser. No. 39, Chapter 6, P. 477 (1978).

[155] R.C. O'Handley, Phys. Rev. B **18**, 2577 (1978).

[156] L. Berger, AIP Conf. Proc. **34**, 355 (1976).

[157] J. Friedel, Del. Nuovo. Cemento. **VII**, 287 (1958).

[158] L. Berger, Physica **91B**, 31 (1977).

[159] B. Velicky, S.Kirkpattrick, and H. Ehrenreich, Phys. Rev. B **175**, 747 (1968).

[160] Hideo Hasegawa and Junjiro Kanamori, J. Phys. Soc. (Japan) **33**, 1599 (1972); **33**, 1607 (1972).

[161] H. Sato, S.A. Werner, and R. Kikuchi, J. Phys. Colloq. (Paris) **35**, C4-23 (1974).

[162] N. Cowlam and A. M. Samah, J. Phys. F: Metal Phys. **11**, 27 (1981).

[163] B. R. Coles, Physica **91B**, 167 (1977).

[164] A.Z. Men'shikov and A. Ye. Teplykh, Phys. Met. Metall. **40**, 174 (1975).

[165] R.M. Bozorth, Ferromagnetism (Van Nostrand, New York, 1959).

[166] A.K. Gangyopadhyay, R.K. Ray, and A.K. Majumdar, Phys. Rev. B **30**, 6693 (1984).

[167] A.Z. Men'shikov, N.N. Kuzmin, V.A. Kazantsev, S.K. Sidorov, and V.N. Kalinin, Phys. Met. Metall. **40**, 174 (1975).

[168] A.K. Majumdar and P.V. Blanckenhagen, J. Magn. Magn. Mater **40**, 227 (1983).

[169] V.I. Pecherskaya, D. N. Bol'shutkin, and A. V. Butenko, Sov. J. Low Temp. Phys. **15**, 9 (1989).

[170] A. V. Butenko, D. N. Bol'shutkin, and V. I. Pecherskaya, Sov. Phys. JETP **71**, 983 (1990).

[171] S. Banerjee and A.K. Roychowdhury, Phys. Rev. B **52**, 3452 (1995); T.K. Nath and A.K. Majumdar, J. Appl. Phys. **70**, 5828 (1991).

[172] A.K. Gangyopadhyay, R.K. Ray, and A.K. Majumdar, Phys. Rev. B **30**, 1801 (1984).

[173] A.K. Majumdar and R.D. Greenough, J. Magn. Magn. Mater. **59**, 57 (1986).

Chapter 2

Experimental Details

Sample preparation and their characterisation, cryostat design, and different aspects of measurement techniques are described briefly in this chapter. In this thesis work, measurements are carried out on a total of 20 samples of two different alloy series, namely γ-CuMn[1] and γ-NiFeCr[2], which are prepared in our institute. The cryostats and the measurement techniques used in the present study are designed and developed during this period.

2.1 Sample preparation and characterization

2.1.1 Sample preparation

Samples of both CuMn (five samples) and NiFeCr (fifteen samples) alloy series are prepared by induction melting of required amount of "spec-pure" grade (5N purity) constituent elements, obtained from Johnson - Mathey Inc. (England). Initially the pure elements are cleaned with organic solvent and then etched with dilute HNO_3, after which the required amounts are cut and weighed carefully. A water - cooled induction furnace with a maximum power of 7 kW, fed by an "Ajax Magnothermic Converter" (which converts the line - frequency of 50 Hz to a value between 20 to 40 kHz depending on power consumption), is used for melting. The required elements are first kept in a high quality alumina crucible which is then placed in a graphite susceptor. Now the whole thing (graphite susceptor along with crucible) is put in a vacuum - sealed quartz tube inside the furnace. The quartz tube is repeatedly evacuated to 10^{-3} torr and flushed with high purity argon gas. Finally, it is sealed after filling with argon gas at much less than atmospheric pressure. During

the heating process, an optical pyrometer is used to monitor the increase in temperature. As soon as the elements get melted, the furnace is turned off to cool the melt in the furnace. For further homogenization, the alloy ingot is put in a quartz capsule which is then evacuated and flushed with argon gas repeatedly. The capsule is finally sealed with a partial pressure of argon gas (a few mm) and put in a vertical furnace for 48 hours at a temperature slightly less than the melting point of the alloy (for CuMn it is 900 ^{0}C while for NiFeCr it is 1150 ^{0}C; for details see phase diagrams in Chapter 1 (Figs.1.7 and 1.9). The ingot is then dropped fast in water to quench it to room temperature. This water quenching is very important for this kind of alloys for retaining their high temperature crystallographic phase (γ - phase) as well as the random substitutional disorder without chemical clustering[1, 2]. The alloy ingot is now swaged, cold - rolled and cut into various shapes for different measurements. To remove strains introduced in the cold - working processes, the sample pieces are annealed for 24 hours at 900 ^{0}C (for both the alloy series) in sealed quartz capsules under argon atmosphere (a few mm pressure) and then water - quenched

2.1.2 Sample characterization

X-ray diffraction

The crystallographic fcc phase (γ - phase) of both CuMn and NiFeCr alloy series are checked using the powder x-ray diffraction technique by employing a *Rich Seifert Isobyeflex 2002 diffractometer* with CuK_α radiation (λ = 1.5406 Å) as the source. The scanning is done from 2θ = 10 to 150^0 with a speed of 1.2 degrees / minute.

SEM and EDXA analysis

The nominal composition of the alloys are checked by *energy dispersive x-ray analysis* (EDXA) using JEOL (model JSM 840A) scanning microscope and KEVEX (model 2003) multichannel analyser. The instrument is calibrated using "spec-pure" grade pure constituent elements. The composition is checked at several places on the sample piece. The diameter of the probe area is varied from (0.1 - 1) micron by changing the applied probe current. It is also essential to ensure alloy homogenization. The actual composition in both the alloy series is found within 5% of the minor constituents.

2.2 Experimental set - up

Fabrication, associated with the installation of a new liquid helium plant (KOCH - 1400, 20 lt/hr), had started from the very beginning of this thesis work. Later, two experimental set-ups were developed for measurements of electrical resistivity, Hall effect, and magnetoresistance in the temperature range of 1.2 to 300 K. Both of them use locally - made glass dewars, where the liquid helium dewar is hung inside the liquid nitrogen dewar. Before starting an experiment, the vacuum jacket of the helium dewar is evacuated to 10^{-2} torr. Liquid nitrogen is filled in the the outermost dewar and after attaining a temperature below 85 K in the sample zone, liquid helium is slowly transferred into the inner dewar from a 15 litre helium vessel. Enough time is allowed for the sample zone to reach 4.2 K and then by pumping on the He^4 bath, using a high - speed Kinney pump, the lowest temperature of 1.2 K is attained.

2.2.1 Electrical resistivity set - up and measurement techniques

The resistivity cryostat is mainly made of three parts : (1) a brass flange on the top on which electrical feedthroughs, liquid He-transport port and pumping ports are provided, (2) in the middle, a thin - walled stainless steel tube (wall thickness = 0.1 mm) is attached (soft soldered) between the top flange and a small bottom flange (made of brass), and (3) a sample holder with its accessories. In Fig.2.1, the dewars and the cryostat assembly are shown schematically. The sample region in the cryostat is isolated by a demountable single - walled copper can which is attached to the small flange using indium as a low - temperature vacuum seal. During an experiment, this region is evacuated first and then liquid nitrogen and helium are filled in the respective dewars.

The sample holder is made of a solid OFHC (oxygen free high conductivity) copper (Cu) cylinder (diameter(ϕ) = 25 mm and height (h) = 35 mm). The heater wire (manganin with I_{max} = 500 mA) is wound in the middle of the sample holder (along its length) uniformly for a homogeneous heating of the sample (see Fig. 2.1). The sample holder is hung from the small flange by three thin - walled stainless steel tubes which are fixed by soft soldering. Being a bad conductor of heat, the stainless steel tube is very effective in preventing heat leak to the sample holder from the rest of

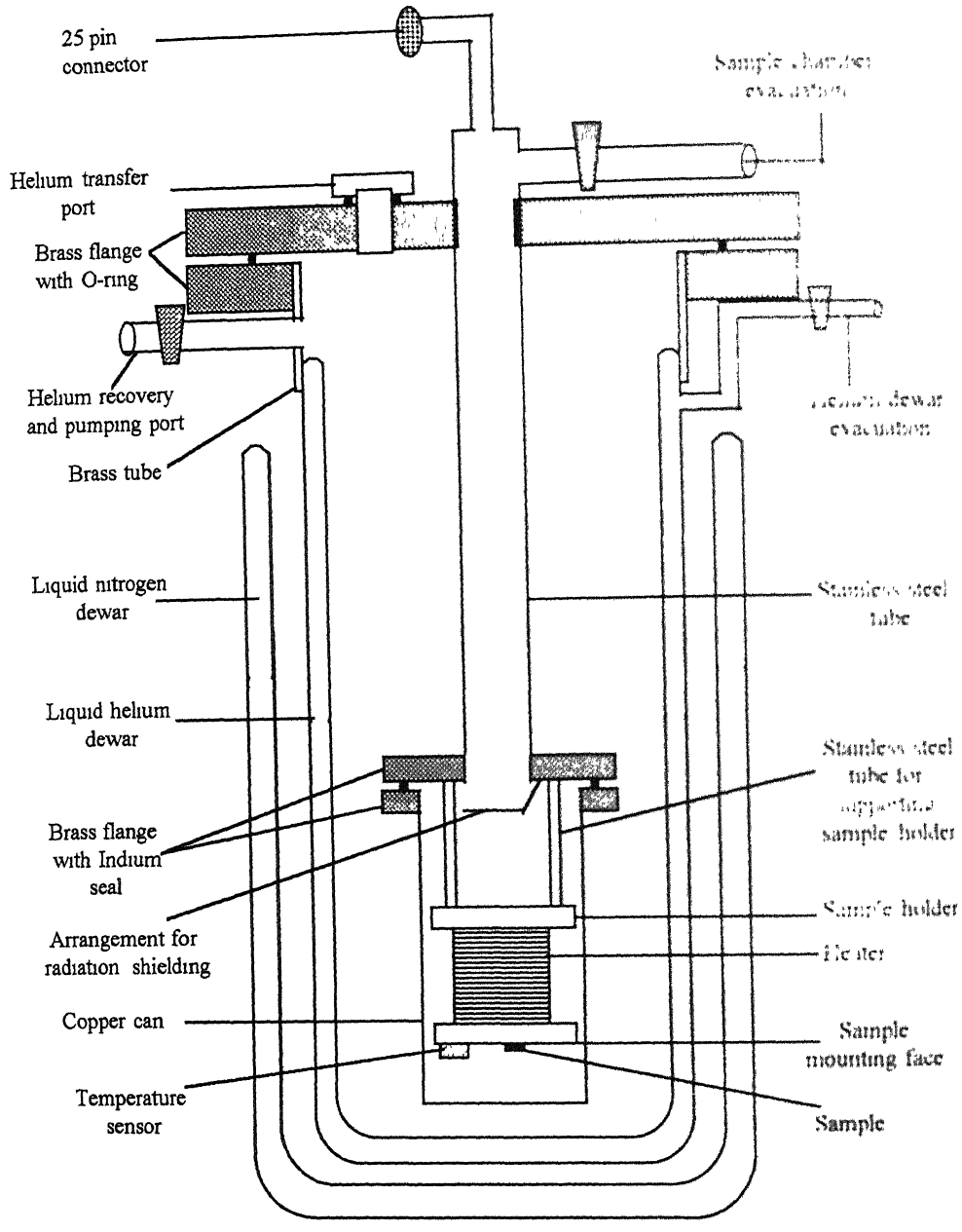

FIG 2.1. Schematic diagram of the cryostat assembly for electrical resistivity measurements.

the cryostat which is at a higher temperature. In addition, a thin - shinned copper strip is attached in between the top of the sample holder and the small flange to reduce radiation loss. On the flat bottom face, the sample is mounted along with a temperature sensor (Fig.2.1). All electrical connections are made from 35 SWG coaxial copper wire. All copper leads are anchored first to the sample holder and then on a copper screw attached to the small flange (not shown in Fig.2.1) to prevent heat leak to the sample and its surrounding where the temperature sensor is attached. This is essential to maintain thermal equilibrium in the sample region. Finally, these wires come all the way to the top brass flange where a 25-pin female connector is used to take the leads out. The temperature is measured using an uncalibrated DT-470 Si-diode (Lake Shore) sensor, which is calibrated with a DT-450 Si-diode sensor (company calibrated) in the temperature range of 1.2 - 300 K. The temperature sensor is mounted very near the sample so that it gives the actual sample temperature.

Measurement technique

The samples ($\simeq$ 20 mm $\times$ 3 mm $\times$ 0.15 mm) are fixed using a thin layer of GE varnish (Oxford Instruments, England) which is a good thermal conductor as well as electrical insulator. This is essential for making a good contact between the sample and the sample holder for attaining thermal equilibrium very fast. The electrical insulation between the sample and the Cu block is checked repeatedly by HIL - 2105 hand-held digital multimeter so as to make sure that the resistance between them is greater than 20 MΩ.

The electrical resistivity is measured using a conventional four - probe dc-technique. The probes are connected by soldering with non-superconducting Zn-Cd alloy, obtained from Oxford Instruments, England. In Fig.2.2, the schematic lay-out of the measuring instruments is shown. For measuring the electrical resistivity, a current in the range of 50 to 100 mA (with a stability better than 10 μA) depending on the sample dimensions and the thermal stability of the sample region is sent by a Keithley 220 programmable current source. The measurement is done in two modes. First one is a sweep - mode which is used for the lowest temperature region (1.2 - 25 K). Here a small heater current is sent by a Keithley 224 current source to increase the sample temperature

very slowly (rate of heating $\simeq$ 1.2 K per hour). During this heating process, the sample region is to be kept in a good vacuum (< 10^{-3} torr). In this mode, data are taken at intervals of 20 - 25 mK with a temperature stability of 2 mK. Hence to complete a measurement till 25 K requires more than 12 hours. On the other hand, the second method (a steady - state mode) is used for the full temperature range from 1.2 to 300 K. The data are taken at intervals of (0.1 - 1) K with a stability of (0.01 - 0.1) K depending on the range of temperature. In this mode, heating is done using a PID (proportional - integral - derivative) temperature controller (Lake Shore, model DRC 93C). The total time required to complete the measurements in the temperature range of (1.2 - 300) K is around 12 hours.

The data acquisition and the temperature control is completely automated using a GPIB interface card (National Instrument, USA), a PC/XT (80286), and a turbo-pascal programme developed for this purpose. As soon as the temperature stabilises to within the specified limits, a forward current (+I) is sent across the sample. After a delay of 10 sec, a set of 20 data points for both temperature and voltage are received from the temperature controller and a Keithley 196 digital multimeter (DMM), respectively. This whole process takes about 20 sec. The mean and the standard deviation (SD) of all these data points are calculated immediately for both temperature (mean = T_+ and SD = $\sigma_T(+)$) and voltage (mean = V_+ and SD = $\sigma_V(+)$). Now these mean and SD are stored into the RAM (random access memory) of the PC/XT. If the temperature is stable, the sample current is reversed (-I). The current reversal is needed to eliminate the effect of thermal voltages. A delay of 10 sec is set for the reverse voltage to settle down. Again another set of 20 data points are taken and the calculation of their mean and SD are carried out (mean temperature = T_- and SD = $\sigma_T(-)$, mean voltage = V_- and SD = $\sigma_V(-)$) and stored in the memory. Now, if the temperature is still stable, then the final voltage and temperature are computed as

$$\begin{aligned} V &= (|V_+| + |V_-|)/2 \\ T &= (|T_+| + |T_-|)/2. \end{aligned} \tag{2.1}$$

Here the criteria for a stable temperature defined in the programme are as follows :

1. After the forward current measurement, $\sigma_T(+) \leq \delta T$.

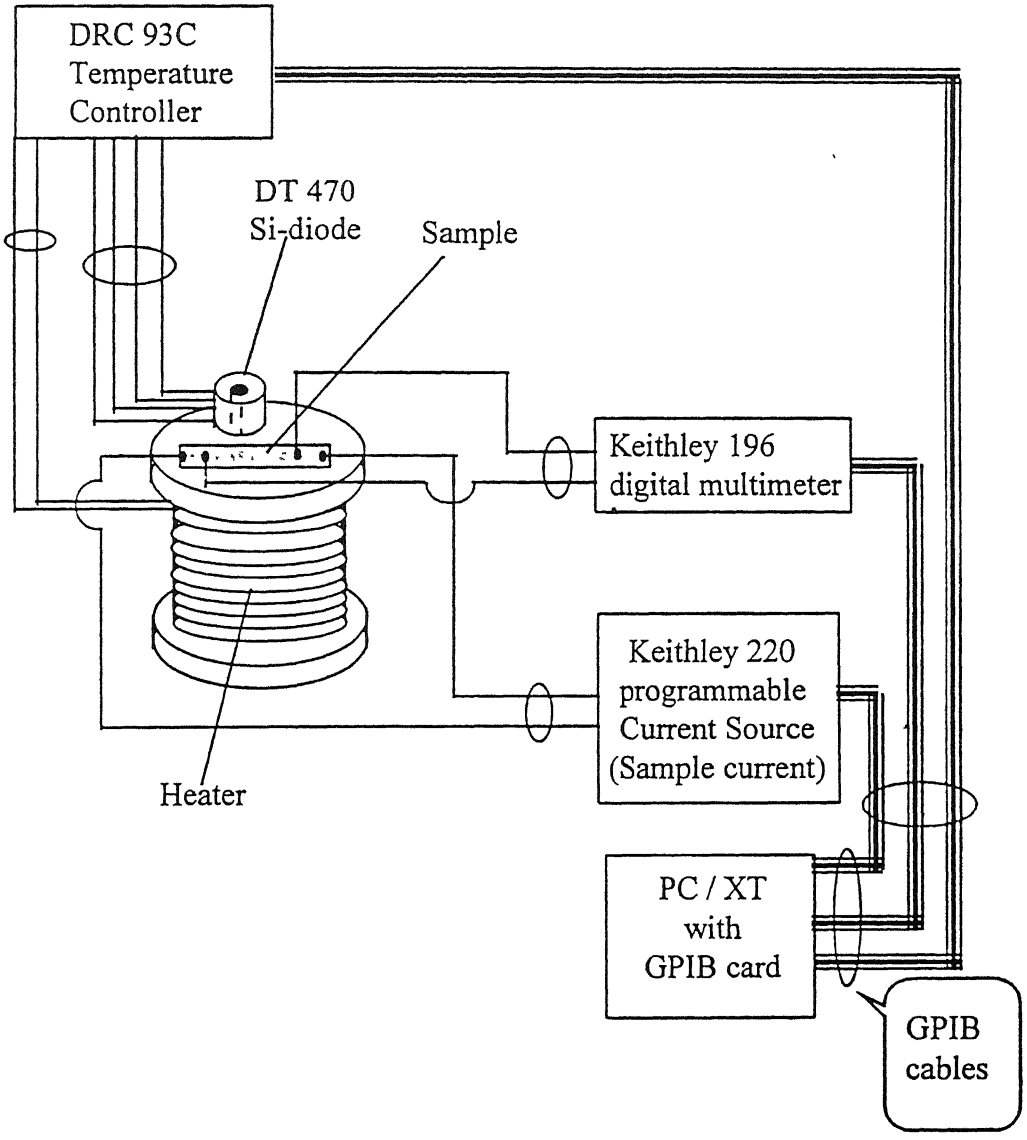

FIG. 2.2. Schematic diagram of the sample holder and the lay-out of the electrical connections for measuring electrical resistivity in the temperature range of 1.2 to 300 K.

2. After the reverse current measurement, $\sigma_T(-) \leq \delta T$.

3. The final condition is $|(T_+ - T_-)| \leq \delta T$.

Here δT has a preassigned value which is set at the very beginning of the measurements. It decides the temperature dispersion within which the data acquisition is permissible. Once the data acquisition is done, the programme will fix the next higher temperature (i.e., $T + \Delta T$ where ΔT has another preassigned value) and, as a result, the heater current will be increased to attain that temperature. The experimental resolution, $\Delta R/R$ of the present data is better than 5 in 10^5 where R is the resistance.

2.2.2 Hall effect and magnetoresistance set - up

In this set-up, an existing Varian V-3800 series electromagnet (pole-piece diameter = 15 inch and separation = 2.5 inch) is used for providing a magnetic field. Hence, tail - dewars (for both liquid helium and nitrogen) are made so that their lower ends (i.e., tail) can fit between the pole pieces of the magnet. The other arrangements regarding the dewar installation remain almost the same as before. Here, the most crucial point is that the inner diameter of the tail of the He dewar is about 20 mm and, hence, the cryostat as well as the sample holder have to be designed accordingly. A multipurpose cryostat is fabricated for making measurements of Hall effect, magnetoresistance, and magnetostriction by changing sample holders only. In Fig. 2.3, the cryostat along with the dewar - assembly are shown schematically. The cryostat essentially consists of two concentric stainless steel tubes where teflon spacers are used to align them co-axially. The outermost tube is fixed between a large top flange and a small flange at the bottom (both made of brass). On the other hand, the inner tube is soft soldered at the top to a hollow brass tube which ultimately comes out from the middle of the top flange through a vacuum sealed adapter (brass), while at the bottom it is attached to the sample holder through a threaded brass adaptor. In this threaded adaptor, different sample holders can be connected to make different measurements. In this cryostat, a provision for changing the sample alignments with respect to the magnetic field direction is made by rotating the inner - tube from the top. The sample chamber is surrounded by a long thin - walled non - magnetic stainless steel chamber which is evacuated using indium wire seal.

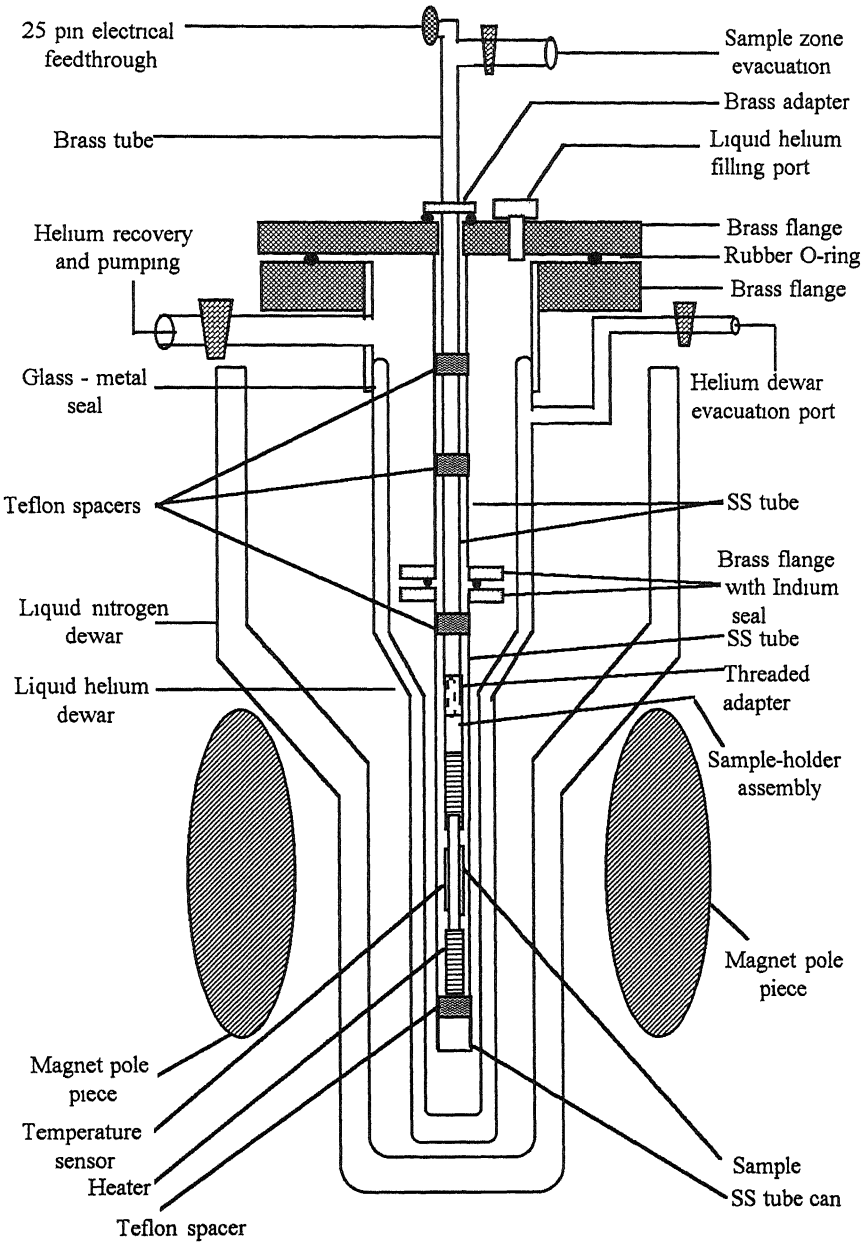

FIG 2.3. Schematic diagram of the multipurpose cryostat assembly to measure both the Hall effect and magnetoresistance.

For the present thesis work, two sample holders are fabricated for the magnetoresistance and Hall effect measurements. Their design is essentially the same and they are shown schematically in Fig.2.4. The sample holders are made of solid OFHC copper rod (diameter = 14 mm and length = 60 mm). For mounting the sample, the middle portion (length = 30mm) of this Cu rod is cut to make a flat face (for Hall effect a rectangular shape (see Fig.2.4a) while for magnetoresistance semi-cylindrical shape (see Fig.2.4b)). However, both the ends (each of length 15 mm) are kept in the cylindrical shape where manganin (heater) wire is wound uniformly for homogeneous heating of the sample zone. At the back of the sample mounting face, a small groove is cut to hold the temperature sensor. For any magnetic measurements, the use of a carbon glass resistor (CGR) as the temperature sensor is preferred because of its low magnetoresistance. In this set-up, a CGR of series CGR-2110 (Lake Shore) is used for temperature measurements. This is calibrated against a DT-450 Si-diode (company calibrated) in the temperature range of 1.2 to 300 K. For electrical connections, 35 SWG co-axial copper wires are used which are twisted before inserting into the cryostat. All the wires are anchored first on the sample holder and then on the brass adaptor to minimize heat leak. Finally all the leads are put inside the inner tube and they ultimately come out from the top brass tube where a 25-pin connector is attached to take these leads out (Fig. 2.3).

Measurement technique for the Hall effect

In the Hall effect set - up, special attention is needed for making voltage - probe contacts. A conventional four - probe dc method is employed to measure the Hall voltage. Theoretically, the Hall probe should be connected on the equipotential line of the sample surface, which is experimentally very difficult to achieve. Hence, during the Hall effect measurements, a misalignment voltage (besides the thermal voltage) always comes into play which needs to be minimised. However both misalignment and thermal voltages can be eliminated by reversing the magnetic field and the current directions, respectively. A large misalignment voltage seriously affects the resolution of the measurements, unless one makes some special arrangement to suppress it. In the present set-up, the voltage probes are attached with a pressure - contact using nut and screw (made of brass), as shown

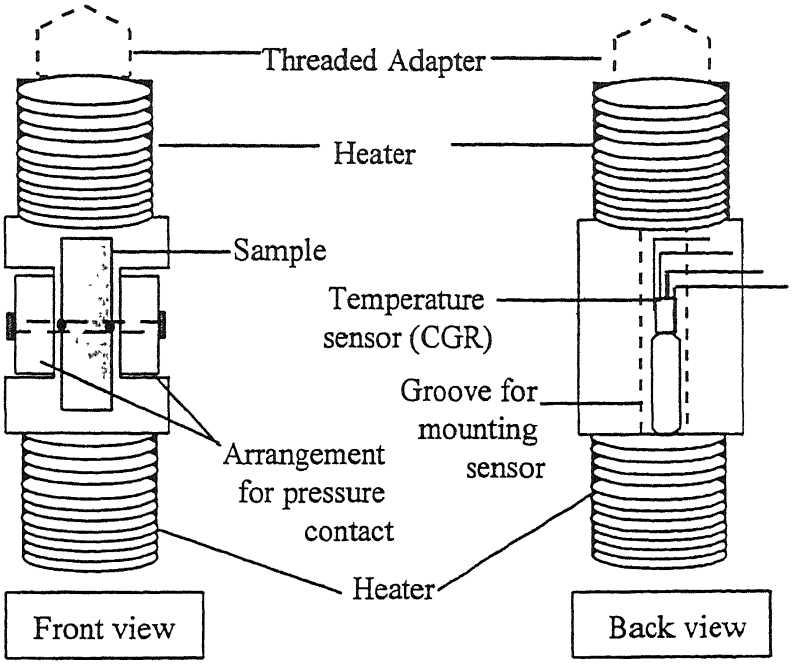

(a) Schematic view of sample holder for the Hall effect measurements.

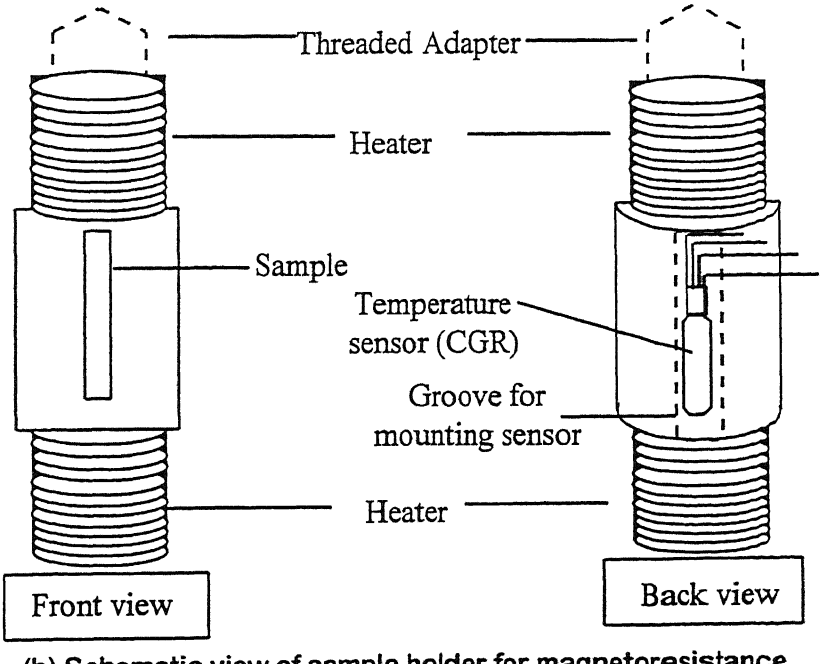

(b) Schematic view of sample holder for magnetoresistance measurements.

FIG. 2.4. Schematic diagram of the front and the back view of the sample holder for (a) the Hall effect and (b) magnetoresistance measurements.

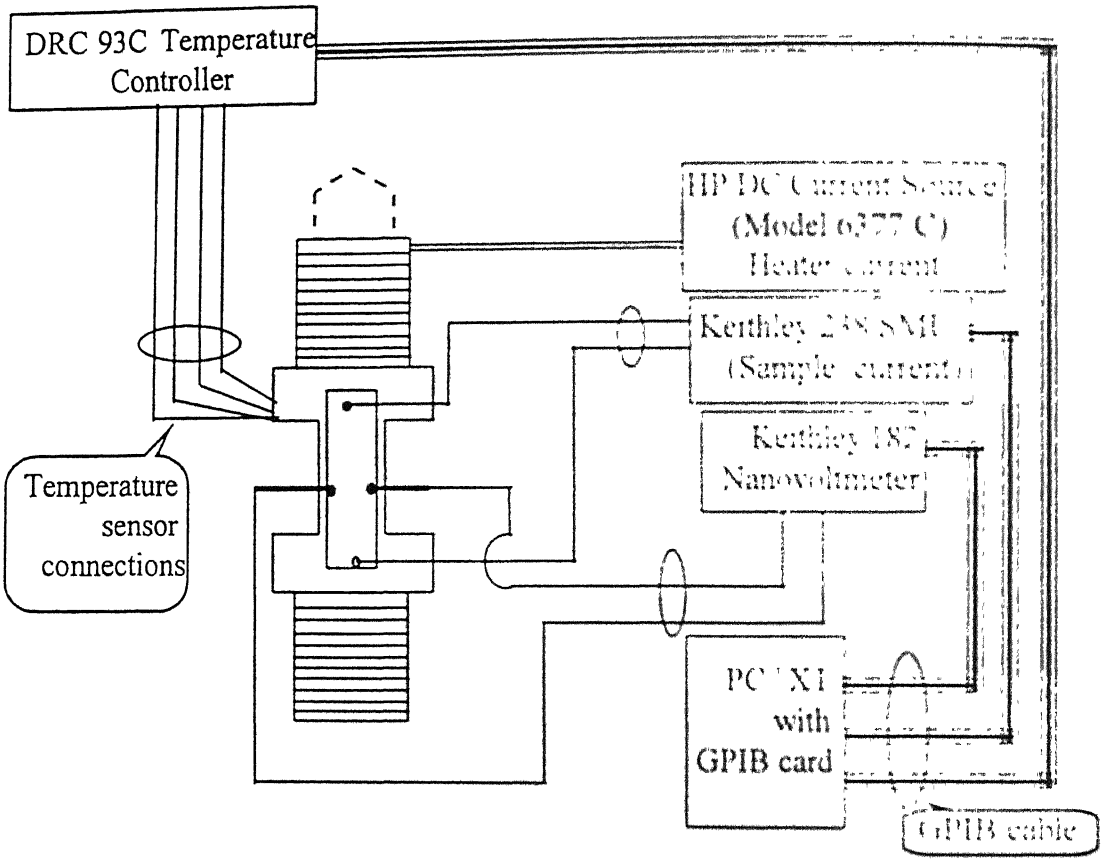

FIG. 2.5. Schematic lay-out of the electrical connections for the Hall effect measurements.

Fig.2.4a (front view). This is adjusted laterally to minimise the misalignment voltage. A small groove is cut on both the sides of the sample mounting face where two fibre - glass - reinforced plastic (a special material developed in IIT / Kanpur) pieces are used to fix the voltage probes. The advantage of using this plastic material is that (1) its temperature coefficient of expansion is almost comparable to those of metals and this helps in retaining the contact at low temperatures and (2) it is a good electrical insulator. On the other hand, the current probes are connected using non-superconducting Zn-Cd solder. The samples for the Hall effect measurements are of dimension 25 mm × 5 mm × 0.15 mm. It is important to note that the measured Hall voltage (V_H) depends only

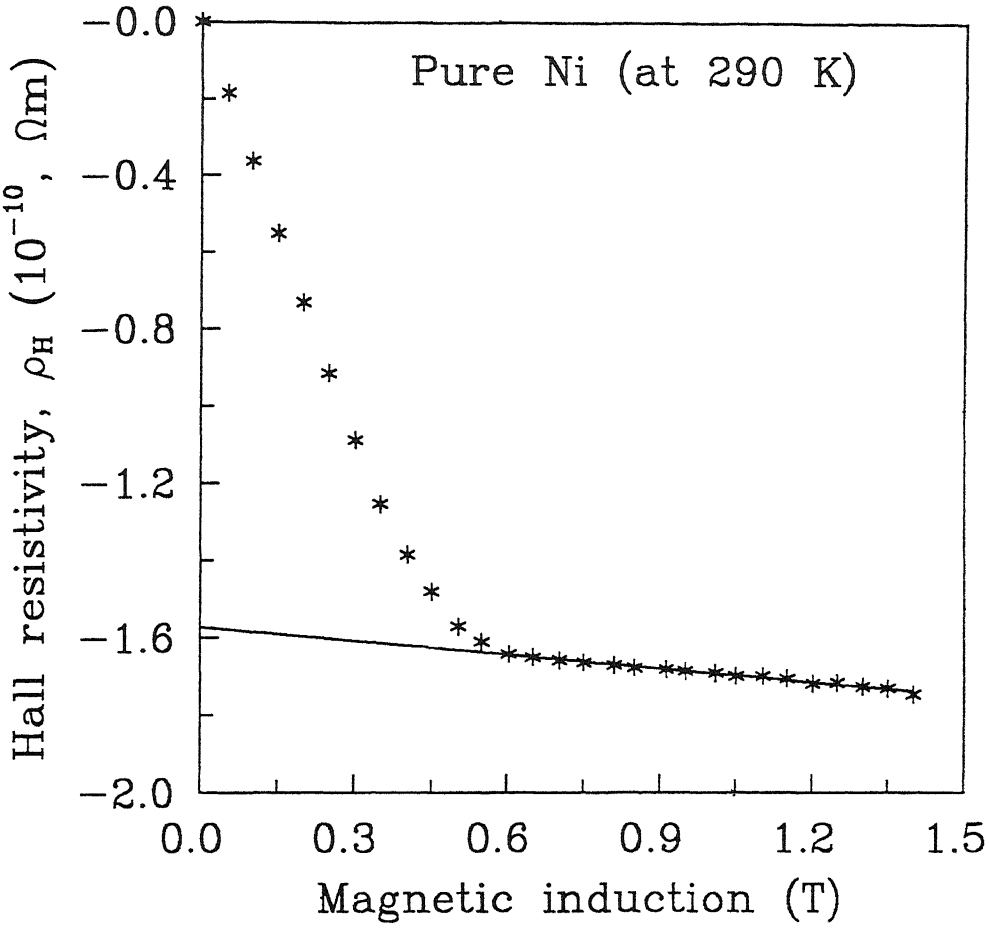

FIG. 2.6. Plot of the Hall resistivity against magnetic induction till 1.4 T for pure Ni at 290 K.

on the sample thickness (d) and is given by

$$V_H = E_y b = R_H J_x B_z b = R_H \frac{I_x}{bd} B_z b = \frac{R_H I_x B_z}{d}, \tag{2.2}$$

where R_H is the Hall coefficient, I_x the applied current, B_z the magnetic induction and b the breadth of the sample. Hence to obtain a large Hall voltage, the sample thickness has to be reduced. Another important point in the Hall effect set-up is that the sample has to be properly aligned with the current and the magnetic field directions. In the flat Hall sample, the magnetic induction B inside it is very nearly the same as $\mu_0 H_{ext}$ since the demagnetisation factor (α) is almost equal to 1 (i.e., $B_{int} = B_{ext} - \alpha\mu_0 M_s = \mu_0 H_{ext} + (1 - \alpha)\,\mu_0 M_s$).

The magnetic induction (till 1.4 tesla) is applied using a Varian V-3800 series electromagnet. A current of 250 mA (with stability of better than 50 μA) is sent through the sample from a Keithley 238 high current source measure unit (SMU). The Hall voltage is measured using a Keithley 182 sensitive digital voltmeter (nanovoltmeter) while the sample temperature is measured using a CGR card (Model - 9318C, Lake Shore) and a Lake Shore DRC 93C temperature controller. In Fig.2.5, the schematic diagram of the electrical connection with the measuring instruments is shown. The data acquisition is completely automated using a GPIB card (National Instrument, USA) and a PC/XT. Since the CGR card can only be used to measure the temperature (i.e., without any temperature control) and the magnet power supply does not have any IEEE interface option, the temperature and the magnetic field controls are done manually. The interfacing programme is modified accordingly. The basic principle in the programme, however, remains almost the same as in the electrical resistivity set-up. After each cycle of forward and reverse currents, the measurement is halted (using the PC keyboard and this is included as an option in the interfacing programme) for sometime ($\simeq$ 2 - 3 minutes) to change the magnetic field externally. After getting the required stable field, the measurements are resumed from the point where it was stopped. The temperature control is done using an HP dc current source (Model 6177C) with 10 - turn potentiometer in the 50 mA current range. The temperature stability is found to be better than 0.1 K below 20 K and 0.2 K above it. The magnetic field / induction is measured using an external Hall probe and an RFL gaussmeter (Model 912) where the stability is found to be better than 3×10^{-4} at 1 tesla.

In the present measurements, the misalignment voltage comes out to be $\leq$ 1 μV and the Hall signal is found in the range of (1 to 2) μV with 250 mA sample current. Hence, to have a high resolution of the data, special care is to be taken, e.g., (1) proper electrical insulation of all the leads, (2) electrical shielding and grounding of the whole system at one point, (3) twisting of the wires to reduce flux noise, and (4) proper thermal equilibrium across the sample as well as the copper leads used for the Hall voltage measurements (so that no thermo-emf is generated). As a result, the experimental resolution is found to be better than 0.5%. Further, to eliminate the misalignment and the thermal voltages, the measurements are done at both forward and reverse directions of field and current, respectively. Finally, the Hall voltage (V_H) comes from the combination of four measured

voltages which can be written as

$$V_H = \frac{1}{2}\left(\frac{(V_+(+H,+I) - V_-(+H,-I))}{2} - \frac{(V_+(-H,+I) - V_-(-H,-I))}{2}\right), \qquad (2.3)$$

where + and - signs represent the data taken at forward and reverse directions. It is important to note here that the sign of the Hall voltage is determined from the actual field (H) and current (I) directions. Alternatively, the actual sign of V_H is found by measuring the Hall voltage of a standard ferromagnetic Ni sample at room temperature where both ordinary (R_0) and extra-ordinary Hall (R_s) coefficients are negative (shown in Fig.2.6, where the Hall resistivity ($\rho_H = V_H/I_x$) is plotted against the magnetic induction (B)). After this calibration, the same current and field directions are maintained for the rest of the measurements. The observed values of R_sM_s for pure Ni (see Fig.2.6) comes out to be -1.57 $\times$ 10^{-10} ($\pm$ 0.01) Ωm which are in good agreement with earlier data[3] (1.7 $\times$ 10^{-10} Ωm). This certainly provides confidence in the present experimental set-up and the measurement procedures. Interestingly, the dispersion in the Hall voltage data comes out to be less than 5 nV.

Measurement technique for magnetoresistance

The magnetoresistance measurements are done in both longitudinal ($\parallel$ B) and transverse ($\perp$ B) orientations at 4.2 K in magnetic inductions till 1.4 tesla (provided by the electromagnet, Varian, V-3800), after properly aligning the sample. The samples used here are of the dimension 14 mm $\times$ 3 mm $\times$ 0.15 mm. A conventional four-probe dc method is employed to measure the resistance. A sample current of 100 mA is sent by a Keithley 220 programmable current source and the potential drop across the sample is measured using a $6\frac{1}{2}$ - digit Keithley 196 digital multimeter. In Fig.2.7, the lay-out of the connections with the measuring instruments is shown. The resolution of the data is found to be better than 5 in 10^5. The temperature of the sample region is measured using a CGR thermometer (Series 2110) and DRC 93C temperature controller (Lake Shore). The magnetic field is measured by a gaussmeter (model - 912, RFL Inc., USA) using an external Hall probe placed in between the pole pieces parallel to the sample holder and the poll faces. The data acquisition is completely automated using a GPIB interface card, a PC/XT, and a turbo-pascal programme. As mentioned earlier, the magnetic field is controlled manually. The measurement procedures are

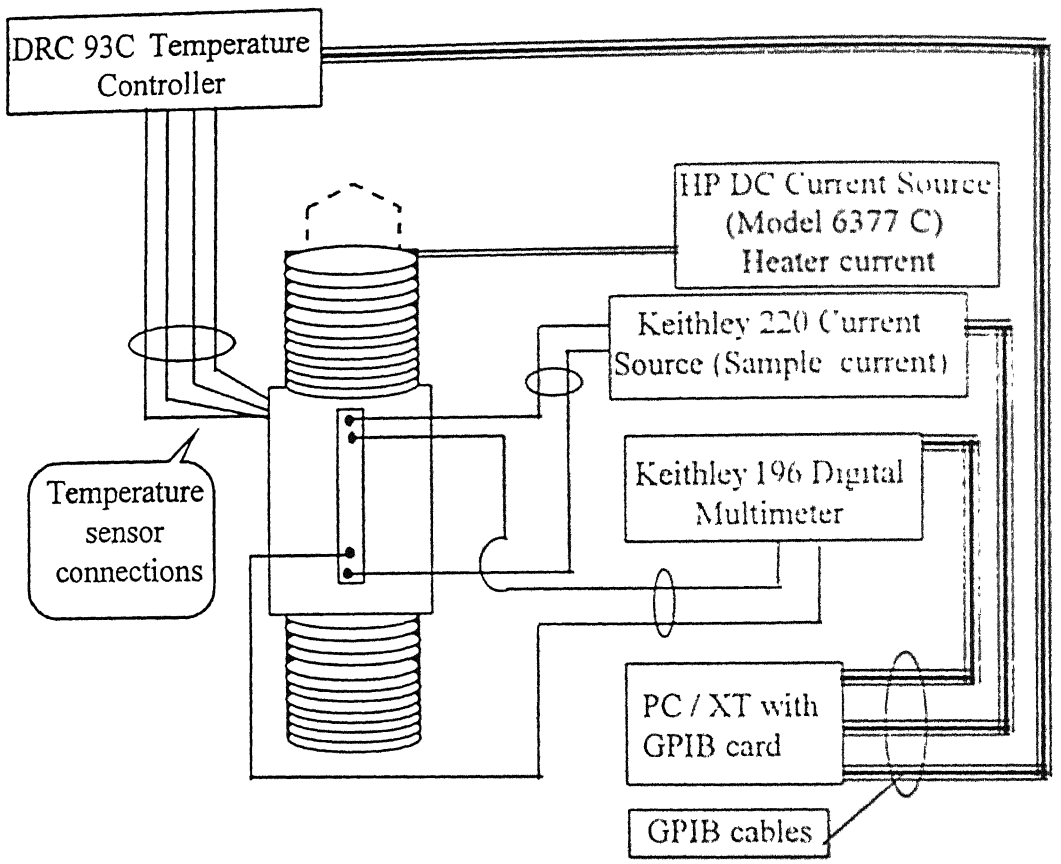

FIG. 2.7. Schematic lay-out of electrical connections for magnetoresistance measurements.

very similar to those of the Hall effect, described above. The only difference is that the reversal of magnetic field is not needed here. However, reversing the current directions is necessary to eliminate thermal voltage. Hence, the final voltage is calculated from the forward and the reverse data using Eq.(2.1).

The high -field magnetoresistance measurements have been made using an ac-resistivity bridge and a 7.5 T superconducting magnet at the University of Giessen, Germany. The data were taken in the sweep mode of the magnet through an automated data acquisition system. The stability at higher temperatures ($T \geq 20$ K) was within 0.1 K whereas it was less than 0.01 K at low temperatures during the 2 hours of a scan. The resolution in the data was about 1 part in 10^5.

2.2.3 Ac-susceptibility set-up and measurement techniques

The ac - susceptibility is measured using an existing set-up and a locally made mutual inductance bridge[4] The basic principle behind this measurement is that when a sample is placed in a ac-field (primary coil), due to the change in mutual inductance, a voltage will appear in the secondary. The value of the ac - susceptibility (χ_{ac}) is found to be proportional to this voltage which is given by

$$V = -\frac{d\phi}{dt} = -N\frac{d(AB)}{dt} = -NA\mu_0\left(\frac{d(M+H)}{dt}\right) = -NA\mu_0\left(\frac{dM}{dH}\frac{dH}{dt} + \frac{dH}{dt}\right), \quad (2.4)$$

or,

$$V = -NA\mu_0(\chi_{ac} + 1)\frac{dH}{dt}, \quad (2.5)$$

where ϕ is the magnetic flux, A the sample cross - section, B the magnetic induction, and H the ac-field ($H = H_0 e^{i\omega t}$).

The experimental set-up consists of glass dewars and a double walled quartz tube where the secondary and the primary coils are fixed. Here two secondary coils are connected in series opposition. This is done to suppress the signal appearing without any sample. However, a small off-balance voltage always remains which is balanced externally to nearly zero by the mutual inductance bridge[4]. It is essential to get a high - resolution off-balance sample signal which is generated after the sample is put inside one of the secondaries. The measurement is done in an ac-field of 1.5 Oe with a frequency 726 Hz in the temperature range of 1.2 to 100 K. The sample voltage is measured in the differential mode of a dual phase lock-in-amplifier while the temperature is measured with a Lake Shore DRC 93C temperature controller using a DT-450 miniature Si-diode (Lake Shore). The data acquisition is completely automated with a GPIB interface card and a PC/AT. However, the temperature is controlled externally by a Hewlett - Packard (HP) dc current source (Model - 6177C).

References

[1] Alok Banerjee, Ph.D. Thesis, Indian Institute of Technology, Kanpur, India, 1992.

[2] A.K. Gangyopadhyay, Ph.D. Thesis, Indian Institute of Technology, Kanpur, India, 1983.

[3] J.P. Jan, in Solid State Physics, edited by F. Seitz and D. Turnbull (Academic, New York 1957), Vol. 5, P. 1.

[4] A. Banerjee, A.K. Rastogi, M. Kumar, A. Das, A. Mitra, and A.K. Majumdar, J. Phys. E Sci. Instrum. **22**, 230 (1989).

Chapter 3

Electrical transport properties

In this chapter, the electrical resistivity (ρ(T)) studies of γ-phase (FCC) binary CuMn and ternary Ni-rich NiFeCr alloys are presented down to 1.2 K. These alloys are all substitutionally disordered with large electrical resistivity values ($\rho_0 \simeq 100\ \mu\Omega$cm, where ρ_0 is the residual resistivity). The mean free path (l_e) of the conduction electrons for the present alloys[1–3], calculated from the relation $\rho = m_e v_F / n e^2 l_e$ using v_F (the Fermi velocity of electron) = 10^6 m/s and n (the carrier concentration) = 10^{29} m^{-3} (taken from the Hall effect data, see Chapter 5), is found out to be 3.5 $\AA$. This is almost of the order of the inter-atomic distance, which is in the range of (4.58 - 4.94) and (3.52 - 3.56) $\AA$ for CuMn[4] and NiFeCr[5] alloys, respectively depending on their composition (obtained from the X-ray diffraction study). In these circumstances, physical phenomena like quantum interference (QIE) and electron - electron interaction (EEI) effects in the weak - localisation limit[2, 6, 7] are quite expected at low temperatures as they are generally observed in amorphous alloys[2]. In fact, the present ρ(T) data have shown resistivity minima below 30 K in both CuMn and NiFeCr alloy series (discussed in details later) which are quite analogous to those of the amorphous alloys.

The prime motivation behind the present study is to identify the physical phenomena responsible for the resistivity minima and also their possible dependence on the alloy compositions and hence their magnetic states. Magnetic scattering will have a dominant role in the electrical resistivity of the present 3d alloys. A knowledge of the magnetic contribution to the resistivity by itself will enrich our understanding of spin - disorder resistivity in concentrated transition metal alloys. In addition to these, phonon contribution is also present. Therefore, it is very interesting to estimate

the magnetic and phonon contributions to the resistivity at low temperatures besides that from the electron - electron interaction effects. This will help us in understanding the role of different competing physical mechanisms responsible for such minima. Here we will describe the data for CuMn alloys first and then those of NiFeCr alloys.

3.1 CuMn alloys

3.1.1 General features of ρ(T) data

High resolution, dc-resistivity data for γ-phase concentrated $Cu_{100-x}Mn_x$ alloys (x = 36, 60, 73, 76, and 83) are taken in the temperature range $1.2 \leq T \leq 30$ K. As it is mentioned earlier (Chapter 1), γ-phase (FCC) Cu-Mn alloys have attracted very special attention due to their complex magnetic phases[8, 9]. The present $Cu_{100-x}Mn_x$ alloys with x = 36, 60, 73, 76, and 83 have exotic magnetic structures at low temperatures. According to the magnetic phase diagram[8] (see Fig.1.8), they are cluster glasses for x = 36, 60, and 73 with T_f between 135 and 149 K and are in the mixed cluster-glass and long-range antiferromagnetic phase for x = 76 and 83 with $T_f \approx$ 145 and 45 K, respectively. Resistivity studies have also shown some interesting features in different regions of Mn concentrations. Resistivity minima in dilute γ-$Cu_{100-x}Mn_x$ (x << 1 at.%) alloys[10] has already been reported and was interpreted as Kondo effect whereas for concentrated alloys (x > 45 at.%), only a rough estimate of the temperatures of the resistivity minima occurring around 20 K and depth of minima ($\frac{\rho(1.2K)-\rho(T_{min})}{\rho(1.2K)}$) of less than 1 % have been reported by Coles[11].

The present ρ(T) data on γ-$Cu_{100-x}Mn_x$ alloys ($36 \leq x \leq 83$) alloys exhibit minima in the range of 2.5 to 24.5 K with the depth of minima of the order of (0.04 - 0.33) %. In Table 3.1, all the details regarding the values of the spin freezing temperature (T_f)[8], the resistivity at 1.2 K, T_{min}, and the depth of minima (%) are given. The present measurements are restricted to 30 K only since the earlier work of Banerjee and Majumdar[8] had already covered, in the same alloy compositions as ours, the temperature range $10 \leq T \leq 300$ K. The raw data (ρ(T) vs T) are presented in Fig. 3.1. Here to get an expanded view of the minima, the plot for the alloy with x = 36 are shown till 20 K only whereas for the others they are shown till 30 K. It is interesting to note that the dispersion in the data is much less than the width of the symbols. The values of T_{min} reported by Coles[11] are

TABLE 3.1. Composition, values of spin - freezing temperature (T_f), resistivity at 1.2 K ($\rho_{1\,2K}$), depth of minimum $\left(\frac{(\rho_{1\,2K}-\rho(T_{min}))}{\rho_{1\,2K}}\right)$ and T_{min} for γ - $Cu_{100-x}Mn_x$ (36 $\leq$x$\leq$ 83) alloys.

$Cu_{100-x}Mn_x$ x (at.%)	T_f (K)	$\rho_{1\,2K}$ ($\mu\Omega$cm)	Depth of minimum (%)	T_{min} (K)
36	135	93	0.04	2.5
60	169	176	0.18	16.5
73	164	184	0.26	16.5
76	145	197	0.33	24.5
83	45	121	0.14	13.5

in good agreement with those of the present investigation, but there it is claimed that no resistivity minima could be observed for x < 45 at. %. However, we have a distinct minimum for x = 36. The resistivity values at 1.2 K for all the alloys are in the range of (93 - 196) $\mu\Omega$cm (see Table 3.1). These values differ by about 5 % from those reported[8] for the same alloy compositions. A typical error of this order is generally there in the measurements of the thickness of the samples and the distance between the voltage probes. The large values of resistivity implies that they are highly disordered materials where the resistivity increases with increasing Mn concentration until x = 76 and then it drops in the Mn-rich x = 83 which, according to Nordheim's rule, is quite expected. So no systematic dependence of T_{min} or the depth of the minima on alloy compositions has been found. However, correlations between the value of the resistivity with T_{min} and the depth of the minima have been observed. They show that the increasing value of resistivity shifts T_{min} to higher temperatures with higher depth of minima. On the other hand, more and more disorder introduced by varying the composition of any alloy system will increase the value of resistivity. Hence it may be concluded that the increasing disorder in alloys can enhance the values of T_{min} as well as the depth of the minima. In Fig. 3.2, we have plotted them against the residual resistivity and found approximate linear relations in both the cases.

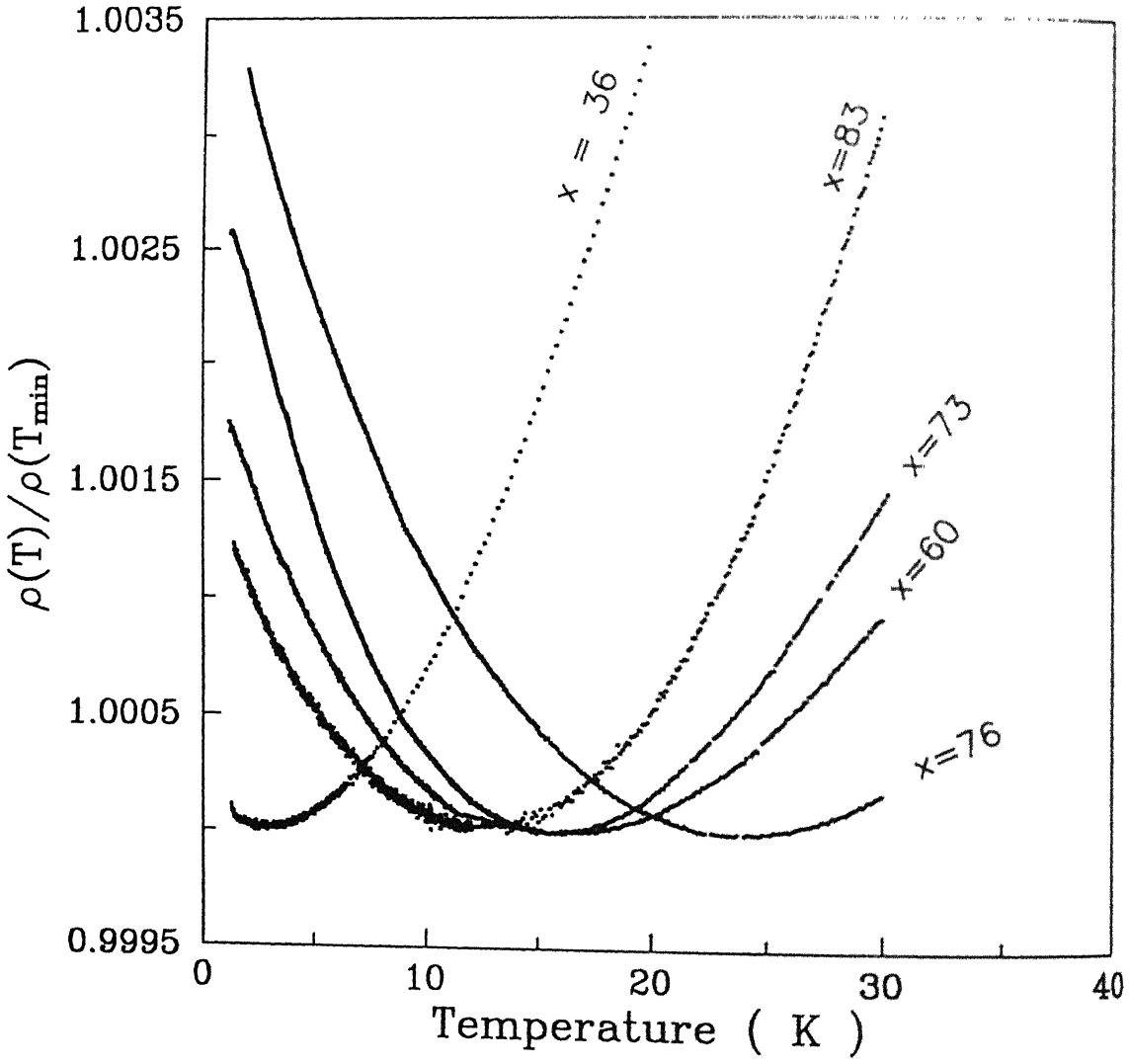

FIG. 3.1. Plot of the resistivity normalised with its value at T_{min} vs temperature for $Cu_{100-x}Mn_x$ alloys with x = 36, 60, 73, 76, and 83 showing distinct minima.

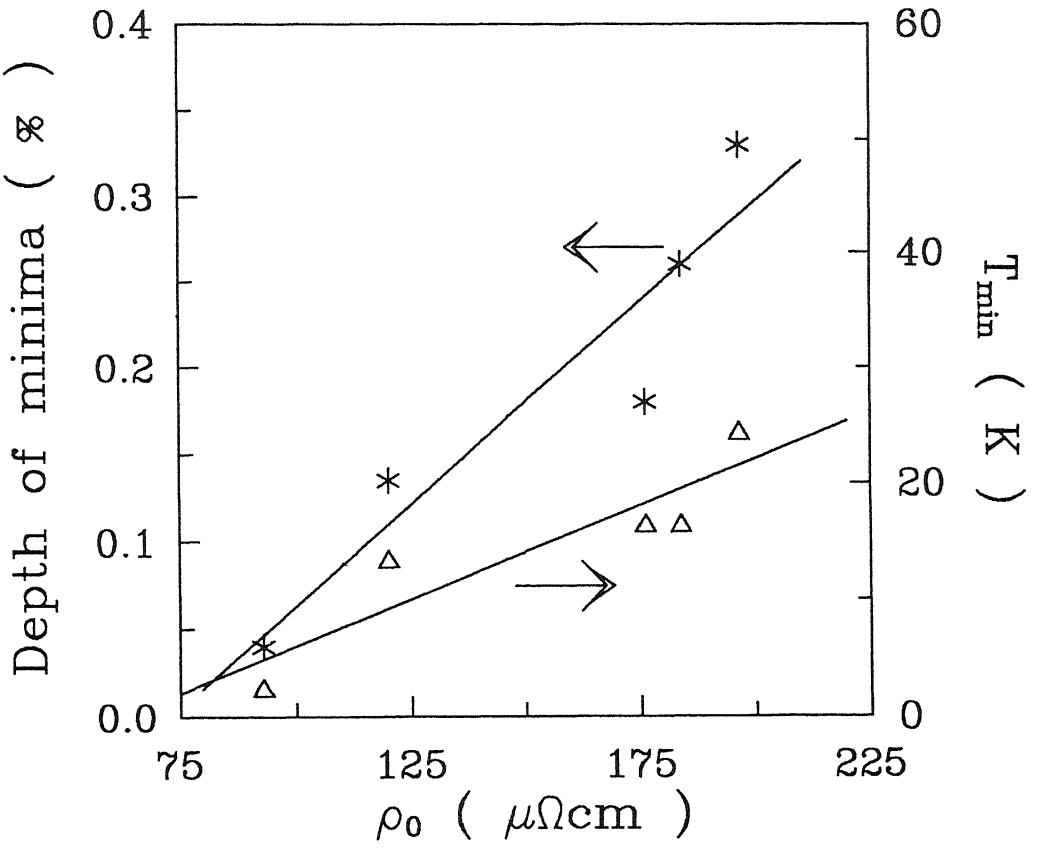

FIG. 3.2. Plot of the dependences of T_{min} and depth of minimum on the values of the residual resistivity of the alloys.

3.1.2 ρ(T) for 1.2 K $\leq$T$\leq$ T_{min}/3

Now we shall examine the various physical phenomena which could describe the resistivity behaviour below minima in $Cu_{100-x}Mn_x$ alloys with x = 60, 73, 76, and 83. The alloy with x = 36 has shown a minimum at 2.5 K. To find the functional dependence of the resistivity of this alloy in the temperature range below T_{min}, measurements have to be done much below 1.2 K which is not accessible to us. So we could not analyse the data of this alloy below T_{min}. However, from the analysis in the temperature range of $T \geq T_{min}$, we have tried to find a plausible dependence of the resistivity below T_{min}. In dilute crystalline alloys, according to the Kondo effect[10] (discussed in details in Chapter 1), the decrease in resistivity with increasing temperature below minima follows

the relation

$$\rho(T) = \rho_0 - m \ln(T). \tag{3.1}$$

Later, theoretical studies of spin-fluctuations in dilute alloys[12] have shown that the resistivity at very low temperatures below the Kondo minima goes as $\rho(T) = \rho_0 - BT^2$. On the contrary, for highly disordered systems, the observed $\sqrt{T}$ dependence of resistivity below minima is generally interpreted in terms of the electron-electron interaction effects in the presence of weak localisation[6, 7]. This theory considers the phase coherence of two electrons both getting localised through elastic impurity scattering. The correction to the electrical conductivity, $\Delta\sigma$, due to the electron-electron (e-e) interaction effect (according to Eq.(1.23)) goes as

$$\sigma(T) = \sigma_0 + \Delta\sigma = \sigma_0 + m_\sigma\sqrt{T}. \tag{3.2}$$

where

$$m_\sigma = \frac{1.3e^2}{4\sqrt{2}\pi^2\hbar}\left[\frac{4}{3} - \frac{3}{2}F_\sigma\right]\left[\frac{k_B}{\hbar D}\right]^{1/2}. \tag{3.3}$$

Here F_σ is the screening constant for Coulomb interaction and D is the diffusion constant. Earlier studies[2, 13–16] on metallic glasses and concentrated crystalline alloys had shown a near-universal value of m_σ which is 6 $(\Omega\text{cmK}^{1/2})^{-1}$. The present alloys are very concentrated and highly resistive, and thus it is very unlikely that they will behave as Kondo alloys. Moreover, the $\rho(T)$ plots (Fig.3.1) below T_{min} in the present alloys go much slower than linear (concave upwards) which can in noway be described by - BT^2 (convex upwards), as predicted by the spin-fluctuation theory[12]. On the other hand, they are highly disordered and so the increase in resistivity below T_{min} may very well be attributed to the e-e interaction effects[1, 6]. For convenience, in the present analysis, Eq.(3.2) has been modified from conductivity to resistivity as

$$\rho(T) = \rho_0 + m_\rho\sqrt{T}, \tag{3.4}$$

where

$$m_\rho = -m_\sigma{\rho_0}^2, \tag{3.5}$$

assuming $m_\sigma\rho_0\sqrt{T} << 1$ and so all the higher order terms of $\sqrt{T}$ are negligible in Eq.(3.4). Whether it is the Kondo effect or the interaction effect, they all occur at temperatures much below T_{min}[1, 2] and hence the temperature range is chosen as 1.2 K $\leq$ T $\leq$ $T_{min}/3$ in the present analysis. In

TABLE 3.2. Composition, values of parameters along with χ^2 for fitting the data to Eq.(3.4) in the temperature range between 1.2 K and $T_{min}/3$, and calculated values of m_σ and density of sates ($N(E_F)$)

$Cu_{100-x}Mn_x$ x (at.%)	ρ_0 ($\mu\Omega$cm)	m_ρ ($\frac{\mu\Omega cm}{K^{1/2}}$)	χ^2 (10^{-10})	m_σ (($\Omega cmK^{1/2})^{-1}$)	$N(E_F)$ (10^{35} $erg^{-1}cm^{-3}$)
60	176.0	-0.15	0.4	4.8	1.4
73	183.7	-0.23	1.7	6.8	2.6
76	196.4	-0.24	2.0	6.2	2.0
83	120.1	-0.08	2.5	5.6	2.6

this range our data have been fitted to both Eqs.(3.1) and (3.4). It is found that the value of the normalised χ^2 of the fit to Eq.(3.4) is an order of magnitude less than that to Eq.(3.1) for all the four samples. Here the normalised χ^2 has been defined as $\frac{1}{N}\sum_{i=1}^{N}\frac{(\rho^i_{raw}-\rho^i_{fit})^2}{\rho^{i\ 2}_{fit}}$. The typical values of χ^2 are 1×10^{-9} and 1×10^{-10} for the ln(T) and $\sqrt{T}$ fits, respectively. The plot (not shown) of the deviation between the raw and the fitted data ($\rho_{raw} - \rho_{fit}$) with temperature for the ln(T) fit (Eq.(3.1)) describes the systematic trend whereas for the $\sqrt{T}$ fit (Eq.(3.4)) it is found to be random for all the alloys. This random nature of deviation can also be considered as a test for the goodness of the fit. Thus it is clear from the above discussion that the present data fit better to the $\sqrt{T}$ dependence of resistivity. The details of the fitting parameters with the values of χ^2 are given in Table 3.2. The coefficient of the $\sqrt{T}$ term, i.e., m_ρ, in these alloys lies in the range ((-0.08) - (-0.24)) $\mu\Omega cm/K^{1/2}$. The calculated values of m_σ (using Eq.(3.5)) are 4.8, 6.8, 6.2, and 5.6 $(\Omega cmK^{1/2})^{-1}$ for x = 60, 73, 76, and 83, respectively and they are in very good agreement with the near-universal value of 6 $(\Omega cmK^{1/2})^{-1}$[2, 13, 14]. A recent study on the electrical conductivity of Fe-rich FeNiCr system[15, 16] below $T_{min}/2$ also found a $\sqrt{T}$ dependence but the values of m_σ are larger than the near-universal one.

According to the generalised Einstein equation[1], the resistivity is related to the density of states at the Fermi level, $N(E_F)$, and the diffusion constant, D, by

$$\rho = \frac{1}{e^2 N(E_F)^2 D} \tag{3.6}$$

On the other hand m_σ is related to D by Eq.(3.3). So the value of $N(E_F)$ can be estimated from Eq.(3.6). Taking $F_\sigma = 0$, the values of D, calculated from Eq.(3.3), are falling between (0.15 - 0.24) cm^2/sec. Hence the values of $N(E_F)$, obtained from Eq.(3.6) and using residual resistivity values from the fitting parameters, are in the range of $(1.4 - 2.6) \times 10^{35}$ erg $^{-1}$cm $^{-3}$. An earlier specific heat study[17] on CuMn had shown that the alloys under the present investigation have their electronic specific heat coefficient (γ) of the order of 10 mJ/moleK^2. Thus the value of $N(E_F)$, calculated from γ using the free-electron theory relation, $N(E_F) = 3\gamma/\pi^2 k_B^2$ is 2.2×10^{35} erg $^{-1}$cm $^{-3}$. This shows that the values of the density of states, obtained in the present work, agree well with those calculated from the experimentally obtained electronic specific heat coefficient[17]. So a good estimation of the density of states at the Fermi level can certainly be made from m_σ. Hence a $\sqrt{T}$ dependence of the resistivity in the temperature range below minima, interpreted as coming from e-e interaction effects, is well justified here in these concentrated $Cu_{100-x}Mn_x$ alloys. On the other hand, the Kondo effect gives a better description of the resistivity behaviour below minima in the dilute regime of this binary alloy system[10]. Therefore CuMn is an unique alloy system where the resistivity minima can be described by both the Kondo and the e-e interaction effects depending on the concentration regime.

3.1.3 ρ(T) for $T_{min}/3 \leq T \leq 30$ K

The analysis of ρ(T) in the temperature range $T_{min}/3 \leq T \leq 30$ K is presented below. Since x = 36 is a rather concentrated alloy with a strong disorder (ρ (1.2 K) = 92.8 $\mu\Omega$cm), one can expect the e-e interaction effects to be responsible for its resistivity minimum as it has already been observed in the case of alloys with higher Mn concentration in the present investigation. Besides the e-e interaction effects, one also expects contributions to the measured resistivity from other competing effects. Phonon contribution, however small it might be at low temperatures, is always present. In addition, the effect of cluster-glass type of magnetic order of the present alloy system will have sufficient magnetic contribution to the resistivity. So the measured resistivity, assuming

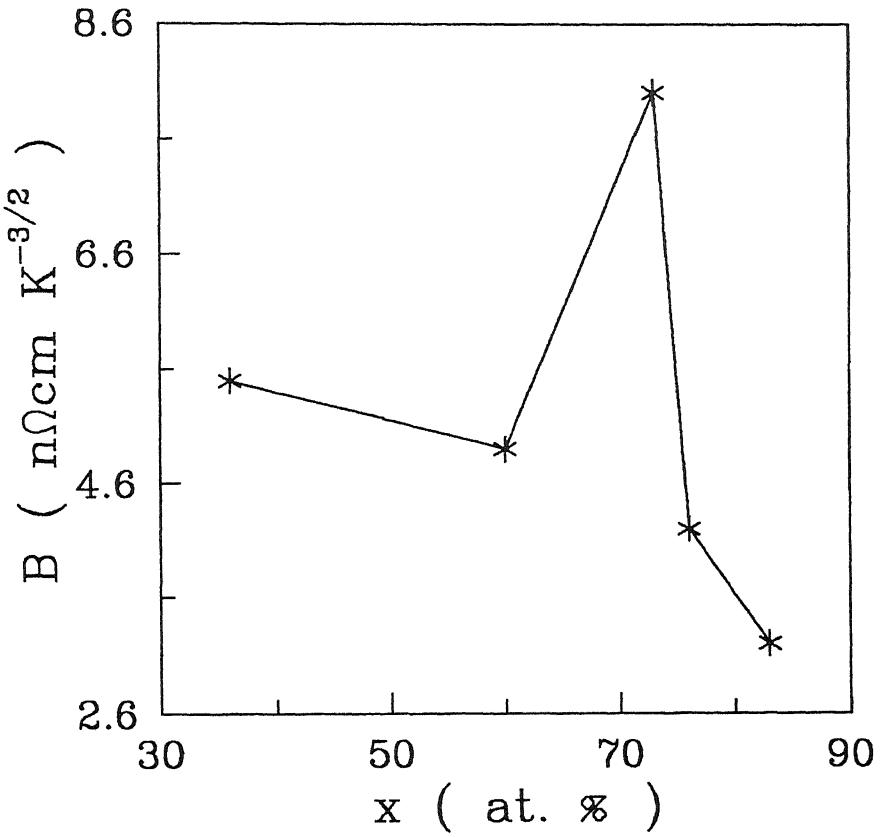

FIG. 3.3. Plot of B (coefficient of the magnetic contribution) of Eq.(3.9) vs Mn concentration, x, in $Cu_{100-x}Mn_x$ alloys.

Matthiessen's rule, is the sum of all those contributions given by

$$\rho(T) = \rho_0 + \rho_{interaction}(T) + \rho_{phonon}(T) + \rho_{magnetic}(T), \tag{3.7}$$

where ρ_0 is the residual resistivity. For phonon contributions, we have taken the standard Bloch - Grüneissen relation

$$\rho_{phonon}(T) = A\left(\frac{T}{\theta_D}\right)^5 \int_0^{\theta_D/T} \frac{z^5 dz}{(e^z - 1)(1 - e^{-z})}, \tag{3.8}$$

where A is a constant and θ_D is the Debye temperature. At very low temperatures (much below the spin-freezing temperature, T_f), magnetic contribution to the resistivity arising from the scattering of conduction electrons by the spin-diffusive modes in spin / cluster glasses, is proportional to $T^{3/2}$,

as proposed by Rivier and Adkins[18]. Later Fischer[19] suggested a (BT^2 - $CT^{5/2}$) (B, C > 0) type of dependence of resistivity at low temperatures ($T < T_f$). In this model, the scattering of conduction electrons by the low-energy spin excitations along with the static disorder of impurity spins was considered. So the final expressions for the resistivity become

$$\rho(T) = \rho_0 + m'_\rho\sqrt{T} + BT^{3/2} + A\left(\frac{T}{\theta_D}\right)^5 \int_0^{\theta_D/T} \frac{z^5 dz}{(e^z - 1)(1 - e^{-z})} \tag{3.9}$$

and

$$\rho(T) = \rho_0 + m'_\rho\sqrt{T} + BT^2 - CT^{5/2} + A\left(\frac{T}{\theta_D}\right)^5 \int_0^{\theta_D/T} \frac{z^5 dz}{(e^z - 1)(1 - e^{-z})} \tag{3.10}$$

The values of θ_D for x = 36, 60, 73, 76, and 83, taken from earlier reports[8], are 325, 305, 305, 325, and 360 K, respectively. First we have fitted the data to Eq.(3.9) and found that they fit very well and the normalised value of χ^2 of the order of 1×10^{-10} is consistent with our experimental accuracy. All the details of the fit are given in Table 3.3. On the other hand, fitting to Eq.(3.10) gives unphysical signs to some of the parameters for all the alloys. The above findings show conclusively that the $T^{3/2}$ type of magnetic contribution along with ρ_0, lattice and e-e interaction effects give the best description of the resistivity in the temperature range between $T_{min}/3$ and 30 K. But the high-temperature (T > 30 K) resistivity study by Banerjee and Majumdar[8] found the (BT^2 - $CT^{5/2}$) (B, C > 0) type of magnetic contribution in the same alloy compositions. They had interpreted the data in terms of the diffusive spin excitations as the dominant source of electron scattering. According to Fischer[19], (BT^2 - $CT^{5/2}$) type of magnetic contribution is valid in the temperature range where the Kondo effect is negligible. This certainly indicates that it is applicable at sufficiently high temperatures above the resistivity minima. It was also shown that instead of (BT^2 - $CT^{5/2}$), a $T^{3/2}$ type of magnetic contribution arises due to the ferromagnetic clusters in spin glasses at temperatures well above minima. However, in CuMn binary alloys the clusters are predominantly antiferromagnetic. On the contrary, the magnetic contribution of $T^{3/2}$ type, as suggested by Rivier and Adkins[18], have their effects in the resistivity at low temperatures ($T \ll T_f$)[20] where resistivity minima are generally found. Therefore both $T^{3/2}$ (Rivier and Adkins, $T \ll T_f$) and (BT^2 - $CT^{5/2}$) or $T^{3/2}$ (both Fischer, $T < T_f$) type of contributions to the resistivity may be expected at different temperature regions in the same alloy compositions where minima occur at temperatures much below T_f. Hence the earlier findings[8] of (BT^2 - $CT^{5/2}$) type of dependence

TABLE 3.3. Composition, values of parameters and χ^2 for fitting the data to Eq.(3.9) in the temperature range between $T_{min}/3$ and 30 K.

$Cu_{100-x}Mn_x$	ρ_0	m'_ρ	B	A	χ^2
x (at.%)	($\mu\Omega$cm)	($\frac{\mu\Omega cm}{K^{1/2}}$)	($\frac{n\Omega cm}{K^{3/2}}$)	($\mu\Omega$cm)	(10^{-10})
36	92.9	-0.05	5.5	77.1	4.7
60	176.2	-0.23	4.9	27.5	1.1
73	183.9	-0.40	8.0	29.2	1.7
76	196.6	-0.35	4.2	81.0	0.3
83	120.1	-0.13	3.2	482	8.2

above 30 K in concentrated CuMn alloys where $T_{min} \simeq 20$ K are quite justified. Another study by Ford and Mydosh[20] had found a $T^{3/2}$ type of magnetic contributions in $Cu_{100-x}Mn_x$ alloys with x$\leq$11 at.% and also in AuCr, AuMn and AgMn systems. There the temperature range of the $T^{3/2}$ fit was 1.5 K $\leq$ T $\leq$ $T_f/4$. The temperature range of the present measurements, 1.2 $\leq$ T $\leq$ 30 K, is below $T_f/4$ (except for the alloy, x = 83, with T_f = 45 K) and this agrees with the range of study of Mydosh and Ford. One interesting point, to be noted from the present findings in concentrated CuMn alloys and also from the earlier report by Ford and Mydosh[20], is that the magnetic contributions of the type $T^{3/2}$ (Rivier and Adkins) are observed in spin glasses only at low temperatures, generally below $T_f/4$. The coefficient B of the $T^{3/2}$ term, according to Rivier and Adkins[18], should have dependence on the magnetic impurity concentration. Earlier resistivity study[20] on $Cu_{100-x}Mn_x$ with x $\leq$ 11 at.% had shown the dependence of B on x. In our case no systematic dependence of B on x has been found (Fig.3.3). But the values of B obtained here are in the vicinity of (3.2 - 8) (nΩ)cm$K^{-3/2}$ which agrees with 7.7 (nΩ)cm$K^{-3/2}$ for the $Cu_{90.3}Mn_{9.7}$ alloy[20].

In Fig.3.4, we have plotted the individual contributions to the resistivity from magnetic, phonon and e-e interactions along with the fitted (sum of all the contributions) and the raw ($\Delta\rho = \rho(T) - \rho_0$) data. Here the fit is so good that the raw and the fitted data are indistinguishable. Moreover, the fits

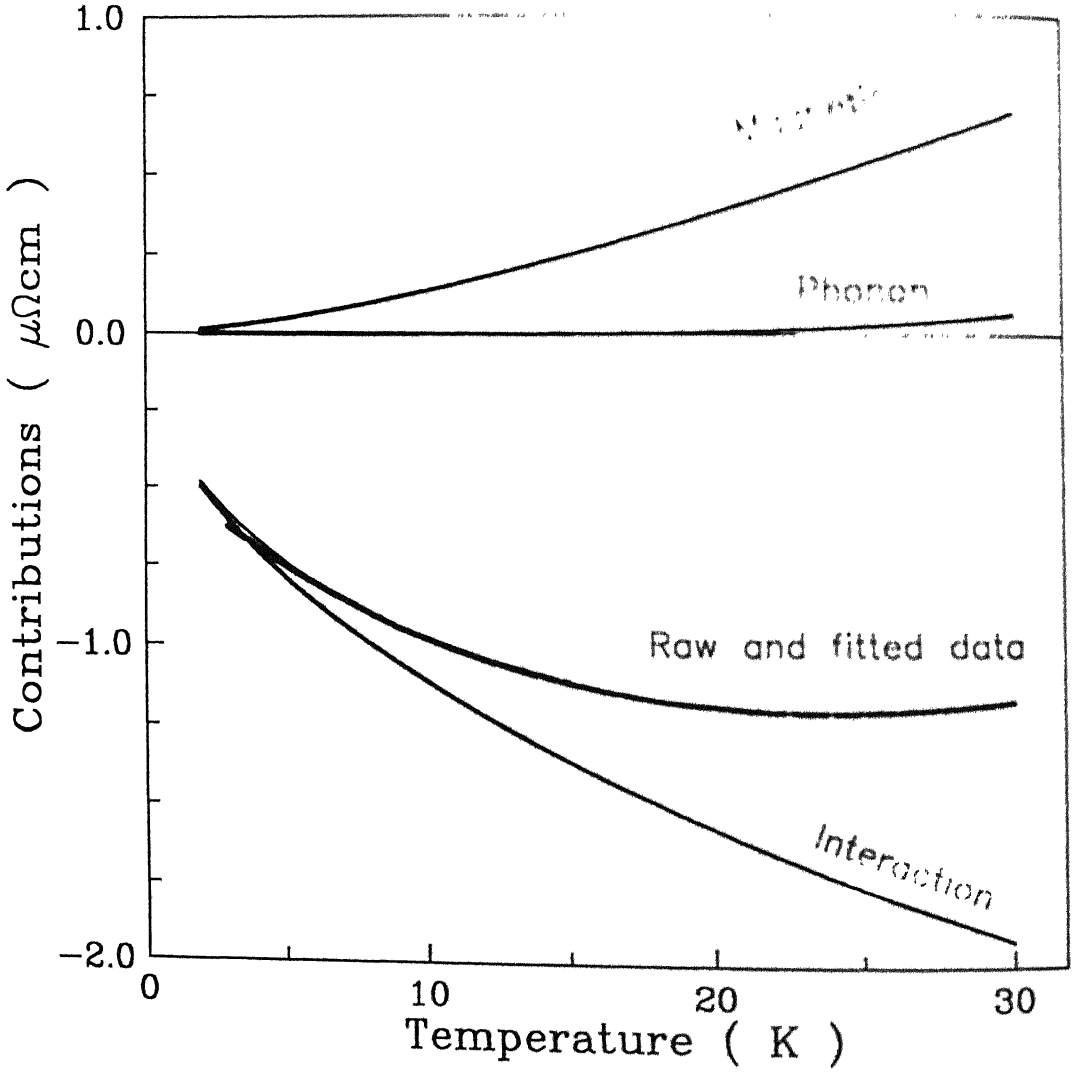

FIG. 3.4. Plot of magnetic ($T^{3/2}$), phonon and electron-electron interaction ($-T^{-1/2}$) contributions along with the raw data and the fit to Eq.(3.9) vs temperature for the alloy with x = 76.

seem to be independent of the detailed magnetic state of the alloys, although the cluster-glass phase is common to all of them. Below $T_{min}/3$ the magnetic and phonon contributions are so small that it is enough to consider the contribution from the interaction effect only, besides ρ_0. The typical values at 8 K for phonon, magnetic and interaction contributions are 2×10^{-5}, 1×10^{-1} and 1 ($\mu\Omega$cm), respectively for the alloy with x = 76. At still lower temperatures the values of phonon and magnetic contributions are much smaller compared to that due to the interaction effects. This can be seen in Fig. 3.4. Therefore the choice of $T_{min}/3$ as the upper limit in the low temperature analysis is quite justified. It is to be noted here that the $\sqrt{T}$ contribution due to the interaction effect should ideally have the same coefficient for both ranges of temperature (1.2 K $\leq$ T $\leq$ $T_{min}/3$ and $T_{min}/3 \leq$ T $\leq$ 30 K). That is why we have chosen to fit the resistivity rather than the conductivity in the 1.2 K $\leq$ T $\leq$ $T_{min}/3$ range. The values of m'_ρ (see Table 3.2) are in good agreement with those of m_ρ (see Table 3.3) considering the fact that the former is obtained along with the residual resistivity, phonon and magnetic contributions in the temperature range $T_{min}/3$ $\leq$ T $\leq$ 30 K whereas m_ρ is obtained along with only the residual resistivity in the range of 1.2 K $\leq$ T $\leq$ $T_{min}/3$. The values differ in the two cases by about only 60 % and this is quite reasonable with so much of variations in the range of temperatures and the fitting parameters. For x = 36, the calculated value of m_σ from the value of m'_ρ using Eq.(3.5) (replacing m_ρ by m'_ρ) is 6.37 $(\Omega\text{cm}K^{1/2})^{-1}$ and it is found to be almost equal to the near-universal value of 6 $(\Omega\text{cm}K^{1/2})^{-1}$. Hence the resistivity minima in the present concentrated $Cu_{100-x}Mn_x$ alloys (x = 36, 60, 73, 76, and 83) are well described by the electron - electron interaction effects.

3.2 NiFeCr alloys

Detailed resistivity measurements in concentrated Ni-rich γ - $Ni_{100-x-y}Fe_xCr_y$ ($8 \leq x \leq 17.5$, $8 \leq y \leq 21$) ternary alloys are also made in the temperature range between 1.2 and 290 K. Recently, the study on the quasibinary Fe-rich $Fe_{100-x}Ni_xCr_{20}$ (14 $\leq$x$\leq$ 30) alloys has clearly shown $\sqrt{T}$ dependence of resistivity well below the minima[21] at low temperatures (< 10 K) whereas at high temperatures (T > 300 K)[22] they exhibit a tendency towards saturation. This is quite amazing, especially when both the effects are observed in different temperature regimes in the same crystalline alloy. On the the other hand, in the Ni-rich side of NiFeCr alloys, Butenko et al.[15, 23]

TABLE 3.4. Sample designation of the alloys with their [illegible] Curie temperature (T_c), spin-freezing temperature (T_f), value of resistivity at [illegible], [illegible] depth minima, and $\Delta\rho/\rho_{300K}$ ($\Delta\rho = \rho_{300K} - \rho_{min}$)

Sample Designation	Alloy Composition	T_c (K)	T_f (K)	[illegible]	[illegible]	Depth of Minima	$\Delta\rho/\rho_{300K}$ (%)
S28	$Ni_{75}Fe_{17}Cr_8$	543	-	58.1	-	0.08	9.6
S29	$Ni_{75}Fe_{13}Cr_{12}$	365	-	89.6	14	0.10	4.9
S33	$Ni_{68}Fe_{17.5}Cr_{14.5}$	320	-	92.4	15	0.11	4.8
S34	$Ni_{73}Fe_{13}Cr_{14}$	315	-	75.8	35.5	0.20	3.7
S48	$Ni_{70}Fe_{12}Cr_{18}$	179	-	71.8	22	0.26	3.8
S41	$Ni_{73.5}Fe_8Cr_{18.5}$	44	9	76.0	27	0.37	3.2
S47	$Ni_{71}Fe_8Cr_{21}$	48	14	80.0	22	0.41	4.3
S50	$Ni_{72}Fe_8Cr_{20}$	60	7	83.7	10	0.19	5.9

have found resistivity minima, but their results do not show any conclusive evidence for the origin of the minima and the nature of the spin - disorder resistivity. Hence, it will be very interesting to study both the resistivity minima as well as the saturation in the present Ni-rich NiFeCr alloys.

3.2.1 Magnetic state of NiFeCr alloys

The designation, composition and transition temperature of the alloys studied here are given in Table 3.4. For convenience in presenting the results, the alloys will be referred by their designations. It has been found that metallic alloys with mixed ferromagnetic and antiferromagnetic exchange interactions have shown, in different temperature regions, several interesting magnetic phases within the same crystallographic phase, e.g., paramagnetic, ferromagnetic or antiferromagnetic, re-entrant spin glass, mixed phase of spin glass with long-range ferromagnetic or antiferromagnetic ordering. The present γ-NiFeCr ternary alloys belong to this category where Ni-Ni interaction is ferromagnetic whereas Fe-Fe and Cr-Cr interactions are both antiferromagnetic[24]. Earlier

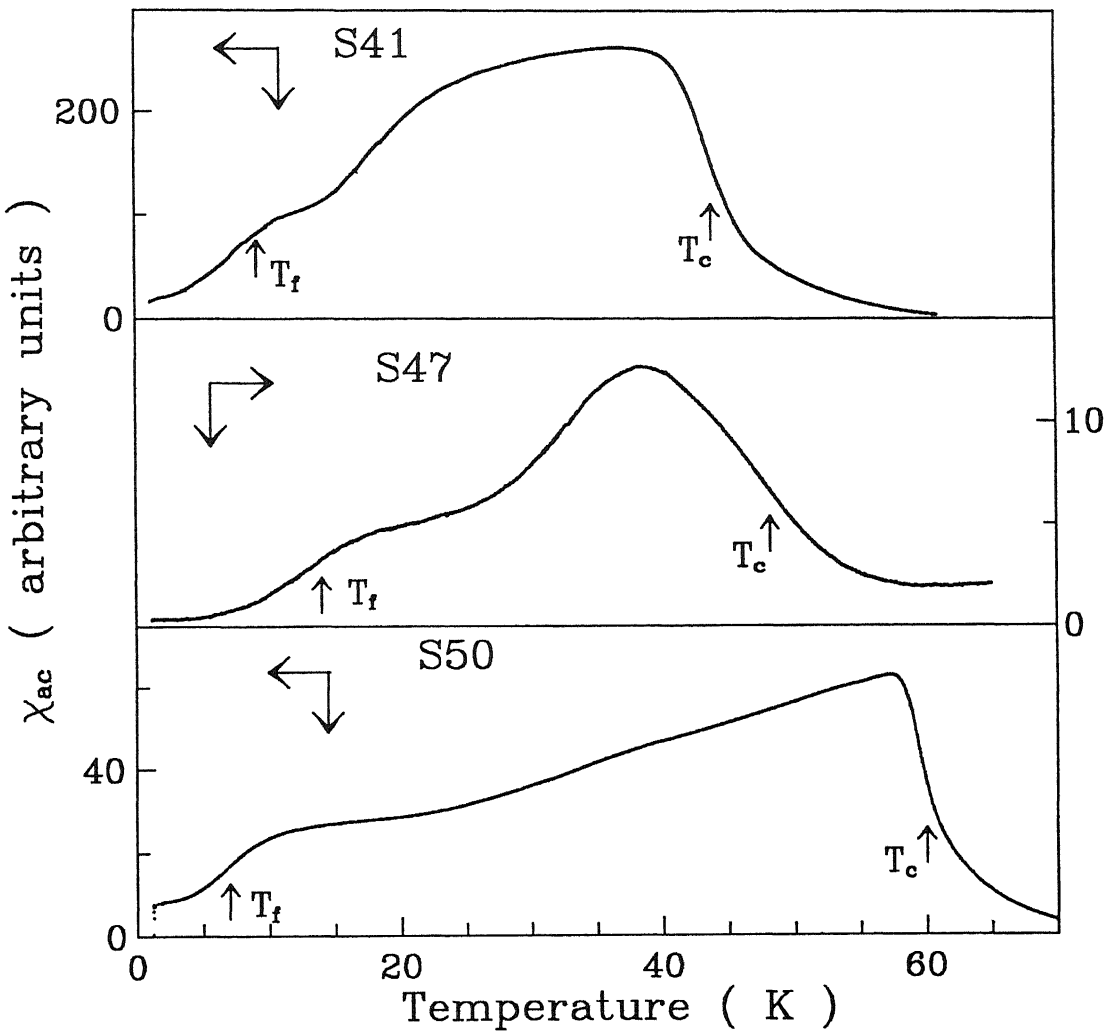

FIG. 3.5. Temperature dependence of the ac susceptibility (χ_{ac}) for alloys S41 ($Ni_{73.5}Fe_8Cr_{18.5}$), S47 ($Ni_{71}Fe_8Cr_{21}$), and S50 ($Ni_{72}Fe_8Cr_{20}$).

neutron diffraction and magnetisation studies by M[illegible] the presence of exotic magnetic phases in Ni-rich Ni[illegible] in different temperature regions. According to their study the [illegible] transitions below 100 K and then to a re-entrant spin glass phase [illegible]. Magnetization in some of the present alloys[26] with low-Cr content [illegible] weak itinerant-electron ferromagnetism with ferromagnetic Curie temperature [illegible] whereas there are no data on the T_c's for the alloys with high Cr content [illegible]. However it was clear that T_c decreased with increasing Cr in this ternary [illegible]. The alloys $Ni_{73}Fe_7Cr_{20}$ (S41), $Ni_{72}Fe_8Cr_{20}$ (S50), and $Ni_{71}Fe_8Cr_{21}$ (S47) are very close to the series studied by Menshic et al.[25]. So in addition to their ferromagnetic state, it is very likely that there is a spin-glass in these alloys at lower temperatures. Linear ac-susceptibility (χ_{ac}) measurements have been made on the above four alloys just to find their low temperature magnetic states. [illegible] measurements down to 1.2 K in alloy S48 do not show any spin-glass transition. Since Gangyopadhayaya et al.[26] have found T_c at 179 K for S48, we have not gone above 100 K. On the other hand, measurements on the rest of the alloys have distinctly shown a second magnetic transition to a spin glass state below 20 K besides the ferromagnetic one. In Fig.3.5, the plots of the absolute values of χ_{ac} (in arbitrary units) versus temperature for alloys S41, S47, and S50 are shown. Ferromagnetic transition (T_c) for alloys S41, S47, and S50 is found at 44, 48, and 60 K, respectively while the second transition (T_f) occurs at 9, 14, and 7 K, respectively. In Table 3.4, the values of T_c for all the alloys and T_f for only alloys S41, S47, and S50 are given. Here the values of T_c for alloys S28, S29, S33, S34, and S48 are taken from an earlier report[26]. On the Fe-rich side of $Fe_{80-x}Ni_xCr_{20}$ alloys a detailed magnetisation study[27] had shown antiferromagnetic, spin-glass, mixed (spin glass with long-range ferromagnetic ordering), and ferromagnetic phases in different regions of composition and temperature. But in the present Ni-rich NiFeCr alloys, we could not detect any long-range ordering in the mixed phase from χ_{ac} measurements. This needs detailed measurements of dc magnetization.

3.2.2 General features of ρ(T) data

High-resolution dc resistivity data for $Ni_{100-x-y}Fe_xCr_y$ ($8 \leq x \leq 17.5$, $8 \leq y \leq 21$) alloys

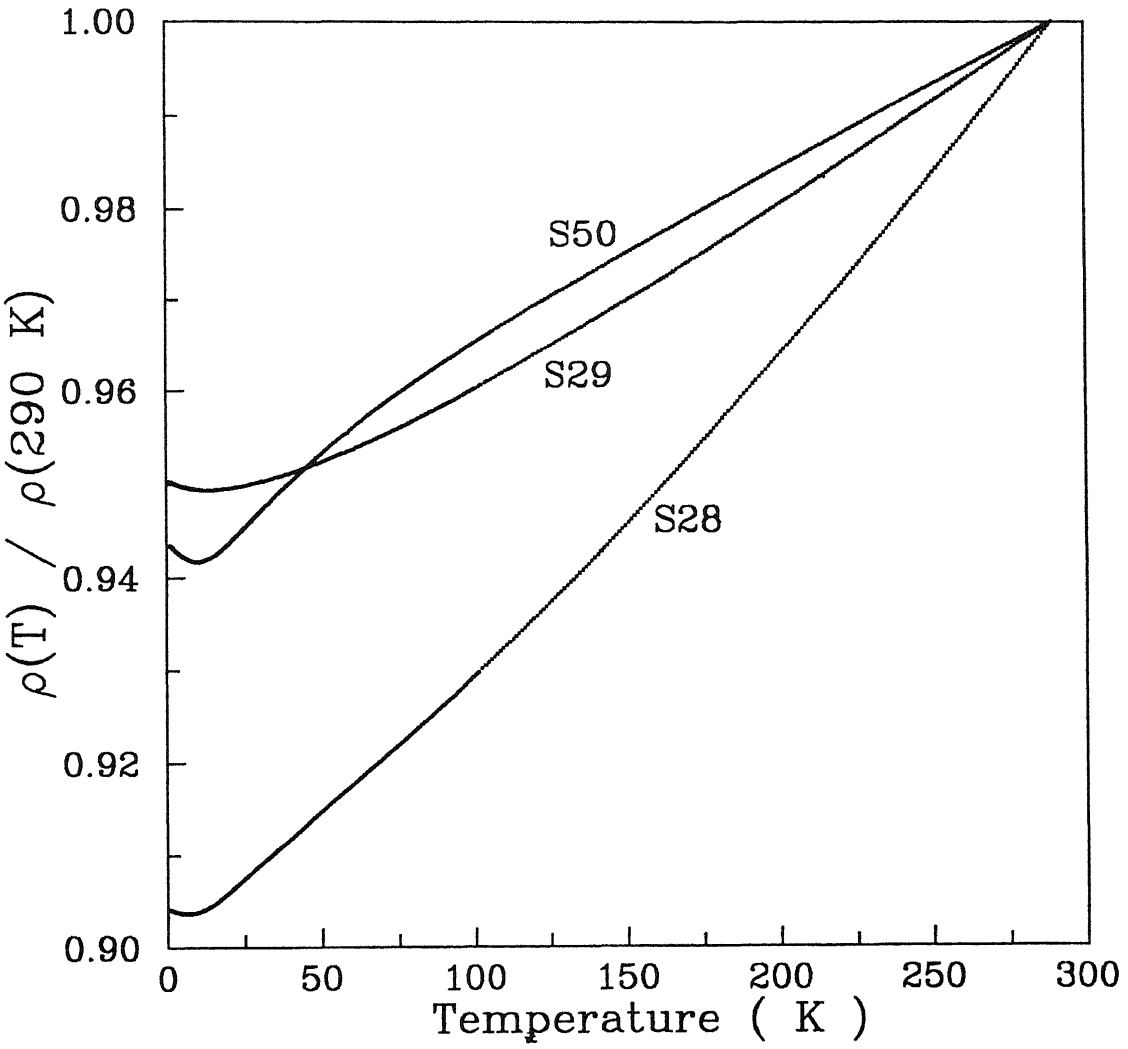

FIG. 3.6. Temperature dependence of the resistivity normalized to its value at 290 K for alloys S28, S29, and S50.

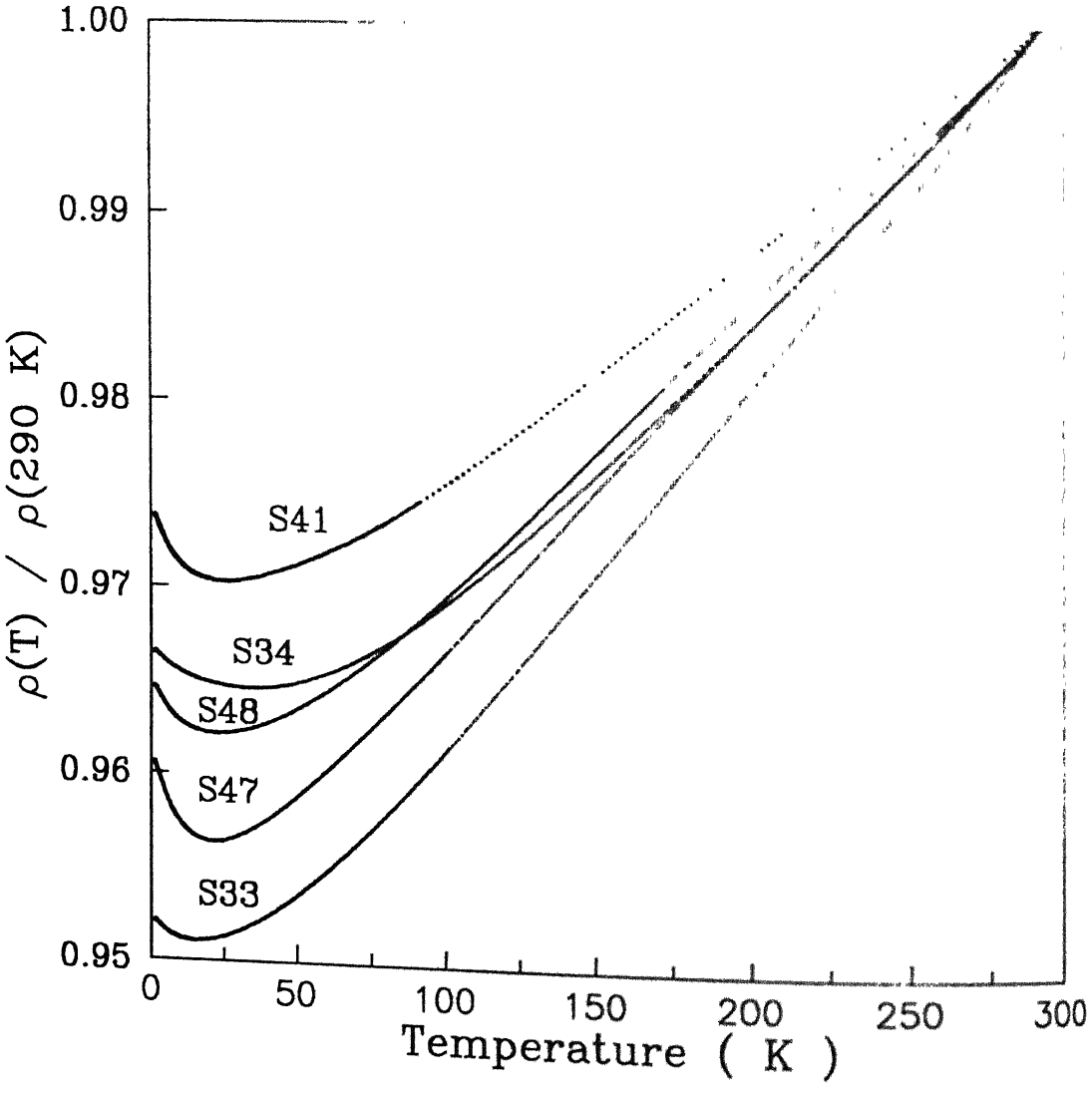

FIG. 3.7. Temperature dependence of the resistivity normalized to its value at 290 K for alloys S33, S34, S41, S47, and S48.

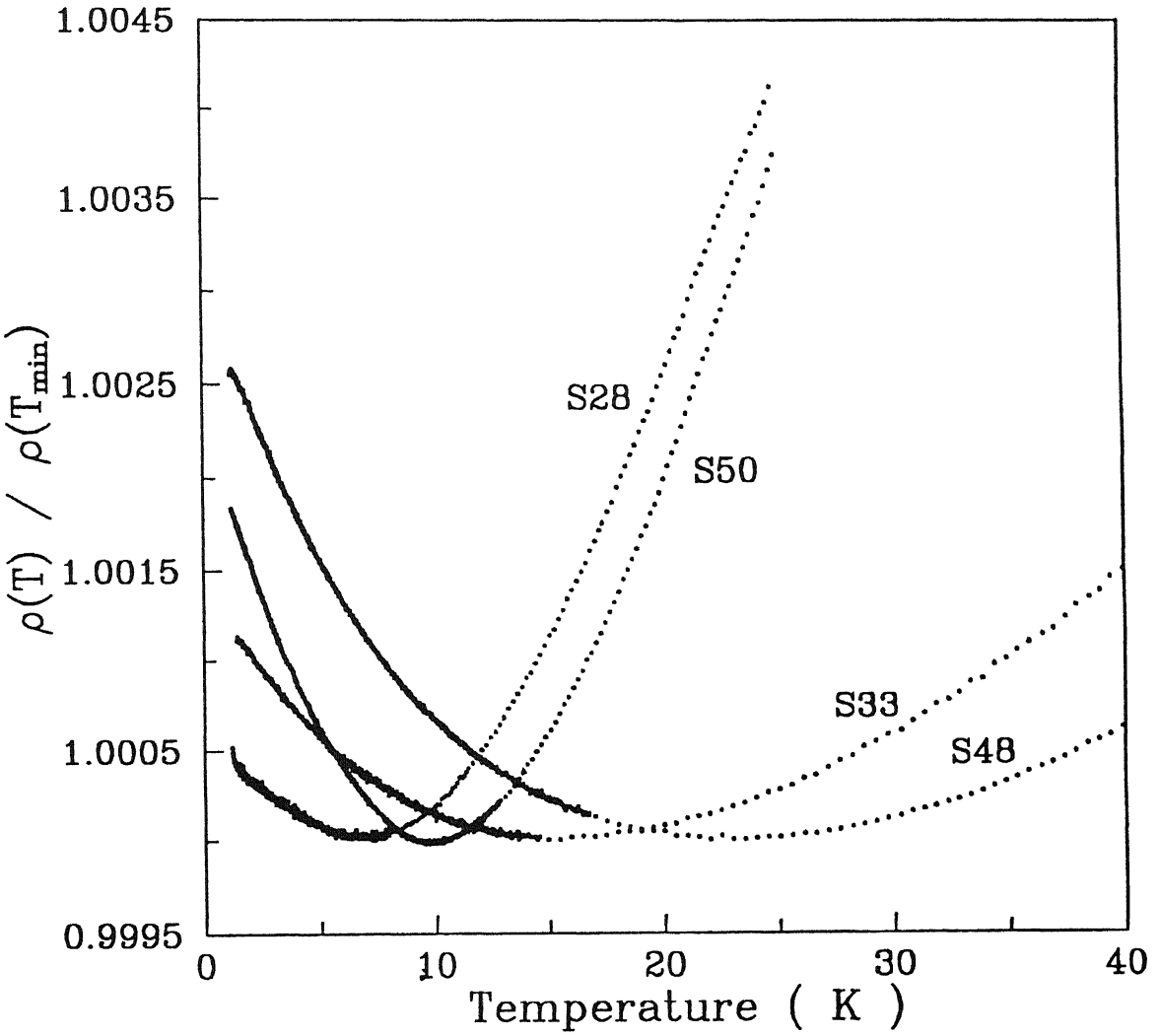

FIG. 3.8. Plot of the resistivity normalized to its value at T_{min} vs temperature till 40 K for alloys S28, S33, S48, and S50.

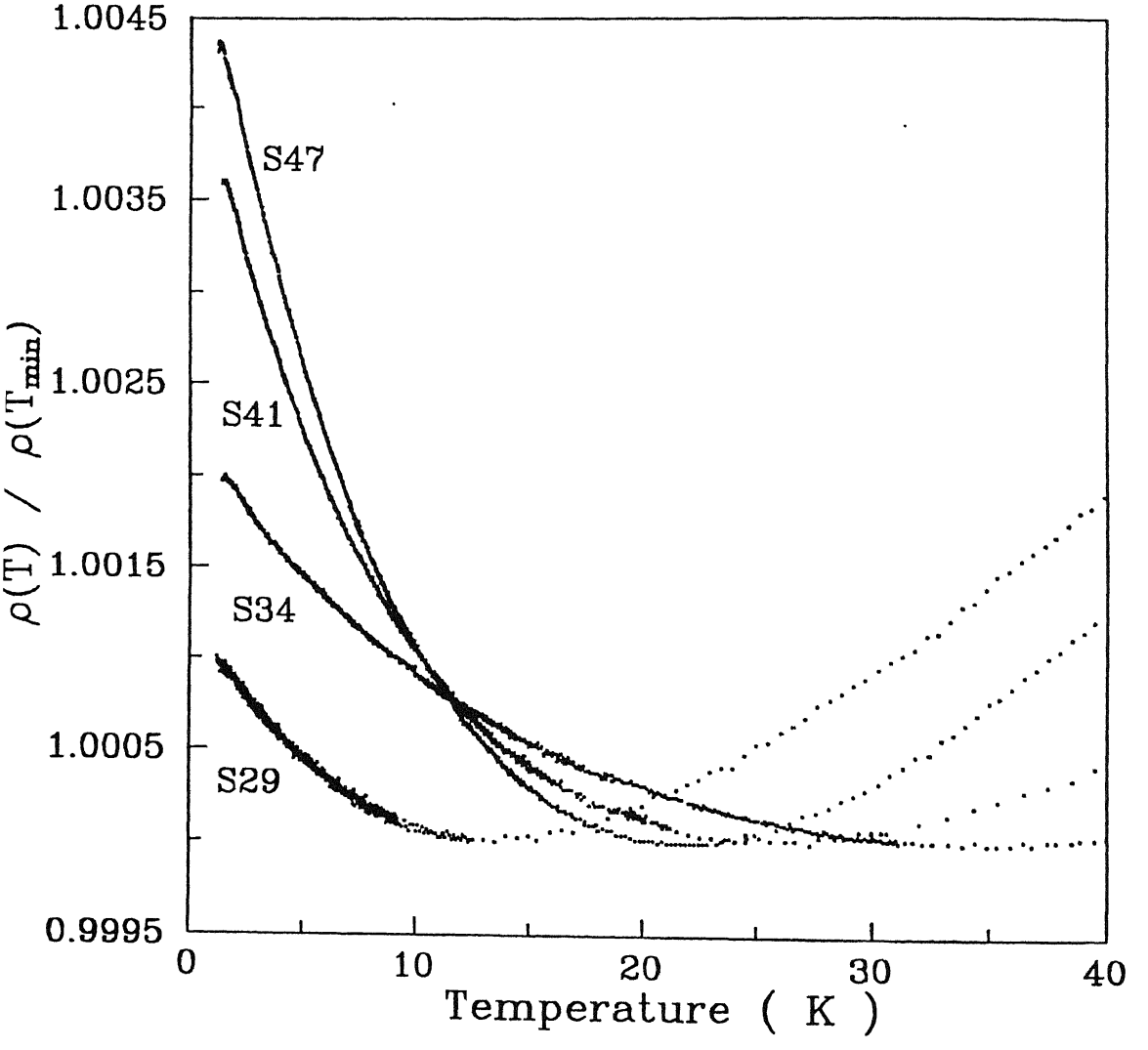

9. Plot of the resistivity normalized to its value at T_{min} vs temperature till 40 K for alloys
)4, S41, and S47.

(Table 3.4) were taken between 1.2 and 290 K. Distinct minima have been observed in all the alloys. In Figs. 3.6 and 3.7, plots of the resistivity normalized to their values at 290 K are given for all the eight alloys. To get a better view of the resistivity minima, low-temperature resistivity data normalized to their values at T_{min}, have been plotted till 40 K in Figs. 3.8 and 3.9. It is very interesting to note that the dispersion in the data is less than the width of the symbols. T_{min} is found between 7 and 35.5 K and the depth of minima (DOM) ($\frac{\rho(1.2K)-\rho(T_{min})}{\rho(1.2K)}$) between 0.05 and 0.37%. The values of resistivity at 1.2 K ($\rho_{1.2K}$), T_{min}, DOM, total change in resistivity, and $\Delta\rho/\rho_{300K}$ ($\Delta\rho = \rho_{300K} - \rho_{min}$ where ρ_{min} = resistivity at T_{min}) are given in Table 3.4. The high values of the electrical resistivity at 1.2 K imply significant disorder in these alloys. It is very difficult to get any systematic dependence of T_{min} or DOM on composition of the present alloys since all the constituents vary. But like the concentrated CuMn alloys, linear dependences of T_{min} and DOM on the values of the resistivity have not been found here. This may be due to the fact that the variation in the resistivity in the present series is found to be very small, about 34 $\mu\Omega$cm, compared to that for the concentrated CuMn alloys where it is about 102 $\mu\Omega$cm. However, a correlation between $\Delta\rho/\rho_{300K}$ with T_{min} and DOM has been found here. In Fig. 3.10, the plots of DOM and T_{min} with $\Delta\rho/\rho_{300K}$ are shown for the present series and some of the Fe-rich FeNiCr alloys[21]. It shows that for large values of $\Delta\rho/\rho_{300K}$ ($\geq$ 15 %), T_{min} and DOM are almost constant whereas a sharp rise in their values are observed for low values of $\Delta\rho/\rho_{300K}$ (< 10 %).

To get an overall view of the temperature dependence of the resistivity, the temperature derivative ($d\rho/dT$) has been calculated from T_{min} to 290 K. In alloys S28, S29, S33 (shown in Fig. 3.11), S34, and S48, the plots of $d\rho/dT$ vs T show a continuous increase with temperatures till about 200 K while they remain constant in the temperature range of 200 to 290 K. The increase till about 200 K is due to the contributions to the electrical resistivity which vary faster than T whereas the linear phonon term is responsible for the constant value of $d\rho/dT$ above 200 K. On the other hand, $d\rho/dT$ in alloys S41 and S47 (T_c's are 44 and 48 K, respectively) exhibits a continuous rise till about 100 K and then it remains constant till 250 K (as in S33, Fig. 3.11). Beyond 250 K there is a decrease in $d\rho/dT$ indicating a tendency towards saturation (not shown). The decrease in $d\rho/dT$ is maximum in alloy S50 where it shows a sharp peak at 40 K. In Fig. 3.11, typical plots of $d\rho/dT$

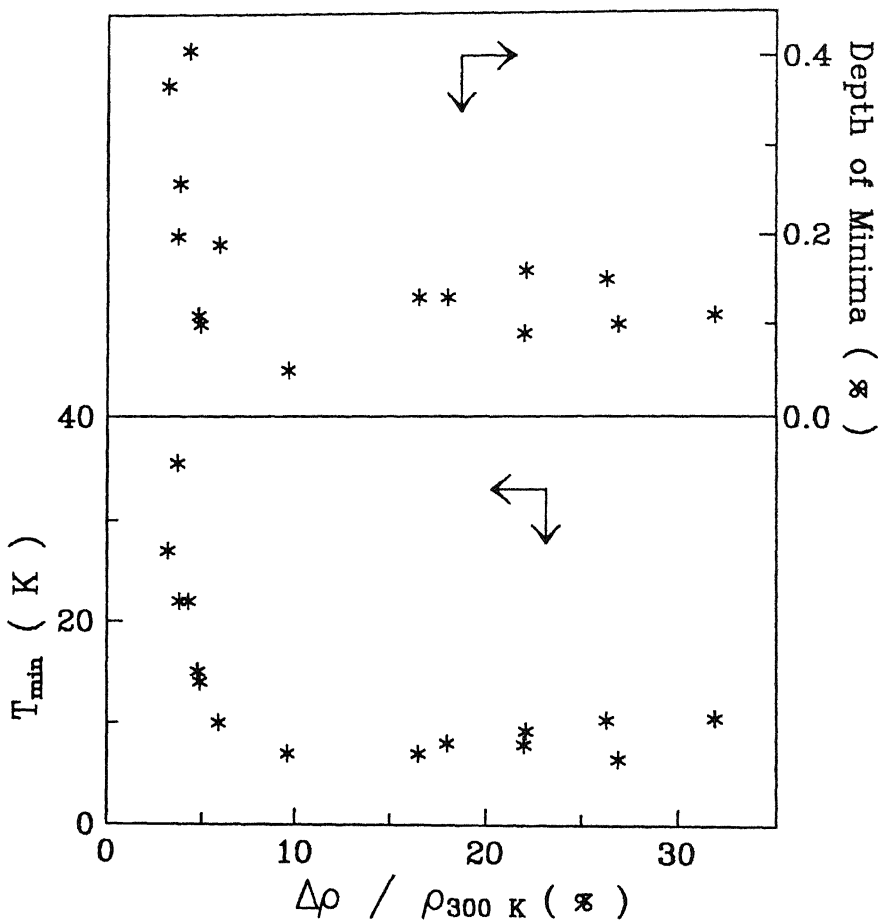

3.10. Dependence of the depth of minima and T_{min} on $\Delta\rho/\rho(300\ K)$ of all the present alloys he Fe-rich $Fe_{100-x}Ni_xCr_{20}$ ($14 \leq x \leq 30$) alloys (Ref.[21]).

mperature are shown for alloys S33 and S50 (inset).

3 $\rho(T)$ for $T \geq 100$ K

e temperature range of 100 to 290 K, the resistivity data of alloy S48 and the low-Cr ($\leq$ 16) alloys (S28 - S34 in Table 3.4) show two distinct regions of temperature dependence. Above K, the linear temperature dependence is ascribed to the high-temperature electron-phonon action where $\rho(T)$ is given by

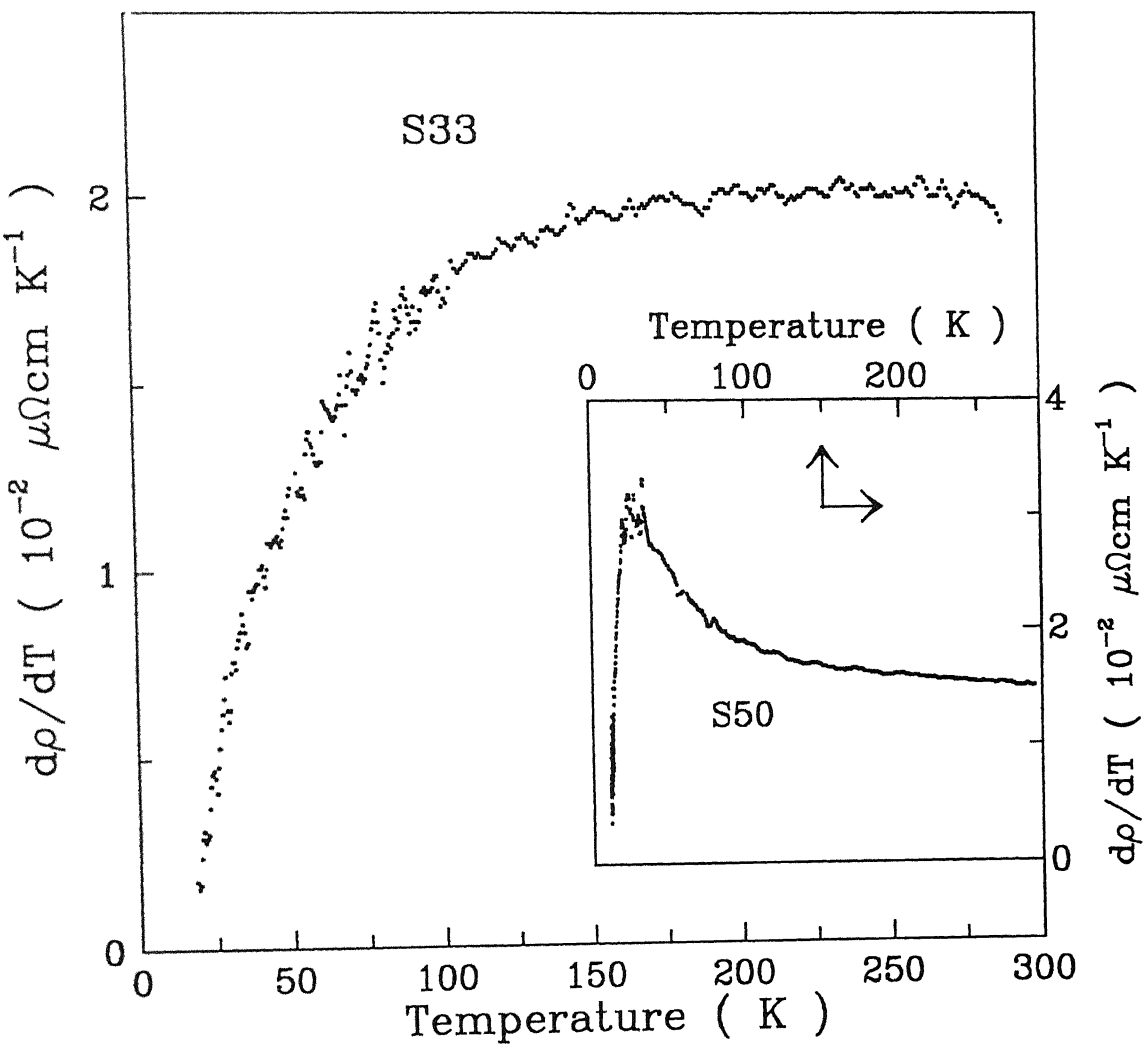

FIG. 3.11. Plot of the first derivative of the resistivity with temperature for alloys S33, and S50 (inset).

$$\rho(T) = \rho_0 + A_1 T. \tag{3.11}$$

The presence of only the phonon term above 200 K (200 - 290 K, see Table 3.5) in the resistivity of alloy S48 is quite reasonable because its T_c is only 178 K. But in the low-Cr alloys where T_c's are in the range of 320 to 543 K, magnetic contribution along with that of phonon is really what is expected. However, fitting the data for the low-cr alloys in a limited temperature range only (see Table 3.5) to Eq.(3.11) gives normalized χ^2, defined as $\frac{1}{N}\sum_{i=1}^{N}\frac{(\rho^i_{raw}-\rho^i_{fit})^2}{\rho^i_{fit}{}^2}$, of the order of 1×10^{-10} which is consistent with our experimental resolution. In the intermediate temperature range of 100 to 200 K, magnetic contributions have to be considered. Kasuya first gave a qualitative description of the temperature dependence of ρ_{mag} considering the molecular field approach[28] and the spin - wave description[29]. But this seems to be valid only at very low temperatures compared to T_c. Later Goodings[30] has found $\rho_{mag} \propto T^2$ considering scattering of conduction electrons by both localised and itinerant electrons. He has also shown in his calculation that the coefficient of the T^2 term is of the order of 10^{-5} $\mu\Omega$cm K^{-2}. In the present weak itinerant ferromagnetic alloys[26], magnetic contribution should certainly have a T^2 type of dependence. In addition, the present temperature range of 100 to 200 K is near $\theta_D/2.5$ (θ_D = Debye temperature) where θ_D's for these alloys are around 380 K[31]. Hence only the high-temperature phonon contribution is expected. Thus ρ(T) can be written as

$$\rho(T) = \rho_0 + B_1 T^2 + A_2 T, \tag{3.12}$$

where B_1 and A_2 are the coefficients of the magnetic and phonon contribution terms, respectively. Fitting the data for alloy S48 and all the low-Cr ($\leq$ 15 at.%) alloys to Eq.(3.12) is found to be very satisfactory resulting in normalized χ^2 of the order of 10^{-10}. The values of the coefficients and the normalized χ^2 along with their range of fits are given in Table 3.5. The most important feature of these fits to Eq.(3.12) is that the coefficient of the T^2 term (B_1) comes out to be of the same order as the theoretical value ($10^{-5}\mu\Omega$cm K^{-2})[30]. This is the only ternary alloy system reported where such a good agreement is obtained. Moreover, this finding certainly indicates that the magnetic contribution is arising from the combined s-s and s-d scattering. Recent studies on Fe-rich FeNiCr alloys[21] have found unexpectedly two orders of magnitude higher values of B_1.

On the contrary, resistivity data of alloys S41 and S47 have shown a linear temperature dependence almost from 100 K onwards till about 250 K. Since these alloys have their T_c's around 60 K, one does not expect magnetic contribution in this range of temperature. Very good fits of the resistivity data of alloys S41 and S47 to Eq.(3.11) have been obtained between 140 to 250 K and between 100 to 220 K, respectively. The details of the fitting parameters along with the χ^2 values are given in Table 3.5. However, no such linear dependence has been observed in the resistivity of alloy S50. This is quite obvious from Fig. 3.6 where the resistivity of the alloy S50 shows a tendency towards saturation right from 40 K onwards. In alloys S41 and S47, similar kinds of behaviour of the resistivity saturation have been found at relatively higher temperatures of around 270 and 230 K, respectively. It is not possible to analyze the data for the resistivity saturation in the alloys S41 and S47 due to the limited range of high-temperature data. Hence we shall try to analyze the data for alloy S50 only in the temperature range of 100 to 290 K. Wiessmann et al.[32] have successfully proposed a model for resistivity saturation where they describe the resistivity of highly disordered materials in terms of a "parallel - resistor" model. Here the Blotzmann transport channel acts in parallel to a non-classical one resulting in

$$\frac{1}{\rho(T)} = \frac{1}{\rho_{sat}} + \frac{1}{\rho_1(T)}, \tag{3.13}$$

where ρ_{sat} is the saturation resistivity and $\rho_1(T) = \rho_0 + A_1 T$ at higher temperatures. Fitting the data for alloy S50 to Eq.(3.13) between 100 and 290 K gives a value of ρ_{sat} much smaller than ρ_0 which is not physically possible. The value of the normalized χ^2 is coming of the order of 5×10^{-8} which is much larger than our experimental accuracy. So the fit to Eq.(3.13) is not at all satisfactory for S50. The value of saturation resistivity (ρ_{sat}) can be written[33] as $\rho_{sat} = 3\hbar a/\alpha^{2/3}e^2$ where $na^3 = \alpha$. Here a is the lattice constant and n is the electron concentration per unit volume. Taking a = 3.55 Å[5] and $n = 10^{29}$ m^{-3}, ρ_{sat} comes out to be about 163 $\mu\Omega$ cm which is large compared to its resistivity at room temperature. So it is quite obvious that one has to go to much higher temperatures to observe saturation.

TABLE 3.5. Sample designation, range of fit, fit functions, their fitted parameters, and normalised χ^2.

Sample Designation	Range of Fit (K)	Fit of ρ(T) to	ρ_0 ($\mu\Omega$cm)	A_1 ($\mu\Omega$cm K^{-1}) (10^{-2})	B_1 ($\mu\Omega$cm K^{-2}) (10^{-5})	χ^2 (10^{-10})
S28	250 - 290	$\rho_0 + A_1T$	56.6	2.7		2.2
	90 - 230	$\rho_0 + A_1T + B_1T^2$	58.0	1.5	2.3	5.2
S29	240 - 290	$\rho_0 + A_1T$	88.4	2.1		3.1
	120 - 220	$\rho_0 + A_1T + B_1T^2$	88.8	1.6	1.0	6.2
S33	220 - 290	$\rho_0 + A_1T$	91.2	2.0		1.3
	100 - 200	$\rho_0 + A_1T + B_1T^2$	91.5	1.6	1.0	3.1
S34	220 - 290	$\rho_0 + A_1T$	74.5	1.3		1.7
	110 - 200	$\rho_0 + A_1T + B_1T^2$	75.2	0.7	1.7	6.1
S48	200 - 290	$\rho_0 + A_1T$	70.9	1.2		0.7
	90 - 170	$\rho_0 + A_1T + B_1T^2$	71.1	0.9	1.2	1.7
S41	150 - 270	$\rho_0 + A_1T$	74.9	1.0		2.8
S47	100 - 230	$\rho_0 + A_1T$	79.0	1.5		5.5

3.2.4 $\rho(T)$ for $T_{min}/2 \leq T \leq 2T_{min}$

In this temperature range, special attention has to be paid to get a more exact picture of different competing physical phenomena responsible for the resistivity minima. In this range the alloys with both high as well as low-Cr content are all ferromagnetic. Hence magnetic contribution of the type T^2, which has already been observed in the high temperature (100 to 200 K) resistivity of alloy S48 and low-Cr alloys ($\leq$ 16 at. %), should be present here. Besides this, the usual electron-phonon scattering will have their low temperature contribution to the resistivity. According to the Bloch-Grüneissen formula, the phonon contribution to the resistivity in the low-temperature limit will have a T^5 dependence. Later on Wilson[34] modified the above relation considering the s-d scattering in addition to the s-s one and found a T^3 dependence in the low-temperature limit. However, both the models give a linear dependence at high temperatures. Phonon contribution of the type T^3 is certainly expected in the present alloys where all the constituents are 3d metals. In addition to these, the physical processes responsible for the increase in resistivity with decreasing temperature below minima will have dominant contribution to the resistivity in this temperature range. Detailed analysis on the resistivity below T_{min} (given in the next section) has shown very conclusively that the e-e interaction effects in the weak localisation limit is responsible for the minima where $\rho_{int}(T) \propto (-\sqrt{T})$. So the resistivity, assuming Matthiessen's rule, can be written as

$$\begin{aligned} \rho(T) &= \rho_0 + \rho_{int}(T) + \rho_{mag}(T) + \rho_{phonon}(T) \\ &= \rho_0 + m'_\rho\sqrt{T} + B_2T^2 + A_3T^3. \end{aligned} \tag{3.14}$$

In the concentrated CuMn alloys, the phonon contribution is found to be negligible compared to those from the magnetic and e-e interaction effects in the same temperature range. Hence neglecting the phonon term, Eq.(3.14) can be written as

$$\rho(T) = \rho_0 + m'_\rho\sqrt{T} + B_2T^2. \tag{3.15}$$

Nevertheless, we have fitted the data to both Eq.(3.14) and (3.15) for all the alloys. Fitting to Eq.(3.14) has resulted in an unphysical sign of A_3. This is quite common in such fits with a large number of parameters. However, a fit to Eq.(3.15) was found to be very satisfactory for all the alloys. But the resulting values of the coefficient of the magnetic contribution (B_2) are an order

TABLE 3.6. Sample designation, range of fit, values of fitted parameters, and normalised χ^2 for Eqs.(3.16) and (3.15) for alloys with low ($\leq$ 15 at. %) and high-Cr ($\geq$ 18 at. %) contents, respectively.

Sample Designation	Range of Fit (K)	ρ_0 ($\mu\Omega$cm)	m'_ρ ($\mu\Omega$cm K$^{-1/2}$) (10^{-2})	A_3 ($\mu\Omega$cm K^{-3}) (10^{-6})	B_2 ($\mu\Omega$cm K^{-2}) (10^{-5})	χ^2 (10^{-10})
S28	2 - 15	58.2	-2.4	30.5	-	2.3
S29	5 - 25	89.7	-4.2	8.3	-	4.7
S33	5 - 25	92.4	-4.5	6.6	-	2.2
S34	12 - 60	75.9	-4.0	0.6	-	1.2
S48	9 - 35	71.7	-4.9	2.8	-	5.9
S41	11 - 40	75.9	- 8.9	-	16.8	5.0
S47	10 - 35	80.1	- 12.8	-	30.0	8.8
S50	5 -15	83.8	-15.1	-	119.7	4.4

of magnitude higher than those obtained at higher temperatures (B_1) for S48 and the low-Cr ($\leq$ 15 at.%) alloys and also in the calculations by Goodings[30]. Earlier resistivity measurements on pure Fe, Ni, and Co by White and Woods[35] gave the coefficient of the magnetic contribution (T^2) of the order of $10^{-5}\mu\Omega$ cm K^{-2} below 10 K. However, this increase in the value of B_2 in the low-temperature regime could be ascribed to the presence of some additional contribution of near similar functional form (A_3T^3 due to electron - phonon scattering). Hence to isolate the magnetic contribution, we assume that its value is the same as in the temperature range of 100 to 200 K for alloy S48 and the low-Cr content ($\leq$ 15 at.%) alloys. Thus Eq.(3.14) is modified as

$$\begin{aligned} \rho'(T) &= \rho(T) - \rho_{mag}(T) \\ &= \rho_0 + m'_\rho\sqrt{T} + A_3T^3, \end{aligned} \tag{3.16}$$

where $\rho_{mag} = B_1T^2$. Subtracting the magnetic contribution from the raw data taking values of B_1 from the high-temperature fit (see Table 3.5), the modified data (ρ(T) - B_1T^2) have been fitted to Eq.(3.16). They show excellent fits with normalized χ^2 of the order of 10^{-10} which is again consistent with our experimental resolution. All the fitting parameters and the temperature ranges are given in Table 3.6. It is found that the coefficient of the low-temperature phonon term is of the order of 10^{-6} $\mu\Omega$cm K^{-3} except for alloy S28 where it is an order of magnitude higher. Interestingly, the calculated phonon contribution (A_3T^3) is found to be an order of magnitude higher than the magnetic contribution (B_1T^2) in this temperature range. On the contrary, the separation of phonon and magnetic contributions following the above arguments is not possible for Cr-rich S41, S47, and S50 alloys where T_c's are 44, 48, and 60 K, respectively. In addition, a second transition at a lower temperature to a spin-glass phase is observed at 9, 14, and 7 K, respectively (see Table 3.4). Hence, besides the T^2 type of ferromagnetic contribution, a $T^{3/2}$ or (BT^2 - $CT^{5/2}$) (B,C >0) type of dependence of resistivity due to the spin-glass phase should show up for $T << T_f$[8, 19]. The present range of temperature is hardly low compared to T_f so to have a spin-glass contribution. To summarize, magnetic scattering gives the most dominant contribution to the resistivity besides the phonon part and the contributions to the T^2 term effectively come from phonon and magnetic scattering only.

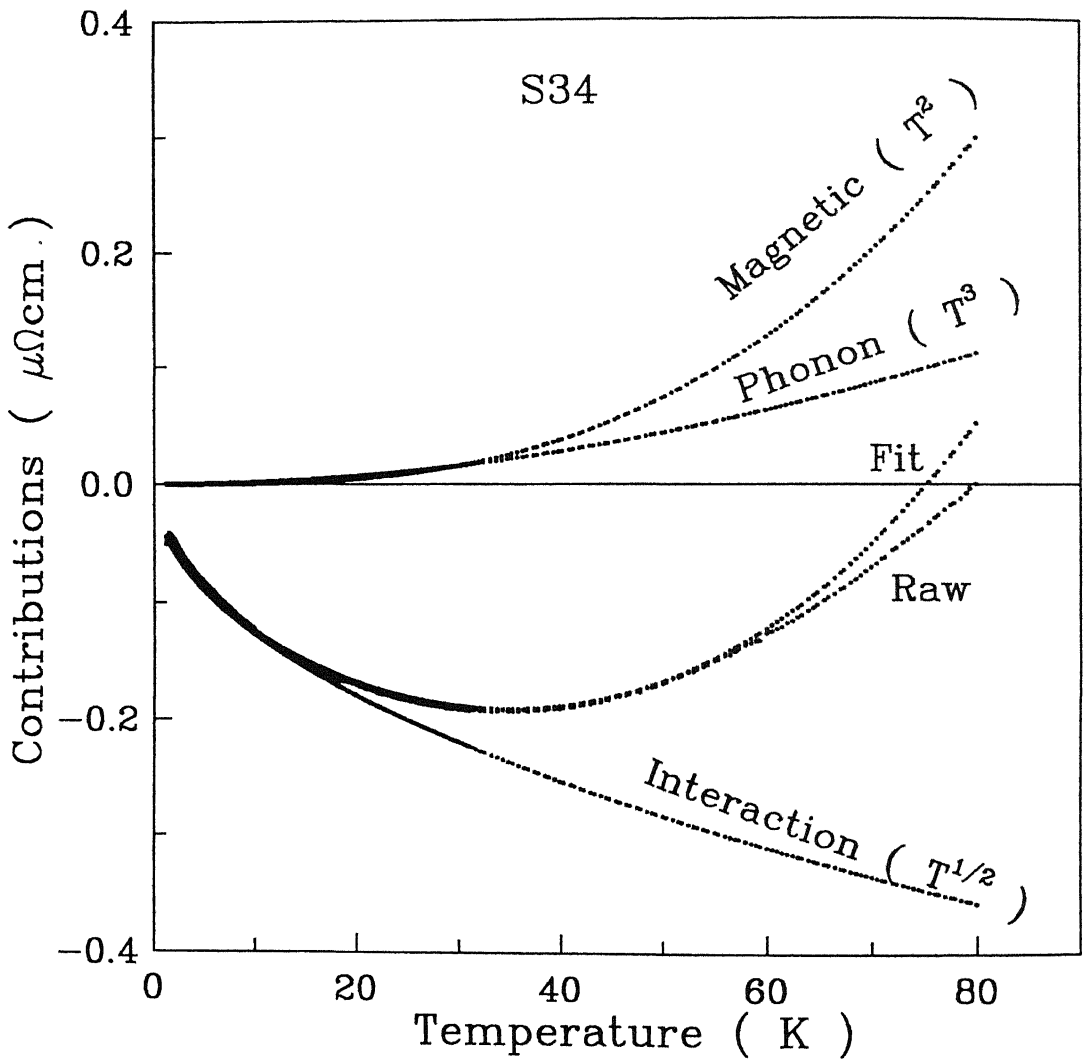

FIG. 3.12. Plot of the individual contributions to the resistivity coming from magnetic (T^2), phonon (T^3), and e-e interaction effects along with the raw and the best-fitted data vs temperature for alloy S34.

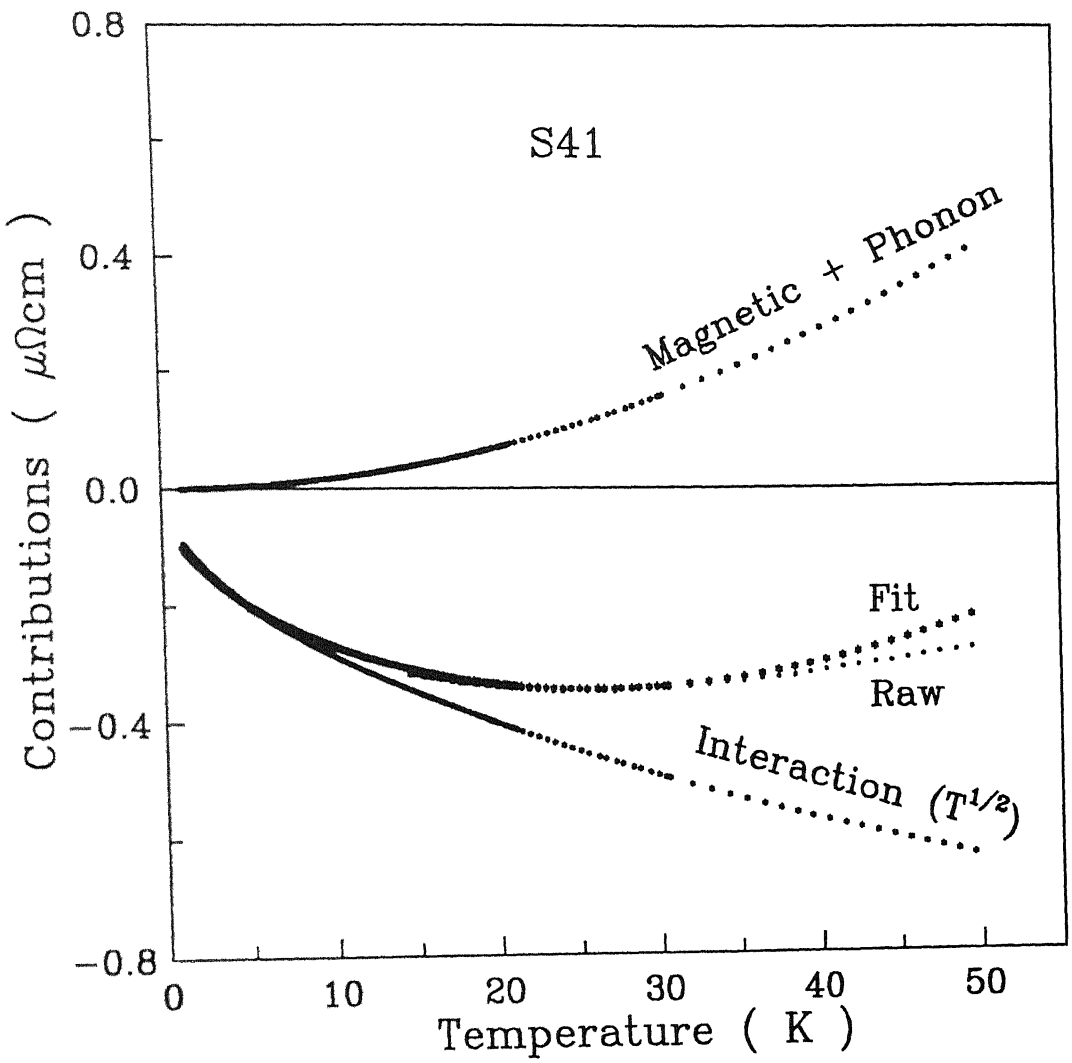

FIG. 3.13. Plot of the individual contributions to the resistivity coming from combined magnetic and phonon, and e-e interaction effects along with the raw and the best-fitted data vs temperature for alloy S41.

TABLE 3.7. Sample designation, values of fitted parameters along with χ^2 for Eq.(3.4) and the corresponding calculated values of m_σ and $N(E_F)$.

Sample Designation	ρ_0 ($\mu\Omega$cm)	m_ρ ($\mu\Omega$cm $K^{-1/2}$) (10^{-2})	χ^2 (10^{-10})	Calculated Values	
				m_σ $((\Omega cm)^{-1} K^{1/2})$	$N(E_F)$ $(erg^{-1}cm^{-3})$ (10^{35})
S28	58.2	-	-	7.2	4.7
S29	89.7	-4.5	2.5	5.6	1.8
S33	92.4	-5.2	0.8	6.0	2.0
S34	75.9	-4.5	1.1	7.6	3.9
S48	71.8	-7.4	0.9	14.3	15.0
S41	75.9	- 10.4	2.2	18.0	22.3
S47	80.2	- 14.2	2.0	22.2	32.2
S50	83.8	-9.6	0.8	13.6	11.6

For more vivid presentation of the individual contributions to the resistivity, we have plotted each of them along with the best-fitted (sum of all the contributions) and the raw ($\Delta\rho = \rho(T) - \rho_0$) data in Figs. 3.12 and 3.13 for alloy S34 and S41, respectively. In Fig. 3.13, the plot for the combined phonon and magnetic contributions has been shown for alloy S41. The raw and the best-fitted data are indistinguishable below T_{min} in both the alloys. Below $T_{min}/2$ the magnetic and phonon contributions are so small that it is enough to consider the contribution from the interaction effects only, besides ρ_0. It is to be noted here that the individual contributions are all less than 0.4 $\mu\Omega$cm. The typical values at 10 K for phonon, magnetic and interaction contributions are 5×10^{-3}, 6×10^{-3}, and 1×10^{-1} (all are in $\mu\Omega$cm), respectively for alloy S34 where ρ_0 is as large as 76 $\mu\Omega$cm.

3.2.5 ρ(T) for 1.2 K $\leq$T$\leq$ $T_{min}/2$

Here our emphasis will be to describe the resistivity behaviour well below minima. As it was mentioned earlier, the present alloys are rather concentrated with residual resistivity of (72 - 92) $\mu\Omega$cm (except alloy S28 where $\rho_0 \simeq 53$ $\mu\Omega$cm). Also these alloys are ferromagnetic[26] in the temperature range where the resistivity minima are observed ($T_{min} << T_c$). Hence the Kondo effect is an unlikely candidate for its origin. Nevertheless, we have tried to fit the data to both ln(T) (Eq (3.1)) and $\sqrt{T}$ (Eq.(3.4)) from 1.2 K to $T_{min}/2$.

Fitting the data of alloy S28 in the temperature range of 1.2 K - T_{min} is not possible. Its T_{min} of 7 K is too low and one has to go much below 1.2 K to check the ln(T) or $\sqrt{T}$ dependence. However, in the previous section, a very consistent result for alloy S28 was found from fitting the data to the e-e interaction effects along with phonon and magnetic terms (Eq.(3.16)) in the temperature range of 1.2 to 15 K. Fitting the data for the rest of the alloys (except S28) to Eqs.(3.1) and (3.4) shows two distinct features. First, the values of the normalised χ^2 for the fits to Eq.(3.4) ($\simeq 1 \times 10^{-10}$) are found to be an order of magnitude lower than that to Eq.(3.1) ($\simeq 1 \times 10^{-9}$). Secondly, the plot of $(\rho_{raw} - \rho_{fit})/\rho_{fit}$ with temperature for the $\sqrt{T}$ fit (Eq.(3.4)) is found to be random whereas that for the ln(T) fit (Eq.(3.1)) shows a systematic trend. A typical plot of the deviations is shown in Fig. 3.14 for alloy S34. Such random variation of $(\rho_{raw} - \rho_{fit})/\rho_{fit}$ with temperature is considered to be a better test for the goodness of a fit. Hence it is beyond doubt that the ρ(T) data are much better described by the $\sqrt{T}$ dependence in this temperature range. The random nature of the residuals as well as the order of magnitude smaller values clearly establish -$\sqrt{T}$ dependence of ρ. All the details of the fitting parameters along with χ^2 are given in Table 3.7. The values of m_ρ, the coefficient of the $\sqrt{T}$ term of Eq.(3.4), are found in the range ((-4.5) - (-14.2)) $\times 10^{-2} \mu\Omega\text{cm}/K^{1/2}$ which is in good agreement with the values of m'_ρ (see Table 3.6). According to a number of earlier studies on amorphous and crystalline alloys[2, 13, 14], m_σ comes out to be of the order of 6 $(\Omega\text{cm}K^{1/2})^{-1}$, almost a near-universal value. The present values of m_σ, calculated from the relation $m_\rho = -m_\sigma \rho_0^2$ (Eq.(3.5)), are in the range of (6 - 22) $(\Omega\text{cm}K^{1/2})^{-1}$ for all the alloys (Table 3.7). The alloys with low-Cr content (< 15 at.%) have m_σ in the range of (5.6 - 7.5) $(\Omega\text{cm}K^{1/2})^{-1}$ which is in very good agreement with the near-universal value[2, 13, 14, 16, 21] of 6 $(\Omega\text{cm}K^{1/2})^{-1}$, whereas those with

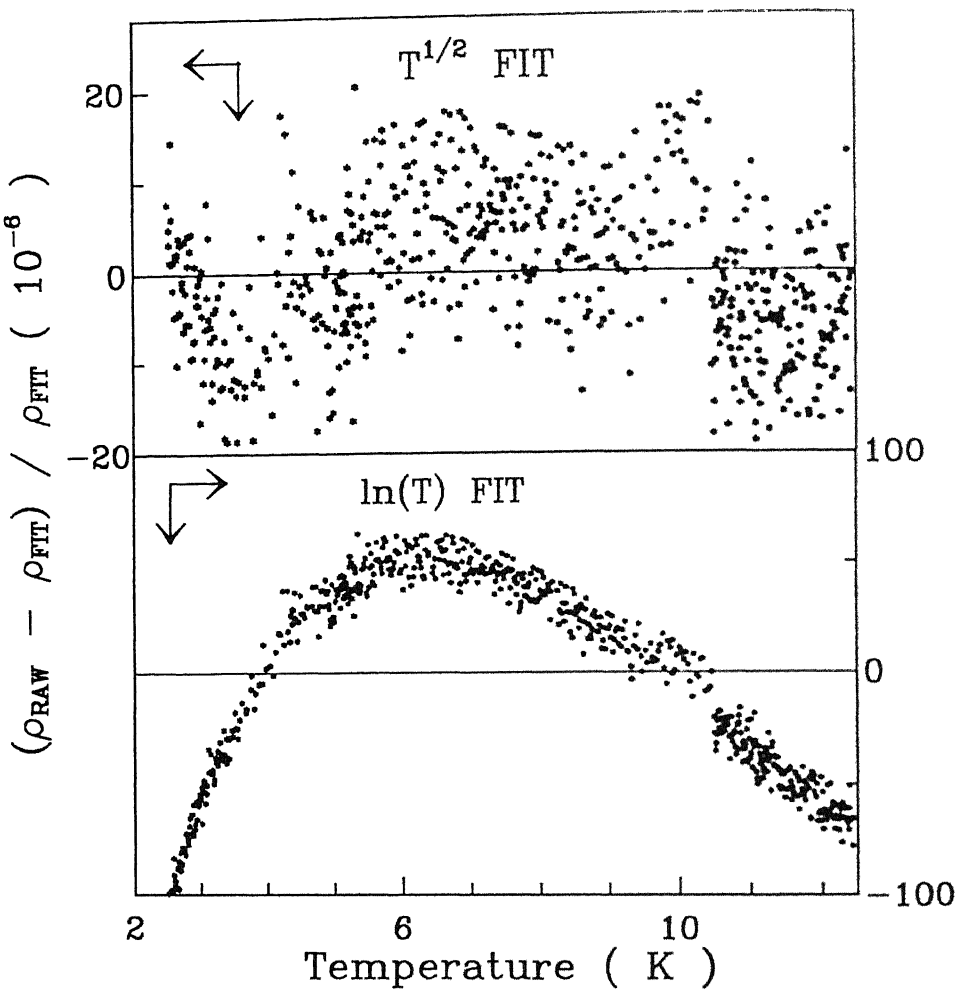

FIG. 3.14. A typical example of the temperature dependence of the residuals for fitting the data to Eq.(3.4) and Eq.(3.1), respectively for alloy S34.

high-Cr content ($\geq$ 18 at.%) give higher values of m_σ, viz, (13 - 22) $(\Omega \mathrm{cm} K^{1/2})^{-1}$. A recent study of the electrical conductivity of Fe-rich $Fe_{80-x}Ni_xCr_{20}$ system[21] (14 $\leq$x$\leq$ 30) below $T_{min}/2$ also finds a $\sqrt{T}$ dependence, but the observed values of m_σ = (12 - 14) $(\Omega \mathrm{cm} K^{1/2})^{-1}$ are on the higher side. The calculated values of N(E_F), using Eqs.(3.3) (with $F_\sigma = 0$) and (3.6), are in the range of (2 - 32) $\times$ 10^{35} $\mathrm{erg}^{-1}\mathrm{cm}^{-3}$ (see Table 3.7). According to an earlier specific heat study[31], $N(E_F)$ in the present alloys are found to be of the order of 15 $\times$ 10^{35} $\mathrm{erg}^{-1}\mathrm{cm}^{-3}$ which is again in good agreement with the present values. This certainly provides another support to the interpretation of the resistivity minima as coming primarily from the e-e interaction effects.

3.2.6 Calculation of ρ_0 using the two-current model

It is important to get some theoretical estimates of the values of the residual resistivity for these ferromagnetic crystalline alloys. Here we have calculated ρ_0 using the two-current model[36] and Mattheissen's rule and compared them with the experimental values. In fact, the residual resistivity (ρ_0) of any alloy arises from the scattering of electrons by impurities and defects. The present $Ni_{100-x-y}Fe_xCr_y$ ternary alloys have high residual resistivities. But the variation in the residual resistivity (ρ_0) with the alloy composition is rather small. Here we have used the two-current model[36] and also Matthiessen's rule to calculate ρ_0. The two-current model has successfully explained the resistivities of dilute and moderately concentrated ($\approx$ 5 at.%) transition metal alloys. The idea behind the two-current model is that the 3d band of the transition metals are split into spin-up and spin-down bands in the presence of ferromagnetic exchange interaction. This ultimately results in different relaxation times for spin-up and spin-down electrons and they conduct in parallel. At very low temperatures, if the interaction between the impurities is neglected, the residual resistivity of the dilute binary alloy $M_{100-x}A_x$, where M and A are the host and the impurity respectively, can be written as

$$\rho_0 = x\frac{\rho_A\uparrow \rho_A\downarrow}{\rho_A\uparrow + \rho_A\downarrow}. \tag{3.17}$$

Here $\rho_A\uparrow$ and $\rho_A\downarrow$ are the spin-up and the spin-down resistivities of the impurity. In the case of a ternary alloy $M_{100-x-y}A_xB_y$ where both A and B are impurities, the resistivity at low temperatures can be written as

$$\rho_\sigma = x\rho_{\sigma A} + y\rho_{\sigma B}, \tag{3.18}$$

where σ is either $\uparrow$ or $\downarrow$. However, in Matthiessen's rule, the sum of the residual resistivities of the two impurities determines the residual resistivity of the alloy. Here it is assumed that in both the cases the residual resistivity of the impurity is independent of temperature. Earlier Fert and Campbell had found very consistent results using the two-current model in Ni and Fe - based dilute binary and ternary alloys[36] for different 3d impurities. According to them, the values of resistivity of Fe and Cr as impurities in Ni-based alloys are ρ_0^{Fe} = 0.35, ρ_0^{Cr} = 5, $\rho_{0\uparrow}^{Fe}$ = 0.37, $\rho_{0\downarrow}^{Fe}$ = 7.4, $\rho_{0\uparrow}^{Cr}$ = 16.1, and $\rho_{0\downarrow}^{Cr}$ = 7.2 (all are in $\mu\Omega$cm per at.%). Hence it is rather simple to calculate ρ_0 for the present Ni-rich NiFeCr alloys although a very good agreement between the calculated

ABLE 3.8. Alloys with their sample designation, composition and values of residual resistivity ρ_0) obtained from experiments, two-current model and Matthiessen's rule.

Sample esignation	Alloy Composition	Residual resistivity, ρ_0 ($\mu\Omega$cm) Experimental Values	Two-current model	Matthiessen's rule
S28	$Ni_{75}Fe_{17}Cr_8$	58.1	77.8	45.9
S29	$Ni_{75}Fe_{13}Cr_{12}$	89.6	95.0	64.5
S33	$Ni_{68}Fe_{17.5}Cr_{14.5}$	92.8	118.4	78.6
S34	$Ni_{73}Fe_{13}Cr_{14}$	75.8	106.1	74.6
S48	$Ni_{70}Fe_{12}Cr_{18}$	71.8	125.3	94.2
S41	$Ni_{73.5}Fe_8Cr_{18.5}$	76.0	110.7	95.3
S47	$Ni_{71}Fe_8Cr_{21}$	79.9	130.1	107.8
S50	$Ni_{72}Fe_8Cr_{20}$	83.7	125.0	102.8

nd the experimental values is not expected. The calculated values of ρ_0 using the two-current nodel and Matthiessen's rule are given in Table 3.8 which clearly shows that the deviation from Iatthiessen's rule is always positive. A comparison with the corresponding experimental values f ρ_0 (see Table 3.8) shows that the variation in ρ_0 with composition is predicted to be more y Matthiessen's rule than the two-current model while the experimental ρ_0's have still weaker ependence. This discrepancy mainly comes from the fact that the values of ρ_0^{Fe}, ρ_0^{Cr}, ... etc., used or the calculation of these concentrated alloys, are actually for dilute NiCr and NiFe alloys[36].

References

[1] J. S. Dugdale, Contemp. Phys. **28**, 547 (1987).

[2] M.A. Howson and B.L. Gallagher, Physics Reports **170**, 265 (1988).

[3] J. Mydosh, Spin Glasses : An Experimental Introduction (Taylor and Francis, London, Washington DC, 1993).

[4] Alok Banerjee, Ph.D. Thesis, Indian Institute of Technology, Kanpur, India, 1993.

[5] Anup Kumar Gangyopadhyaya, Ph.D. Thesis, Indian Institute of Technology, Kanpur, India, 1983.

[6] P. A. Lee and T. V. Ramakrishnan, Rev. Mod. Phys. **57**, 287 (1985).

[7] B. L. Altshuler and A. G. Aranov, Solid State Commun. **30**, 115 (1979); B. L. Altshuler and A. G. Aranov, *Electron-Electron Interactions in Disordered Solids*, edited by A.L. Efros and M. Pollak (North - Holland,Amsterdam) 1985.

[8] A. Banerjee and A. K. Majumdar, Phys. Rev. B **46**, 8958 (1992).

[9] N. Cowlam and A. M. Samah, J. Phys. F: Metal Phys. **11**, 27 (1981).

[10] J.Kondo, Prog. Theoret. Physics, **32**, 37 (1964); J. S. Dugdale, " The Structures and Properties of Solids 5 - The Electrical Properties of Metals and Alloys", Edward Arnold Publications, UK (1977).

[11] B. R. Coles, Physica **91B**, 167 (1977).

[12] N. Rivier and M.J. Zuckermann, Phys. Rev. Lett. **21**, 904 (1968).

[13] R. W. Cochrane and J. O. Storm-Olsen, Phys. Rev. B **29**, 1088 (1984).

[14] A. Das and A. K. Majumdar, Phys. Rev. B **43**, 6042 (1991).

[15] A. V. Butenko, D. N. Bol'shutkin, and V. I. Pecherskaya, Sov. Phys. JETP **71**, 983 (1990).

[16] S. Banerjee and A. K. Roychowdhury, Solid State Commun. **83**, 1047 (1992).

[17] J. E. Zimmerman and H. Sato, J. Phys. Chem. Solids **21**, 71 (1961).

[18] N. Rivier and J. Adkins, J. Phys. F: Metal Phys. **5**, 1745 (1975).

[19] K. H. Fischer, Z. Phys. B **34**, 45 (1979).

[20] P. J. Ford and J. A. Mydosh, Phys. Rev. B **14**, 2057 (1976).

[21] S. Banerjee and A. K. Roychowdhury, Phys. Rev. B **50**, 8195 (1994).

[22] T.K. Nath and A.K. Majumdar, Phys. Rev. B **53**, 12148 (1996).

[23] V.I. Pecherskaya, D. N. Bol'shutkin, and A. V. Butenko, Sov. J. Low Temp. Phys. **15**, 9 (1989).

[24] A.K. Majumdar and P.V. Blanckenhagen, J. Magn. Magn. Mater. **40**, 227 (1983).

[25] A.Z. Menshikov, G.A. Takzey, and A. Ye. Teplylykh, Phys. Met. Metall. **54**, 41 (1982).

[26] A.K. Gangyopadhyay, R.K. Ray, and A.K. Majumdar, Phys. Rev. B **30**, 6693 (1984).

[27] A.K. Majumdar and P.V. Blanckenhagen, Phys. Rev. B **29**, 4079 (1984).

[28] T. Kasuya, Progr. Theoret. Phys. (Kyoto) **16**, 58 (1956).

[29] T. Kasuya, Progr. Theoret. Phys. (Kyoto) **22**, 227 (1959).

[30] D.A. Goodings, Phys. Rev. **132**, 542 (1963).

[31] V.I. Pecherskaya, D. N. Bol'shutkin, A. V. Butenko, V.N. Belinson, V.I. Ovcharenko, V.A. Pervakov, and N. Yu. Tyutryumova, Sov. J. Low Temp. Phys. **14**, 9 (1988).

[32] H. Wiessmann, M. Gurvitch, A.K. Ghosh, B. Schwartz, M. Strongin, P.B. Allen, and J.W. Halley, Phys. Rev. Lett. **38**, 782 (1977).

[33] M. Gurvitch, Phys. Rev. B **28**, 544 (1983).

[34] A.H. Wilson, Proc. Roy. Soc. (London) **A167**, 580 (1938).

[35] G K. White and S.B. Woods, Phil. Trans. Roy. Soc. London **A251**, 273 (1958).

[36] A. Fert and I.A. Campbell, J. Phys. F: Metal Phys. **6**, 849 (1976).

Chapter 4

Magnetoresistance

In the last chapter, the temperature dependence of the electrical resistivity (ρ(T)) for both binary CuMn and Ni-rich ternary NiFeCr alloys was discussed in details where the electron - electron interaction (EEI) effects was found to be responsible for the low - temperature resistivity minima. Theoretically, application of a magnetic field[1–3] is another source of dephasing other than inelastic scattering which could destroy the phase coherence of electrons and hence weak - localisation. As a result, the field dependence of weak - localisation as well as EEI effects are expected to show up in the magnetoresistance data of these two alloy series in the temperature range where the resistivity minima were observed. Earlier studies[4–6] in some non - magnetic amorphous alloys have clearly shown the presence of interaction effects in ρ(T) in the temperature range of 100 mK to 20 K. But in the interpretation of the magnetoresistance data[5], the field dependence of EEI effects along with localisation term comes into play only at lower temperatures below 1 K. Here we have presented magnetoresistance data in both transverse and longitudinal orientations for both CuMn and NiFeCr alloys. One of the motivations behind this investigation is to find a satisfactory description of the field dependence of the magnetoresistance and to check whether the interpretation of the magnetoresistance data is consistent with that of the electrical resistivity (ρ(T)).

Earlier studies[7, 8] had shown that addition of a few atomic percent of Cr in Ni and Fe-based alloys could decrease the value of the FAR (ferromagnetic anisotropy of resistivity) drastically. It is important to note that the value of the FAR was reported[8] as zero for 10.1 at.% of Cr in $Ni_{100-x}Cr_x$ alloys. Since then, there is as such no detailed report on the FAR in Cr-rich alloys.

The present NiFeCr alloys are all ferromagnetic at 4.2 K with widely varying Cr (2 to 21 at.%) content. Here our prime intention is to interpret the composition dependence of the FAR in terms of the split - band model[9] and to correlate them with the earlier observed the γ_{HS}= 0 line[10] in the ternary phase diagram. In addition, it will be interesting to see how the present FAR decreases with increasing Cr content in these NiFeCr alloys and also to explore the possible physical reasons for such changes.

4.1 CuMn alloys

4.1.1 General description of the data

A detailed investigation of both the transverse and the longitudinal magnetoresistances in concentrated crystalline γ-$Cu_{100-x}Mn_x$ alloys (x = 36, 60, 73, 76, and 83) are presented here till a magnetic induction of 7.5 T. The measurements in the transverse mode (TMR) are done at 4.2, 20.5, and 63 K whereas those in the longitudinal mode (LMR) are done only at 4.2 K. Interestingly, most of the earlier studies in $Cu_{100-x}Mn_x$ alloys are restricted to the dilute Mn regime ($x \leq 4.4$ at.%) where it is a canonical SG with a negative magnetoresistance[11]. The present alloys have exotic magnetic structures at low temperatures (see Fig. 1.8). The alloys with x = 36, 60, and 73 are cluster glasses with T_f between 135 and 149 K whereas x = 76 and 83 are in the mixed cluster-glass and long-range antiferromagnetic phase below 145 and 45 K, respectively[12]. The LMR data ($\Delta\rho/\rho$) at 4.2 K are shown in Fig. 4.1 whereas the TMR's are shown in Figs. 4.2, 4.3, and 4.4 for 4.2, 20.5, and 63 K, respectively in magnetic inductions up to 7.5 T. For better view of the low - magnetoresistance region, some are not plotted all the way till 7.5 T. The plots show that the dispersion in the data is comparable to the width of the symbols in most of the cases. The values of the LMR at 7.5 T for all the alloys along with their residual resistivity (ρ_0), and the temperatures of the resistivity minima (T_{min}) are given in Table 4.1 while the values of the TMR are given in Table 4.2. The plots show a positive magnetoresistance for the Mn-rich ($x \geq 60$) alloys and an overall negative one for x = 36. However, the data at 4.2 K in alloy x=36 (Figs. 4.1 and 4.2) show a distinct positive magnetoresistance till 3 T beyond which it becomes negative. The above positive $\Delta\rho/\rho$ is found to disappear at higher temperatures (20.5 and 63 K).

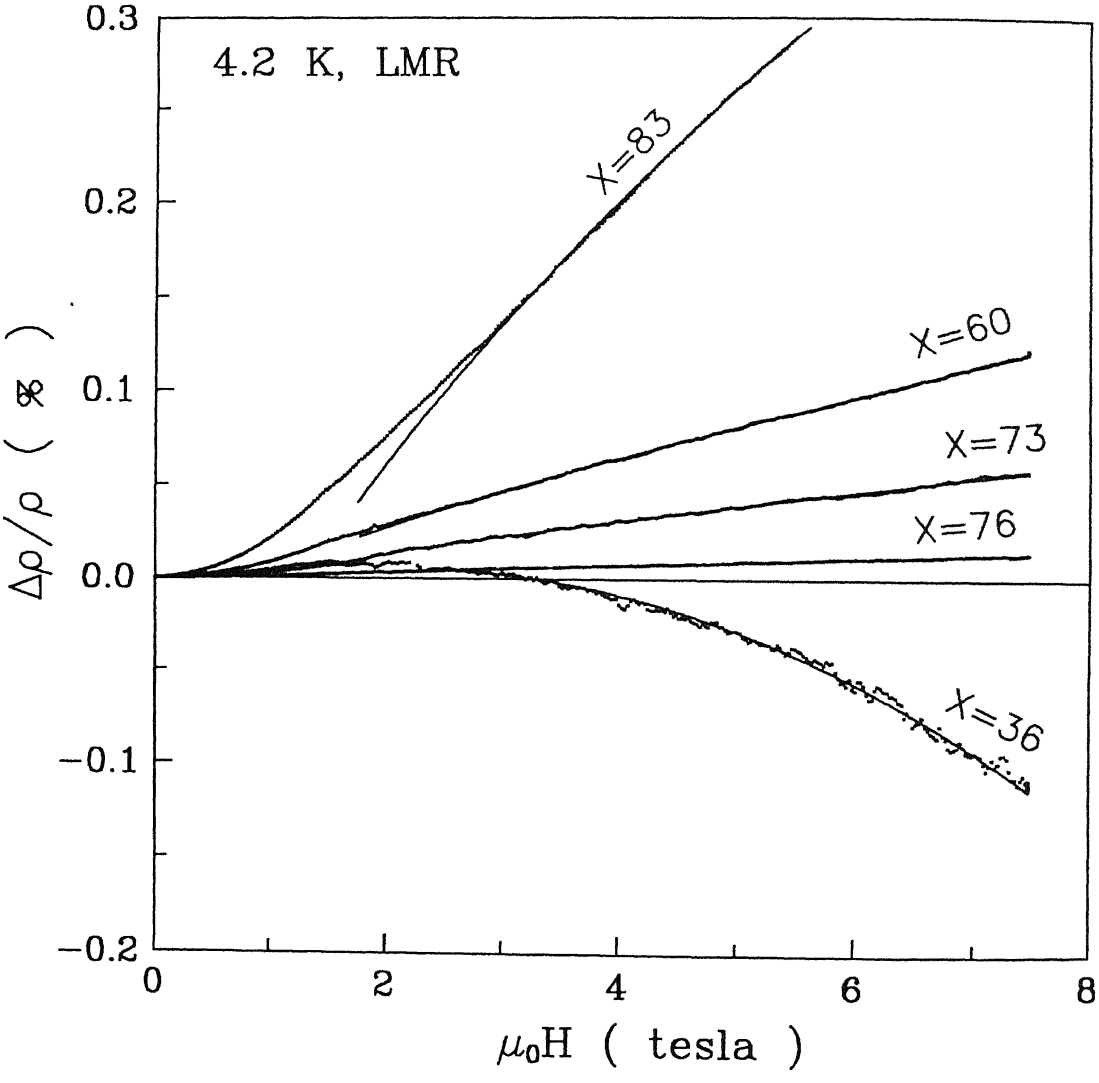

FIG. 4.1. Plots of the longitudinal magnetoresistance (LMR) data ($\Delta\rho/\rho$ vs μ_0H) in the range of 0 to 7.5 T and the best-fitted curves between 4 and 7.5 T for $Cu_{100-x}Mn_x$ (x = 36, 60, 73, 76, and 83) alloys at 4.2 K. Here μ_0H is the magnetic induction in tesla.

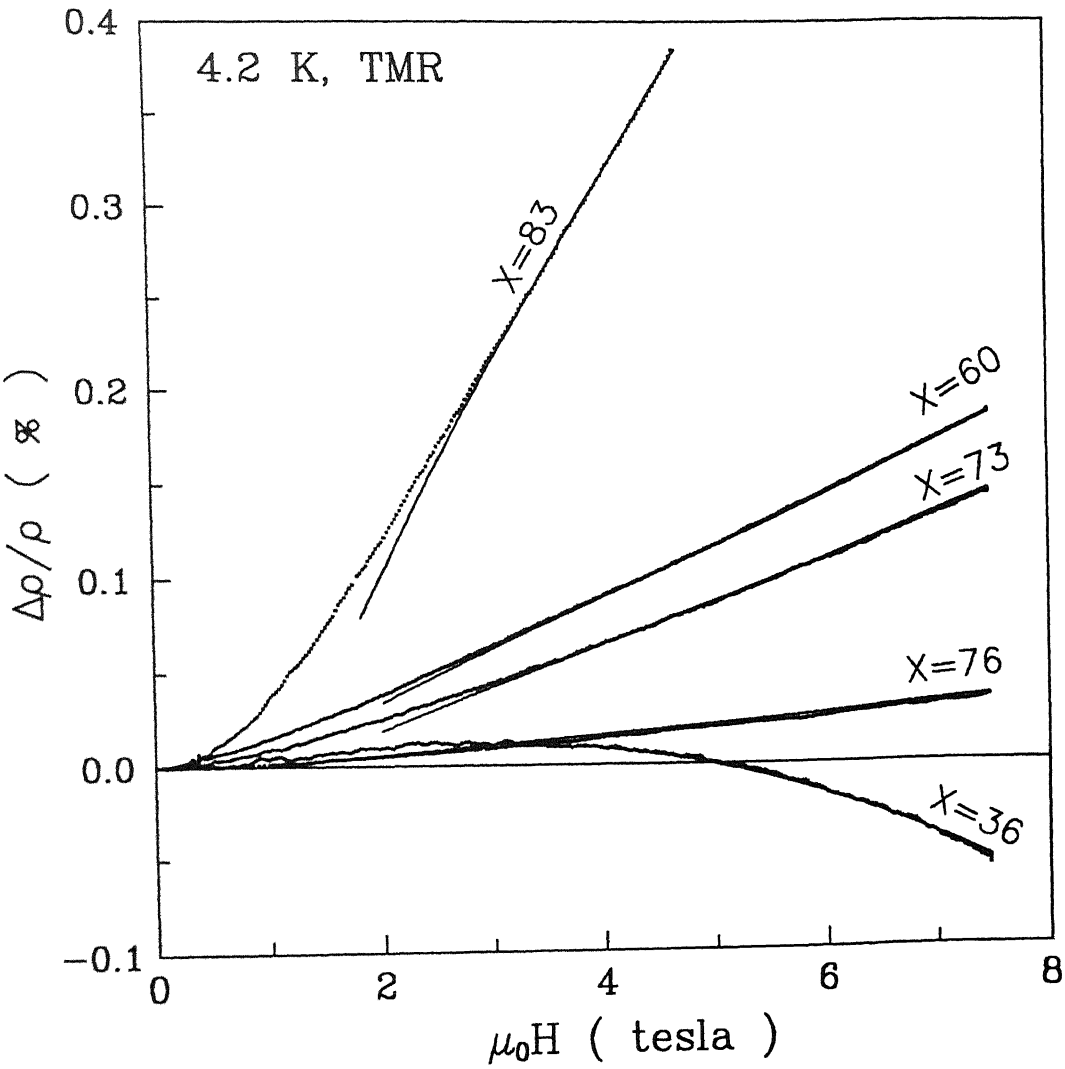

FIG. 4.2. Plots of the transverse magnetoresistance (TMR) data ($\Delta\rho/\rho$ vs μ_0H) in the range of 0 to 7.5 T and the best-fitted curves between 4 and 7.5 T for $Cu_{100-x}Mn_x$ (x = 36, 60, 73, 76 and 83) alloys at 4.2 K.

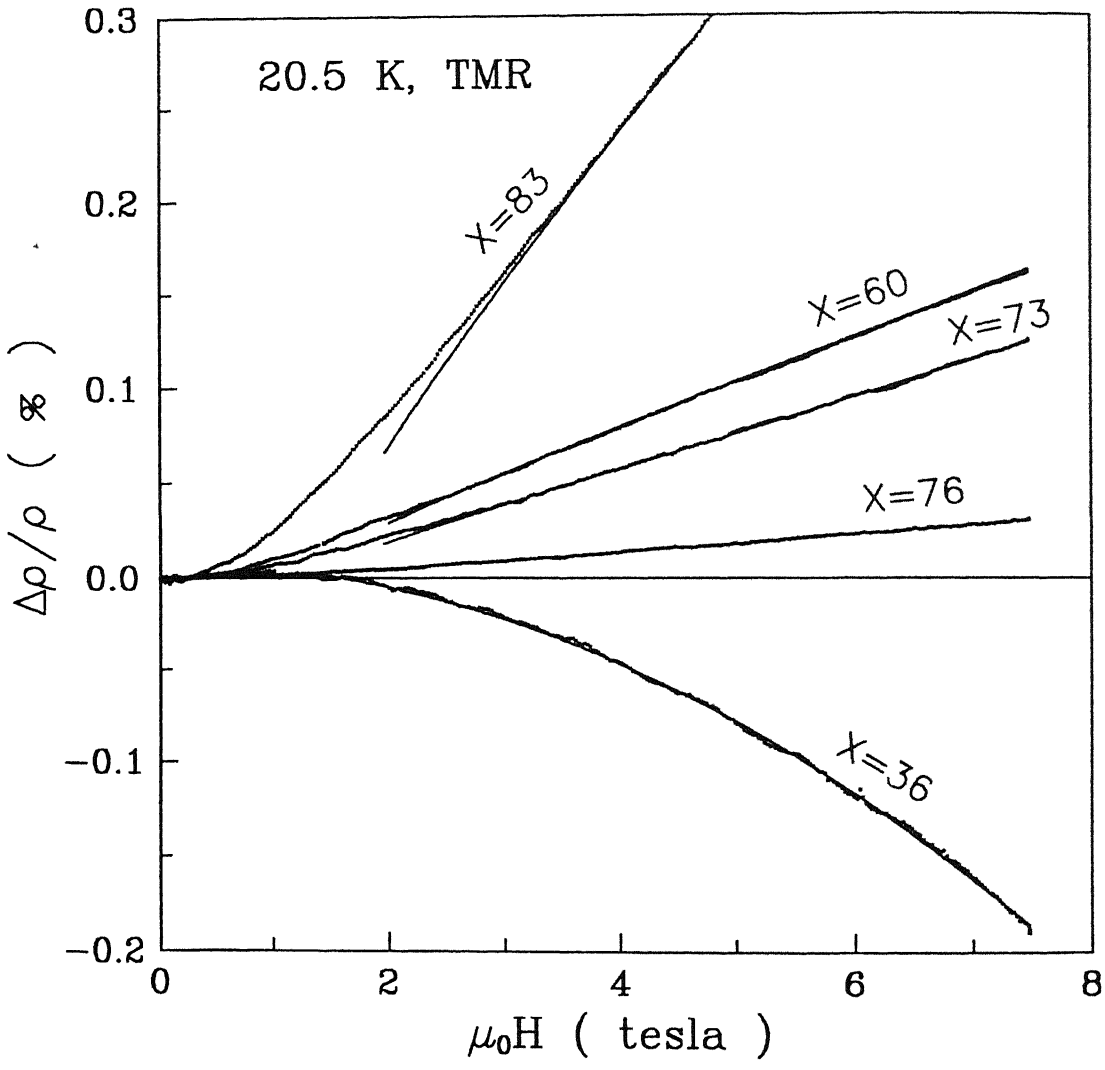

FIG. 4.3. Plots of the transverse magnetoresistance (TMR) data ($\Delta\rho/\rho$ vs μ_0H) in the range of 0 to 7.5 T and the best-fitted curves between 4 and 7.5 T for $Cu_{100-x}Mn_x$ (x = 60, 73, 76, and 83) alloys at 20.5 K. For x=36, both the TMR data and the best - fitted curve are shown between 0 and 7.5 T.

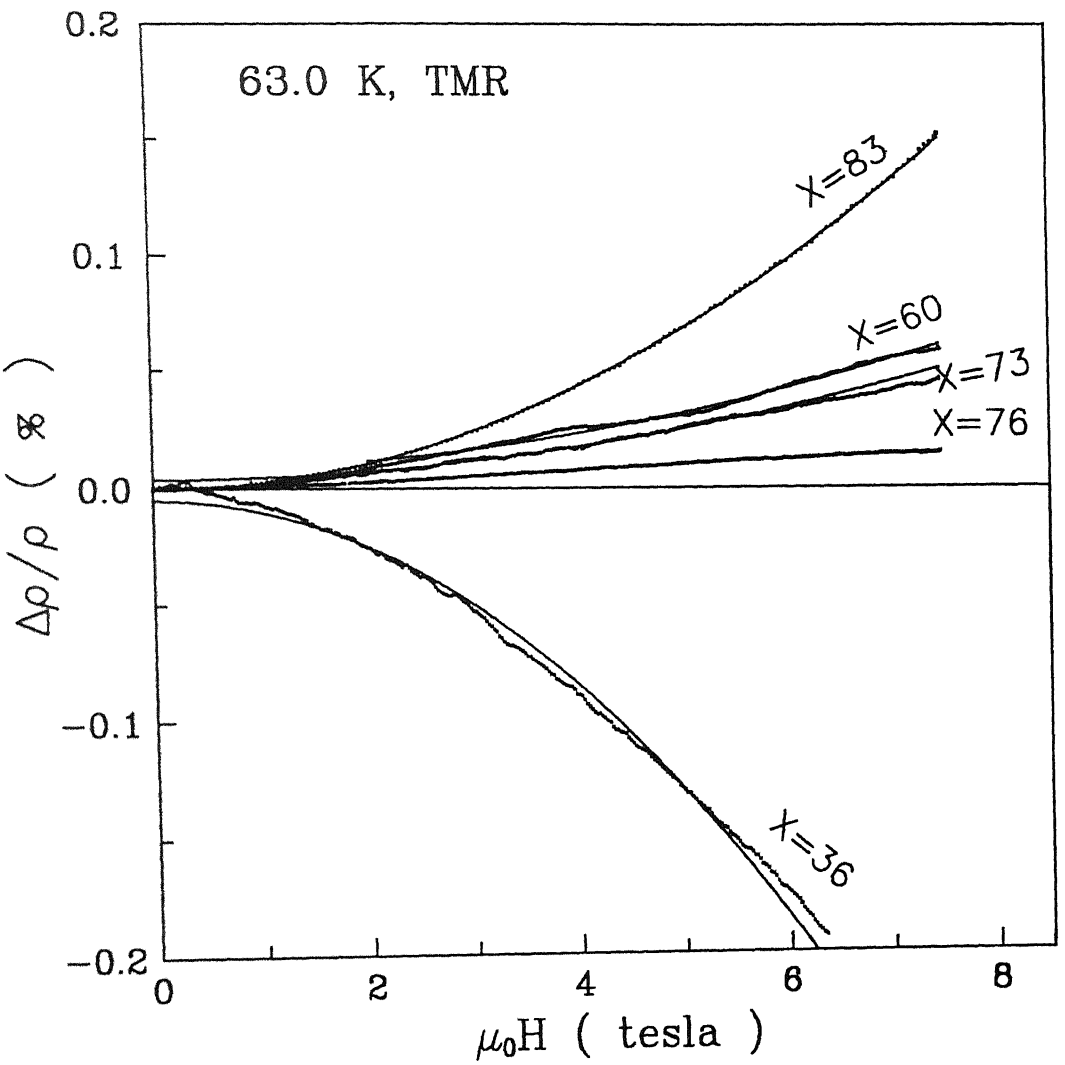

FIG. 4.4. Plots of the transverse magnetoresistance (TMR) data ($\Delta\rho/\rho$ vs μ_0H) and the best-fitted curves between 0 and 7.5 T for $Cu_{100-x}Mn_x$ (x = 36, 60, 73, and 83) alloys at 63 K. For x=76, the TMR data are shown in the range 0 to 7.5 T and the best-fitted curve is between 4 and 7.5 T.

4.1.2 Results and discussion

It is to be noted that the nature of the LMR and TMR curves at 4.2 K for all the alloys are very similar. But the values of the LMR is found to be smaller compared to those of the TMR except for x=36 A negative magnetoresistance similar to that of the spin - glass phase is quite expected in alloy x=36, since it is in the critical region of the magnetic phase diagram[12] where a transition from the spin-glass (SG) to the cluster-glass (CG) phase is observed (see Fig. 1.8). Interestingly, the data for x=36 show more negative TMR at higher temperatures. This clearly indicates that the SG type of contribution is indeed dominant in this particular alloy. Earlier studies on canonical spin glasses[11], including CuMn alloys, have shown that T_f (SG transition temperature) increases with concentration and the magnitude of the negative TMR increases with temperature till $\approx T_f$ and then it decreases with T. Here $T_f \simeq 150$ K[12] and hence the above behaviour of the TMR till 63 K is justified. The positive $\Delta\rho/\rho$, observed in these concentrated alloys (including even the low-field data for x=36 at 4.2 K), is in contrast to the earlier findings of negative magnetoresistance in the dilute regime of $Cu_{100-x}Mn_x$ ($x \leq 10$)[11]. To find whether the normal magnetoresistance[13] ($(\Delta\rho/\rho)_N = C_N H^2$ where $C_N = 1/(2ne\rho)^2$, (see Eq. (1.26))) could be responsible for the observed positive TMR, we estimate it using $n \simeq 10^{28}$ electrons/m^3 and find that $(\Delta\rho/\rho)_N \simeq 10^{-6}$ at 5 T which is much smaller than the present $\Delta\rho/\rho$ values ($(2 - 66) \times 10^{-4}$). This suggests that the normal magnetoresistance can hardly explain the magnitude of the positive $\Delta\rho/\rho$. Moreover, the present alloys are compositionally disordered with large residual resistivities ($\rho_0 \simeq 150$ $\mu\Omega$cm). As it was discussed in Chapter 3, the electrical resistivity measurements (ρ(T)) have clearly identified the EEI effects as responsible for the resistivity minima in these alloys. Here one should note that the similarity in the behaviour of the LMR and TMR data gives a possible indication for the presence of weak localisation/EEI effects.

From our earlier discussion in Chapter 1, it is clear that a positive magnetoresistance is expected from both spin-orbit interaction and EEI effects. Theoretically, to find at least a moderate spin-orbit contribution, one should have an alloy of heavy elements, like 4d or 5d series of elements. In an extensive study, Bieri et al.[6] have shown the dominant presence of spin-orbit interaction in the magnetoresistance of $Cu_{50}Lu_{50}$, $Pd_{80}Si_{20}$, $Cu_{50}Y_{50}$, and $Cu_{57}Zr_{43}$ alloys where Y, Zr, and Pd are in

TABLE 4.1. $Cu_{100-x}Mn_x$ alloys with their Mn concentration (x), T_{min}, ρ_0, values of LMR at 7.5 T, equations of fit, and the corresponding parameters for the data at 4.2 K from 4 to 7.5 T.

Mn (x)	T_{min} (K)	ρ_0 ($\mu\Omega$ cm)	$\Delta\rho/\rho$ at 7.5 T (%)	Eqn. of fit	A (10^{-4})	B (10^{-4} $T^{-1/2}$)	C_N or C_3 (10^{-5} T^{-2})
36	2.5	93	-0.11	$A+B\sqrt{H}+C_3H^2$	-9.4	7.2	-3.83
60	16.5	176	0.12	$A+B\sqrt{H}+C_NH^2$	-5.5	5.7	0.35
73	16.5	176	0.06	- ditto -	-1.7	2.3	0.25
76	24 5	197	0.02	- ditto -	-0.4	0.6	0.07
83	12.5	120	0.39	- ditto -	-29.6	24.4	0.42

4d series whereas Lu is a 5d element. One should note that an overall positive magnetoresistances can only be expected from a strong spin-orbit interaction whereas for a moderate one, a downturn of the data is generally observed[5, 6]. The present alloys are made of only 3d elements and thus theoretically it is not possible to invoke strong spin-orbit interaction. They have also not shown any kind of downturn till 7.5 T (except for x=36). So even a moderate spin-orbit interaction could not be assumed. Hence the contribution from the spin-orbit interaction should be rather negligible in these CuMn alloys. Moreover, an earlier experimental observation in Cu-based $Cu_{20}Mg_{80}$ alloy has shown much smaller spin-orbit contribution as compared to that of the localisation effect ($H'_{so} < H_{loc}$, see Table I of Ref.[6]).

On the other hand, these CuMn alloys have shown a distinct positive magnetoresistance which can now be attributed only to the dominant EEI effects. It turns out that the spin - splitting (Eq. (1.40)) and the orbital (Eq. (1.43)) contributions of the interacting electrons to the magnetoresistance have the same field dependence. So it is difficult to isolate them from one another[14] as well as from the weak localisation. However, the orbital contribution is found to be very small[6, 15] in the temperature range of T > 1.2 K and in magnetic fields H $\leq$ 6 T. It becomes dominant only at much lower temperatures and higher fields. Henceforth, we will take only the spin-splitting contribution (Eq.(1.40)) as representing the electron-electron interaction effects. Besides the EEI effects,

a negative contribution from the localisation effects (Eqs. (1.36) and (1.37)) is also expected, as found in $Cu_{50}Ti_{50}$[5] and $Y_{80}Si_{20}$[6] alloys. Hence the expression for the magnetoresistance, coming from quantum interference effects (QIE), can be written (using Eqs. (1.36), (1.37), and (1.40)) as

$$\begin{aligned}(\Delta\rho/\rho)^{QIE} &= (\Delta\rho/\rho)^{int} + (\Delta\rho/\rho)^{loc} \\ &= A + B^{int}\sqrt{H} - B^{loc}\sqrt{H} \\ &= A + B\sqrt{H} \qquad \text{(for high fields)} \end{aligned} \tag{4.1}$$

and

$$\begin{aligned}(\Delta\rho/\rho)^{QIE} &= (\Delta\rho/\rho)^{int} + (\Delta\rho/\rho)^{loc} \\ &= C^{int}H^2 - C^{loc}H^2 \\ &= CH^2 \qquad \text{(for low fields),} \end{aligned} \tag{4.2}$$

where A = -1.3α_1, $\alpha_1 = \frac{\rho e^2 F_\sigma}{4\pi^2\hbar}\sqrt{\frac{k_B T}{2\hbar D}}$, B = ($B^{int}$ - B^{loc}), C = (C^{int} - C^{loc}), $B^{int} = \frac{\rho e^2 F_\sigma}{4\pi^2\hbar}\sqrt{\frac{g\mu_B}{2\hbar D}}$, $B^{loc} = \frac{0.605 e^2\rho}{2\pi^2\hbar}\left(\frac{e}{\hbar}\right)^{1/2}$, $C^{int} = 0.053\alpha_1(\frac{g\mu_B}{k_B T})^2$, and $C^{loc} = \frac{e^2\rho}{96\pi^2\hbar H_i^{3/2}}\left(\frac{e}{\hbar}\right)^{1/2}$. The symbols F_σ, D, g, and μ_B stand for the screening constant, diffusion constant, Lande-g-factor, and Bohr magneton, respectively while the others have their usual meanings. The field dependence of both $(\Delta\rho/\rho)^{int}$ and $(\Delta\rho/\rho)^{loc}$ (see Eqs. (4.1) and (4.2)) are identical in both high and low-field regimes and hence it is very difficult to isolate them. To get estimates of the contributions of the EEI and the localisation effects, we have calculated the coefficients B^{int} and B^{loc} (Eqs. (4.1) and (4.2)) using the values of F_σ=1, D=0.2 $\times$ 10^{-4} m^2s^{-1}, and g=2. They come out of the order of 8 $\times$ 10^{-4} and 5 $\times$ 10^{-4} (both are in $T^{-1/2}$ units), respectively. It shows clearly that the EEI effect is dominant (B = (B^{int} - B^{loc}) = + 3 $\times$ 10^{-4} $T^{-1/2}$) and this is certainly consistent with our observed positive magnetoresistance. Moreover, the EEI effect has already been observed in the ρ(T) measurements till $2T_{min}$. The present disordered alloys have very low diffusion constant (D $\sim$ 0.2 $\times$ 10^{-4} m^2s^{-1}, taken from the interpretation of ρ(T) data). This is much smaller compared to that observed in $Cu_{20}Mg_{80}$ alloy ($\simeq$ 7.7 $\times$ 10^{-4} m^2s^{-1})[6] (where the weak - localisation effect is found to be dominant in $\Delta\rho/\rho$).

As a result, the small value of D for the present CuMn alloys enhances the contribution of the EEI effect, since $\Delta\rho/\rho \propto 1/\sqrt{D}$ (see Eq.(1.40)). Hence a positive magnetoresistance coming from the dominant EEI effects is quite justified. In addition, a quadratic field dependence due to the normal magnetoresistance ($(\Delta\rho/\rho)_N = C_N H^2$), however small it is, is also expected here. The analysis for the Mn-rich alloys ($x \geq 60$) are presented first for convenience and that for x=36 is given later. Assuming Matthiessen's rule, the final expressions for the magnetoresistance are given by

$$\begin{aligned} \Delta\rho/\rho &= (\Delta\rho/\rho)^{QIE} + (\Delta\rho/\rho)_N \\ &= A + B\sqrt{H} + C_N H^2 \qquad \text{(for high fields)} \qquad (4.3) \\ &= C_2 H^2, \qquad \text{(for low fields)} \qquad (4.4) \end{aligned}$$

where $C_2 = C + C_N$. Here H is actually the magnetic induction, commonly referred to as the magnetic field having the unit of tesla. The data, taken at 4.2 and 20.5 K, for the Mn-rich alloys ($x \geq 60$), fit very well to Eq.(4.3) in the range of 4 to 7.5 T (high-field limit) as shown in Figs. 4.1 - 4.3 where the raw data are found to be almost indistinguishable from the best-fitted curves. The details of the fitting parameters are given in Tables 4.1 and 4.2 for longitudinal and transverse modes, respectively. One of the interesting findings in the present fittings is that the LMR and TMR data at 4.2 K show a similar kind of functional dependence on H (see Tables 4.1 and 4.2 , respectively). The values of the fitting parameters for the LMR data are found to be lower as compared to those of the TMR which is really expected as $(\Delta\rho/\rho)_{LMR} < (\Delta\rho/\rho)_{TMR}$. The fit in all the alloys shows that the value of the constant A is negative in agreement with the theory (see Tables 4.1 and 4.2, and Eq.(4.1))). On the other hand, the coefficient B (= (B^{int} - B^{loc}), see Table 4.2) is found to be positive showing dominant EEI effect ($B^{int} > B^{loc}$). The values of the coefficient B, obtained from the fit, are in the range of (1 - 8) $\times$ 10^{-4} $T^{-1/2}$ for all the alloys except x=83 where it is unexpectedly high ((24 - 31) $\times$ 10^{-4} $T^{-1/2}$). These values of B are in reasonably good agreement with our calculated value of 3 $\times$ 10^{-4} $T^{-1/2}$ and this certainly gives us confidence in the present interpretation. In addition, the values of B (see Tables 4.1 and 4.2) also indicate that the contributions from the EEI effect are higher compared to that of the localisation effect in the alloys with x=36, 60, 73, and 83 whereas for x=76, they are found to be almost comparable. The overall decrease of the positive TMR with temperature (Figs. 4.2 - 4.4) is justified from the theoretical point of view (Eq.(4.1)). However, no definite statement could be made for the temperature dependence of the individual

coefficients A and B.

The above fittings (done at 4.2 and 20.5 K only) did not include 63 K since it is is too high a temperature to expect weak localisation along with EEI effects in x = 60, 73, and 83 where T_{min}'s are found at 16.5, 16.5, and 12.5 K, respectively. Here the data fit only to the normal magnetoresistance ($(\Delta\rho/\rho)_N = C_N H^2$) for the entire range of 0 to 7.5 T. The fitting parameter, C_N (the coefficient of the normal magnetoresistance term), is found to be in good agreement with the findings at 4.2 and 20.5 K (see Table 4.2). However, the alloy with x = 76, where T_{min} is rather high (24.5 K), has shown surprisingly good fit to Eq.(4.3) at 63 K in the same range of field as at 4.2 and 20.5 K. To check this, the data are also fitted to $(\Delta\rho/\rho)_N = C_N H^2$ resulting in systematic residuals ($(data)_{fit}$ - $(data)_{raw}$) and an order of magnitude higher value of the normalised χ^2. The plots of the raw data and the best-fitted curves are shown in Fig. 4.4. The value of B, obtained from the fitting to Eq.(4.3) for x=76 at 63 K, is found to be consistent with the results at 4.2 and 20.5 K whereas that of the normal magnetoresistance comes out to be much smaller (Table 4.2). This discrepancy can be ascribed to the small value of TMR (0.02 %) at 63 K. According to the Kohler's rule[13] (see Eq.(1.27)), the plot between the normal magnetoresistance, $(\Delta\rho/\rho)_N$, and $\mu_0 H/\rho$ should follow an universal curve for a particular alloy at all temperatures (Kohler's plot). But at much higher fields, it may break down depending on the nature of the Fermi surface. In Fig. 4.5 we have plotted the normal magnetoresistance data ($(\Delta\rho/\rho)_N = C_N H^2$) against ($\mu_0 H/\rho$) at 4.2, 20.5 and 63 K (curves 1, 2, and 3, respectively) taking the values of C_N from the fit[16]. The data are found to fall almost on one curve for all the Mn-rich alloys ($x \geq 60$) at all temperatures till 5 T. Above 5 T, they start deviating from each other as expected.

In the low-field limit, the TMR and the LMR data for all the alloys with $x \geq 60$ fit very well to Eq.(4.4) in the range of 0 to 1 T at 4.2 and 20.5 K. The TMR data at 63 K of only x=76 have shown a good fit to Eq.(4.4). All the details of the fitting parameters are given in Table 4.3. In Fig. 4.6, the TMR data and the best-fitted curves for the alloys with x = 60, 76, and 83 are shown at 4.2 K for the low-field region. Due to the same H^2 dependence, the low-field QIE coefficient C (= (C^{int} - C^{loc})) has been coupled with that of the normal magnetoresistance (C_N). Unlike the estimate of

TABLE 4.2. $Cu_{100-x}Mn_x$ alloys with their Mn concentration (x), temperature of TMR measurements, value at 7.5 T, range of fit, equations of fit, and the corresponding parameters.

Mn (x)	Temp. (K)	$\Delta\rho/\rho$ at 7.5 T (%)	Range of fit (T)	Eqn. of fit	A or A′ (10^{-4})	B (10^{-4} $T^{-1/2}$)	C_N or C_3 (10^{-5} T^{-2})
	4.2	-0.06	4.0 - 7.5	$A+B\sqrt{H}+C_3H^2$	-10.9	8.4	-3.12
36	20.5	-0.19	0 - 7.5	$A'+C_3H^2$	0.5	-	-3.3
	63.0	-0.26	- ditto -	- ditto -	-0.7	-	-4.75
	4.2	0.18	4.0 - 7.5	$A+B\sqrt{H}+C_NH^2$	-8.2	7.8	1.00
60	20.5	0.16	- ditto -	- ditto -	-7.6	7.1	0.78
	63.0	0.06	0 - 7.5	$A'+C_NH^2$	0.9	-	0.91
	4.2	0.14	4.0 - 7.5	$A+B\sqrt{H}+C_NH^2$	-6.8	5.9	0.91
73	20.5	0.13	- ditto -	- ditto -	-5.3	5.0	0.76
	63.0	0.05	0 - 7.5	$A'+C_NH^2$	-0.4	-	0.84
	4.2	0.04	4.0 - 7.5	$A+B\sqrt{H}+C_NH^2$	-1.0	1.0	0.29
76	20.5	0.03	- ditto -	- ditto -	-1.0	1.0	0.22
	63.0	0.02	- ditto -	- ditto -	-1.1	0.9	0.02
	4.2	0.66	4.0 - 7.5	$A+B\sqrt{H}+C_NH^2$	-34.4	30.7	2.88
83	20.5	0.50	- ditto -	- ditto -	-28.5	24.2	2.38
	63.0	0.15	0 - 7.5	$A'+C_NH^2$	-0.02	-	2.70

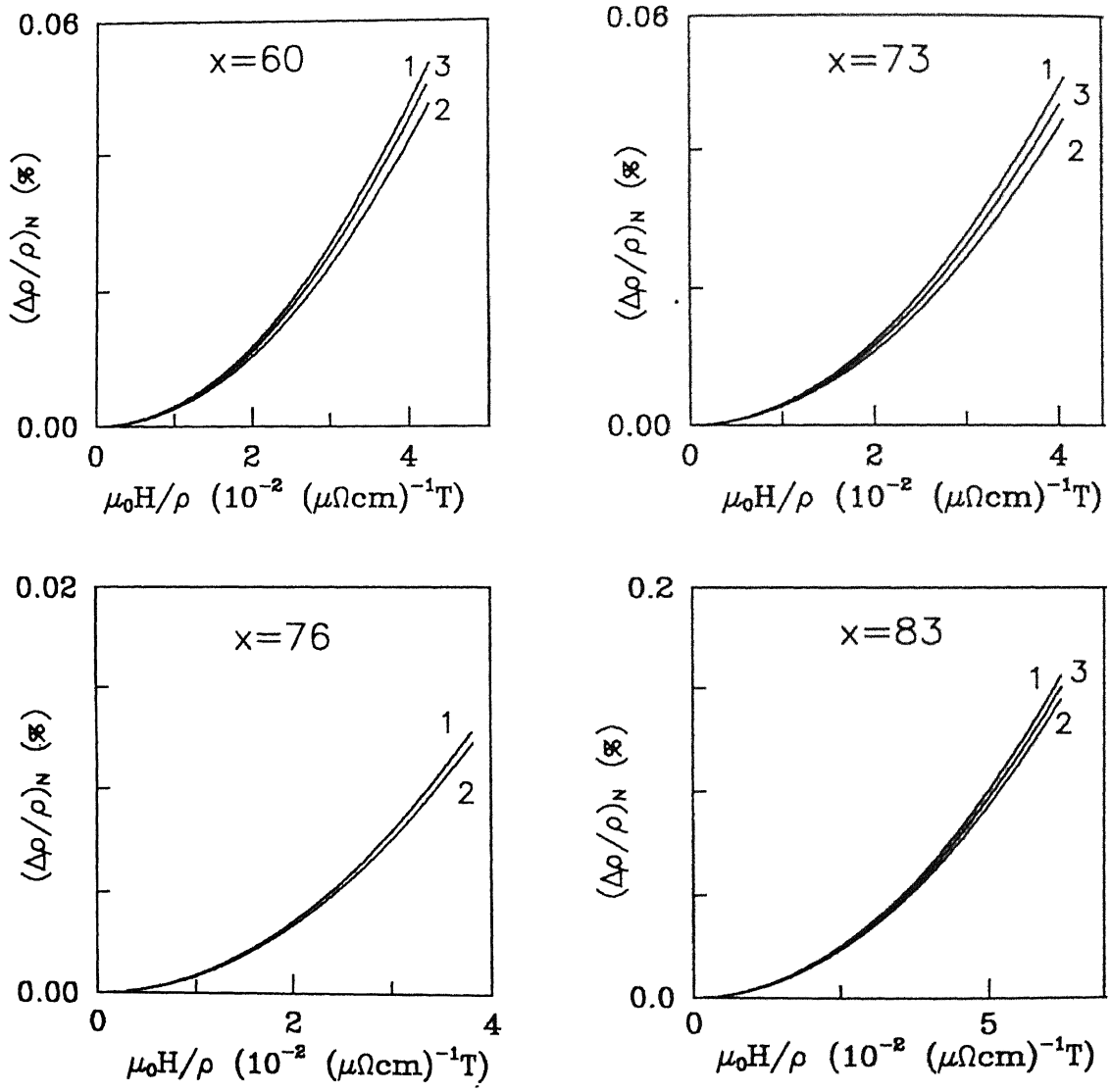

FIG. 4.5. Kohler's plots (normal magnetoresistance ($(\Delta\rho/\rho)_N$) vs (μ_0H/ρ)) for the alloys with x = 60, 73, 76, and 83. Here the numbers 1, 2, and 3 represent the data at 4.2, 20.5, and 63 K, respectively.

B, here it is very difficult to get a theoretical estimate of C of the low-field term ($\propto H^2$), since the value of the inelastic spin-relaxation rate(τ_i^{-1}) is not available for these alloys. However, fitting of the high-field data independently gave the values of the coefficient C_N. One should expect that the values of C_N, obtained from the high-field fit, will remain the same in the low-field fit as well. After subtracting the high-field fit value of C_N from C_2, C is calculated for the Mn-rich alloys (x $\geq$ 60). The large positive values of C (see Table 4.3), thus obtained, again indicate the dominant contribution of the EEI effects compared to the localisation effects ($C^{int} >> C^{loc}$) in the low-field regime. In summary, the present findings in CuMn alloys certainly provide another strong support to the interpretation of the transport properties in terms of the dominant EEI effects.

In alloy x=36, a negative magnetoresistance, similar to that of the SG phase[11, 17], is quite expected. Moreover, the relatively large value of ρ_0 (93 $\mu\Omega$ cm) clearly indicates a fairly disordered state which has shown up in ρ(T) in the form of a resistivity minimum (T_{min} = 2.5 K). Therefore, the CG contribution ($(\Delta\rho/\rho)_{CG} = \beta_{CG}H^2$) has to be considered in the magnetoresistance of this alloy along with those of the EEI/localisation effects (Eqs.(4.1) and (4.2)) and the normal magnetoresistance ($(\Delta\rho/\rho)_N = C_N H^2$). The contributions to the magnetoresistance of these two competing scattering mechanisms, viz, the positive one from the EEI/localisation effects and the negative one from the CG phase are responsible for the downturn of the data at 4.2 K. Thus Eqs.(4.3) and (4.4) can be modified as

$$\Delta\rho/\rho = (\Delta\rho/\rho)^{QIE} + (\Delta\rho/\rho)_N + (\Delta\rho/\rho)_{CG}$$

$$= A + B\sqrt{H} + C_3H^2 \qquad \text{(for high fields)} \qquad (4.5)$$

$$= C_4H^2, \qquad \text{(for low fields)} \qquad (4.6)$$

where $C_3 = C_N - \beta_{CG}$, is the sum of the coefficients of the normal and the cluster-glass terms and $C_4 = C + C_3 = (C^{int} - C^{loc}) + (C_N - \beta_{CG})$, gives the combined effects of interaction, localisation, normal, and cluster-glass terms. Unlike the other alloys, one should not expect the EEI/localisation effects at higher temperatures in x=36 since its T_{min} is only at 2.5 K. Hence the expressions for magnetoresistance, for T > 4.2 K can be written, for all fields, as

$$\Delta\rho/\rho = (\Delta\rho/\rho)_N + (\Delta\rho/\rho)_{CG}$$

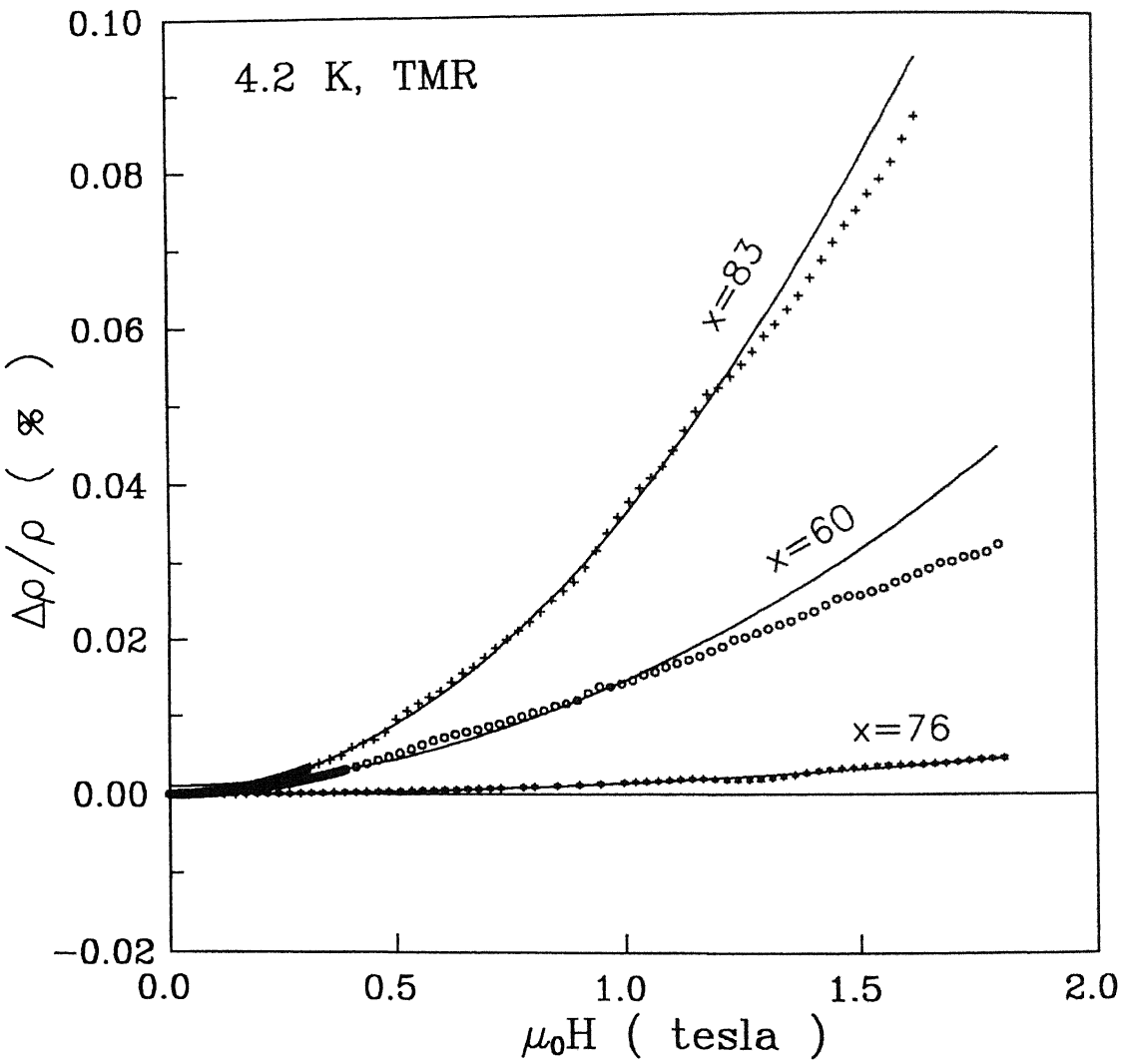

FIG. 4.6. Plots of $\Delta\rho/\rho$ vs $\mu_0 H$ and the best-fitted curves between 0 and 1 T for alloys with x = 60, 76, and 83 at 4.2 K (x = 36 and 73 are excluded for clarity). Here $\Delta\rho/\rho < 10^{-3}$.

$$= C_3 H^2 \qquad \text{(for all fields)}, \tag{4.7}$$

where C_3 (= C_N - β_{CG}) has the same meaning as in Eq.(4.5). The LMR and the TMR data at 4.2 K show very good fits to Eq.(4.5) in the range of 4 to 7.5 T (see Tables 4.1 and 4.2). The plots of the best-fitted curve and the raw data in the range of 4 to 7.5 T are found to be almost indistinguishable in Figs.4.1 and 4.2, respectively for the LMR and the TMR. The observed positive value of B (see Tables 4.1 and 4.2) clearly establishes the dominant EEI contribution to the magnetoresistance ($B^{int} > B^{loc}$) compared to the localisation. The coefficient C_3 is found to be negative indicating a dominant CG contribution compared to the normal magnetoresistance ($\beta_{CG} >> C_N$). However, fitting of the low-field data to Eq.(4.6) in the range of 0 to 1 T shows a positive coefficient of the H^2 term, C_4 (= C + C_3), which is interpreted as due to the dominant EEI contribution (C > C_3, i.e., C^{int} > (C^{loc} + C_3)). The value of C, the coefficient of the low-field EEI term, is estimated following the arguments used for the Mn-rich alloys (x $\geq$ 60). The details of the low-field parameters are given in Table 4.3. The data at 20.5 and 63 K have shown good fits to Eq.(4.7) in the whole range of 0 to 7.5 T. This is really justified in x=36 with the lowest T_{min} of 2.5 K. It is very difficult to isolate the coefficients of the cluster-glass (β_{CG}) and the normal magnetoresistance (C_N) contributions from C_3 (= C_N - β_{CG}) in the present case. Since the alloy with x=60 is compositionally nearest to x=36, the normal magnetoresistance contribution can be considered to be roughly of the same order in x=36 and 60. This assumption helps us atleast in estimating the coefficient β_{CG} of the cluster-glass term. Taking C_N = 1 $\times$ 10^{-5} T^{-2}, the values of β_{CG} come out as 4.1, 4.3, and 5.8 (in units of 10^{-5} T^{-2}) at 4.2, 20.5, and 63 K, respectively. These values show an increase in the cluster-glass term with temperature. This is quite expected as it has been already observed in canonical spin glasses[11] (including CuMn alloys). To summarize, the positive magnetoresistance in concentrated γ - CuMn alloys can be attributed to the dominant presence of EEI effects.

4.2 NiFeCr alloys

4.2.1 General description of the data

Measurements are made in both longitudinal and transverse orientations on some fifteen different compositions of Ni-rich γ - $Ni_{100-x-y}Fe_xCr_y$ ($6 \leq x \leq 23$; $2 \leq y \leq 21$) alloys at 4.2 K in magnetic inductions till 1.4 T. The present alloys are all ferromagnetic at 4.2 K. All details regarding the

alloy designation, composition, Curie temperature (T_c), and resistivity value at 4.2 K ($\rho_{4.2K}$) are given in Table 4.4. The values of T_c for almost all the alloys are taken from an earlier report on dc-magnetisation[18] except for S41, S47, and S50 where they are obtained from the present ac-susceptibility measurements (discussed in Chapter 3). The typical behaviour of the magnetoresistance ($\Delta\rho/\rho$) for low - Cr content ($x \leq 15$) and high - Cr content alloys ($x \geq 18$) are shown in Figs. 4.7 and 4.8, respectively. The plots for both longitudinal (LMR) and transverse magnetoresistance (TMR) for alloys S9, S26, S32, and S40 are given in Fig. 4.7 whereas those for S41 and S47 are presented in Fig. 4.8. In the low - Cr content alloys, the LMR and the TMR are positive and negative, respectively at low fields, but as the field increases, they both become positive. This low-field anisotropy in the magnetoresistance is better known as the ferromagnetic anisotropy of resistivity (FAR)[13]. At this stage, our interest is to analyze the data well above the anisotropy region and so we will not discuss the FAR now. On the other hand, in the high - Cr content alloys, both the LMR and the TMR are negative and nearly isotropic (see Fig. 4.8), i.e., the FAR ($(\Delta\rho/\rho)_{LMR}$ - $(\Delta\rho/\rho)_{TMR}$) in the present alloys decreases with increasing Cr concentration. However, the isotropic nature of the magnetoresistance in the high - Cr content alloys is found to be quite interesting. Recently similar behaviour has been observed in Cr-rich $Fe_{80-x}Ni_xCr_{20}$ alloys[16].

4.2.2 Field dependence of magnetoresistance

The slopes ($\frac{1}{\rho}\frac{d\rho}{dH}$) for both the LMR and the TMR data beyond technical saturation are coming positive in the low-Cr content alloys (see Fig. 4.7) whereas they are negative in the high-Cr content alloys. In conventional ferromagnets, a negative slope is generally expected which is explained in terms of both the reduced electron-magnon scattering as well as the slow increase in magnetisation with applied field beyond saturation[13]. Earlier, a similar kind of positive magnetoresistance beyond technical saturation was observed in some Cr containing crystalline[8, 19] and amorphous[19] alloys. This was described by the dominance of the positive normal magnetoresistance[13] ($\propto H^2$), arising due to the Lorentz force acting on the conduction electrons, over the negative ferromagnetic contribution. Very recently a positive magnetoresistance[20] in Cr-rich $Cr_{100-x}Fe_x$ amorphous thin films is attributed to the strong spin - orbit interaction[6] in the weak localisation limit. This is quite surprising since strong spin - orbit interaction is expected only

TABLE 4.4. Sample designation, alloy composition, ferromagnetic Curie temperature (T_c), and value of resistivity ($\rho_{4.2K}$) at 4.2 K.

Alloy No.	Alloy Compositions	T_c (K)	$\rho_{4.2K}$ ($\mu\Omega$cm)
S35	$Ni_{77}Fe_{21}Cr_2$	778‡	31
S9	$Ni_{85.5}Fe_{11}Cr_{3.5}$	620‡	40
S26	$Ni_{80}Fe_{16}Cr_4$	693‡	52
S32	$Ni_{69.5}Fe_{23}Cr_{7.5}$	635‡	60
S28	$Ni_{75}Fe_{17}Cr_8$	543‡	61
S29	$Ni_{75}Fe_{13}Cr_{12}$	365‡	82
S51	$Ni_{67}Fe_{21}Cr_{12}$[a]	470‡	87
S33	$Ni_{68}Fe_{17.5}Cr_{14.5}$	320‡	88
S40	$Ni_{73.5}Fe_{11.5}Cr_{15}$	260‡	87
S42	$Ni_{78}Fe_6Cr_{16}$	185‡	85
S34	$Ni_{73}Fe_{13}Cr_{14}$	315‡	82
S48	$Ni_{70}Fe_{12}Cr_{18}$	179‡	78
S41	$Ni_{73.5}Fe_8Cr_{18.5}$	44	81
S50	$Ni_{72}Fe_8Cr_{20}$	60	84
S47	$Ni_{71}Fe_8Cr_{21}$	48	84

‡ Values taken from Ref. 10.

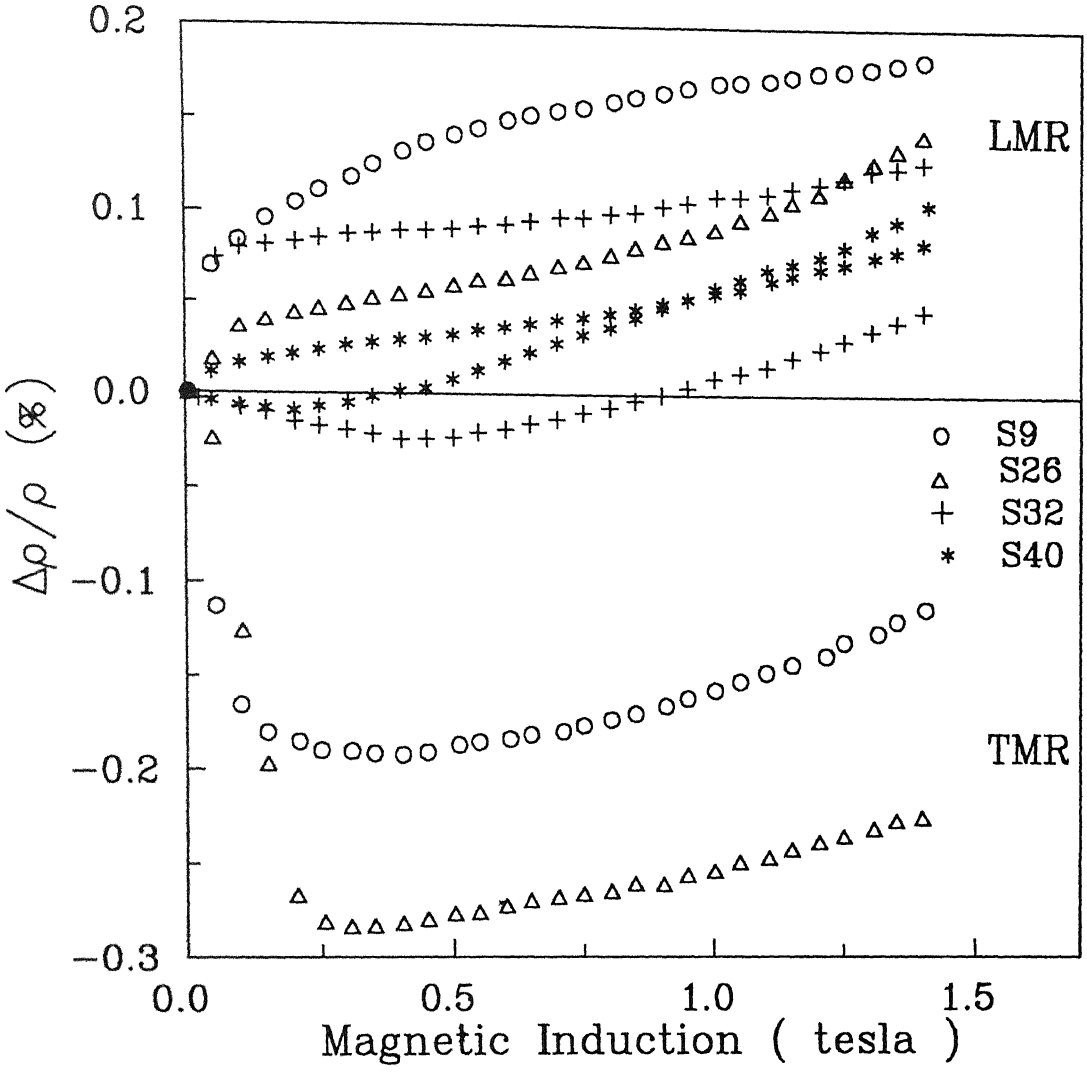

FIG. 4.7. Longitudinal (LMR) and transverse (TMR) magnetoresistance for alloys S9, S26, S32, and S40 at 4.2 K till 1.4 T of applied magnetic induction (μ_0H).

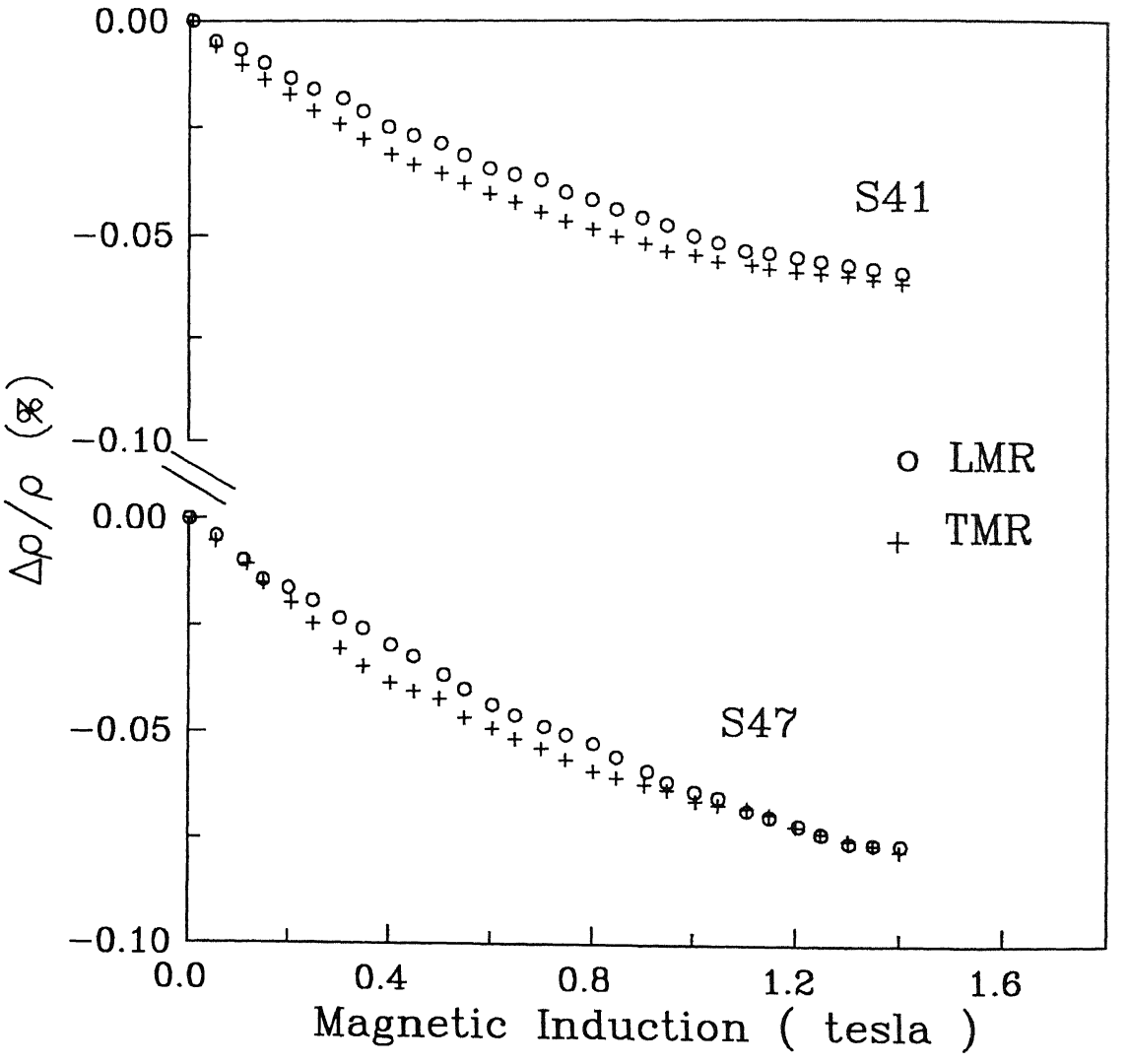

FIG. 4.8. Longitudinal (LMR) and transverse (TMR) magnetoresistance for alloys S41 and S47 at 4.2 K till 1.4 T of applied magnetic induction (μ_0H).

in alloys with 4d or 5d series of elements[6] (e.g., CuLu, CuPd, etc.). Now we discuss the positive magnetoresistance in the low - Cr content alloys first. The present alloys have fairly large values of resistivity ($\rho_{4.2K} \simeq$ (31 - 88) $\mu\Omega$cm) (see Table 4.4). The constituents of these alloys are all 3d elements and hence the spin - orbit interaction is unlikely to be strong. Moreover, the electrical resistivity study (in Chapter 3) on some of the present alloys (i.e., S28, S29, S33, S34, S48, S41, S47, and S50) has shown resistivity minima which have been interpreted satisfactorily in terms of the electron - electron interaction effects in the weak localisation limit[2, 3]. Hence, the dominant presence of the EEI effects (discussed earlier in details for CuMn alloys) seems responsible for the present positive magnetoresistance. However, according to the electron-electron interaction effects, a $\sqrt{H}$ dependence (Eqs.(1.40) and (1.41)) is generally expected at very high fields (h >> 1, i.e., H $\geq$ 5 T at 4.2 K) and an H^2 dependence (Eqs.(1.40) and (1.42)) at much lower fields (h << 1, i.e., H $\leq$ 2 T)[5, 6]. The present measurements are till 1.4 T and hence the data should be fitted only to the low - field limit. In addition, a positive normal magnetoresistance (see Eq. (1.26)) is generally expected in metals and alloys[13]. It is very important to have a rough estimate of the contribution coming from this normal magnetoresistance since both Eqs.(1.26) and (1.42) have the same H^2 dependence. From the Hall effect studies in these alloys (which will be discussed later in Chapter 5), the ordinary Hall coefficient (R_0) is found to be of the order of 5 $\times$ 10^{-11} ΩmT^{-1}. An order of magnitude estimate of n (the carrier concentration) $\simeq$ 10^{29} m^{-3} has been made from the equation R_0 = 1/ne. Hence $(\Delta\rho/\rho)_N$ (using Eq.(1.26)) is found to be of the order of 10^{-8} at 1 T which is negligible compared to the present values of (1 - 10) $\times$ 10^{-4} (see Fig. 4.9). In Fig. 4.9 the MR data for alloys S28, S29, S33, and S48 are presented above the FAR region in both the longitudinal and transverse orientations. It is to be noted that the plots (Fig. 4.9) for both the LMR and the TMR are shifted along the Y-axis for better clarity. However, the change in $\Delta\rho/\rho$ in Fig. 4.9 is on an absolute scale. Here the positive MR in both the orientations are attributed to the dominant presence of the electron - electron interaction effets in the low-field limit. The expression for magnetoresistance due to the EEI effects in the low-field limit comes out to be

$$(\Delta\rho/\rho)^{int} = C_{int}H^2, \tag{4.8}$$

where

$$C_{int} = 0.053\frac{e^2\rho F_\sigma}{4\pi^2\hbar}\left(\frac{k_BT}{2D\hbar}\right)^{1/2}\left(\frac{g\mu_B}{k_BT}\right)^2. \tag{4.9}$$

Fitting both the LMR and the TMR data to Eq.(4.8) gives normalised $\chi^2 \simeq 5 \times 10^{-5}$ which is consistent with our experimental resolution. In Fig. 4.9, the plots for the raw and the best-fitted data are found to fall almost on the same curve. The values of C_{int}, the coefficient of the H^2 term, are obtained in the range of (1 - 5) $\times$ 10^{-6} T^{-2} which is almost the same for both the orientations as expected theoretically. These values are found to be an order of magnitude smaller than those in CuMn alloys (see Table 4.3). To conclude, the present findings of an H^2 dependence of both the LMR and TMR data till 1.4 T have certainly reinforced the interpretation of ρ(T) at low temperatures in terms of the electron - electron interaction effects. On the other hand, the ac-susceptibility study (discussed earlier in Chapter 3) in the high - Cr content alloys S41, S47, and S50 has shown a second magnetic transition at 9, 14, and 7 K, respectively besides the ferromagnetic one at their respective Curie temperatures. According to the earlier neutron diffraction and dc-magnetisation studies[21], this low-temperature transition represents a spin-glass phase. The present magnetoresistance data are taken only at 4.2 K which is lower than the spin-glass transition temperatures. Hence a negative magnetic contribution arising from the spin-glass/cluster-glass phase[17] is quite expected which could completely suppress the positive contribution. In addition, the isotropic behaviour of the magnetoresistance provides another indication for such dominance of spin - glass / cluster - glass contribution[11]. However, to say something more conclusively in both the low and high - Cr content alloys, one has to do the measurements at much higher fields ($\simeq$ 10 T)[6] and at lower temperatures ($\leq$ 1 K) which are not accessible to us.

4.2.3 Ferromagnetic anisotropy of resistivity

4.2.3.1 General introduction

In the last few decades, lot of efforts have been made experimentally[7–9, 19, 22–26] as well as theoretically[7, 9, 13, 27–33] to understand the ferromagnetic anisotropy of resistivity (FAR) in Ni and Fe - based alloys. Interestingly, most of the earlier studies[7–9, 22, 25] were focussed on alloys with large FAR ($\simeq$ (10 - 20)%). In an extensive study[8], Van Elst had pointed out long back that adding a few atomic percent of Cr in Ni and Fe-based alloys could decrease the value of FAR sharply. It is important to note that the value of the FAR is reported[8] as zero for 10.1 at.%

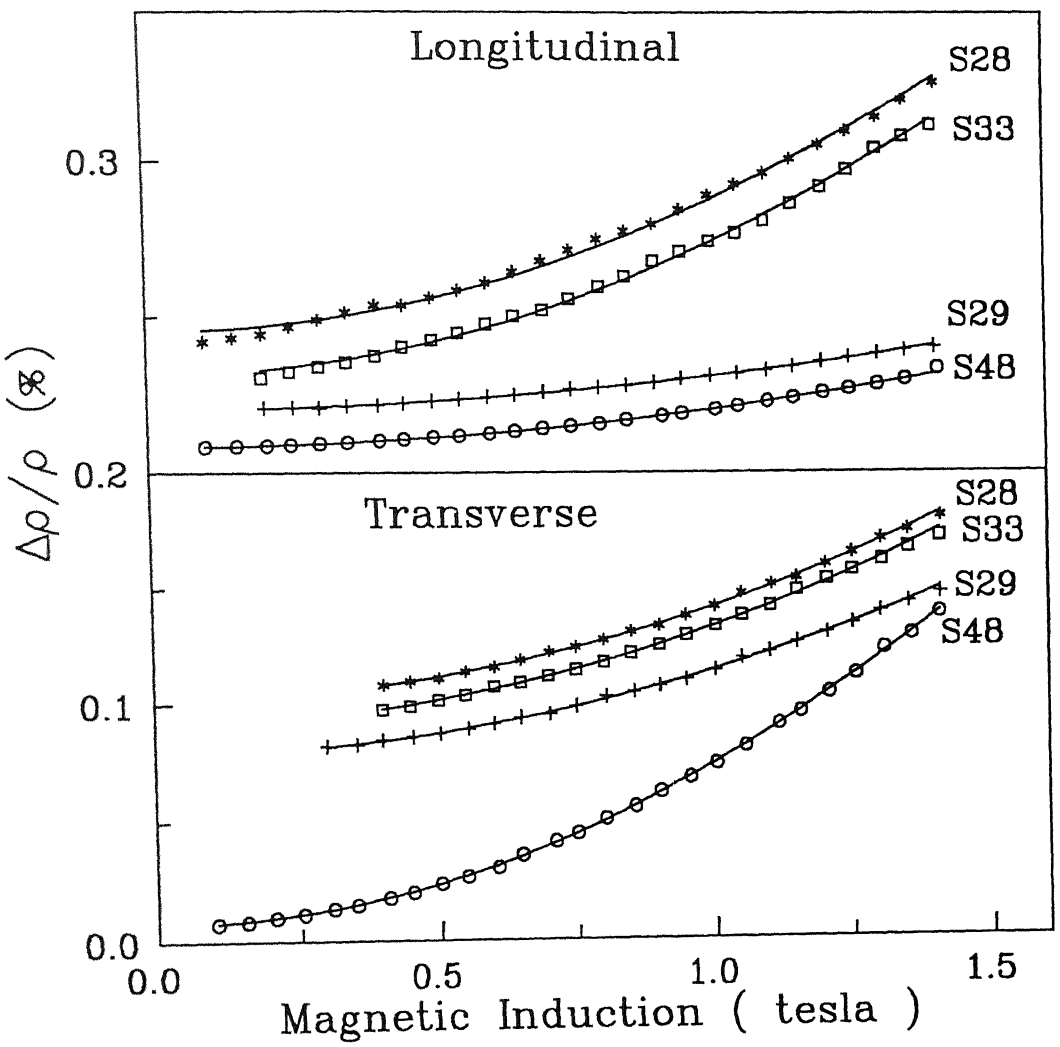

FIG. 4.9. Plots of longitudinal and transverse magnetoresistance ($\Delta\rho/\rho$ vs μ_0H) and their best-fitted (Eq.(4.8)) curves till external magnetic inductions of 1.4 T for alloys S28, S29, S33, and S48 at 4.2 K. Only the regions beyond FAR are shown.

Cr in $Ni_{100-x}Cr_x$ alloys. On the other hand, the behaviour of FAR in ternary alloy systems was found to be rather complicated and hence difficult to interpret. Later Berger and others[9, 27, 34, 35] have suggested that the split-band (SB) model could provide a satisfactory explanation for the composition dependence of FAR, EHC, and linear saturation magnetostriction in NiFeCu ternary alloys. The above SB model can also be applied to binary alloys. As a consequence, most of the earlier studies had dealt with binary alloys where the FAR was found to be very large (10 - 20)%. Till now, except for some scattered reports on amorphous alloys[23, 35], no detailed investigation on FAR along with EHC and linear magnetostriction coefficient (λ_s) has been made in any ternary crystalline systems suggested in the SB model except NiFeCu. In this work, the magnetoresistance is measured and FAR is calculated using Eq. (1.30) in some fifteen different compositions of chrome - permalloys γ - $Ni_{100-x-y}Fe_xCr_y$ ($6 \leq x \leq 23; 2 \leq y \leq 21$) at 4.2 K in magnetic inductions till 1.4 T. The values of the FAR are found to be much smaller than 0.1 % for high-Cr content (>12 at.%) alloys. The values of the FAR for all the alloys at 4.2 K are given in Table 4.5. The maximum value of the demagnetisation factor β is in the transverse direction and it is of the order of 2×10^{-2} and hence $\beta M_S \simeq 100$ Oe. The value of the zero-field electrical resistivity ρ^0 (see Eq.(1.28)) is obtained by averaging over directions of spontaneous magnetisation which for any cubic crystal can be written[19] as

$$\begin{aligned} \rho^0 &= \frac{1}{3}\rho_{\|s} + \frac{2}{3}\rho_{\perp s} \\ &= \rho + \frac{1}{3}\Delta\rho_{\|s} + \frac{2}{3}\Delta\rho_{\perp s}, \end{aligned} \tag{4.10}$$

where ρ is the residual resistivity. A random distribution of domains, however, in these concentrated crystalline alloys is not obvious. However, the values of $\rho_{4.2K}$ are found to be much higher compared to those of $\Delta\rho_{\|s}$ and $\Delta\rho_{\perp s}$ (see Table 4.5) and thus $\rho^0 \simeq \rho_{4.2K}$.

Earlier, the change of sign of the EHC[10] and the coefficient of the linear magnetostriction[36] (λ_s) (i.e., $R_s = \lambda_s = 0$) in the present alloy series could not be explained in terms of the split-band model. However, the study was restricted to only some low Cr-content alloys where their Curie temperatures (T_c) were found around and above the room temperature. Now the Hall resistivity (ρ_H) has been measured in alloys S29, S41, S48, S47, and S50 at 4.2 K till external magnetic inductions of 1.4 T. The behaviour of ρ_H for alloys S41, S48, S47, and S50 are shown in Fig. 4.10.

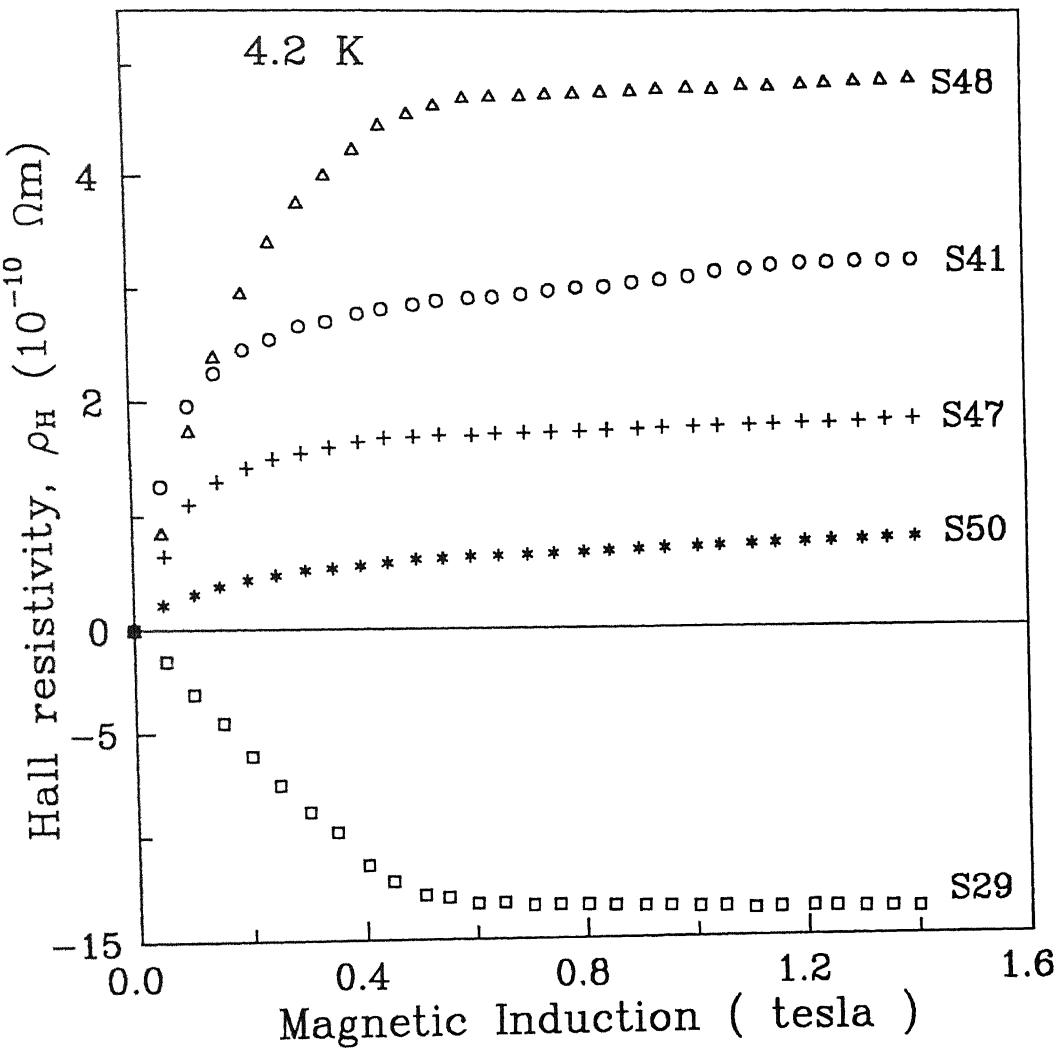

FIG. 4.10. Hall resistivity (ρ_H) data for alloys S29, S41, S48, S47, and S50 at 4.2 K till 1.4 T of applied magnetic induction (μ_0H).

TABLE 4.5. Sample designation, alloy composition, value of resistivity ($\rho_{4.2K}$), FAR, extra-ordinary Hall resistivity (R_sM_s), and extra-ordinary Hall conductivity (γ_{HS}).

Alloy No.	Alloy Compositions	$\rho_{4\,2K}$ ($\mu\Omega$cm)	FAR (%)	R_sM_s (10^{-9} Ωm)	γ_{HS} (10^3 Ω^{-1} m^{-1})
S35	$Ni_{77}Fe_{21}Cr_2$	31	0.76	+0.9‡	+9.4
S9	$Ni_{85.5}Fe_{11}Cr_{3.5}$	40	0.38	-6.6‡	-41.3
S26	$Ni_{80}Fe_{16}Cr_4$	52	0.26	-1.5‡	-5.5
S32	$Ni_{69.5}Fe_{23}Cr_{7.5}$	60	0.16	+4.9‡	+13.6
S28	$Ni_{75}Fe_{17}Cr_8$	61	0.11	-1.9‡	-5.1
S29	$Ni_{75}Fe_{13}Cr_{12}$	82	0.05	-1.3	-1.9
S51	$Ni_{67}Fe_{21}Cr_{12}$[a]	87	0.05	+5.9‡	+7.8
S33	$Ni_{68}Fe_{17.5}Cr_{14.5}$	88	0.04	+2.7‡	+3.5
S40	$Ni_{73.5}Fe_{11.5}Cr_{15}$	87	0.04	-2.9‡	-3.8
S42	$Ni_{78}Fe_6Cr_{16}$	85	0.07	-0.7‡	-1.0
S34	$Ni_{73}Fe_{13}Cr_{14}$	82	0.07	-0.7‡	-1.0
S48	$Ni_{70}Fe_{12}Cr_{18}$	78	0.02	+0.5	+0.8
S41	$Ni_{73.5}Fe_8Cr_{18.5}$	81	0.02	+0.3	+0.5
S50	$Ni_{72}Fe_8Cr_{20}$	84	0.00	+0.05	+0.1
S47	$Ni_{71}Fe_8Cr_{21}$	84	0.01	+0.2	+0.3

‡ Values taken from Ref. 10.

The values of R_0 and R_sM_s are obtained from the slope and the intercept of the linear fit of the Hall resistivity data beyond saturation. The sign of both R_0 and R_sM_s are positive for alloys S48, S41, S47, and S50 whereas they are negative for S29. The values of R_0 are found of the order of (2 - 5) $\times$ 10^{-11} ΩmT^{-1} whereas those of R_sM_s are in the range of (0.05 - 1.3) $\times$ 10^{-9} Ωm (see Table 4.5). The absolute values of R_sM_s are found to be almost comparable with those of ρ_H since the values of R_0B_z (at 1 tesla) are more than two orders of magnitude smaller than those of R_sM_s. On the contrary, the electrical resistivity at 4.2 K is found to be almost three times greater than the Hall resistivity (see Table 4.5). According to the side-jump effect[37–39], this is quite expected in the present concentrated alloys. In Table 4 5, the values of R_sM_s in the remaining alloys are taken from earlier reports[10]. The values of the extra-ordinary Hall conductivity (γ_{HS} = R_sM_s/ρ^2) are calculated using the values of $\rho_{4\,2K}$.

4.2.3.2 Description of FAR using the split-band model

Smit[7] and Van Elst[8] had shown long back that the FAR reaches a maximum of 20% in $Ni_{100-x}Fe_x$ and $Ni_{100-x}Co_x$ alloys with x $\simeq$ 18 which corresponds to almost the same 27.7 electrons per atom ratio. Later on, R_s[9, 10, 23, 25, 27] and λ_s[34–36] were found to change their signs exactly at the same alloy composition (x = 18 at.%)[22, 27]. Later in ternary NiFeCu alloys, the line $R_s \simeq \lambda_s \simeq 0$ was found to deviate a lot from the line of 27.7 electron / atom ratio. This was, however, interpreted in terms of the split-band (SB) model. The constituents (i.e., Ni, Fe, and Cr) of the present alloy series have their valence difference Z $\geq$ 2. As result, they form their own distinct 3d subbands separated from each other on the energy scale (as in Fig. 1.6) where the bands of Ni will be at the bottom (since it is most attractive to electrons) while those of Cr will be at the top. The degeneracy between Fe 3d$\downarrow$ and Ni 3d$\downarrow$ bands (see Fig. 1.6) will cross the Fermi level when the alloy compostitions, according to Eq. (1.62), are related by

$$3C_{Fe} + (10 + Z)C_{Cr} = 0.55 \quad (4.11)$$

$$i.e.,\ 3C_{Fe} + 6C_{Cr} = 0.55, \quad (4.12)$$

the valence difference (Z) between Cr and Ni being -4.

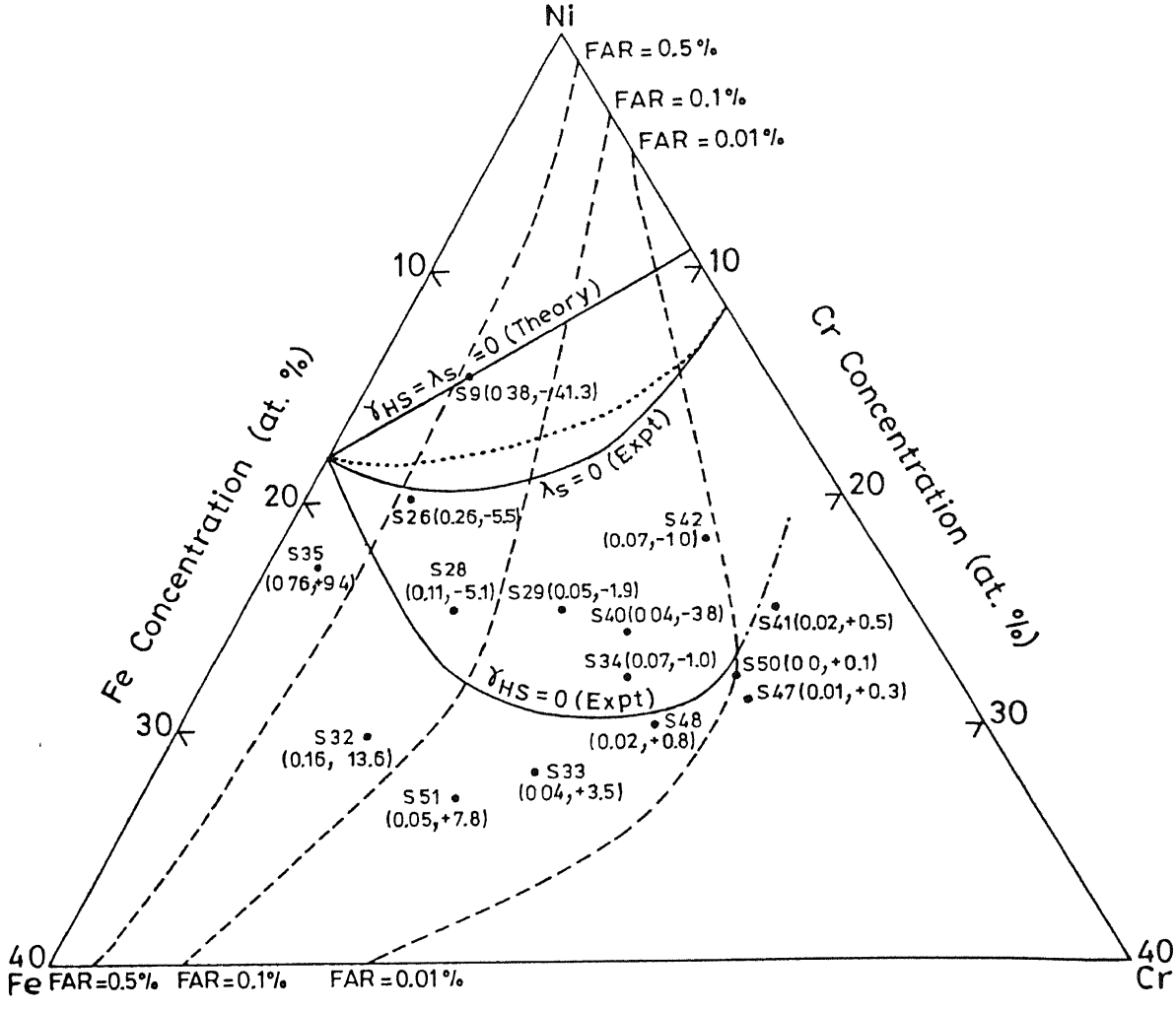

FIG. 4.11. Ternary phase diagram for NiFeCr alloys. The alloys are represented by their sample designation. The numbers, given in the bracket after each sample designation, are the values of the FAR (in %) and γ_{HS} (in units of $10^3\ \Omega^{-1}m^{-1}$), respectively. The dashed lines are contours of constant FAR. The experimentally obtained γ_{HS}=0 line (where the data for the solid line are taken from Ref. 10 and the dot-dashed line is the extended one from the present work, for details see Table 4.5) is shown along with the theoretically predicted straight line (according to the split-band model (Eq. (4.12)). The data for the experimental λ_s=0 (solid) line are taken from Ref. 36. For the dotted line, see text.

The FAR is found to be much less than 1 % in the present alloys. It is interesting to note that the alloys with high Cr-content (i.e., 16 at.% or more) have almost zero FAR. This is consistent with the earlier data[8] of Van Elst. However, most of the studies, reported so far in support of the split-band model, have focussed on the alloys (NiFe, NiCo, NiFeCu[9] (all are fcc), FeV, and FeCr[25] (all are bcc)) where a large FAR ((10 - 20) %) was observed. According to those, a maximum FAR ($\simeq$ (10 -20)%) is expected when the point T of the 3d spin-down band of Ni approaches the Fermi level (Fig. 1.6). But this is not the case in the present γ-NiFeCr alloys. In the ternary phase diagram (Fig. 4.11), the constant FAR lines are plotted using the present values. The FAR is found to decrease with increasing Cr concentration. The maximum FAR is found to be in the region where the alloy $Ni_{80}Fe_{20}$ lies. This is quite expected since the alloy γ-$Ni_{80}Fe_{20}$ has an FAR of 18%, the maximum value reported so far for any bulk crystalline alloy[8]. This certainly implies that the addition of Cr smears the orbital degeneracy so that the average energy difference between the 3d branches in the vicinity of the Fermi level increases, which, in turn, destroys the FAR.

Coming back to the Hall effect studies, the extended γ_{HS} = 0 line is drawn on the ternary phase diagram (Fig. 4.11) of the present NiFeCr alloys using their positive and negative values along with the theoretical line, predicted by the SB model (Eq.(4.12)). In Fig. 4.11, the alloys are represented by their sample designation (Table 4.5). The two numbers in the bracket, given after each sample designation, show the values of the FAR (in %) and γ_{HS} (in units of 10^3 $(\Omega m)^{-1}$) at 4.2 K for the corresponding alloy. The experimental γ_{HS}=0 line is found to lie much below the theoretical line as it was found in the earlier report[10]. The experimental line exhibits a curvature, instead of a straight line as predicted by the SB model (Eq.(4.12)). This curvature is found to be more pronounced in the high-Cr region of the phase diagram (Fig. 4.11). But the most important observation in the present study is that the ridges of the constant FAR lines are found to follow more or less exactly the experimental γ_{HS}=0 line in the direction of increasing Cr concentration. This is consistent with the idea behind the SB model, but the experimental γ_{HS}=0 line and the ridges of the constant FAR lines deviate a lot from where they are theoretically predicted. This is quite puzzling. In an earlier study[36], the experimental λ_s=0 line (shown in Fig. 4.11) also exhibited a

ırvature in the ternary phase diagram for the present alloys. The probable reason for such a large ɔviation could be attributed to the concentration dependent values of (10+Z) (hereafter referred) as Z_{eff}) in Eq.(4.12) which is taken as a constant (for the present NiFeCr alloys, Z_{eff} = 6) in ıe SB model. According to the Friedel's VBS model[40], the average number of Bohr magneton er atom for the present alloys should follow a similar kind of relation with impurity concentration i.e., M in the alloy NiFeM; Eq.(4.12)) and can be written as

$$\begin{aligned} \mu_{av} &= \mu_{matrix} - (10+Z)C_M \\ &= 0.61 + 2C_{Fe} - Z_{eff}. \end{aligned} \tag{4.13}$$

Earlier, the values of Z_{eff}, calculated from the dc-magnetisation data[18], were obtained in the ange of 3.0 - 4.2 which is smaller than the expected value of 6. In addition, Z_{eff} is found to ɔe highly concentration dependent. Substituting the values of Z_{eff} in Eq.(4.12), the modified heoretical line for R_s=λ_s=0 comes much closer to the experimental λ_s=0 line (still far away from the experimental R_s=0 line) with a small curvature in the Cr-rich region[10] (see dotted line in the ternary phase diagram (Fig. 4.11). In addition, an earlier neutron diffraction study[41] had shown that the presence of Fe in Ni matrix (i.e., in NiFe alloys) does not influence the moment on the nearby Ni atoms. The moments at the Ni and the Fe sites are found to be 0.6 and (2.8 $\pm$ 0.2) (in units of Bohr magneton μ_B). On the other hand, Cr as impurity in Ni matrix introduces a large-spread magnetic moment disturbance[41] around Cr sites which is interpreted as an extended localised states in Ni alloys. The moment at the Cr site is found to be (0.7 $\pm$ 1.1) μ_B. Hence the bands for the present Cr-rich NiFeCr alloys are not so completely split as they are assumed in the SB model[41]. This can be a plausible reason for such a large discrepancy between the experimental findings and the theoretical lines. Earlier studies in FeCr and FeV alloys[25] had pointed out similar discrepancy, but not as large as it is in the present ternary alloys. Intensive theoretical as well as experimental investigations are needed to resolve this. Nevertheless, for the first time, a complete study of FAR (< 1 %) along with the corresponding γ_{HS}=0 and the earlier reported λ_s=0 lines is presented here for any ternary NiFeM system. These compositions should lead to technologically important materials with very high initial permeability.

Now we try to explore the plausible reasons for such small values of FAR in the present γ-

NiFeCr alloys. It is very important to point out here that the addition of 2 at.% of Cr in NiFe alloys reduces the FAR drastically almost from 18% (in $Ni_{80}Fe_{20}$) to 0.76% (in $Ni_{77}Fe_{21}Cr_2$ (S35)). This is consistent with the earlier reported values[8] of 0.79 % in $Ni_{99}Cr_1$. Very recently, this has also been found in amorphous alloys where FAR decreases with increasing Cr concentration[42, 43]. In Table 4.5, the values of the FAR are listed where the maximum is found around 0.76% for S35 while the minimum is less than 0.01% for S50. It is to be noted here that the high resolution of the present data allows us to observe convincingly FAR of less than 0.1%. It is well known that the ferromagnetic anisotropy of resistivity is a manifestation of the spin-orbit interaction[9] and is usually expressed as

$$FAR = (A_{so}/\Delta E)^2 + ..., \tag{4.14}$$

where the dots indicate higher order terms, A_{so} is the spin-orbit parameter, and ΔE the energy difference between branches of the 3d band near the Fermi level. Earlier the coherent potential approximation calculations[44] in $Ni_{90}Fe_{10}$ and $Ni_{90}Cr_{10}$ alloys have shown $(\Delta E)^{\downarrow}_{Fe-Ni} \simeq 0.56$, $(\Delta E)^{\downarrow}_{Cr-Ni} \simeq 0.52$, $(\Delta E)^{\uparrow}_{Fe-Ni} \simeq$ -0.06, and $(\Delta E)^{\uparrow}_{Cr-Ni} \simeq 0.7$ (all values are in units of half the band width of the respective impurity). Here the signs $\downarrow$ and $\uparrow$ represent the spin-down and the spin-up bands, respectively. It is interesting to see that the FAR is almost unaffected by the energy difference between spin-down bands of FeNi and CrNi (where Fe and Cr are impurities in Ni matrix), since $(\Delta E)^{\downarrow}$ is almost the same in both the cases. On the contrary, the large energy difference in the spin-up bands for NiCr compared to that of NiFe alloy is found to be mostly responsible for such low values of the FAR. $(\Delta E)^{\uparrow}_{Cr-Ni}$ is found to be an order of magnitude greater than $(\Delta E)^{\uparrow}_{Fe-Ni}$, which implies that addition of Cr in Ni matrix can effectively reduce the FAR by two orders of magnitude (see Eq.(4.14)). This is in excellent agreement with the experimental values of less than 0.02 % in S41 ($Ni_{73.5}Fe_8Cr_{18.5}$) and the earlier observed value of 18 % in $Ni_{80}Fe_{18}$ alloy. Hence, such small values of FAR in the present γ-NiFeCr alloys are quite understandable.

4.2.3.3 Description of FAR in the two-current conduction model

In the two - current conduction band model[28, 29, 31], the FAR is given by Eq.(1.34). In the low - temperature limit $\rho_{\uparrow\downarrow} \simeq 0$ (no mixing) and hence Eq.(1.34) reduces to

ABLE 4.6. Sample designation, alloy composition, values of resistivity for spin-down ($\rho_\downarrow$) and pin-up ($\rho_\uparrow$) bands at 4.2 K, and their ratio α (= $\rho_\downarrow/\rho_\uparrow$).

Alloy No.	Alloy Compositions	$\rho_\downarrow$ (4.2 K) ($\mu\Omega$cm)	$\rho_\uparrow$ (4.2 K) ($\mu\Omega$cm)	α (= $\rho_\downarrow/\rho_\uparrow$)
S35	$Ni_{77}Fe_{21}Cr_2$	86	49	1.77
S9	$Ni_{85.5}Fe_{11}Cr_{3.5}$	95	69	1.38
S26	$Ni_{80}Fe_{16}Cr_4$	118	93	1.26
S32	$Ni_{69.5}Fe_{23}Cr_{7.5}$	130	112	1.16
S28	$Ni_{75}Fe_{17}Cr_8$	129	116	1.11
S29	$Ni_{75}Fe_{13}Cr_{12}$	174	166	1.05
S51	$Ni_{67}Fe_{21}Cr_{12}$	178	169	1.05
S33	$Ni_{68}Fe_{17.5}Cr_{14.5}$	180	173	1.04
S40	$Ni_{73.5}Fe_{11.5}Cr_{15}$	178	171	1.04
S42	$Ni_{78}Fe_6Cr_{16}$	176	166	1.07
S34	$Ni_{73}Fe_{13}Cr_{14}$	170	159	1.07
S48	$Ni_{70}Fe_{12}Cr_{18}$	158	155	1.02
S41	$Ni_{73.5}Fe_8Cr_{18.5}$	164	161	1.02
S50	$Ni_{72}Fe_8Cr_{20}$	168	168	1.00
S47	$Ni_{71}Fe_8Cr_{21}$	169	167	1.01

$$FAR = \gamma[(\rho_\downarrow/\rho_\uparrow) - 1] = \gamma(\alpha - 1), \tag{4.15}$$

where $\alpha = \rho_\downarrow/\rho_\uparrow$ and γ ($\simeq 0.01$) is a constant[29] independent of the scattering process. The TCC model is quite successful in explaining FAR in both crystalline[22, 28, 29] and amorphous[24] alloys. In strong ferromagnets[28, 29] like NiFe and NiCu alloys[29], the calculated values of FAR are in very good agreement with experiments.

It is interesting to note here that Eq.(4.15) provides an important criterion for determining

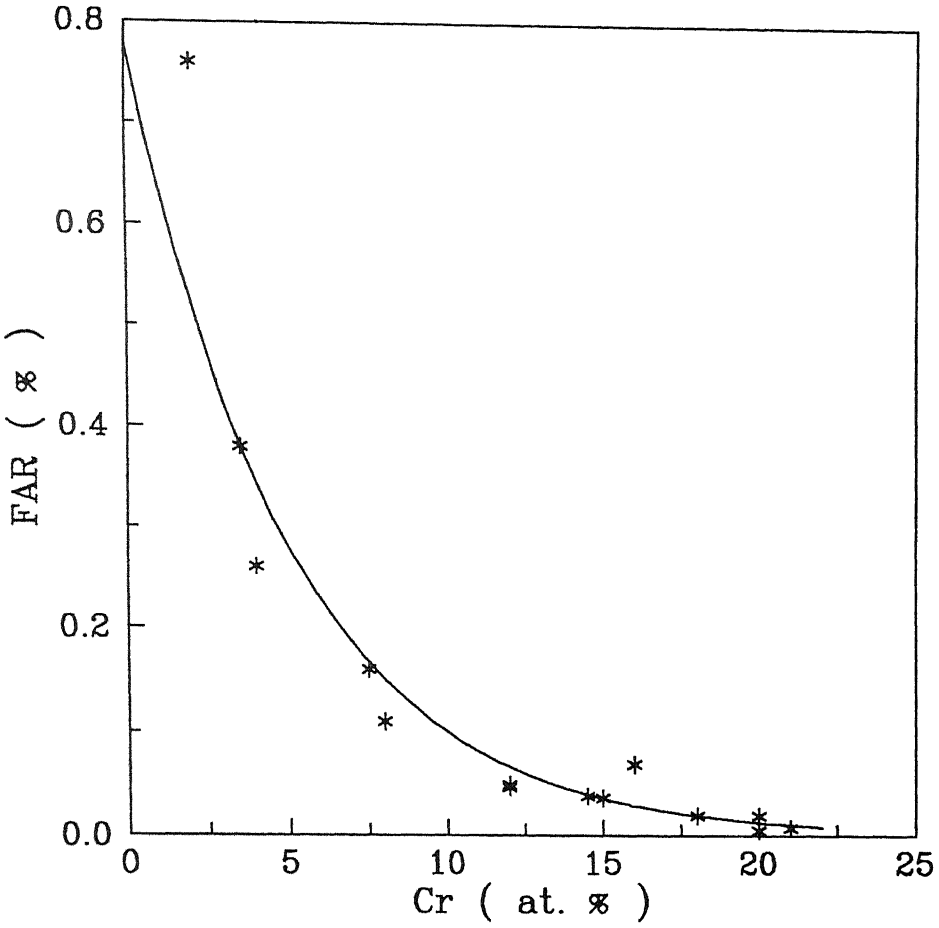

FIG. 4.12. Plot of the FAR against the Cr concentration (in at.%).

strong/weak itinerant-electron ferromagnetism in a given alloy. According to Stoner[45], a strong ferromagnet is considered to have one subband completely full while in a weak ferromagnet both spin-up and spin-down subbands are partially filled. In strong ferromagnets like Ni, the conduction process takes place mostly through the spin-down subband, which implies that the contribution to the resistivity comes mostly from $\rho\downarrow$ (i.e., $\rho\downarrow >> \rho\uparrow$) resulting in $\alpha >> 1$. Hence, a large FAR is expected in a strong ferromagnet. This is in good agreement with the large values of FAR in NiFe and NiCu. On the other hand, in a weak ferromagnet $\rho\uparrow$ and $\rho\downarrow$ are found to be almost comparable (i.e., $\alpha \simeq 1$) since both spin-up and spin-down subbands are available for conduction. As a result, its FAR will be very small (see Eq.(4.15)). Earlier, Kaul and Rosenberg[24] had

employed the above idea to amorphous $(Fe\text{-}Ni)_{80}B_{20}$ and $(Fe\text{-}Ni)_{80}P_{14}B_{20}$ alloys to describe their ferromagnetic state. This, however, contradicts the earlier high-field magnetic data[31, 46]. Later on, Malozemoff[31] proposed a modified TCC model for describing FAR in both amorphous and concentrated crystalline alloys. The dc-magnetisation study[18] on the present alloy series has clearly shown a transition from strong to weak itinerant-electron ferromagnetism with increasing Cr concentration. In Table 4.5, one can find that the FAR values exhibit a sharp decrease with increasing Cr content. The plot for the FAR with Cr concentration is shown in Fig. 4.12, where the FAR is found to fall almost exponentially and becomes nearly zero beyond $C_{Cr} \geq 12$ at.%. In order to get an estimate of $\rho^{\uparrow}$ and $\rho^{\downarrow}$, the expressions for them are derived[24] from Eqs.(1.31) and (4.15) as

$$\rho_{\downarrow} = \rho_0 \left[\gamma^{-1}(\mathrm{FAR}) + 2\right] \tag{4.16}$$

and

$$\rho_{\uparrow} = \rho_{\downarrow} \left[\gamma^{-1}(\mathrm{FAR}) + 1\right]^{-1}. \tag{4.17}$$

The calculated values of $\rho_{\uparrow}$, $\rho_{\downarrow}$, and α for all the alloys at 4.2 K are shown in Table 4.6. It is to be noted here that instead of ρ_0, $\rho_{4.2K}$ is used in the above calculations since, according to the electrical resistivity study (Chapter 3), the values of ρ_0 and $\rho_{4.2K}$ are found to be almost the same. However, the difference, if any, falls within the error limits of the measurements of the sample dimensions. In Table 4.6, the value of $\rho_{\downarrow}$ is found to be two times greater than $\rho_{\uparrow}$ in low Cr-content alloys (e.g. S35). But as Cr concentration increases, they almost become comparable. It is very interesting to see that the value of α $(= \rho_{\downarrow}/\rho_{\uparrow})$ comes out to be almost one in Cr-rich alloys ($C_{Cr} \geq 12$). This clearly indicates that with increasing Cr concentration the present NiFeCr alloys moves towards weak itinerant ferromagnetism in good agreement with the dc-magnetisation study[18]. This is probably the first time when the magnetic state of a crystalline Cr-rich ternary alloy series is correlated with the FAR using the TCC model.

References

[1] J. S. Dugdale, Contemp. Phys. **28**, 547 (1987).

[2] P. A. Lee and T. V. Ramakrishnan, Rev. Mod. Phys. **57**, 287 (1985).

[3] B. L. Altshuler and A. G. Aranov, *Electron-Electron Interactions in Disordered Solid*, edited by A.L. Efros and M. Pollak (North - Holland,Amsterdam), 1985.

[4] M.A. Howson and D. Greig, Phys. Rev. B **30**, 4805 (1984).

[5] M.A. Howson and D. Greig, J. Phys. F **16**, 989 (1986).

[6] J.B. Bieri, A. Fert, G. Creuzet, and A. Schuhl, J. Phys. F **16**, 2009 (1986).

[7] J. Smit, Physica **16**, 612 (1951).

[8] H.C. Van Elst, Physica **25**, 708 (1959).

[9] H. Ashworth, D. Sengupta, G. Schnakenberg, L. Shapiro, and L. Berger, Phys. Rev. **185**, 172 (1969).

[10] A.K. Gangyopadhyay, R.K. Ray, and A.K. Majumdar, Phys. Rev. B **30**, 1801 (1984).

[11] A.K. Nigam and A.K. Majumdar, Phys. Rev. B **27**, 495 (1983).

[12] A. Banerjee and A. K. Majumdar, Phys. Rev. B **46**, 8958 (1992).

[13] J.P. Jan, in Solid State Physics, edited by F. Seitz and D. Turnbull (Academic, New York, 1957), Vol. 5, P. 27.

[14] D.V. Baxter, R. Richer, A.L. Trudeau, R.W. Cochrane, and J.O. Strom-Olsen, J. Phys. France **50**, 1673 (1989).

15] B.L. Altshuler, A.G. Aranov, A.I. Larkin, and D.E. Khmelnitskii, Sov. Phys. - JETP **54**, 411 (1981).

[16] S. Banerjee and A.K. Roychowdhury Phys. Rev. B **52**, 3453 (1995); T.K. Nath and A.K. Majumdar, J. Appl Phys. **70**, 5828 (1991).

[17] Abhijit Mookerjee, J. Phys. F **10**, 1559 (1980); M.T. Béal-Monod and R.A. Weiner, Phys. Rev. B **170**, 552 (1968).

[18] A K. Gangyopadhyay, R.K. Ray, and A.K. Majumdar, Phys. Rev. B **30**, 6693 (1984).

[19] A.K. Nigam and A.K. Majumdar, Physica **95B**, 385 (1978).

[20] Y. Öner, A. Kilic, M. Özdemir, H. Celik, and S. Senoussi, J. Phys C **8**, 11121 (1996).

[21] A.Z. Menshikov, G.A. Takzey, and A. Ye. Teplykh, Phys. Met. Metall. **54**, 41 (1982); A.K. Majumdar and P.V. Blanckenhagen, Phys. Rev. B **29**, 4079 (1984).

[22] T.R. McGuire and R.I. Potter, IEEE Trans. Magnetics **MAG-11**, 1018 (1975).

[23] R.C. O'Handley, Phys. Rev. B **18**, 2577 (1978).

[24] S.N. Kaul and M. Rosenberg, Phys. Rev. B **27**, 5698 (1983).

[25] L. Berger, AIP Conf. Proc. **34**, 355 (1976).

[26] H. Ma, Z. Wang, H.P. Kunkel, and Gwyn Williams, J. Phys. C **4**, 1993 (1992).

[27] L. Berger, Physica **30**, 1141 (1964).

[28] I.A. Campbell, A. Fert, and O. Joul, J. Phys. C **3**, S95 (1970).

[29] I.A. Campbell, A. Fert, and O. Joul, J. Magn. Magn. Mater. **5**, 23 (1977); J. Phys. F: Metal Phys. **6**, 849 (1976).

[30] J. Banhart and H. Ebert, Europhys. Lett. **32**, 517 (1995).

[31] A.P. Malozemoff, Phys. Rev. B **32**, 6080 (1985).

[32] L. Berger, P.P. Freitas, J.D. Warner, and J.E. Schmidt, J. Appl. Phys. **64**, 5459 (1988).

[33] L. Berger, J. Appl. Phys. **67**, 5549 (1990).

[34] L. Berger, Phys. Rev. **138**, A1083 (1965).

[35] R.C. O'Handley, Phys. Rev. B **18**, 930 (1978); R.C. O'Handley and L. Berger, Inst. Phys. Conf., Ser. No. 39, Chapter 6, P. 477 (1978).

[36] A.K. Majumdar and R D. Greenough, J. Magn. Magn. Mater. **59**, 57 (1986).

[37] L. Berger and G. Bergmann, in The Hall Effect and its Applications, edited by C.L. Chien and C.R. Westgate (Plenum, New York, 1980), p. 55.

[38] T.R. McGuire, R.J. Gambino, and R.C. O'Handley, ibid, p. 137.

[39] L. Berger, Phys. Rev. B **32**, 4559 (1970).

[40] J. Friedel, Del. Nuovo. Cemento. **VII**, 287 (1958).

[41] M.F. Collins and G.G. Low, Proc. Phys. Soc. **86**, 535 (1965).

[42] A. Das and A.K. Majumdar, J. Appl. Phys. **70**, 6323 (1991).

[43] R. Kern, M. Naka, U. Gonsor, H. Fujimori, and I. Okamoto, J. Magn. Magn. Mater. **31-34**, 1471 (1983).

[44] Hideo Hasegawa and Junjiro Kanamori, J. Phys. Soc. Japan **33**, 1599 (1972); **33**, 1607 (1972).

[45] E.C. Stoner, Proc. Roy. Soc. London, Ser A **165**, 372 (1938).

[46] R.C. O'Handley and D.S. Boudreau, Phys. Status Solidi A **45**, 607 (1978).

Chapter 5

Hall effect

5.1 Introduction

In this chapter, we have presented the temperature dependence of Hall effect in some NiFeCr alloys. Earlier, most of the studies[1–7] in crystalline as well as amorphous alloys were focussed on the concentration dependence of the Hall effect whereas not much attention has been paid to its temperature dependence. Recently some precise measurements of Hall effect have shown clearly in non-magnetic CuTi and CuZr amorphous alloys[8–10] that the ordinary Hall coefficient (R_0) decreases slowly with temperature. The dominant presence of electron - electron interaction effects (EEI) in the weak-localisation limit[11] is considered to be its cause. The electrical resistivity (ρ(T)) study in the present NiFeCr alloys (discussed earlier in Chapter 3) has also shown resistivity minima which have been interpreted by the electron - electron interaction (EEI) effects along with other conventional electron - magnon and electron - phonon scattering mechanisms. In addition, these alloys are all ferromagnetic in the temperature range below 50 K[12, 13]. As a result, ρ_H below T_c will have contributions from both ordinary and extra-ordinary Hall terms (see Eq. (1.47)). The motivation behind the present work is to study the temperature dependence of the ordinary (OHC) and the extraordinary (EHC) Hall coefficients in NiFeCr crystalline ferromagnets showing resistivity minima.

TABLE 5.1. Sample designation with their composition, ferromagnetic Curie temperature (T_c), T_{min}, value of resistivity at 1.2 K ($\rho_{1\,2K}$), depth of minimum, $\Delta\rho/\rho_{300K}$ ($\Delta\rho = \rho_{300K} - \rho_{min}$) along with values of Hall resistivity (ρ_H) beyond saturation (at 1 T), R_sM_s, R_s, and R_0 at 1.4 K.

Sample No.	S29	S48	S41
Alloy composition	$Ni_{75}Fe_{13}Cr_{12}$	$Ni_{70}Fe_{12}Cr_{18}$	$Ni_{73\,5}Fe_8Cr_{18\,5}$
T_c (K)	365	179	44
T_{min} (K)	14	22	27
$\rho_{1\,2K}$ (10^{-8} Ωm)	89.6	71.8	76.0
Depth of minima (%)	0.10	0.26	0.37
$\Delta\rho/\rho_{290K}$ (%)	4.9	3.8	3.2
ρ_H (10^{-10} Ωm)	-13.6	4.9	3.2
R_sM_s (10^{-10} Ωm)	-13.01 (± 0.03)	4.80 (± 0.02)	2.77 (± 0.01)
R_0 (10^{-11} ΩmT^{-1})	-5.5 (± 0.3)	1.4 (± 0.1)	4.2 (± 0.4)
R_s (10^{-9} ΩmT^{-1})	-2.66 (± 0.01)	1.60 (± 0.01)	2.34 (± 0.01)

5.2 Results and discussion

5.2.1 General description of the data

The measurements are done till magnetic inductions of 1.4 T in Ni-rich γ-$Ni_{75}Fe_{13}Cr_{12}$ (S29), $Ni_{70}Fe_{12}Cr_{18}$ (S48), and $Ni_{73\,5}Fe_8Cr_{18.5}$ (S41) alloys at several temperatures in the range of (1.4 - 80) K, (1.4 - 186.3) K, and (1.4 - 30.3) K, respectively. The ferromagnetic Curie temperatures (T_c) for S29, S48, and S41 alloys are at 365, 179, and 44 K, respectively. These alloys are substantially disordered with large residual resistivity ($\rho_0 \simeq 100$ μohm cm) and small $\Delta\rho/\rho_{290K}$ (≤ 5 % where $\Delta\rho = \rho(290\text{ K}) - \rho(1.2\text{ K})$). The electrical resistivity study exhibits increase in ρ(T) with decreasing temperature below T_{min} (see Chapter 3). In Table 5.1, all the details of the alloy composition, T_c, $\rho_{1\,2K}$, T_{min}, depth of minimum ($= \frac{\rho(1.2K)-\rho(T_{min}}{\rho(1\,2K)}$), and $\Delta\rho/\rho_{290K}$ are given. Typical Hall resistivity (ρ_H) vs magnetic induction data are shown in Figs. 5.1, 5.2 and 5.3 for alloys S41, S48 and S29, respectively at some selected temperatures for better clarity. The absolute value of ρ_H beyond

saturation for all the three alloys exhibit a decrease with increasing temperature. ρ_H is found to be positive for both S41 and S48 whereas it is negative for S29. The values of ρ_H beyond saturation at 1.4 K are given in Table 5.1 where one finds that the magnitude of ρ_H for alloy S29 is three to four times greater than those for alloys S48 and S41. The values of R_sM_s and OHC (R_0) are obtained from the intercept and the slope, respectively of a linear fit of ρ_H beyond saturation. Typical error in the values of R_sM_s and R_0 are given in Table 5.1. The sign of the OHC and R_sM_s are found to be positive in both S48 and S41 whereas they are negative in S29. A negative OHC is generally expected in alloys of simple metals where the majority charge carriers are electrons. However, a positive OHC is found in pure Fe and some of its dilute alloys. This has been explained in terms of their band structure and the two-band model[14]. In recent times, some amorphous 3d alloys have shown positive OHC which is explained by the negative slope of the S-shaped dispersion (E vs. k) curves due to s-d hybridisation[15]. In s-d hybridisation, the OHC becomes positive when the Fermi energy (E_F) is located at the middle of the 3d band whereas it is negative when E_F lies at the top. Berger had proposed a model, called the split-band model[5, 16], using which the sign of the EHC of binary and ternary Ni and Fe based alloys are explained successfully. In an earlier report[6], the sign reversal of the EHC (R_s) in various compositions of the present Ni-rich γ-NiFeCr alloys has been discussed in terms of the split-band model. The Fermi level crossing some degeneracy at the top of the Ni 3d spin-down band[5, 6] is found responsible for the sign change in R_s. In the ternary phase diagram of NiFeCr alloys[6], one can easily find that the alloys with negative EHC have their E_F at the top of the 3d spin-down band. As the concentration of Fe and Cr increases the Fermi level goes down to the middle of the Ni 3d spin-down band resulting in a positive R_s. The positive sign of EHC in S41 and S48 and the negative sign in S29 are consistent with the above[6] ternary phase diagram.

Hereafter, we will consider only the absolute values of ρ_H, R_sM_s, OHC, and EHC, unless their sign is specifically mentioned. It is very interesting to note from Table 5.1 that ρ_H beyond saturation at 1.4 K are three orders of magnitude smaller than the residual resistivity (ρ_0) in all the alloys. The values of the OHC are found in the range of (1.4 - 5.5) $\times$ 10^{-11} ΩmT^{-1} and are of the same order as observed earlier in dilute crystalline FeCr and FeCo alloys[4]. The extra-ordinary term (R_sM_s)

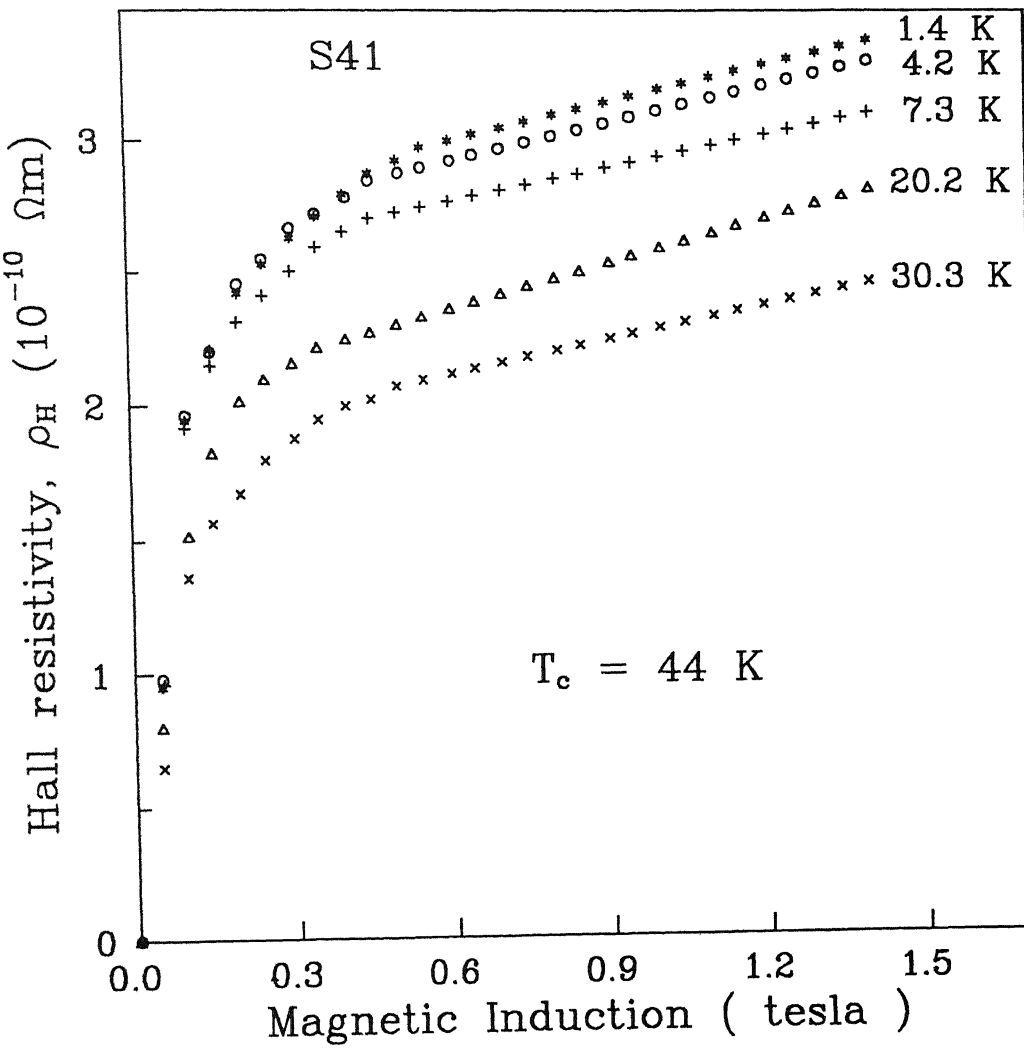

FIG. 5.1. Plot of the Hall resistivity (ρ_H) for alloy S41 ($Ni_{73.5}Fe_8Cr_{18.5}$) in magnetic inductions till 1.4 T at 1.4, 4.2, 7.3, 20.2, and 30.3 K.

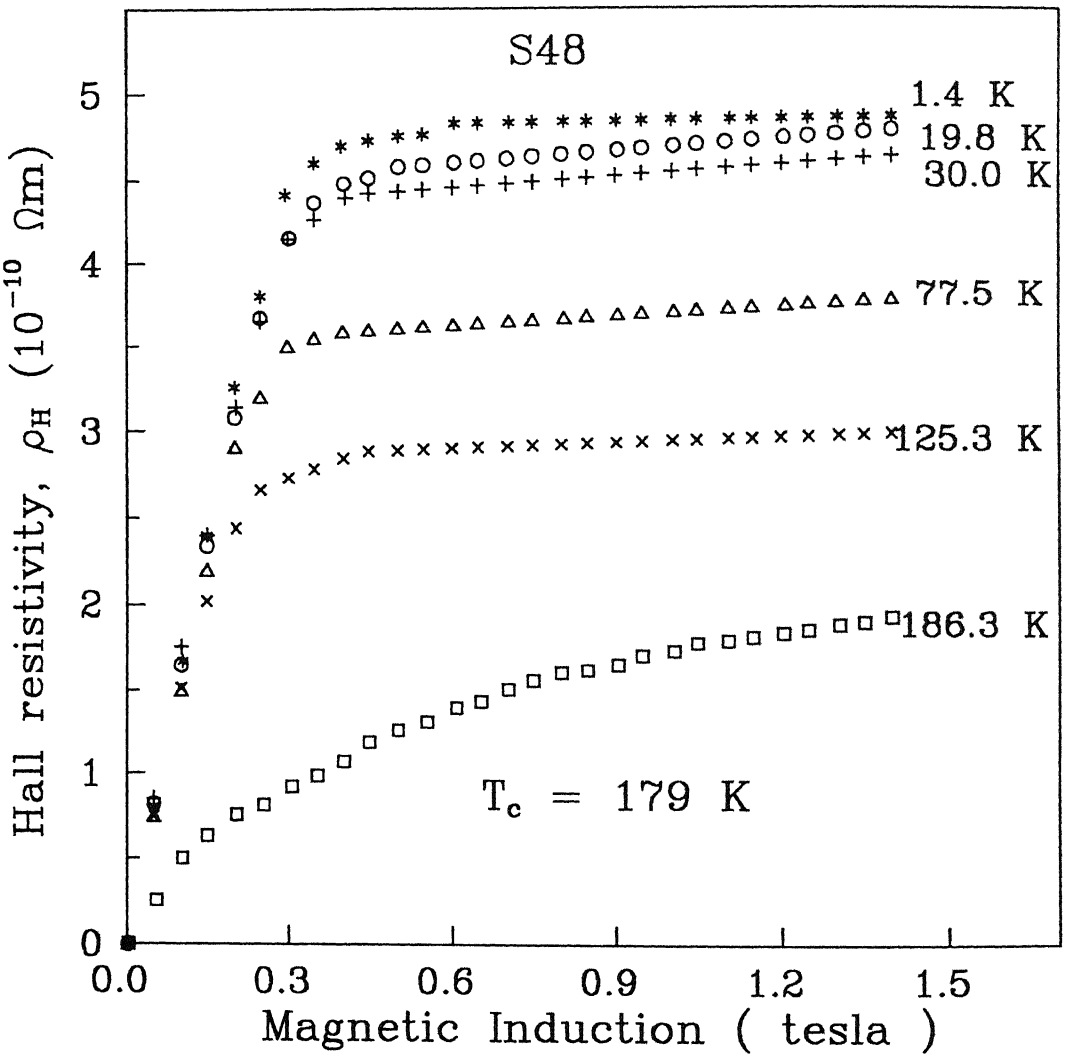

FIG. 5.2. Plot of the Hall resistivity (ρ_H) for alloy S48 ($Ni_{70}Fe_{12}Cr_{18}$) in magnetic inductions till 1.4 T at 1.4, 19.8, 30.0, 77.5, 125.3, and 186.3 K.

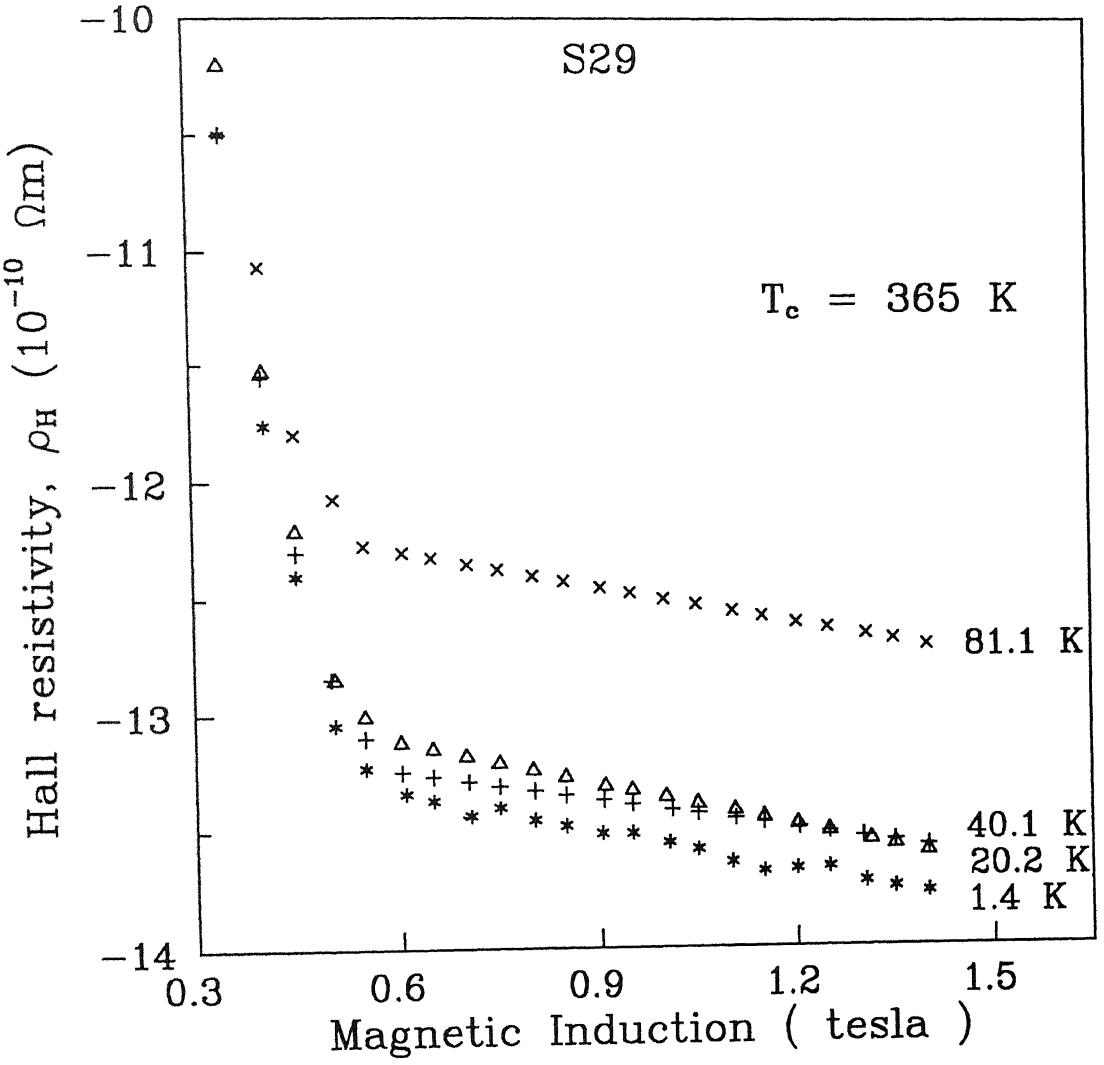

FIG. 5.3. Plot of the Hall resistivity (ρ_H) for alloy S29 ($Ni_{75}Fe_{13}Cr_{12}$) in magnetic inductions of 0.3 to 1.3 T at 1.4, 20.2, 40.1, and 81.1 K.

ABLE 5.2. Temperature of measurements along with the values of saturation of magnetisation, $_0$, R_sM_s, and R_s for alloy S41 ($Ni_{73.5}Fe_8Cr_{18.5}$).

Temperature of measurements (K)	M_s (10^{-2} tesla)	R_0 (10^{-11} ΩmT^{-1})	R_sM_s (10^{-10} Ωm)	R_s (10^{-10} ΩmT^{-1})
1.4	11.83	4.2	2.77	23.41
3.2	11.77	4.5	2.66	22.60
4.2	11.72	4.8	2.62	22.30
5.0	11.71	4.6	2.59	22.10
6.1	11.67	4.1	2.56	21.90
7.3	11.61	4.2	2.50	21.50
8.5	11.55	4.6	2.46	21.30
8.9	11.52	4.6	2.43	21.10
9.7	11.47	4.3	2.42	21.15
10.1	11.45	5.5	2.41	21.07
11.2	11.37	4.8	2.38	20.95
12.2	11.26	5.8	2.35	20.87
13.2	11.17	4.6	2.33	20.86
14.3	11.05	5.1	2.29	20.72
20.2	10.26	5.7	2.08	20.30
25.6	9.35	4.7	1.97	21.05
30.3	8.38	4.3	1.85	22.07

TABLE 5.3. Temperature of measurements along with the values of saturation of magnetisation, R_0, R_sM_s, and R_s for alloy S48 ($Ni_{70}Fe_{12}Cr_{18}$).

Temperature of measurements (K)	M_s (10^{-2} tesla)	R_0 (10^{-11} ΩmT^{-1})	R_sM_s (10^{-10} Ωm)	R_s (10^{-10} ΩmT^{-1})
1.3	29.93	1.4	4.80	16.04
4.2	29.87	1.5	4.68	15.68
6.2	29.83	1.7	4.64	15.55
8.0	29.78	1.8	4.58	15.38
10.0	29.72	1.9	4.56	15.34
14.2	29.54	2.4	4.49	15.20
19.8	29.23	2.5	4.41	15.09
25.3	28.88	2.7	4.33	14.99
30.0	28.85	2.3	4.32	14.97
36.2	28.08	3.1	4.19	14.92
41.1	27.67	3.3	4.12	14.90
61.1	25.87	3.2	3.91	15.10
77.5	20.56	3.0	3.44	16.72
100.5	15.94	2.7	3.18	19.95
125.3	12.83	2.1	2.73	21.26

TABLE 5.4. Temperature of measurements along with the values of saturation of magnetisation, R_0, R_sM_s, and R_s for alloy S29 ($Ni_{75}Fe_{13}Cr_{12}$).

Temperature of measurements (K)	M_s (10^{-2} tesla)	R_0 (10^{-11} ΩmT^{-1})	R_sM_s (10^{-10} Ωm)	R_s (10^{-10} ΩmT^{-1})
1.4	48.86	- 5.5	- 13.01	- 26.63
4.2	48.71	- 5.4	- 13.01	- 26.71
7.5	48.66	- 5.2	- 13.00	- 26.72
10.0	48.64	- 4.6	- 13.03	- 26.79
12.5	48.61	- 4.5	- 13.02	- 26.78
15.6	48.59	- 4.4	- 13.03	- 26.82
18.1	48.54	- 4.2	- 13.02	- 26.83
20.2	48.49	- 4.1	- 13.00	- 26.81
25.1	48.43	- 4.6	- 12.99	- 26.82
30.0	48.28	- 5.1	- 12.93	- 26.78
40.1	47.92	- 5.2	- 12.75	- 26.61
81.1	45.75	- 5.0	- 11.99	- 26.21

is found to be (1.85 - 2.77), (2.73 - 4.80), and (11.99 - 13.01) (all are in 10^{-10} Ωm) for alloys S41, S48, and S29, respectively. The values of the EHC (R_s), evaluated from the above R_sM_s, are obtained in the range of (14.90 - 26.83) $\times$ 10^{-10} ΩmT^{-1} which is two orders of magnitude greater than the OHC ones. The values of ρ_H, R_0, R_sM_s, and R_s for all the temperature of measurements are given in Table 5.2, 5.3 and 5.4 for alloys S41, S48, and S29, respectively. It is interesting to note that the present values of the EHC are an order of magnitude greater than those of the dilute crystalline FeCr alloys[4] and nearly equal to those of the concentrated Ni-rich NiCu alloys[17]. However, they are an order of magnitude smaller compared to those of the amorphous 3d alloys[2, 18]. Since $R_s >> R_0$, the Hall resistivity (ρ_H) beyond saturation is almost equal to R_sM_s, i.e. $\rho_H \simeq R_sM_s$. Hence, such a large extraordinary contribution to ρ_H can certainly be attributed to the side-jump effect (see Eqs. (1.58) and (1.59)).

5.2.2 Temperature dependence of R_0 and R_s

The temperature dependence of the OHC (R_0) is shown in Fig. 5.4 where it is found to be almost a constant. However, a small bump is observed around T_{min} which is not understood. On the other hand, the temperature dependence of the EHC (R_s) for S41, S48, and S29, shown in Fig. 5.5, exhibit minima at 20, 40, and 20 K, respectively which are of the same order as the T_{min} of the resistivity (see Table 5.1). However, the decrease in R_s till their minima are found around 11, 7, and 1 % for alloys S41, S48, and S29, respectively which are quite large compared to the depth of the minima (see Table 5.1) of their ρ(T). Recently large changes in Hall coefficient as compared to those of the electrical resistivity have been observed in some amorphous alloys[10, 19].

In conventional ferromagnetic crystalline metals and alloys[1, 17, 20], with increasing temperatures ρ(T) is generally found to increase which, in turn, enhances the absolute value of the EHC (Eqs. (1.56) and (1.59)). As a result, with increasing temperatures the positive EHC becomes more positive (e.g., Fe) and the negative EHC more negative[20] (e.g., Ni). Here in Fig. 5.5, one finds that the temperature dependence of the positive EHC in alloys S41 and S48 are consistent with the minima of the ρ(T) data (see Figs. 3.8 and 3.9). On the contrary, the negative EHC in alloy S29 shows a behaviour exactly opposite to what is expected. As the resistivity increases

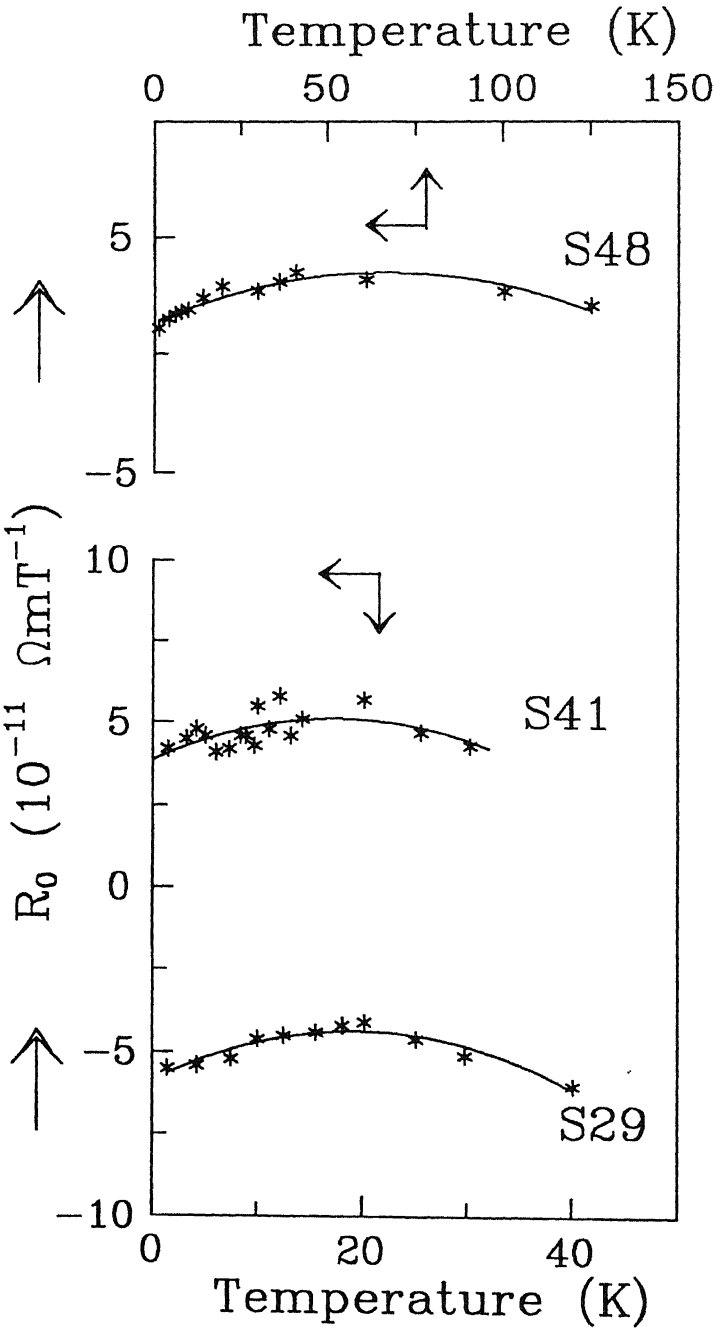

FIG. 5.4. Plot of the temperature dependence of the OHC (R_0) for alloys S48, S41, and S29.

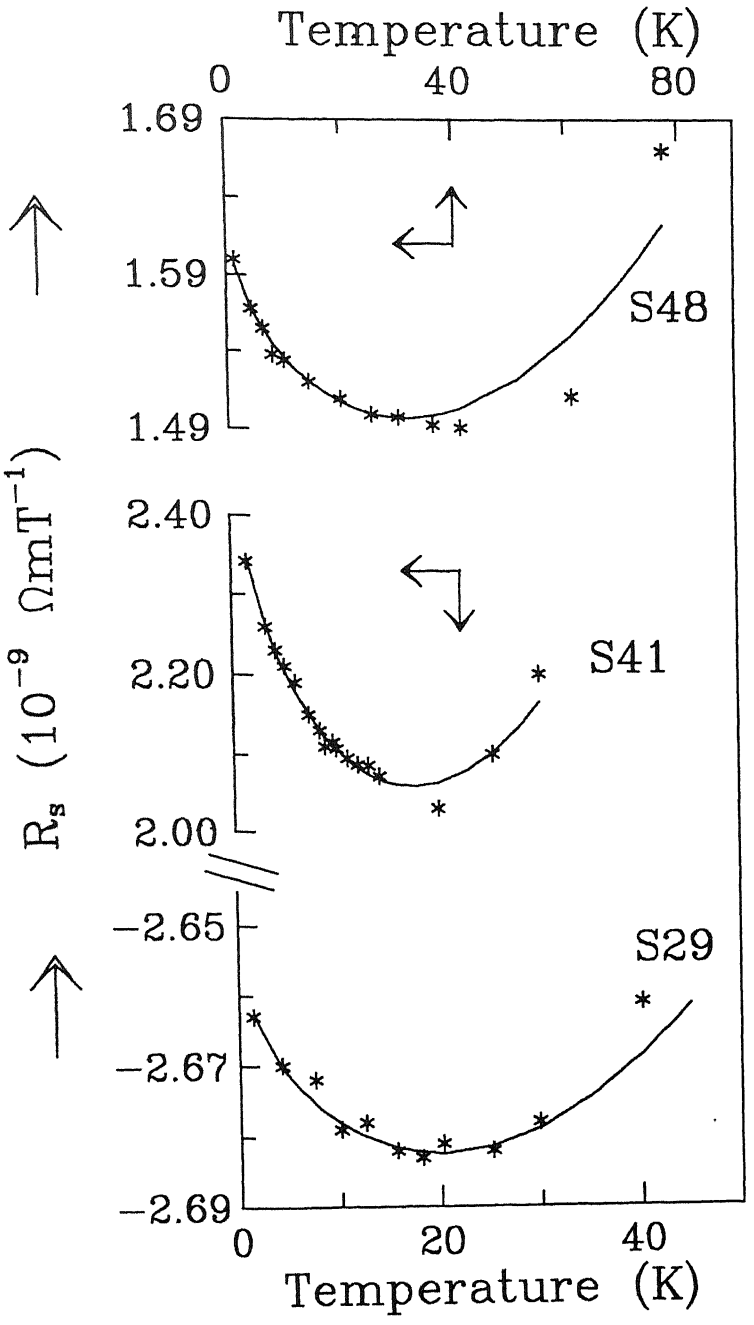

FIG. 5.5. Plot of the temperature dependence of the EHC (R_s) and their fits to Eq.(5.1) for alloys S41 and S48. For S29, see text.

TABLE 5.5. Sample designation, parameters obtained from fitting to Eq.(5.1), and the calculated values of the coefficients of ρ(T) fit to Eq.(3.15).

				calculated values		
Sample No.	R_s^0 (10^{-9}) $\Omega m T^{-1}$	m_H (10^{-11}) $\Omega m K^{-1/2} T^{-1}$	B_H (10^{-14}) $\Omega m K^{-2} T^{-1}$	K (10^3) $(\Omega m T)^{-1}$	m_ρ (10^{-9}) $\Omega m\ K^{-1/2}$	B (10^{-11}) $\Omega m\ K^{-2}$
S48	1.6	-3.3	4.6	3.2	-7.4	1.0
S41	2.5	-14.6	49.3	4.4	-22.2	7.5

below as well as above T_{min}, the negative EHC instead of becoming more negative on both sides of T_{min}, it becomes less negative. In other words, R_s vs T plot of S29 should have been a mirror image about the temperature axis of S41 and S48. This is found to be rather puzzling. A similar behaviour[20] had been observed in pure Co where the negative EHC shows a minimum at 80 K and finally it becomes positive at room temperature[20]. This can not be explained by the usual scattering mechanisms ($R_s = K\rho^n$). Using the earlier interpretation of the ρ(T) data ($\rho(T) = \rho_0 - m_\rho\sqrt{T} + BT^2$; here we have neglected the phonon contribution), the temperature dependence of the EHC can be written as (assuming side-jump mechanism)

$$\begin{aligned} R_s(T) &= K(\rho(T))^2 \\ &\simeq R_s^0 - m_H\sqrt{T} + B_H T^2 \quad \text{(neglecting higher order terms)}, \end{aligned} \tag{5.1}$$

where $R_s^0 = K\rho_0^2$, $m_H = 2K\rho_0 m_\rho$, and $B_H = 2K\rho_0 B$. Here the term $R_s^0 = K\rho_0^2$ can be called the residual EHC which is solely dependent on the composition of the alloy. The data for the positive EHC give a very good fit to Eq.(5.1) in the temperature range of 1.4 - 40 K which can be seen from Fig.5.5. The values of the normalised χ^2 (= $1/N\sum_{i=1}^{N}((\text{raw})_i - (\text{fit})_i)^2/(\text{fit})_i^2$), obtained from the fittings, are of the order of 3×10^{-5} which is close to our experimental resolution. In Fig. 5.5, the best-fitted curves for alloys S41 and S48 are extrapolated to show deviations at higher temperatures. All the

details of the fitting parameters are given in Table 5.5. The values of R_s^0 for S48 and S41, obtained from the fittings, are coming as 1.6 and 2.5 (all are in 10^{-9} ΩmT^{-1}) respectively. The values of K (see Eq.(1.59)), calculated from R_s^0 using the zero-field residual resistivity (ρ_0), are coming an order of magnitude smaller than the theoretically predicted[3, 4] one ($\simeq 5 \times 10^4$ $(\Omega mT)^{-1}$). Here it is to be noted that, with the assumption of short-range potential, K is derived to be a constant which is independent of the type of scattering centers including even phonons[3]. But in the dilute FeCr alloys[4], K is found to be an order of magnitude larger than the theoretical one. On the other hand, in the Ni-rich concentrated NiCu alloys[17] the values of K are obtained in the range of (8×10^3 - 1×10^5) $(\Omega mT)^{-1}$ depending on the temperature of fit. Hence a large deviation in the value of K is quite expected in highly concentrated alloys where the assumption of short-range potential does not hold good. Moreover, this is probably the first time when the value of K is extracted from the temperature dependence of the EHC of any concentrated crystalline alloy where the residual resistivity is an order of magnitude larger than the earlier reported values in conventional crystalline ferromagnetic alloys[1, 4, 14, 17]. However, the present values of K in alloys S48 and S41 are coming almost the same (see Table 5.5). On the contrary, the values of m_H (in the units of 10^{-11} $\Omega mK^{-1/2}T^{-1}$) and B_H (in the units of 10^{-14} $\Omega mK^{-2}T^{-1}$) are found to be 3.3 and 4.6, and, 14.6 and 49.3 for alloys S48 and S41, respectively. The values of m_ρ and B, calculated from the fitting parameters m_H and B_H of Eq.(5.1), are found to be an order of magnitude higher than those obtained from the fitting of the ρ(T) data (in Chapter 3, Table 3.7). The large changes in R_s(T) till their minima compared to those of ρ(T) is likely to be the main reason for such deviations. Moreover, this is not unexpected as these values are obtained from two different experiments and especially the R_s(T) data are extracted out of the very small Hall voltages. Thus the minima in the positive R_s(T) can certainly be attributed indirectly (through ρ(T)) to the dominant presence of the EEI effects. On the other hand, as mentioned earlier, the minimum in the negative R_s(T) for alloy S29 can not be similarly interpreted since it should have shown a maximum instead. However, the best-fitted line (which has no physical significance) through the experimental data is shown for S29 in Fig. 5.5 only to demonstrate the minimum. None the less, this shows clearly that the dispersion in the present EHC (R_s(T)) data is less than 0.5%. However, it is not possible to calculate Δy from Eq.(1.60) since the values of the Fermi wave vector is not available for the present alloys. To the

est of our knowledge, this is the only report where such strong minima in the EHC are found for ny concentrated crystalline ferromagnet.

References

[1] L. Berger and G. Bergmann, in The Hall Effect and its Applications, edited by C.L. Chien and C.R. Westgate (Plenum, New York, 1980), p. 55.

[2] T.R. McGuire, R.J. Gambino, and R.C. O'Handley, ibid, p. 137.

[3] L. Berger, Phys. Rev. B **32**, 4559 (1970).

[4] A.K. Majumdar and L. Berger, Phys. Rev. B **7**, 4203 (1973).

[5] H. Ashworth, D. Sengupta, G. Schnakenberg, L. Shapiro, and L. Berger, Phys. Rev. **185**, 172 (1969).

[6] A.K. Gangyopadhyay, R.K. Ray, and A.K. Majumdar, Phys. Rev. B **30**, 1801 (1984).

[7] D.G. Naugle and K. Rhie, "Ordering disorder : Prospect and Retrospect in Condensed Matter Physics, Proceedings of the Indo-US Workshop, Hyderabad, India, 29 Dec 1992 - 5 Jan 1993.

[8] B.L. Gallagher, D. Greig, and M.A. Howson, J. Phys. F : Metal Phys. **14**, L225 (1984).

[9] M.A. Howson and B.L. Gallagher, Physics Reports **170**, 265 (1988).

[10] A. Schulte, W. Haensch, G. Fritsch, and E. Lüscher, Phys. Rev. B **40**, 3581 (1989).

[11] B.L. Altshuler, A.G. Aronov, A.I. Larkin, and D. Khmel'nitskii, Sov. Phys.-JETP **54**, 411 (1981).

[12] A.K. Majumdar, K.D.D. Rathnayaka, and D.G. Naugle (to be published).

[13] A.K. Gangyopadhyay, R.K. Ray, and A.K. Majumdar, Phys. Rev. B **30**, 6693 (1984).

4] J.P. Jan, in Solid State Physics, edited by F. Seitz and D. Turnbull (Academic, New York, 1957), Vol. 5, P. 1.

5] G.F. Weir, M.A. Howson, B.L. Gallagher, and G.J. Morgan, Phil. Mag. **47**, 163 (1983).

5] L. Berger, Physica **30**, 1141 (1964).

7] S.N. Kaul, Phys. Rev. B **20**, 5122 (1979).

8] U. Mizutani, Progress in Material Science **28**, 97 (1983).

9] D. Müller, J.W. Schünemann, and K. Bärner, J. Magn. Magn. Mater. **110**, 161 (1991).

0] N.V. Volkenshtein and G.V. Fedorov, Sov. Phys. JETP **11**, 48 (1960).

Chapter 6

Conclusions and Scope for further work

To conclude, the present thesis has covered detailed investigations of the low - temperature electrical resistivity and magnetoresistance in disordered crystalline Mn-rich CuMn and Ni-rich NiFeCr alloys, and the temperature dependence of Hall effect in some Ni-rich NiFeCr alloys. A few interesting but anomalous behaviours have emerged which, however, could not be explained by conventional theories. The effects under the weak - localisation limit which are expected only in substantially disordered alloys, are found to be the cause for some such anomalies. An attempt has been made to understand how the degree of disorder in these alloys affects the electron transport. Dominant physical mechanisms are identified and isolated very convincingly. Besides these, we have made a comprehensive study on the composition dependence of the ferromagnetic anisotropy of resistivity (FAR) in NiFeCr alloys and tried to understand them in terms of both the split - band and the two - current conduction models. The plausible reasons for the observed decrease in the values of the FAR with increasing Cr content have also been explored. Below we have summarised some of the important observations and conclusions of the present thesis. The scope for further work is spelt out at the end.

.1 Conclusions

- **Electrical resistivity**

1. CuMn alloys

The electrical resistivity in concentrated γ-$Cu_{100-x}Mn_x$ alloys (x = 36, 60, 73, 76, and 83) is measured between 1.2 and 30 K. In this temperature range, the alloys with x = 36, 60, and 73 are cluster glasses while those with x = 76 and 83 show mixed cluster-glass and long-range antiferromagnetic phase. The present alloys are all substitutionally disordered with large residual resistivity ((93 - 196) $\mu\Omega$cm). The ρ(T) data exhibit distinct resistivity minima for all the alloys at T_{min} lying between 2.5 and 24.5 K. One of the most interesting observations in the present study is the linear correlation between the resistivity and the depth of the minima (DOM) as well as the T_{min} of the alloys, which shows that increasing value of the resistivity shifts T_{min} to higher temperatures with larger DOM. On the other hand, the increasing value of the resistivity is a clear signature of an enhanced disorder in the alloys. Hence, in disordered alloys, it is quite natural to have resistivity minima at higher temperatures with larger DOM. This, in fact, is nothing but a manifestation of the Mooij correlation.

Resistivity well below the minima ($\leq T_{min}/3$) is found to follow a $\sqrt{T}$ type of dependence which has been interpreted in terms of the electron-electron (e-e) interaction effects in the weak localisation limit. Interestingly, in the temperature range 1.2 K $\leq$ T $\leq T_{min}/3$, the e-e interaction effects is found to have a dominant contribution to the resistivity while those from magnetic and phonon scattering are negligible. The values of m_σ, calculated from the coefficient (m_ρ) of $\sqrt{T}$ term, come out to be in the range of (4.8 - 6.8) $(\Omega cm K^{1/2})^{-1}$. These are in good agreement with the near-universal value of 6 $(\Omega cm K^{1/2})^{-1}$. The diffusion constant D, calculated from m_ρ, is found to lie between (0.15 - 0.24) cm^2/sec. Also the density of states at the Fermi level ($N(E_F)$), estimated from ρ_0, D, and m_ρ, are in the range of (1.4 - 2.6) $\times$ 10^{35} $erg^{-1}cm^{-3}$. These values agree very well with 2.2 $\times$ 10^{35} $erg^{-1}cm^{-3}$, obtained from the early specific heat study. All the above facts provide a strong support to

the present interpretation of the data.

In the higher temperature range of $T_{min}/3 \leq T \leq 30$ K, besides the e-e interaction effects, magnetic contribution of the type $T^{3/2}$ and phonon contribution given by the standard Bloch - Grüneissen relation have been observed. All these contributions are succesfully isolated from each other. It is also concluded that the $T^{3/2}$ contribution to the resistivity due to the spin diffusive modes in spin / cluster glasses is observed at low temperature ($T \leq T_f/4$) whereas (BT^2 - $CT^{5/2}$) type of magnetic contribution is found at much higher temperatures compared to T_{min}. This is the first report showing the simultaneous presence of the $T^{3/2}$ type of magnetic contribution alongwith that from the e-e interaction effects. It also reveals that both $T^{3/2}$ and (BT^2 - $CT^{5/2}$) (B, C > 0) terms can be observed in the same alloys in different temperature ranges. The above conclusions are found to be independent of the details of the magnetic state of the alloys.

2. NiFeCr alloys

Detailed electrical resitivity measurements in concentrated Ni-rich γ - $Ni_{100-x-y}Fe_xCr_y$ ($8 \leq x \leq 17.5$, $8 \leq y \leq 21$) chrome - permalloys have been made in the temperature range of $1.2 \leq T \leq 290$ K. The alloys with low Cr - content ($\leq$ 15 at.%) are ferromagnetic while those with high Cr ($\geq$ 18 at.%) show exotic low-temperature magnetic behaviour with T_c (ferromagnetic Curie temperature) and T_f (spin - freezing temperature) below 60 and 20 K, respectively. The resistivity data of all the alloys exhibit distinct minima lying between 7 and 35.5 K. Above T_{min}, the data show a positive temperature coefficient of resitivity. Unlike the CuMn alloys, no such correlation between the resistivity and the DOM as well as the T_{min} can be found, since the values of $\rho_{1.2K}$ in the present alloys are almost the same. However, both the DOM and the T_{min} are found to be strongly dependent on the total change in the resistivity between 1.2 K to 290 K ($\Delta\rho/\rho_{290K}$, where $\Delta\rho = \rho_{290K} - \rho_{1.2K}$). This is quite interesting. According to the Mooij correlation, the alloys with positive TCR are more disordered when their TCR's are very small (i.e., for $\rho \simeq 150$ $\mu\Omega$cm, TCR $\simeq$ 0). This is exactly what is found here. The values of the DOM and the T_{min} are found to be nearly

constant for $\Delta\rho/\rho_{300K} > 15$ % whereas they show a sharp rise for $\Delta\rho/\rho_{300K} < 10$ %. This indicates that for small positive TCR, the DOM and the T_{min} increase very fast showing the enhanced disorder in the alloys.

In the high temperature region, the resistivity of S48 and the low Cr - content alloys ($\leq$ 15 at.%) shows a linear temperature dependence above 200 K whereas those for S41 and S47 are linear from even 100 K upwards. This is explained in terms of the high temperature electron phonon scattering. On the other hand, the resistivity for alloy S50 shows a clear tendency towards saturation right from 40 K which, however, could not be explained by the parallel - resistor model. The theoretically - estimated value of the saturation resistvity ($\rho_{sat} \simeq 163$ $\mu\Omega$cm) is found to be almost two times as large as ρ_{290K}. Hence to interpret the above behaviour in the present alloys, one has to do measurements at much higher temperatures. In the temperature range of 100 to 200 K, magnetic contribution ($\propto T^2$) along with the linear phonon term have been observed for S48 and the low-Cr alloys. Interestingly, the coefficient of the T^2 term comes out to be of the order of 1×10^{-5} $\mu\Omega$cm which agrees very well with the theoretical value. This clearly shows that the magnetic contribution to the electrical resistivity arises due to the s-d and s-s scattering. This is the first study on any concentrated ternary system where a magnetic contribution ($\propto T^2$) is found so convincingly.

At low temperatures, the resistivity well below minima (1.2 K $\leq T \leq T_{min}/2$) is described by the e-e interaction effects with a characteristic $\sqrt{T}$ dependence. A typical plot of the deviations between the raw and the fitted data ($(\rho_{raw} - \rho_{fit})/\rho_{fit}$) against temperature for $\sqrt{T}$ and lnT fits demonstrates the goodness of the $\sqrt{T}$ fit. The calculated values of m_σ for low - Cr content alloys are found in the range of (5.6 - 7.5) $(\Omega cm K^{1/2})^{-1}$ in good agreement with the near-universal value of 6 $(\Omega cm K^{1/2})^{-1}$, whereas those for high-Cr content alloys give higher values of m_σ, viz, (13 - 22) $(\Omega cm K^{1/2})^{-1}$. On the other hand, the density of states at the Fermi level ($N(E_F)$), estimated from the coefficient of the $\sqrt{T}$ term, comes out to be in the range of (1.8 - 4.7) $\times 10^{35}$ $erg^{-1}cm^{-3}$ and (15 - 32) $\times 10^{35}$ $erg^{-1}cm^{-3}$ for low and high-Cr content alloys, respectively. An earlier specific heat study shows that $N(E_F)$ in

the present alloys are of the order of 15×10^{35} erg^{-1}cm^{-3} which is again in good agreement with the present values, especially those for the high - Cr content alloys. This gives a strong support to the present interpretation of the resistivity minima. However, the above findings are found to be independent of the magnetic state of these alloys. In the temperature range $T_{min}/3 \leq T \leq 2T_{min}$, besides the e-e interaction effects, magnetic ($\propto T^2$) and phonon ($\propto T^3$) contributions have been distinctly identified as well as isolated. The plots of all these contributions vs temperature clearly show how the different competing physical phenomena are responsible for the resistivity minima. In addition to these, the residual resistivities for all the alloys are estimated using the two-current model and Matthiessen's rule. The agreement with the experimental values is reasonable.

- **Magnetoresistance**

1. CuMn alloys

High - field magnetoresistance in γ-$Cu_{100-x}Mn_x$ alloys (x = 36, 60, 73, 76, and 83) are measured till 7.5 T in both longitudinal (LMR) and transverse (TMR) orientations at 4.2 and at 4.2, 20.5, and 63 K, respectively. The data show positive magnetoresistance till 7.5 T in the Mn-rich ($x \geq 60$) alloys while an overall negative one in the alloy with x=36 at all temperatures. However, the data at 4.2 K in x=36 clearly demonstrate a positive magnetoresistance till 3 T which becomes negative at higher fields. The resemblance of the TMR and the LMR data at 4.2 K in all the alloys can be taken as an indication for electron - electron interaction / localisation effects. The positive contribution to the magnetoresistance from the spin - orbit interaction in the weak - localisation limit is expected to be dominant only in the alloys of heavy elements (i.e., 4d or 5d series of elements). Hence, it is rather unphysical to consider the spin-orbit interaction as responsible for the positive magnetoresistance in the present CuMn alloys where all the constituents are 3d metals. Moreover, from the electrical resistivity study, it is found that the present alloys have very low diffusion constant ($D \sim 0.2 \times 10^{-4}$ m^2 s^{-1}), which, in turn, enhances the electron - electron interaction effects (EEI) ($(\Delta\rho/\rho)_{int} \propto 1/\sqrt{D}$). Over and above, the resistivity studies have clearly established the presence of EEI effects till $2T_{min}$. Hence the present positive magnetoresistance can certainly be attributed to the dominant presence of electron - electron interaction effects. In addition,

a negative magnetoresistance due to localisation effects has been included in the present interpretation. However, its contribution is calculated theoretically and found to be much smaller compared to that of the EEI effects. Besides these, a quadratic field dependence of the normal magnetoresistance ($\propto H^2$), however small it's contribution may be, is considered for a complete description of the data.

In both the high (4 to 7.5 T) and the low-field (0 to 1 T) limits, the dominant presence of EEI effects has been clearly identified. The data at 4.2 and 20.5 K for the Mn-rich ($x \geq 60$) alloys fit very well to the combined EEI and localisation effects in the presence of the normal magnetoresistance term. However, 63 K is too high a temperature for observing the EEI / localisation effects and indeed the data fit only to the normal magnetoresistance terms rather well for x=60, 73, and 83. Interestingly, the data even at 63 K for alloys x=76 show a good fit to the EEI/localisation and normal magnetoresistance terms in both the low and the high - field limits. This can be ascribed to the high value of its T_{min} ($\sim$ 24.5 K). The values of B, the coefficient of the $\sqrt{H}$ term (the combined EEI and localisation term in the high-field limit), are in good agreement with the theoretically calculated one. The coefficient (C) of the low-field limit of the combined EEI and localisation terms has been successfully isolated from the coefficient (C_N) of the normal magnetoresistance term. The normal magnetoresistance, estimated from the fitting parameters, follows the Kohler's rule for all the Mn-rich ($x \geq 60$) alloys.

On the other hand, an overall negative magnetoresistance is quite expected in the alloy x=36 since it is in the critical region of the magnetic phase diagram where a transition from the spin-glass (SG) to the cluster-glass (CG) phase is observed. Hence, a dominant negative magnetoresistance (- $\beta_{CG}H^2$) coming from the SG/CG effect is considered in the interpretation. The data at 4.2 K (where $\Delta\rho/\rho$ is positive till 3 T) are described by the dominant EEI/localisation terms coupled with the normal magnetoresistance and the SG/CG terms. However, the data at 20.5 and 63 K fit only to the normal and the SG/CG terms since these temperatures are very high compared to T_{min} ($\simeq$ 2.5 K). The present interpretation of the

magnetoresistance in all the alloys is found to be consistent with that of the ρ(T) data. This is the only study where such good qualitative as well as quantitative descriptions of the field dependence of dominant EEI effects are presented for any bulk crystalline alloy system along with localisation, cluster-glass and normal magnetoresistance effects. Moreover, the present study clearly demonstrates a transition of magnetoresistance from negative to positive values as the alloy compositions change from the SG to the CG regime.

2. NiFeCr alloys

Magnetoresistance in both longitudinal and transverse orientations are measured in some fifteen different compositions of Ni - rich γ - $Ni_{100-x-y}Fe_xCr_y$ ($6 \leq x \leq 23$; $2 \leq y \leq 21$) permalloys at 4.2 K in magnetic inductions till 1.4 T. These alloys are all ferromagnetic at 4.2 K. In the low Cr-content alloys ($y \leq 18$), the LMR is found to be positive while that of the TMR is negative. However, beyond technical saturation, the slope of both the LMR and the TMR data are found to be positive. This low-field anisotropy in the magnetoresistance arises from the inherent spin - orbit interaction present in a ferromagnet. Both the LMR and the TMR data beyond technical saturation and till 1.4 T have shown an H^2 dependence which is attributed to a dominant presence of the electron - electron interaction effects in the low - field limit. The contribution of the normal magnetoresistance to the present data is estimated to be negligibly small. On the other hand, in the high Cr-content alloys ($y \geq 18$), both the LMR and the TMR are found to be negative and nearly isotropic. This is quite puzzling. However, this may be ascribed to the dominant SG/CG contribution. To say something more conclusively, measurements have to be done at much higher fields and several temperatures.

The ferromagnetic anisotropy of resistivity (FAR) for the present $Ni_{100-x-y}Fe_xCr_y$ ($6 \leq x \leq 23$; $2 \leq y \leq 21$) alloys are evaluated from the LMR and the TMR data. The FAR values in the present alloys are found to be very small. A maximum value of 0.76 % is found in the alloy $Ni_{77}Fe_{21}Cr_2$ with 2 at.% of Cr. But as the Cr content increases, the value of the FAR decreases drastically and for $Ni_{72}Fe_8Cr_{20}$ it becomes almost zero. The Hall resistivity till 1.4 T is measured at 4.2 K for $Ni_{75}Fe_{13}Cr_{12}$, $Ni_{70}Fe_{12}Cr_{18}$, $Ni_{73.5}Fe_8Cr_{18.5}$, $Ni_{72}Fe_8Cr_{20}$, and

$Ni_{71}Fe_8Cr_{21}$ alloys. The experimental γ_{HS}=0 line is plotted on the ternary phase diagram using the present Hall effect data and the earlier reported values of γ_{HS}. The experimental line is found to deviate strongly from the theoretical line. In addition, the experimental line has shown a pronounced curvature in the Cr-rich ($\simeq$ 20 at.%) region in contrast to the straight line predicted by the split-band model. On the same diagram, the nearly constant FAR lines are also drawn. The most important observation is that the ridges of the constant FAR lines are found to follow exactly the experimental γ_{HS}=0 line. Also, the initial permeability (μ) for these compositions should be very high making them useful as transformer core materials. All these are in good agreement with the idea behind the SB model. However, the experimental γ_{HS}=0 line and the line joining the ridges of the constant FAR lines are found to lie far away from where they are theoretically expected. This is quite interesting. One of the reasons for such a discrepancy is found to lie in the composition dependence of Z_{eff} which, according to the split-band model, is a constant. Besides this, according to the earlier neutron diffraction data, a complete band splitting, as predicted by the split - band model, is quite unexpected for the present Cr-rich alloys and this might be another reason behind the above discrepancy. Intensive theoretical as well as experimental investigations are needed to resolve it.

According to the coherent potential approximation calculations, there is a large energy difference between the spin-up bands of Cr and Ni. This may be responsible for such small values of FAR in the high Cr-content alloys. On the other hand, according to the two-current conduction model, the decrease in the FAR values with increasing Cr could be interpreted in terms of the alloys moving from strong to weak-itinerant ferromagnetism. This is in excellent agreement with the earlier dc-magnetisation data of the present alloys. Here, for the first time, detailed qualitative as well as quantitative description of such small FAR's in high Cr-content alloys are interpreted more or less convincingly.

- **Hall effect**

Very precise Hall resistivity (ρ_H) data are taken in magnetic inductions till 1.4 T in ferromagnetic γ-$Ni_{75}Fe_{13}Cr_{12}$ (S29), $Ni_{70}Fe_{12}Cr_{18}$ (S48), and $Ni_{73.5}Fe_8Cr_{18.5}$ (S41) alloys at several

temperatures which are well below the Curie temperatures of the respective alloys. The OHC (R_0) and R_sM_s are found to be positive in alloys S48 and S41 whereas they are negative in alloy S29. The values of R_s (EHC) are coming two orders of magnitude larger than those of the OHC whereas the values of ρ_H beyond saturation are found to be three orders of magnitude smaller than those of ρ_0. Hence the present large extra-ordinary contribution can be ascribed to the side-jump effect ($R_s \propto \rho^2$). The electrical resistivity study in the present alloys has shown minima, i.e., ρ(T) decreases with increasing temperature till T_{min}. Therefore, the temperature dependence of R_s is also expected to have a similar anomaly at low temperatures. The OHC is found to be almost temperature independent with a broad maximum. On the other hand, the EHC, irrespective of their sign, has shown a strong temperature dependence with a minimum at around T_{min}, much the same way as ρ(T). The behaviour of the positive EHC in alloys S41 and S48 is consistent with the resistivity minima which is explained convincingly by electron - electron interaction effects. On the other hand, the negative EHC in alloy S29 behaves exactly opposite to that theoretically expected ($R_s(T) = -K(\rho(T))^2$). Instead of getting more negative, it becomes more positive below as well as above T_{min}. This is found to be quite puzzling and in noway can be interpreted by current theories. Nevertheless, this is the only study where such a strong negative temperature dependence of EHC has been observed in any concentrated crystalline ferromagnetic alloy.

6.2 Scope for further work

- In the present thesis, the interpretation of the electron - electron interaction (EEI) effects describing the electrical resistivity data is done convincingly in the temperature range 1.2 to 10 K. However, the range is quite narrow. Also, the EEI effects are expected to become more dominant at lower temperatures below 1.2 K. Hence, the interpretation will be much more conclusive if the measurements are extended below 1.2 K.

  On the other side, the tendency towards resistivity saturation at high temperatures is found very clearly in the high Cr-content ($\geq$ 18 at.%) NiFeCr alloys which, however, can not be

analysed in the present temperature range till 290 K. It will be of interest if one does the measurements much above 290 K.

- The detailed low - temperature magnetic state of high Cr-content ($\geq$ 18 at.%) Ni-rich ferromagnetic NiFeCr alloys is not at all known. The present study has clearly shown that, besides the ferromagnetic phase, there is a second transition at lower temperatures. It is, therefore, very essential to establish the low - temperature magnetic phases through dc - magnetisation, ac-susceptibility, and neutron diffraction studies.

- The magnetoresistance study of CuMn alloys is done till 7.5 T at 4.2, 20.5, and 63 K where the data are interpreted in terms of the combined electron - electron interaction and localisation effects. To make the interpretation more complete, it is very necessary to isolate these two effects from each other. This is possible only if measurements are extended to higher fields (> 10 T) and at various temperatures down to a few millikelvin.

On the other hand, in NiFeCr alloys the magnetoresistance measurements were done till 1.4 T and at 4.2 K only. The data in such a small field range and at only one temperature are very difficult to interpret satisfactorily, especially in terms of the electron - electron interaction or the quantum interference effects. Detailed investigations at various temperatures and in higher fields (> 10 T) are needed to arrive at more definite conclusions.

- The ridges in the constant FAR lines at 4.2 K are found to follow exactly the experimental γ_{HS}=0 line in the ternary phase diagram of NiFeCr alloys. This is very much consistent with the idea behind the split - band model. However, the above experimental lines lie far away from the theoretically predicted one. This interesting behaviour needs further look from both theoretical (band structure) and experimental view points.

- Earlier, in conventional ferromagnets, the temperature dependence of FAR was found to depend strongly on electron - impurity and electron - phonon scattering. Hence it will be interesting to study the temperature dependence of the FAR in the present disordered alloys where resistivity minima are observed.

- The temperature dependence of the Hall effect data in the present NiFeCr alloys has shown minima in $R_s(T)$, irrespective of their sign. The minima in the positive $R_s(T)$ are interpreted quite satisfactorily in terms of the resistivity minima. But the negative $R_s(T)$ could not be explained by existing theories. To get a more complete picture of the effect of resistivity minima on Hall resistivity data, detailed investigations are needed on a large number of magnetic as well as non-magnetic alloys.